TRC2202

Updating ARDOT Liquefaction Evaluation Procedures

Clinton M. Wood
Suman Mitra
Sagar Barua
Mohammad Rahimi

University of Arkansas - Fayetteville
College of Engineering, Department of Civil Engineering

Final Report

March 2024

TRC2202

Updating ARDOT Liquefaction Evaluation Procedures

Clinton M. Wood
Suman Mitra
Sagar Barua
Mohammad Rahimi

University of Arkansas - Fayetteville
College of Engineering, Department of Civil Engineering

Final Report

March 2024

Arkansas Department of Transportation

Notice of Nondiscrimination

The Arkansas Department of Transportation (ARDOT) complies with all civil rights provisions of federal statutes and related authorities that prohibit discrimination in programs and activities receiving federal financial assistance. Therefore, the Department does not discriminate on the basis of race, sex, color, age, national origin, religion (not applicable as a protected group under the Federal Motor Carrier Safety Administration Title VI Program), disability, Limited English Proficiency (LEP), or low-income status in the admission, access to and treatment in the Department's programs and activities, as well as the Department's hiring or employment practices. Complaints of alleged discrimination and inquiries regarding the Department's nondiscrimination policies may be directed to Civil Rights Officer Joanna P. McFadden (ADA/504/ Title VI Coordinator), P. 0. Box 2261, Little Rock, AR 72203, (501) 569-2298, (Voice/TTY 711), or the following email address: joanna.mcfadden@ardot.gov.

Free language assistance for Limited English Proficient individuals is available upon request.

This notice is available from the ADA/504/Tittle VI Coordinator in large print, on audiotape and Braille

Disclaimer:

The contents of this report reflect the views of the authors, who are responsible for the facts and the accuracy of the data presented herein. The contents do not necessarily reflect the official views or policies of ARDOT and they assume no liability for the contents or use thereof. This report does not constitute a standard, specification, or regulation. Comments contained in this report related to specific testing equipment and materials should not be considered an endorsement of any commercial product or service; no such endorsement is intended or implied.

TECHNICAL REPORT DOCUMENTATION

1. Report No. TRC2202	**2. Government Accession No.**	**3. Recipient's Catalog No.**	
4. Title and Subtitle Updating ARDOT Liquefaction Evaluation Procedures		**5. Report Date** March 2024	
		6. Performing Organization Code	
7. Author(s) Clinton M. Wood and Suman Mitra		**8. Performing Organization Report No.**	
9. Performing Organization Name and Address Department of Civil Engineering University of Arkansas 4190 Bell Engineering Center Fayetteville, Arkansas 72701		**10. Work Unit No. (TRAIS)** **11. Contract or Grant No.** Project TRC2202	
12. Sponsoring Agency Name and Address Arkansas Department of Transportation PO Box 2261 Little Rock, Arkansas 72203-2261		**13. Type of Report and Period Covered** FINAL **14. Sponsoring Agency Code**	
15. Supplementary Notes			

16. Abstract

There is a significant amount of uncertainty when designing piles for bridge foundations in liquefiable soil. Currently, Arkansas Department of Transportation (ARDOT) engineers use a standard penetration test (SPT)-based liquefaction spreadsheet developed 10 years ago to evaluate liquefaction triggering. Since this spreadsheet was developed, updates to the liquefaction triggering procedures have been published, making the spreadsheet out-of-date. In addition, recommendations regarding skin friction and end bearing of piles in liquefiable soils have been published, providing additional guidance regarding the design of these piles. Moreover, additional methods of liquefaction evaluation using the cone penetration test (CPT) and shear wave velocity (V_s) provide additional means of evaluating liquefaction potential. This project plans to update ARDOT's liquefaction triggering evaluation methodology with the newest procedures and incorporate additional empirical liquefaction hazard estimates such as the liquefaction potential index (LPI). This will provide ARDOT with the tools necessary to design pile foundations in liquefiable soils using the most up-to-date guidance and methods.

17. Key Words Liquefaction, SPT, CPT, V_s, LPI	**18. Distribution Statement**		
19. Security Classification (of this report) Unclassified	**20. Security Classification (of this page)** Unclassified	**21. No of Pages** 189	**22. Price**

SI* (MODERN METRIC) CONVERSION FACTORS

APPROXIMATE CONVERSIONS TO SI UNITS

Symbol	When You Know	Multiply By	To Find	Symbol
		LENGTH		
in	inches	25.4	millimeters	mm
ft	feet	0.305	meters	m
yd	yards	0.914	meters	m
mi	miles	1.61	kilometers	km
		AREA		
in^2	square inches	645.2	square millimeters	mm^2
ft^2	square feet	0.093	square meters	m^2
yd^2	square yard	0.836	square meters	m^2
ac	acres	0.405	hectares	ha
mi^2	square miles	2.59	square kilometers	km^2
		VOLUME		
fl oz	fluid ounces	29.57	milliliters	mL
gal	gallons	3.785	liters	L
ft^3	cubic feet	0.028	cubic meters	m^3
yd^3	cubic yards	0.765	cubic meters	m^3
	NOTE: volumes greater than 1000 L shall be shown in m^3			
		MASS		
oz	ounces	28.35	grams	g
lb	pounds	0.454	kilograms	kg
T	short tons (2000 lb)	0.907	megagrams (or "metric ton")	Mg (or "t")
		TEMPERATURE (exact degrees)		
°F	Fahrenheit	5 (F-32)/9 or (F-32)/1.8	Celsius	°C
		ILLUMINATION		
fc	foot-candles	10.76	lux	lx
fl	foot-Lamberts	3.426	$candela/m^2$	cd/m^2
		FORCE and PRESSURE or STRESS		
lbf	poundforce	4.45	newtons	N
lbf/in^2	poundforce per square inch	6.89	kilopascals	kPa

APPROXIMATE CONVERSIONS FROM SI UNITS

Symbol	When You Know	Multiply By	To Find	Symbol
		LENGTH		
mm	millimeters	0.039	inches	in
m	meters	3.28	feet	ft
m	meters	1.09	yards	yd
km	kilometers	0.621	miles	mi
		AREA		
mm^2	square millimeters	0.0016	square inches	in^2
m^2	square meters	10.764	square feet	ft^2
m^2	square meters	1.195	square yards	yd^2
ha	hectares	2.47	acres	ac
km^2	square kilometers	0.386	square miles	mi^2
		VOLUME		
mL	milliliters	0.034	fluid ounces	fl oz
L	liters	0.264	gallons	gal
m^3	cubic meters	35.314	cubic feet	ft^3
m^3	cubic meters	1.307	cubic yards	yd^3
		MASS		
g	grams	0.035	ounces	oz
kg	kilograms	2.202	pounds	lb
Mg (or "t")	megagrams (or "metric ton")	1.103	short tons (2000 lb)	T
		TEMPERATURE (exact degrees)		
°C	Celsius	1.8C+32	Fahrenheit	°F
		ILLUMINATION		
lx	lux	0.0929	foot-candles	fc
cd/m^2	$candela/m^2$	0.2919	foot-Lamberts	fl
		FORCE and PRESSURE or STRESS		
N	newtons	0.225	poundforce	lbf
kPa	kilopascals	0.145	poundforce per square inch	lbf/in^2

TABLE OF CONTENTS

LIST OF FIGURES

LIST OF TABLES

LIST OF ABBREVIATIONS, ACRONYMS, AND SYMBOLS

AASHTO	Association of State Highway and Transportation Officials
a_{max}	Design peak horizontal acceleration
ARDOT	Arkansas Department of Transportation
C_B	Borehole diameter correction factor
C_E	Hammer energy correction factor
C_N	Overburden stress correction factor
CPT	Cone penetration test
C_R	Rod length correction factor
CRR	Cyclic resistance ratio
C_S	Sampler liner correction factor
CSR	Cyclic stress ratio
DWF	Duration weighting factor
D_R	Relative density
E_S	Young's modulus
FC	Fines content
F_R	Normalized friction ratio
f_s	Sleeve friction
FS	Factor of safety
G_O	Small strain shear modulus
I_C	Soil behavior index
K	Permeability
K_O	In-situ stress ratio
K_σ	Overburden correction factor
K_α	Sloping ground correction factor
K_C	Grain size characteristics correction factor
KM_W	Seismic moment magnitude scaling factor
LL	Liquid limit
LPI	Liquefaction potential index
LRFD	Load and resistance factor design
M	1-D constrained modulus
MODOT	Missouri Department of Transportation
M_W	Earthquake moment magnitude
MSF	Magnitude safety factor
N	Raw blow count value
N_{60}	Blow count corrected for hammer efficiency
$(N_1)_{60}$	Corrected blow count
$(N_1)_{60,CS}$	Equivalent clean-sand blow count value
NCEER	National Center for Construction Education and Research
NEA	Northeast Arkansas

NMSZ	New Madrid Seismic Zone
OCR	Over-consolidation ratio
Pa	Atmospheric pressure
PI	Plasticity index
PL	Plastic limit
P_L	Probability of liquefaction
PGA	Peak ground acceleration
q_c	Raw tip resistance
$(q_{C1N})_{CS}$	Normalized clean-sand cone penetration resistance
$q_{c,1,mod}$	Modified normalized tip resistance
q_t	Corrected cone tip resistance
Q_{tn}	The normalized cone resistance
r_d	Stress reduction factor
SBT_n	Normalized soil behavior type
SCPT	Seismic cone penetration test
SSGMRA	Site-specific ground motion response analysis
SPT	Standard penetration test
S_U	Undrained shear strength
$S_{U(rem)}$	Remolded undrained shear strength
USCS	Unified Soil Classification System
USGS	US Geological Survey
V_s	Shear wave velocity
V_{S1}	Overburden stress corrected shear wave velocity
$V_{S,40}$	Average shear wave velocity at the top 40 ft
$V_{S,100}$	Average shear wave velocity at the top 100 ft
wc	Moisture content
σ'v	Effective vertical stress
ψ	State parameter
ϕ'	Peak drained friction angle

EXECUTIVE SUMMARY

As part of this study, the existing Arkansas Department of Transportation (ARDOT) standard penetration test (SPT)-based liquefaction triggering spreadsheet is updated with the inclusion of new cone penetration test (CPT) and shear wave velocity (V_s)-based liquefaction triggering spreadsheets. These SPT, CPT, and V_s-based liquefaction triggering spreadsheets will aid in evaluating liquefaction triggering using the most up-to-date methods. The format, primary input page, and graphs of these spreadsheets are kept very similar to the existing SPT spreadsheet, ensuring a minimal learning curve for the user of the basic spreadsheet. Second, a user guide for all three spreadsheets is provided in Chapter 3 to help understand how these spreadsheets work. The guide describes the inputs and outputs of the spreadsheet along with how to utilize the results of the spreadsheet. Also, to understand whether liquefaction manifestation will be an issue, the liquefaction potential index (LPI) by Iwasaki et al. (1978) and LPI_{ISH} by Maurer et al. (2015) are also included in the spreadsheets. These spreadsheets were verified using previously developed spreadsheets, codes, hand calculations, and commercial software packages.

In the new SPT spreadsheet, the Boulanger and Idriss (2014) relationship (an update to the 2008 version) and the Cetin et al. (2018) relationship (an update to the 2004 version) for liquefaction triggering are included. The previous Youd et al. (2001) approach is also included in the spreadsheet, which has not been revised since 2001 (except in the change of the K_σ limit). The Moss et al. (2006), Boulanger and Idriss (2014), and Youd et al. (2001) (also known as Robertson and Wride 1998) techniques are all included in the CPT spreadsheet. Kayen et al. (2013) and Youd et al. (2001) (also known as Andrus and Stokoe 2000) are included in the V_s liquefaction spreadsheet. The CPT and V_s spreadsheets can convert the raw data to the desired units required to perform the analysis. In the CPT spreadsheet, a rolling average is programmed into the data analysis to smooth the plots, which can help the user better understand the results and remove large spikes. This spreadsheet can also determine the water table if the information is not given in the CPT data. In addition to the continuous comparison tab, a discontinuous 5'/2.5' layered comparison tab is also provided in the CPT and V_s-based spreadsheets to compare co-located SPT, CPT, and V_s data and complete a sensitivity study using the spreadsheet to understand any differences between the procedures and methods.

After developing the SPT, CPT, and V_s-based liquefaction triggering spreadsheets, several analyses are completed using constant raw inputs (SPT-N, q_c, V_s) to compare the liquefaction triggering procedures

and understand the contributing factors behind their differences. When constant SPT-N values of 20 blows/ft are used in the SPT spreadsheet, the Youd et al. (2001) procedure shows the least liquefiable layers. Also, Cetin et al. (2018) generate lower cyclic resistance ratio (CRR) values than the others even though $(N_{1,60})_{cs}$ is similar for all three procedures, which makes this method the most conservative of all three SPT procedures. The factor of safety (FS) values from the Cetin et al. (2018) procedure are higher than their 2004 procedure. This is caused by the new model coefficients in the probabilistic liquefaction triggering relationship for CRR, which generates higher CRR values at shallow depths. For the other two procedures, the percentage of change (old procedure versus new procedure) in the factor of safety results is not significant. In the CPT spreadsheet, constant tip resistance and raw tip resistance (q_c) of 250 ksf are used; similar to the SPT analysis, the Youd et al. (2001) procedure shows the least liquefiable layers, whereas the Boulanger and Idriss (2014) procedure is found to be the most conservative CPT procedure. From the V_s-based analysis results of constant V_s of 200 m/s, the Kayen et al. (2013) procedure is the most conservative V_s-based procedure.

After the constant input analysis, these spreadsheets are used to understand the differences between the methods and analyze real project data from Arkansas. Site-specific comparisons of the SPT, CPT, and V_s liquefaction triggering procedures for two different sites in eastern Arkansas are presented and discussed. For the Turrell site, sets of data were produced for the TRC1204 and TRC1502 ARDOT research projects, which include SPT data gathered by ARDOT, CPT data gathered by the Missouri Department of Transportation (MoDOT), and V_s data gathered by MoDOT using seismic CPT. The second dataset was collected in Monette, Arkansas, for an ARDOT project. SPT testing was performed for the initial design efforts while seismic CPT testing was performed as part of this research work. Extensive analyses are conducted using the co-located SPT, CPT, and V_s evaluation data to understand not only the similarities and differences but also the driving factors behind these differences.

From the analysis performed at the Monette site using the co-located data, the SPT methods are in good agreement with the CPT-based procedure of Boulanger and Idriss (2014) from the surface to 80 ft depth. At depths below that, Moss et al. (2006) shows good agreement with the SPT-based results. It is important to note that the CPT-based approaches of Youd et al. (2001) and Boulanger and Idriss (2014) generally consider the deeper layers more liquefiable than the SPT-based approaches. Moreover, Kayen et al.'s (2013) V_s-based procedure shows similar results to the CPT-based procedure of Boulanger and Idriss (2014) in shallow depths (from the ground surface to 60 ft depth). Below this depth, the CPT-based procedure of Boulanger and Idriss (2014) shows non-liquefiable layers, whereas the Kayen et al.

(2013) method demonstrates the possibility of these layers being liquefiable. This is likely driven by the V_s measures being averaged more through the soil column, making them less sensitive to the rapid changes in stiffness in the soil profile than the CPT results. From the LPI analysis, this site is susceptible to severe liquefaction as all the in-situ methods show LPI and LPI_{ISH} higher than 15.

From the analysis performed at the Turrell site, CPT-based procedures consistently have a higher factor of safety than the SPT methods, which is quite different from the results observed from the Monette data. Moreover, the CPT-based FS is consistently greater compared to the SPT results. From the discontinuous V_s results, the V_s-based FS is found higher than the SPT-based FS but lower than the CPT-based FS at a depth below 65 ft. At depths deeper than 65 ft, the V_s-based FS from Youd et al. (2001) and Kayen et al. (2013) is higher than both SPT- and CPT-based results. The V_s-based results of Kayen et al. (2013) indicate the layers from 30 ft to 40 ft depth from the boring surface are liquefiable, similar to the SPT-based results but in contrast with the CPT-based results. Moss et al.'s (2006) CPT-based procedure and Youd et al.'s (2001) V_s-based procedure show the least liquefiable layers for this site, whereas all SPT-based procedures and Kayen et al.'s (2013) V_s-based procedure have the most liquefiable layers. From the LPI analysis results, this site is susceptible to severe liquefaction as the SPT-based and V_s-based analyses show LPI and LPI_{ISH} higher than 15, whereas the CPT-based results show moderate to no liquefaction severity.

The cost-saving analysis results from the bridge redesign in Monette, Arkansas, performed by Wood and Baker (2018) as a part of the TRC1603 research project, are used to compare the in-situ liquefaction analysis results and to find out if any further changes are needed if the updated spreadsheets and new in-situ measurements (i.e., CPT and V_s) are used. From the analysis, minor to no potential cost savings can be achieved if CPT and V_s results are used instead of SPT results, using the American Association of State Highway and Transportation Officials' (AASHTO) general seismic design procedure (PGA = 0.917 g) and the site-specific ground motion response analysis (PGA = 0.611 g). However, that does not mean that using multiple approaches is without benefits. Using more than one approach at a site provides redundancy to the design, and the CPT-based approach provides higher resolution, providing more information on the thickness of potential liquefiable and non-liquefiable layers.

The primary task of the research discussed herein is to help ARDOT update the SPT-based procedures used to evaluate earthquake-induced soil liquefaction triggering, particularly for deep soil deposits. The CPT method improves upon this lack of resolution by providing a near-continuous estimate of soil properties with depth. This provides more accurate estimates of liquefaction triggering. In addition, CPT

has been shown to provide more accurate estimates of soil strength, especially for soils softer than SPT. The addition of using V_s along with CPT and SPT has the benefits of a better understanding of the aging of the sandy deposits. Aging or cementation in sandy soils increases soil liquefaction resistance. The measurement of aging is improved with V_s as compared to CPT and SPT, which are large strain tests that tend to damage the cementation without fully measuring its contribution to the strength of the soil. The current liquefaction spreadsheet used by ARDOT is deterministic, meaning it only provides a yes or no answer with a factor of safety. The inclusion of estimates of the severity of surface manifestation has benefits in helping understand whether the consequences of liquefaction will be significant for a project. There are times when thin or deep layers are the only ones that are determined to liquefy for a project. In these cases, the impacts of liquefaction are reduced, decreasing the potential impacts due to liquefaction.

CHAPTER 1: INTRODUCTION

BACKGROUND AND SIGNIFICANCE OF WORK

Northeast Arkansas is in the heart of the New Madrid Seismic Zone (NMSZ), an area of the United States that has some of the highest design ground motions in the nation. This large seismic hazard is the result of past large-magnitude earthquakes occurring within the NMSZ. It is a major seismic zone located in the southern and midwestern parts of the United States, stretching to the southwestern part of Kentucky and through southeastern Missouri, the northeastern part of Arkansas, the western part of Tennessee, and the northwest part of Mississippi. This region was the site of several large earthquakes in 1811 and 1812, estimated to have been around a magnitude 7 or 8. The tremors were felt as far away as New York, and the force of the quake caused the Mississippi River to temporarily flow backward. Since then, the NMSZ has been without any major incidents, but it is still considered a significant risk for future seismic activity. It is important to note that while large earthquakes in the NMSZ are infrequent, they can be extremely destructive when they do occur. The NMSZ is still active today, producing hundreds of small earthquakes each year, most of them too small to be felt. This is due to the unique geology of this region: The seismic waves produced by earthquakes in this region tend to propagate very efficiently, leading to tremors over a larger area than would be expected from an earthquake of comparable magnitude in a place like California.

Due to its location within the NMSZ, northeastern Arkansas has some of the largest design earthquake ground motions in the continental United States. The unknown seismic response of deep, soft soils in the Mississippi embayment makes these massive earthquake ground motions extremely hazardous. Furthermore, due to the limitations in guidance in the current literature on what to do in these situations, the Arkansas Department of Transportation (ARDOT) and others involved in bridge construction in the NMSZ are forced to drive piles for bridge foundations to significant depths to mitigate against the loss of strength in these potentially liquefiable soils during an earthquake. This is both costly and time-consuming. In addition, there is still a significant amount of uncertainty when designing piles for bridge foundations in liquefiable soil. Currently, ARDOT engineers use a Standard Penetration Test (SPT)-based liquefaction spreadsheet developed 10 years ago to evaluate liquefaction triggering. The previous spreadsheets adopted the SPT liquefaction triggering procedures of Youd et al. (2001), Idriss and Boulanger (2008), and Cetin et al. (2004). Since this spreadsheet was developed, updates to the liquefaction triggering procedures of the latter two procedures have been published,

making the spreadsheet out-of-date. Moreover, liquefaction evaluation using the cone penetration test (CPT) and shear wave velocity (V_s) methods provide additional means of evaluating liquefaction potential. This work aims to update the current SPT-based liquefaction triggering spreadsheet of Idriss and Boulanger (2008) and Cetin et al. (2004), with the newest procedures of Boulanger and Idriss (2014) and Cetin et al. (2018). Additionally, a new CPT-based liquefaction triggering spreadsheet, containing the procedures of Youd et al. (2001), Boulanger and Idriss (2014), and Moss et al. (2006), and a V_s-based liquefaction triggering spreadsheet, containing the procedures of Youd et al. (2001) and Kayen et al. (2013), are developed; and these spreadsheets will incorporate additional empirical liquefaction hazard estimates such as the liquefaction potential index (LPI). This will provide ARDOT with the tools necessary to evaluate liquefaction triggering for pile foundations in liquefiable soils using the most up-to-date guidance and methods. This work also systematically evaluates differences between the previous and current SPT-based liquefaction-triggering relationships along with current CPT and V_s relationships. The similarities and differences in the methods between the relationships are also studied when evaluating the liquefaction in the Mississippi embayment.

OBJECTIVES OF THIS STUDY

The primary task of this study is to review and update procedures used to evaluate earthquake-induced soil liquefaction triggering. Specific subtasks of this research project are included below.

(1) Update the SPT liquefaction triggering spreadsheet with the most up-to-date triggering procedures.

The three most popular SPT liquefaction triggering relationships—Youd et al. (2001), Cetin et al. (2004), and Idriss and Boulanger (2008)—were utilized to produce the current ARDOT liquefaction spreadsheet, which Cox and Griffiths developed in 2010 to predict the liquefaction potential of soil deposits. This spreadsheet is first updated and improved by programming the Boulanger and Idriss (2014) relationship (an update to the Idriss and Boulanger [2008] relationship and slight modification of the 2012 procedure) and the Cetin et al. (2018) relationship (an update to the Cetin et al. [2004] relationship) relationships for the liquefaction triggering relationships. The spreadsheet is programmed with the probabilistic and deterministic frameworks provided by the two relationships. Since the Youd et al. (2001) approach has not been revised since 2001, it is unchanged as the original method in the spreadsheet (except for changing the K_σ limit). The spreadsheet also includes the liquefaction susceptibility calculation method developed by Bray and Sancio (2006) based on plasticity. This offers

the most up-to-date approach for assessing a soil's plasticity-based liquefaction potential. The spreadsheet is designed in Excel, much like the one before it, guaranteeing that it will operate with the current workflow.

(2) Investigate software and develop spreadsheets for CPT and V_s-based liquefaction triggering evaluations.

Liquefaction spreadsheets for CPT and V_s data are also prepared in addition to updating the SPT liquefaction spreadsheet. Additionally, since the previous spreadsheet was created, the collection of CPT and V_s data for ARDOT bridge projects has increased. The addition of the CPT and V_s-based liquefaction evaluations provides redundancy to the current SPT approaches and improves the accuracy of liquefaction estimations. The Moss et al. (2006), Boulanger and Idriss (2014), and Youd et al. (2001) (also known as Robertson and Wride [1998]) techniques are all included in the CPT spreadsheet. Kayen et al. (2013) and Youd et al. (2001) (also known as Andrus and Stokoe [2000]) are included in the V_s liquefaction spreadsheet. In addition to programming the CPT and V_s procedures in a spreadsheet like the SPT procedure, commercial software packages (CPet-it, C-Liq) are explored to conduct the liquefaction analysis and to validate the results of the spreadsheets. These software packages have some advantages but also generally have the limitation of only providing the results of one liquefaction-triggering relationship.

(3) Incorporate empirical estimates of liquefaction surface manifestation into the ARDOT methodology.

Although the main objective of the research is to estimate liquefaction potential through triggering relationships, simply determining if liquefaction is likely to trigger does not assist engineers in understanding whether liquefaction manifestation will be an issue. Because of this, it is crucial to determine whether surface manifestation will be considerable and to include these estimates in the ARDOT methodology. As a result, the LPI, created by Iwasaki et al. in 1978, is included in the spreadsheets. The LPI offers a depth-weighted index of the likelihood of liquefaction triggering that relates to liquefaction surface manifestation. In the LPI method, the factor of safety for liquefaction is compounded by a linear weighting factor from 0 to 20 m below the surface. This indicates that layers close to the surface are more likely to manifest at the surface than deeper layers. The spreadsheets also include LPI_{ISH} in addition to LPI. LPI_{ISH} is a modification of LPI that incorporates the Ishihara (1985) concept of a non-liquefiable crust that is typical of some Arkansas sites that have a thick layer of clay

covering a liquefiable sand layer and uses a power-law depth weighting factor as opposed to a linear depth–weighting factor used for LPI. It has been demonstrated that the LPI_{ISH} procedure, created by Maurer et al. (2015), reduces false positives and more correctly depicts the liquefaction manifestation during the earthquake in Christchurch, New Zealand.

(4) Evaluate the spreadsheet using sites in Arkansas with co-located SPT, CPT, and V_s data.

Co-located SPT, CPT, and V_s data are used to evaluate the spreadsheet after it has been created. For the Turrell site, sets of data were produced for the TRC1204 and TRC1502 ARDOT research projects. This dataset includes SPT data gathered by ARDOT, CPT data gathered by MoDOT, and V_s data gathered by MoDOT using seismic CPT. This offers a useful comparison of the different approaches at a specific location where numerous measurements were taken. The second dataset was collected in Monette, Arkansas, for an ARDOT project. SPT testing was performed for the initial design efforts while seismic CPT testing was performed as part of this research work. This offers a second location where various in-situ techniques can be used to conduct co-located liquefaction analyses. The spreadsheet findings are checked against those from hand calculations and those from the software programs discussed previously that were used to calculate the liquefaction potential. The evaluation results are used to do a cost-benefit analysis on the pile design for the Monette bridge and Turrell site. In addition, utilizing the project's new data and updated spreadsheets, the liquefaction potential of the Monette bridge from TRC1603 is reevaluated. This gives an estimation of the advantages and prospective cost savings of this research.

Report Overview

This report is composed of five chapters. Chapter 1 includes some general information and an introduction to this project. Chapter 2 encompasses a review of relevant literature, which includes pertinent information regarding soil liquefaction-triggering procedures. Chapter 3 is a user's guide, which should serve to clarify any questions that may arise while implementing the liquefaction triggering spreadsheets and include valuable information about the bridge sites. Chapter 4 summarizes the liquefaction-triggering results from the bridge sites in Arkansas. The results obtained from each of the three spreadsheets (SPT, CPT, and $V_{s)}$ are compared in-depth to determine what factors most influence the differences between procedures. It also includes a cost-savings analysis for using different liquefaction evaluation procedures. Chapter 5 presents the overall conclusions, recommendations, and future scope of this work.

CHAPTER 2: LITERATURE REVIEW

INTRODUCTION

Liquefaction is a process that occurs during an earthquake where saturated cohesionless soil temporarily loses its strength and behaves more like a liquid than a solid. This is due to the increase in pore water pressure and reduction of effective stress between solid particles generated by shear strains due to ground shaking, which causes the soil particles to lose contact with each other and behave more like a fluid. The phenomenon typically occurs in loose, water-saturated, granular soils such as sandy or silty soils. As a result, structures and buildings on top of these soils can sink or tilt, and buried structures, like pipelines can float to the surface. Figure 1 provides a simplistic description of the phenomenon of liquefaction and discusses the basic behavior of soil during liquefaction.

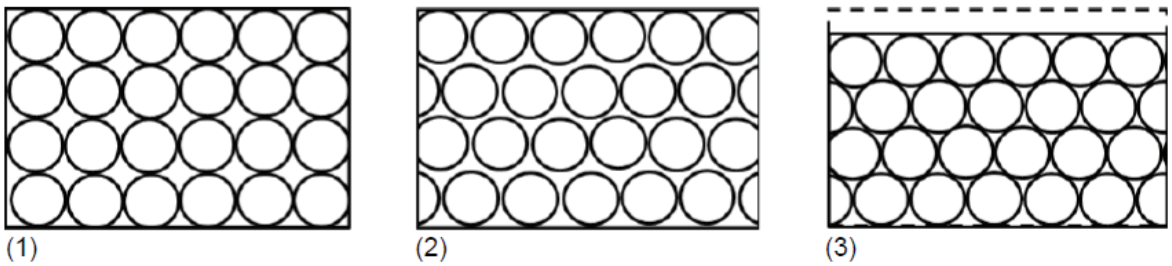

FIGURE Idealized schematic of liquefiable soils. (1) Before an earthquake, individual soil grains are held in place by frictional or adhesive contact forces, creating a solid soil structure with water filling the spaces between the grains. Note the grain-to-grain contact. (2) After initiation of liquefaction, particle rearrangement with no change in volume (e.g., a lateral shift of a half diameter of every other row of particles in the figure) causes the particles to lose contact and go into suspension, causing the porewater pressure to increase as gravity load is transferred from the soil skeleton to the porewater. (3) As water flows out of the soil, the soil particles settle into a denser configuration, the soil skeleton once again carries the load, and the porewater pressure decreases (back to the initial steady state value).

Figure 1. Basic Description of Soil Liquefaction (Modified from NASEM 2018)

Liquefaction is a severe natural hazard, and its occurrence and impact during earthquakes have been widely recognized globally. It involves a process where saturated soils lose their strength due to an increase in pore-water pressure during seismic activities. Over the years, various methods and models have been developed to predict and assess the potential for soil liquefaction during earthquakes. This review examines several of these models, focusing on those using the SPT, CPT, and V_s as central tools for evaluation.

SPT LIQUEFACTION–TRIGGERING RELATIONSHIPS

In the field of geotechnical earthquake engineering, soil liquefaction refers to the transformation of granular material from a solid state into a liquefied state due to an increase in pore water pressure. The SPT is a popular method for assessing soil susceptibility to liquefaction. The test consists of driving a split-spoon sampler into the soil using a 140 lb hammer dropped 30”. The number of blows required to drive the sampler the last 12” of an 18” total drive is defined as the N value. The raw N value must be adjusted for hammer energy and other test parameters along with overburden stress for liquefaction analysis. This literature review aims to investigate the evolution of SPT-based liquefaction-triggering relationships, their validity, strengths and weaknesses, and the direction of recent research. It seeks to analyze various research studies and advancements on the subject, focusing on their development, accuracy, applicability, and overall impact on the geotechnical engineering field.

The SPT liquefaction triggering relationships are vital tools in the analysis of seismic soil behavior. These relationships are integral in assessing a soil’s propensity toward liquefaction, a phenomenon that typically occurs during earthquakes, causing significant infrastructural damage and loss of life. SPT was first introduced in 1902 by the Raymond Pile Company. The usefulness of SPT in assessing liquefaction potential was recognized in the 1970s, leading to the development of empirical relationships (Seed and Idriss 1971). These relationships, based on case histories of past earthquakes, defined the liquefaction-triggering relationship using SPT values.

The major relationships include those proposed by Seed and Idriss (1971, 1982), Youd et al. (2001), Idriss and Boulanger (2004, 2008), and Boulanger and Idriss (2014), Moss et al. (2006), and Cetin et al. (2004, 2014). These studies proposed relationships that consider several factors, such as the magnitude of the earthquake, the overburden stress, soil type, fines content, and age of the deposit. With each new relationship, improvements were made, incorporating more case histories and addressing the limitations of the previous relationships.

The early work in the late 1970s and early 1980s by Seed and Idriss is a foundational pillar in SPT-based liquefaction triggering relationships. They proposed a method where the liquefaction potential of a site is assessed using data from the SPT and a calculated factor of safety. If the cyclic stress ratio (CSR) is greater than the cyclic resistance ratio, liquefaction is likely to occur. The NCEER Workshop (1996) brought together numerous researchers to develop a set of guidelines for evaluating liquefaction

potential. They provided standard procedures for normalizing SPT data, which is critical for evaluating liquefaction potential.

Youd et al.'s (2001) SPT-based relationship improved upon the initial Seed and Idriss method by addressing several of its limitations and incorporating new findings from field investigations of liquefaction. They proposed a new liquefaction resistance correlation with the SPT data. This new correlation considered factors like the overburden correction factor (K_σ) and fines content (FC). The work by Youd et al. (2001) represented a consensus in the field, incorporating a comprehensive database of case studies in their revised method for SPT-based liquefaction triggering. Juang et al. (2002) proposed the use of Bayesian statistical methods in SPT-based liquefaction evaluation. The use of Bayesian statistics allows for the incorporation of uncertainty in the input parameters, providing a more robust and reliable analysis.

Cetin et al. (2004) proposed a new model that incorporated uncertainty explicitly. They introduced the concept of a "probability of liquefaction" (PL), allowing for a statistical understanding of risk, which marked a shift from the binary (will/will not liquefy) viewpoint in earlier models and subsequently in 2018. Cetin et al. also updated their procedure.

In 2008, Idriss and Boulanger critically reviewed the developments in SPT-based liquefaction triggering methods and proposed a simplified procedure. Their method aimed at reducing complexities in existing models and improving the consistency in predictions. This update to previous relationships recognized the limitations of the existing methods. Moreover, Boulanger and Idriss (2014) emphasized the role of soil plasticity in the evaluation of liquefaction susceptibility, stressing that higher plasticity could decrease susceptibility.

The SPT method has the advantage of liquefaction analysis in that this test is commonly conducted throughout the world, and a sample of soil is obtained for each test. The test has the limitation that there can be variability in the measured raw N values (i.e., hammer energy, equipment differences, etc.), which necessitates correction. In addition, the SPT test measures soil strength at intervals (often 5 ft) and, therefore, provides discontinuous soil information. The test itself has inherent variability and is sensitive to in-situ conditions, testing procedures, and equipment used. There have been efforts to mitigate these factors, with varying success. These relationships are based on empirical data and are, therefore, susceptible to the inherent limitations of empirical models, including uncertainty about predictive accuracy outside the range of case histories (Andrus and Stokoe 2000). Furthermore, the

method is primarily designed for clean, sandy soils and may not provide accurate predictions for other soil types (Boulanger and Idriss 2014).

Current research in this domain has taken a more multidisciplinary approach, employing methods from fields such as machine learning to improve predictions. Also, emphasis is being placed on integrating geospatial information and remote sensing data to assess liquefaction risk at a regional scale, moving beyond individual site assessments. The accuracy of these relationships has been a point of debate, however. Some researchers argue that the relationships are well-calibrated and provide a reasonably accurate assessment of liquefaction potential (Kramer and Mayfield 2007). Recent research has focused on improving the accuracy of these relationships and extending their applicability to other soil types.

SPT liquefaction-triggering relationships represent a significant contribution to geotechnical earthquake engineering. Despite their limitations and uncertainties, they provide a practical tool for assessing the liquefaction potential of soils, informing the design of infrastructure and earthquake hazard mitigation efforts. The continuous refinement of these relationships, coupled with advancements in testing methods and statistical techniques, promises an increasingly accurate tool for predicting and mitigating the devastating effects of soil liquefaction during earthquakes. In summary, SPT-based liquefaction-triggering relationships have evolved, with increased sophistication and the consideration of more influencing factors. However, the accuracy of these relationships depends on the quality of the SPT data, the assumptions made, and the degree to which the empirical relationships represent the site-specific conditions. Despite numerous advancements, predicting liquefaction triggering remains a challenging task due to the inherent variability of soils and the complexity of soil behavior during earthquakes. The development of more sophisticated predictive models is an ongoing area of research in geotechnical earthquake engineering. Figure 2 shows a comparison of the cyclic resistance ratio (CRR) triggering curves of the three adopted SPT relationships. However, it should be noted that a direct comparison of these methods based on CRR-triggering relationships can be deceiving since each uses several factors that influence the result.

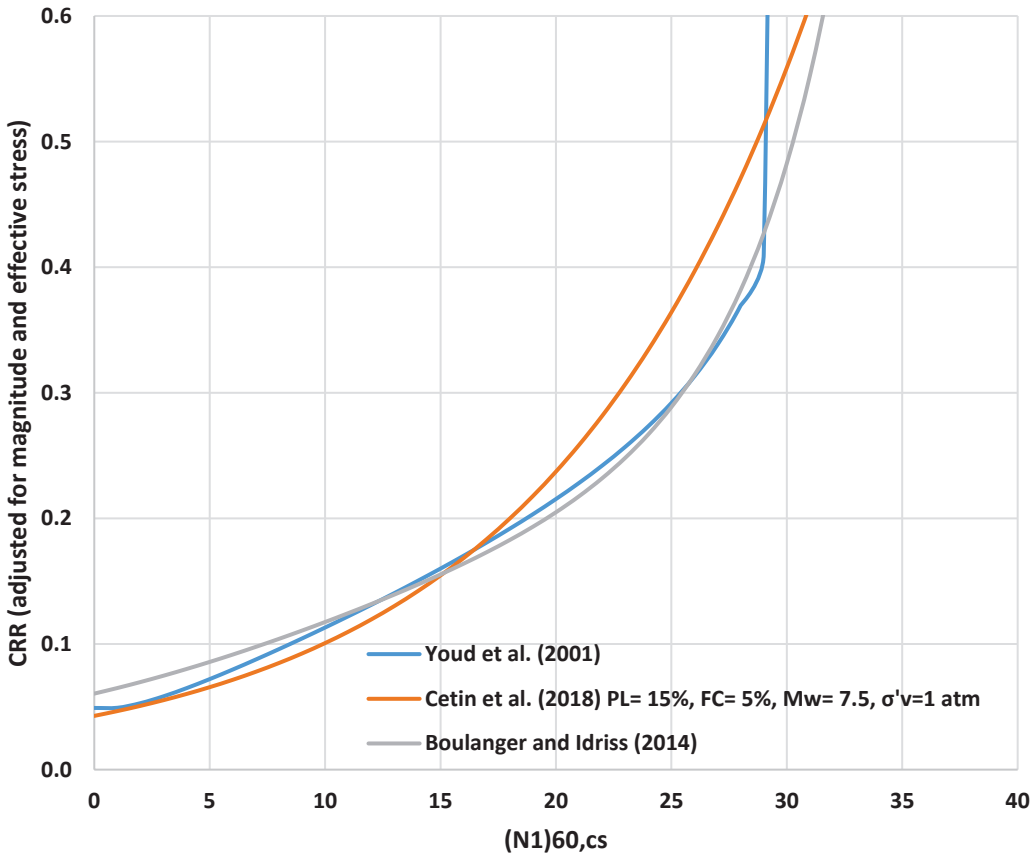

Figure 2. Comparison of SPT CRR Triggering Curves for Liquefaction from Youd et al. (2001), Cetin et al. (2018), and Boulanger and Idriss (2014)

CPT LIQUEFACTION TRIGGERING RELATIONSHIPS

The CPT is a soil testing method that offers continuous in-situ measurement of soil resistance to penetration. It is considered effective in characterizing soil types, stratigraphy, relative density, and other geotechnical parameters.

The seminal work by Robertson and Wride (1998) revolutionized our understanding of soil liquefaction potential by developing an empirical triggering relationship for CPT data. This seminal study provided a procedure to evaluate the potential of soil liquefaction based on CPT data. They proposed a simplified procedure using CPT measurements to evaluate soil susceptibility to liquefaction by using the tip resistance to estimate CRR and the behavior type index (I_c) to estimate soil susceptibility due to plasticity. These parameters indicated the soil's propensity to liquefy under seismic loadings. This made

it possible to improve the accuracy of CPT-based liquefaction assessment in soils with varying fine content.

Ishihara and Yoshimine (1992) explored the use of the normalized soil behavior index (I_c) as a factor in determining soil liquefaction potential, noting its correlation with soil type and grain size distribution. They also contributed to this field by focusing on the limitations of traditional methods in accurately predicting liquefaction in nonplastic silts and clayey soils. They highlighted that soil classification based on plasticity index alone was not sufficient, leading to a novel approach that considers soil grain size and water content, thus expanding the potential applicability of CPT-based liquefaction assessment. Juang et al. (2002, 2003) presented a probabilistic framework for the assessment of soil liquefaction potential using CPT data, which has been influential in establishing risk-based assessment methods. In addition, Zhang et al. (2002) provided an empirical, statistical method for liquefaction potential evaluation that was an enhancement of the Robertson and Wride method, incorporating additional CPT parameters. Advancements in CPT-based methodologies for liquefaction potential assessment were further made by Zhang et al. (2002), who proposed a method based on the factor of safety against liquefaction (FS), accounting for the influence of factors like effective vertical stress (σ'_v), horizontal coefficient of earth pressure (K_o), and overburden pressure. Zhang et al.'s work provided a practical approach, helping engineers to quickly estimate the liquefaction potential, but again, the applicability was for clean sands and sandy silts. Idriss and Boulanger (2008) developed a revised CPT-based liquefaction evaluation method. This method, while sharing some similarities with the Robertson and Wride (1998) approach, includes adjustments to account for fines content and overburden pressure. Furthermore, Boulanger and Idriss (2014) significantly advanced the study of CPT-based liquefaction-triggering relationships. Their study incorporated findings from more recent field case histories, laboratory tests, and an improved understanding of soil behavior under cyclic loading. The primary enhancement introduced by Boulanger and Idriss (2014) was a more detailed consideration of soil behavior, especially concerning soil plasticity. While prior methodologies made use of I_c from CPT data to differentiate between different soil types, Boulanger and Idriss (2014) developed a model to account for plastic fines and the influence of soil type on CRR. Their method incorporates a variable to correct the clean sand equivalent normalized cone tip resistance($q_{c1N})_{cs.}$ This parameter, paired with the effective vertical stress, gives a nuanced assessment of soil's susceptibility to liquefaction under seismic loads. The inclusion of plasticity and the correction factor in their model was a significant advancement, enabling a more accurate prediction of liquefaction potential in soils with varying fines content and plasticity.

Moss et al. (2006) developed a model based on a large CPT database of case histories, focusing on the normalized CPT resistance for liquefaction evaluation. Moss et al.'s approach introduces the concept of "aged" and "youthful" sands to account for soil cementation effects, showing promising results in numerous case studies. Moss et al. (2006) made significant strides in advancing CPT-based liquefaction-triggering relationships. Contrary to the traditional deterministic methods, Moss et al.'s approach first integrated both probabilistic and deterministic elements, hence broadening the scope and providing a more nuanced understanding of soil behavior under seismic loading. The methodology also stands out because it accounts for the influence of soil type, particularly the fines content, which was often overlooked or inadequately considered in earlier methods. Their research provided an enhanced method for estimating the CRR based on CPT data. The CRR is a crucial parameter in evaluating the potential for soil liquefaction, as it represents the soil's resistance to cyclic loading. In their study, the team developed a model that accounted for the inherent uncertainty in the liquefaction process. They generated a new CPT-based correlation for evaluating CRR, taking the penetration resistance, depth, and soil type into consideration. The probabilistic nature of the method also helped to provide a more risk-informed assessment of liquefaction potential, which is vital for decision-making in civil engineering projects. Figure 3 shows a comparison of the CRR triggering curves of the three adopted CPT relationships. However, it should be noted that a direct comparison of these methods based on CRR-triggering relationships can be deceiving since each uses several factors that influence the result.

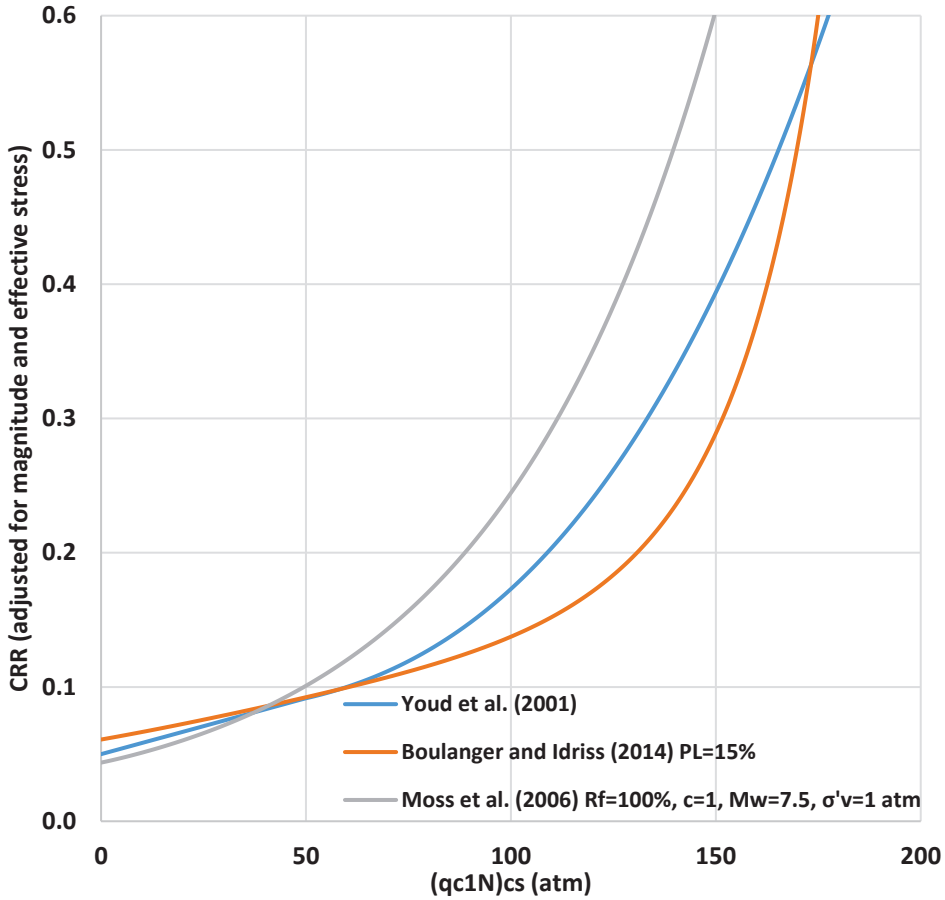

Figure 3. Comparison of CPT CRR Triggering Curves for Liquefaction from Robertson and Wride (1998)/Youd et al. (2001), Moss et al. (2006), and Boulanger and Idriss (2014)

V_S LIQUEFACTION TRIGGERING RELATIONSHIPS

Shear wave velocity (V_s) is a fundamental geotechnical parameter that characterizes the stiffness and strength of the soil. It represents the velocity at which shear waves propagate through a medium. Research has shown that the V_s is related to the resistance of granular soils against liquefaction. The V_s-based liquefaction triggering procedure utilizes this relationship to assess the liquefaction potential of soils. Over the years, numerous studies have contributed to the development of the V_s-based liquefaction triggering procedure. One significant advancement is the establishment of empirical correlations between V_s and liquefaction susceptibility. These correlations allow engineers to estimate the liquefaction potential based on readily available V_s data. Furthermore, researchers have explored the incorporation of other geotechnical parameters, such as the fines content and soil density in

conjunction with V_s to improve the accuracy of liquefaction assessments. This multi-parameter approach provides a more comprehensive understanding of soil behavior during seismic events.

Andrus and Stokoe (2000) developed liquefaction resistance criteria from field measurement of V_s and aimed to develop a simplified and practical method for assessing liquefaction potential using readily available V_s data. Andrus and Stokoe (1997) developed a CRR-V_{s1} curve for uncemented Holocene-age soils with 5% or less fines using field performance data from 20 earthquakes and over 50 measurement sites. Andrus and Stokoe (2000) revised this curve based on the latest information and an extended database that includes 26 earthquakes and more than 70 measurement sites. The database included information on ground motions, soil properties, and observed liquefaction occurrences. Based on their analysis, the researchers established a relationship between the normalized V_s ($V_s/V_{s,1}$) and the CSR required for liquefaction initiation. This model allowed engineers and geotechnical practitioners to estimate the liquefaction resistance of a soil deposit using only the V_s value and a few additional parameters. These charts assisted in quantifying the likelihood of liquefaction occurrence for different soil deposits.

In their research, Kayen et al. (2013) aimed to develop a comprehensive and reliable method for evaluating the liquefaction potential of soils using V_s measurements. They utilized a large dataset consisting of 440 liquefaction case histories from around the world to develop their methodology. The study employed both probabilistic and deterministic approaches to assess liquefaction potential. The probabilistic approach involved statistical analyses of the liquefaction database, including the computation of liquefaction probability curves. These curves provided a means to estimate the likelihood of liquefaction occurrence at various levels of CSR for a given V_s value. Kayen et al. (2013) proposed a simple empirical relationship between CRR and V_s, considering factors such as relative density and earthquake magnitude. Kayen et al. (2013) also considered the variability and uncertainties associated with liquefaction assessments. They used Bayesian and structural reliability methods to estimate the PL to refine the assessment and improve its accuracy.

V_s-based liquefaction triggering procedures have evolved significantly, offering improved predictions of soil liquefaction potential. While SPT and CPT-based methods have traditionally been employed, the development of empirical relationships and the utilization of advanced laboratory testing and geophysical techniques have contributed to more accurate assessments. However, it is important to continue refining and validating these procedures using extensive field case studies and considering site-specific factors to ensure reliable predictions. Further research and advancements in technology are

necessary to enhance our understanding of V_s and its role in assessing liquefaction hazards. Figure 4 shows a comparison of the CRR triggering curves of the two adopted V_s relationships. However, it should be noted that a direct comparison of these methods based on CRR-triggering relationships can be deceiving since each uses several factors that influence the result.

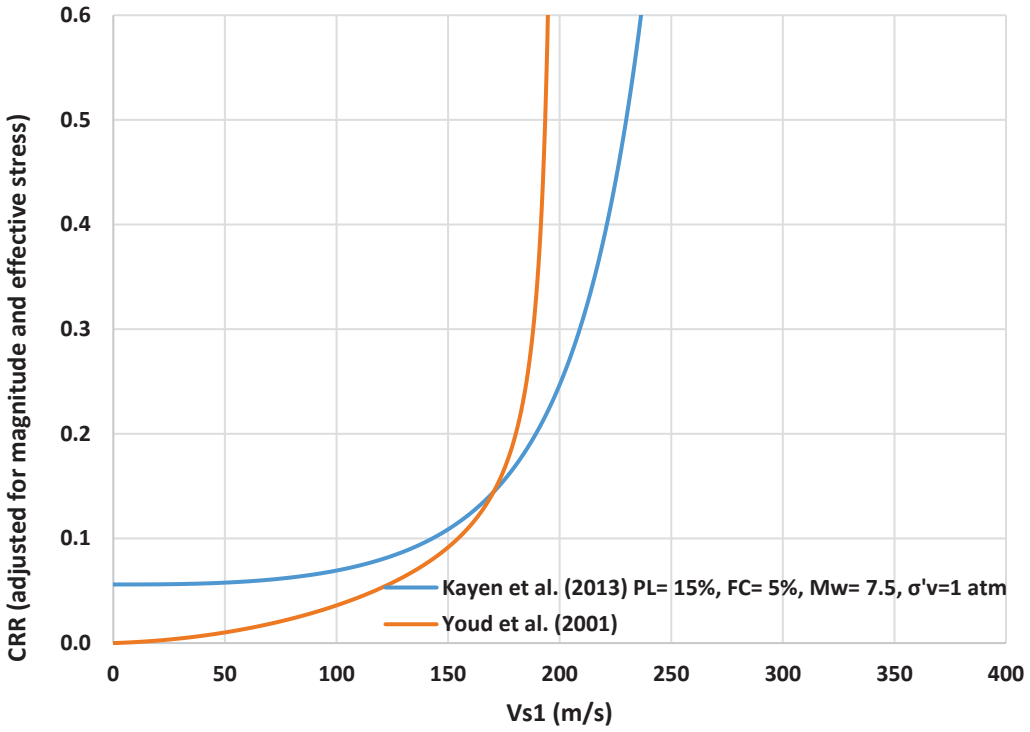

Figure 4. Comparison of V_s CRR Triggering Curves for Liquefaction from Andrus and Stokoe (2000)/Youd et al. (2001) and Kayen et al. (2013)

EMPIRICAL AND SEMI-EMPIRICAL METHODS FOR EVALUATING LIQUEFACTION CONSEQUENCES

The LPI is a probabilistic parameter used in the field of geotechnical engineering to estimate the likelihood of soil liquefaction manifestation due to seismic activity. It is an important topic of study due to the damage that liquefaction can cause in an earthquake, including structural damage and increased landslide risk. The LPI is a simplified yet robust method for assessing the liquefaction manifestation due to seismic activity.

The LPI concept was proposed by Iwasaki et al. (1978) as a practical means to assess the potential for soil liquefaction during an earthquake. The index was based on three main parameters: the depth of the

soil layer susceptible to liquefaction, its relative density, and the magnitude of the seismic loading. The authors developed the index based on observations and field data from previous earthquakes. LPIs less than 5 suggest none to minor liquefaction manifestation, while large LPIs (above 15) imply severe liquefaction manifestation is anticipated. Over the years, Iwasaki and others conducted various field studies to validate and refine the LPI method, which has been applied and validated in numerous field studies around the world. Iwasaki et al. (1982) assessed the LPI with several historical earthquakes and found a good correlation between predicted and observed liquefaction, further establishing the credibility and effectiveness of the index. Maurer et al. (2015) used the Ishihara (1985) boundary curves for surficial liquefaction manifestation to derive an alternative index for assessing liquefaction hazard, LPI_{ISH}. The boundary curves were developed using a power-law depth weighting function that may be more appropriate than the existing linear form. The comparison of adopted depth weighting functions for Iwasaki et al. (1978) and Maurer et al. (2015) is shown in Figure 5.

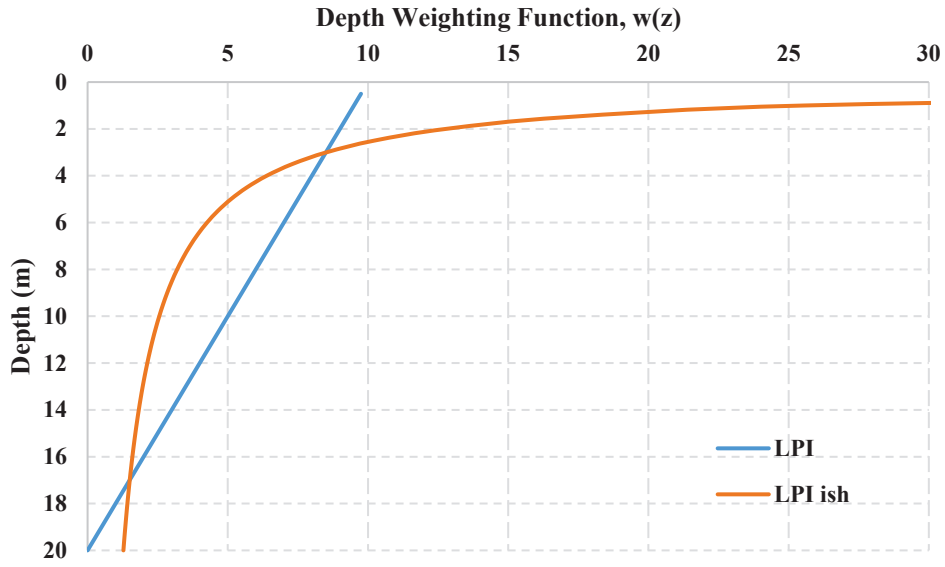

Figure 5. A Comparison of Adopted Depth Weighting Functions for Iwasaki et al. (1978) and Maurer et al. (2015)

Zhou and Chen (2007) made some modifications to the LPI for it to be more accurate. The modifications also discuss its application in creating zoning maps for sand deposits, a critical aspect of pre-construction

geological surveys and earthquake preparedness. Juang et al. (2014) proposed a simplified method to calculate LPI using logistic regression analysis, a more straightforward version and has a more solid statistical basis than the previous ones. Similar estimates of liquefaction severity are provided by other techniques, such as the liquefaction severity number (LSN) (van Ballegooy et al. 2012). Liquefaction-induced settlement estimations can help evaluate the effects of liquefaction in addition to manifestation severity indexes. Simple estimates of computed volumetric stresses are offered by techniques such as those described by Zhang et al. (2002) or Cetin et al. (2009) to predict total settlements for a certain site.

CHAPTER 3: METHODOLOGY AND STUDY AREA

LIQUEFACTION TRIGGERING WORKBOOK REVIEW GUIDE

SPT, CPT, and V_s-based liquefaction triggering procedures have been programmed in three different Microsoft Excel workbooks. This chapter aims to give instructions on using these workbooks to conduct a liquefaction susceptibility analysis. This user's manual should be used as a complement to the worksheet cells' comments because it is not comprehensive. Reading the material while looking at the worksheet in question will make it more comprehensible.

Each worksheet is intended to be used with English units. The user must convert any metric units (except V_s spreadsheet) provided on the boring log or data files to English units before entering them into the workbook. The purpose of this user manual is to guide the use of these workbooks to perform a liquefaction susceptibility evaluation. An item of note is that users must enable iterative calculation within the excel options menu for the spreadsheet to operate correctly.

SPT-based Workbook Review

The three most popular liquefaction triggering procedures (Youd et al. 2001; Cetin et al. 2018; Boulanger and Idriss 2014) have been programmed in Microsoft Excel workbooks. The different tabs of this Excel workbook are divided and color-coded for better understanding. The "Input data tab", which the user will use to input data for analysis, is a green color. The "Comparisons" and "Liquefaction manifestation" tabs are red and show the results of the three liquefaction triggering procedures used in this Excel workbook.

The calculation tab and the supplementary tabs for Youd et al. (2001), Cetin et al. (2018), and Idriss and Boulanger (2014) are yellow, blue, and orange, respectively. The user can also view the references used in this Excel workbook in the last tab titled "References". These tabs are shown in Figure 6. The three calculation tabs for Youd, Cetin, and Idriss and Boulanger are as identical as feasible to make data entry and sharing of information amongst workbooks simpler. A thorough discussion about the Youd et al. (2001) workbook will be examined following a brief section highlighting the commonalities between the workbooks. The workbooks from Cetin et al. (2018) and Idriss and Boulanger (2014) will be thoroughly examined after the discussion of Youd et al. (2001). The discussion of the Cetin et al. (2018) and Idriss and Boulanger (2014) sheets will concentrate on the areas that differ from the workbook by Youd et al.

(2001) as many of the computations are identical to Youd et al. (2001). Discussing the overall style and format of the workbook before starting each section is prudent.

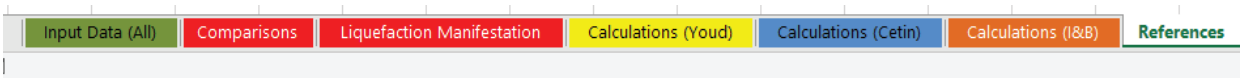

Figure 6. Individual Worksheet Tabs Within the SPT-based Liquefaction Triggering Workbook

Input Data

The Input Data tab in the workbook is where all site-specific data will be manually added to the workbook. An image of the general input information for the Input tab is provided in Figure 7. Most of the input data required for the evaluation of soil liquefaction triggering will come from the boring logs collected during the site investigation and subsequent laboratory testing. The project data should only be updated in the cells marked in light green. No other cells should be changed in this workbook. Rows E5 to E15, the first set of input fields, are located at the top of the Input Data worksheet and are used to identify jobs by their job number, name, location (latitude and longitude), date of boring, drilling equipment, type of drilling, hammer energy, etc. Most of these cells are simply used for documentation. However, the hammer energy correction factor is utilized to convert the observed SPT blow count (N) to the standardized N60 value. The hammer energy ratio (in percent) divided by the typical energy ratio of 60% is the hammer energy correction factor (C_E). There are two uses for the boxes labeled “Data Input by” and “Checked by” in cells L6 and L7. The user can enter Initials manually after the input and output pages have been printed, or they can be typed into the boxes and transferred to the output worksheets. The month, day, and year are separated by a backslash in the numerical format of the “Date” field in cells N6 and N7.

The remaining input cells E17–E23 are used to estimate N_{60} and $(N_1)_{60}$. The design peak horizontal ground acceleration (a_{max} or A_s), earthquake moment magnitude (Mw), boring surface elevation, ground water level (depth below boring surface), sampler type, liner used, and borehole diameter are all cells in this group. Below, each of these topics is covered in further detail.

Job No:	100651 - Cockle Burr Slough		
Job Name:	Monette Bypass		
Station:	616	+	40
Location:	8.0 ft left of Centerline of Construction		
Latitude and Longitude (decimal degrees)	35.89	-90.324	
Logged By :	0		
Boring No:	3		
Date:	41029		
Type of Drilling:	Rotary Wash		
Equipment:	CME 750 w/CME Automatic Hammer		
Hammer Energy Correction Factor:	1.28		

Design Peak Horizontal Ground Acceleration (a_{max}, or A_s) =	0.611	g's
Earthquake Moment Magnitude (M_w) =	7	
Boring Surface Elevation =	237.6	ft
Ground Water Level (depth below boring surface) =	0	ft
Sampler Type: Liner Space [Yes], or No Liner Space [No] =	yes	
Liner Used [Yes], or no Liner Used [No]=	no	
Borehole Diameter =	4	in

Data Input by: Date:

Checked by: Date:

All cells highlighted in this color should be input

All other cells should not be altered!

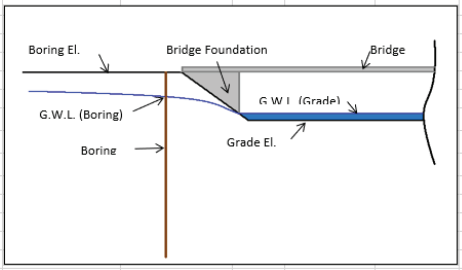

Figure 7. "Input Data (All)" Tab of the SPT-based Worksheet with Job Identification Information and Site-specific Input Options

Design Peak Ground Acceleration and Moment Magnitude

The design peak horizontal ground acceleration and the earthquake moment magnitude must be provided in the Input Data worksheet. External resources, like building regulations and the website of the US Geological Survey, must be used to determine these values (www.usgs.gov). Procedures advised by the relevant regulatory body/building code often regulate the choice of design peak horizontal ground acceleration. The processes should have clauses for obtaining ground motions on "rock" for a specific return period or yearly rate of exceedance, regardless of the code utilized. The code should offer recommendations for adjusting to site-specific soil conditions after collecting the "rock" ground motions. The simplified processes utilized to estimate local site characteristics are often the same for all US codes, even though the chosen exceedance rate varies between codes. Only the AASHTO-recommended practices will be included in this manual as it is primarily intended for individuals involved in bridge design. The peak horizontal ground acceleration corrected for site classification (A_s or a_{max}) is determined based on USGS ground motion maps and the AASHTO code or through a site-specific seismic hazard analysis. The user must be familiar with the latitude and longitude of the bridge's location as well as the seismic site classification based on Table 3.4.2.1-1 of the AASHTO Guide specifications for LRFD seismic bridge design (2nd ed.) to determine this value (reproduced below as Table 1).

Table 1. Site Class definitions reproduced from AASHTO Guide specifications for LRFD seismic bridge design (2nd Edition)

Site Class	Soil Type and Profile
A	Hard rock with measured shear wave velocity, $\overline{v}_s > 5000$ ft/sec
B	Rock with 2500 ft/sec $< \overline{v}_s < 5000$ ft/sec
C	Very dense soil and soil rock with 1200 ft/sec $< \overline{v}_s < 2500$ ft/sec, or with either $\overline{N} > 50$ blows/ft or $\overline{s}_u > 2.0$ ksf
D	Stiff soil with 600 ft/sec $< \overline{v}_s < 1200$ ft/sec, or with either 15 blows/ft $< \overline{N} < 50$ blows/ft or 1.0 ksf $< \overline{s}_u < 2.0$ ksf
E	Soil profile with $\overline{v}_s < 600$ ft/sec, or with either $\overline{N} < 15$ blows/ft or $\overline{s}_u < 1.0$ ksf, or any profile with more than 10 ft of soft clay defined as soil with $PI > 20$, $w > 40\%$, and $\overline{s}_u < 0.5$ ksf
F	Soils requiring site-specific ground motion response evaluations, such as: • Peats or highly organic clays ($H > 10$ ft of peat or highly organic clay, where H = thickness of soil) • Very high plasticity clays ($H > 25$ ft with $PI > 75$) • Very thick soft/medium stiff clays ($H > 120$ ft)

Using the raw SPT blow count (N) numbers from the boring log, the worksheets can automatically compute the seismic site classification based on the average N values over the top 100 ft for Site Classes C, D, and E. However, using the standards listed in Table 1, the user must precisely determine whether the site falls within Site Class E or F. The seismic site classification will be computed and shown in the Calculations and Output Boring El tabs. Each worksheet has a sizable yellow box toward the top that contains the estimated seismic site classification. The boring must be finished to a depth of at least 95 ft below the boring surface elevation for the workbook to calculate the site classification. If the boring is stopped at a depth of less than 95 ft, the site cannot be automatically classified using the worksheet; instead, the user must provide additional judgment to make the seismic site classification. Alternatively, the seismic site classification can be determined using shear wave velocity.

Once the seismic site classification has been determined, A_s/a_{max} can be obtained from the USGS probabilistic ground motion hazard maps. The site can be accessed directly using Seismic Design Web Service Documentation (usgs.gov) in the search bar. Then the user needs to scroll down and click 2009 AASHTO Guide Specifications (AASHTO-2009). It will direct the user to the AASHTO- 2009 web service documentation page. The user must scroll to “Example” and click on the “Request” link, which will take you to a different page. On that page, in the address bar, the user needs to change latitude and longitude to those of interest; change site class to that of interest (A, B, C, D, or E); and finally change the example to a suitable title of the user’s interest. An example of the address bar is shown

(https://earthquake.usgs.gov/ws/designmaps/aashto-2009.json? latitude=35.89&longitude=-90.324&siteClass=D&title=Monette). After that, the user needs to press Enter, and the results for the requested parameter will appear. The horizontal peak ground acceleration (PGA) will be visible in the response section. A sample of the requested output is shown in Figure 8.

Figure 8. Design Horizontal PGA from 2009 AASHTO Guide Specifications

The USGS Unified Hazard Tool can be used to determine the design earthquake moment magnitude using deaggregation, which provides both the magnitude and distance for site-specific locations. The user needs to search for the "USGS Unified Hazard Tool" in a search engine or go to the following website: https://earthquake.usgs.gov/hazards/interactive/index.php. At the Input tab, the user needs to select the edition corresponding to the year of the AASHTO code. The user needs to select the **Dynamic** edition for deaggregation. The 2008 version is still the most up-to-date version for AASHTO at the time of this report. However, this is expected to change in the near future along with a change to the USGS new Hazard toolbox (https://earthquake.usgs.gov/nshmp/) due to the update to the AASHTO code. In this new hazard toolbox, the process is referred to as disaggregation. The process is similar in application. After that, the user needs to enter the latitude and longitude of the site location. Site Class B/C should be selected for Rock conditions regardless of the site class determined previously. For a spectral period, the user needs to select PGA and 5% in a 50-year return period, or enter 975 years, corresponding to the AASHTO 7% probability of exceedance in 75 years. After all inputs have been selected, the user needs to scroll down to the **Deaggregation** tab and select the "**Compute**

Deaggregation" button. When the website has finished loading the deaggregation results, record the distances and magnitudes for the Mean and Mode values. Typically, the Mode magnitude is used for the liquefaction evaluations. Example deaggregation results are presented in Figure 9.

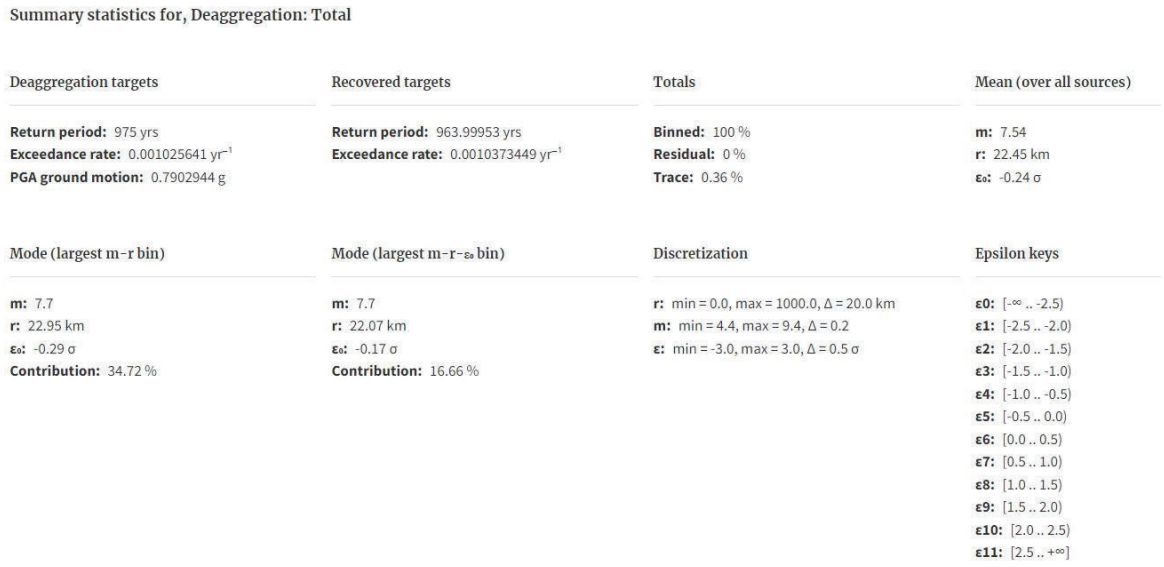

Summary statistics for, Deaggregation: Total

Deaggregation targets	Recovered targets	Totals	Mean (over all sources)
Return period: 975 yrs	**Return period:** 963.99953 yrs	**Binned:** 100 %	**m:** 7.54
Exceedance rate: 0.001025641 yr^{-1}	**Exceedance rate:** 0.0010373449 yr^{-1}	**Residual:** 0 %	**r:** 22.45 km
PGA ground motion: 0.7902944 g		**Trace:** 0.36 %	**ε_0:** -0.24 σ

Mode (largest m-r bin)	Mode (largest m-r-ε_0 bin)	Discretization	Epsilon keys
m: 7.7	**m:** 7.7	**r:** min = 0.0, max = 1000.0, Δ = 20.0 km	**ε0:** [-∞ .. -2.5)
r: 22.95 km	**r:** 22.07 km	**m:** min = 4.4, max = 9.4, Δ = 0.2	**ε1:** [-2.5 .. -2.0)
ε_0: -0.29 σ	**ε_0:** -0.17 σ	**ε:** min = -3.0, max = 3.0, Δ = 0.5 σ	**ε2:** [-2.0 .. -1.5)
Contribution: 34.72 %	**Contribution:** 16.66 %		**ε3:** [-1.5 .. -1.0)
			ε4: [-1.0 .. -0.5)
			ε5: [-0.5 .. 0.0)
			ε6: [0.0 .. 0.5)
			ε7: [0.5 .. 1.0)
			ε8: [1.0 .. 1.5)
			ε9: [1.5 .. 2.0)
			ε10: [2.0 .. 2.5)
			ε11: [2.5 .. +∞]

Figure 9. Determination of Moment Magnitude Using the USGS Unified Hazard Tool

Sampler Type and Borehole Diameter Correction Factor

The Sampler Type cell must indicate if the sampler has room for liners or not (input Yes or No), and the Liner Used cell must state whether the sampler was used with or without liners (enter Yes or No). ARDOT frequently uses samplers without liners instead of those without liner space. The Sampler Type input cell should be filled in with Yes, and the Liner Used input cell should be filled in with No. The borehole correction factor, which only applies to boreholes greater than 4.53 in (115 mm), is considered when using the Borehole Diameter input cell (4.5 in). The diameter of the borehole should be specified on the boring logs.

Depth-dependent Input Data

All the remaining input data is depth dependent. Figure 10 displays the column headers for columns A through J. The numbers in the first two columns, Sample Number and Elevation at Sample Location,

were computed right in the workbook. These columns should only include information that helps the user keep track of specific sample locations (depths) across the workbook; the user should enter no values into them directly. The remaining data input column headers are covered in more detail below to clarify them. The depth at which each SPT sample was taken below the surface is shown in feet. The distance between SPT sample sites is often fixed, such as 2.5 or 5 ft. This information is provided in the boring logs. User input of the Unified Soil Classification System (USCS) classification is required for each depth. If adequate laboratory tests (such as grain size analysis and Atterberg Limits) have been carried out on the split-spoon samples, this information should be recorded on the boring log. The user should input both symbols for dual classes separated by a dash with no spaces (i.e., SW-SP). If the USCS designation is missing, the user must utilize the basic soil descriptors listed on the boring log to apply a USCS designation for each sample. If no extra information is supplied, the user can assume CL for clays, ML for silts, SP for sands, and GP for gravels, as mentioned in the worksheet's cell remark. To correlate unit weight and establish whether the soil is "cohesive" or "cohesionless", a USCS classification is required. If a USCS designation is not entered, no output information will be accessible.

The boring log contains the raw blow count. To apply additional correction factors, a value of "1" should be entered if the recorded value is "0" (i.e., the weight of the rod). Since liquefaction susceptibility has been demonstrated to rely on fines content (FC), split-spoon samples recovered during testing should, if possible, be used to quantify FC. Leave the cell empty if the FC has not been measured, and a conservative value (i.e., an FC of 5%) will be assigned. Leave the cell empty, and a typical value will be provided based on the USCS designation and blow count data if the unit weight has not been tested in the lab (which it seldom is). The correlation provided by Teng (1962) provides the foundation for the unit weight correlation. It is presented in the Calculation Tables worksheet and addressed in further sections. Plastic Limit, Liquid Limit, and In-situ Water Content assist in establishing the fine-grained liquefaction susceptibility of the soil based on the Bray and Sancio (2006) criteria. The V_s column is required to calculate the average shear wave velocity over 40 ft. The workbook can calculate this column using a correlation. The undrained shear strength of the soil, S_U column, is used to calculate the undrained shear strength for the cohesive layers. Leave these cells empty if this information has not been established or the soil is not plastic.

		Must Enter: Depth, USCS Classification (estimate if unknown), Fines content, Unit weight and N value									
Sample Number	Elevation at Sample Location (ft)	Depth to Sample Location (ft)	USCS Classification	Raw SPT Blow Count, N	Fines Content (%)	Measured Unit Weight of Soil (pcf)	Shear Wave Velocity, V_S	Plastic Limit, PL	Liquid Limit, LL	In-Situ Water Content, w_c	Undrained Shear Strength of the Soil, Su (psf)

Figure 10. Headings for Depth-dependent Parameters in the "Input Data (All)" Tab of the SPT-based Worksheet

Calculations Worksheet (Youd et al. [2001])

The worksheets for calculations and calculation tables provide the framework of the whole workbook. Data is copied into the different output worksheets and moved from the Input Data worksheet into these worksheets. Unless a calculation error is discovered, these workbooks should not be altered. These workbooks will not have to be examined during typical evaluations if the user is familiar with liquefaction calculations. The user will be given a review of each of the columns so they can comprehend how these worksheets compute and use data. Additionally, many of the column titles in the workbooks have cell comments describing the purpose of the respective column.

The user will notice that most input into the Input Data worksheet has been copied to the Calculations worksheet when viewing it for the first time (Figure 6). The Calculations worksheet cannot be edited or have data entered again. To avoid this error, the cells are locked. In the cells E23–E29, right below the input data, several common blow count correction parameters that are not depth-dependent—such as hammer energy, borehole diameter, and sampler liner—are provided (Table 2). In this block of cells, the magnitude scaling factor (MSF) is also provided. To make it simple for the user to track the worksheet's evolution, the cells provide references to the precise formulae and tables from the Youd et al. (2001) paper used to get these factors. It should be noted that cell E29 was initially designated as the location for the sloping ground correction factor (K_α). However, due to the lack of agreement on handling static driving shear stresses in soil liquefaction triggering, this function was eliminated from the workbook. The cell is filled with "NA" to alert the user that this workbook does not consider the correction factor for sloping terrain.

The large yellow boxes represent the seismic site classification previously mentioned in Section 3 in Figure 11. The soil boring log must go at least 95 ft below grade elevation for the grade elevation site

classification to be calculated automatically. Below is more information about the calculations used to produce these site categories.

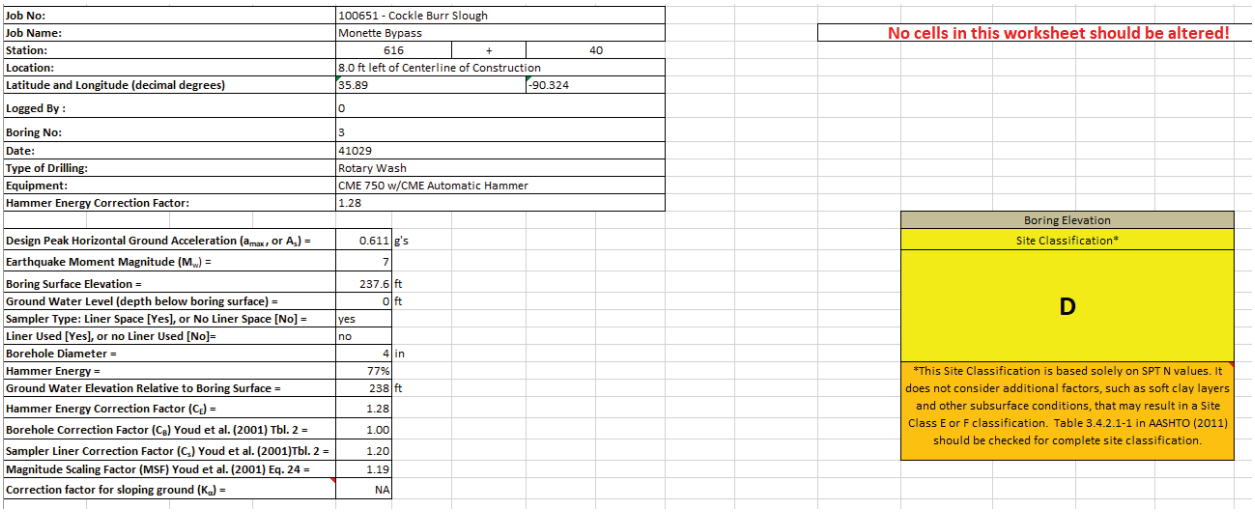

Job No:	100651 - Cockle Burr Slough		
Job Name:	Monette Bypass		
Station:	616	+	40
Location:	8.0 ft left of Centerline of Construction		
Latitude and Longitude (decimal degrees)	35.89	-90.324	
Logged By :	0		
Boring No:	3		
Date:	41029		
Type of Drilling:	Rotary Wash		
Equipment:	CME 750 w/CME Automatic Hammer		
Hammer Energy Correction Factor:	1.28		

No cells in this worksheet should be altered!

Design Peak Horizontal Ground Acceleration (a_{max}, or A_s) =	0.611	g's
Earthquake Moment Magnitude (M_w) =	7	
Boring Surface Elevation =	237.6	ft
Ground Water Level (depth below boring surface) =	0	ft
Sampler Type: Liner Space [Yes], or No Liner Space [No] =	yes	
Liner Used [Yes], or no Liner Used [No]=	no	
Borehole Diameter =	4	in
Hammer Energy =	77%	
Ground Water Elevation Relative to Boring Surface =	238	ft
Hammer Energy Correction Factor (C_E) =	1.28	
Borehole Correction Factor (C_B) Youd et al. (2001) Tbl. 2 =	1.00	
Sampler Liner Correction Factor (C_s) Youd et al. (2001)Tbl. 2 =	1.20	
Magnitude Scaling Factor (MSF) Youd et al. (2001) Eq. 24 =	1.19	
Correction factor for sloping ground (K_α) =	NA	

Boring Elevation
Site Classification*
D

*This Site Classification is based solely on SPT N values. It does not consider additional factors, such as soft clay layers and other subsurface conditions, that may result in a Site Class E or F classification. Table 3.4.2.1-1 in AASHTO (2011) should be checked for complete site classification.

Figure 11. "Calculations (Youd)" Tab of the SPT-based Worksheet with Job Identification and Site Classification

Depth-dependent Calculations

The remaining calculations are connected to a specific SPT sample site and are all depth dependent. The user will observe that there are many more filled-in columns in the Calculations worksheet than in the Input Data worksheet (i.e., from column K through column AR). The headings in the Calculations worksheet will be examined here in the same order that they are displayed in the worksheet for the sake of clarity. Details on the column's purpose will follow each column title. The user is informed that additional helpful comments may be included in the worksheet's cells. Red triangles in the cell's top-right-hand corner denote these remarks. The user may readily follow the worksheet development since, if possible, the equations from the Youd et al. (2001) paper used to program for the computations are referenced in the column titles. To avoid repetition, the column heads taken directly from the Data worksheet will not be covered again. In addition, several of the calculation column headers have been combined for discussion. Below is a discussion of the calculations made in columns K through R. These column headers are shown in Figure 12 for reference.

Boring Elevation Calculation Table.							
			Site Classification				
General Soil Type	Plasticity Index, PI	w_c/LL	Thickness (ft)	d_i/N_i for Site Classification	Cumulative d_i/N_i for Site Classification	Drill Rod Length with 5' stickup (ft)	Rod Length Correction Factor, C_R Youd et al. (2001) Tbl 2

Figure 12**. Column Headers from Column K to Column R in the "Calculations (Youd)" Tab of the SPT-Based Worksheet**

General Soil Type (Column K): To identify whether a soil sample is often "cohesive" or "cohesionless", this column employs a LOOKUP function based on the USCS soil classification. The Calculation Tables worksheet contains a table named General Soil Classification based on USCS that was utilized to generate this decision.

Plasticity Index, PI (Column L): The plasticity index (PI) of the soil is calculated in this column using the plastic limit (PL) and liquid limit (LL) values entered in the Input Data worksheet. The column will provide a "cohesive" or "cohesionless" classification based on the General Soil Type if the required index tests have not been carried out.

wc/LL (Column M): If these values were given in the Input Data worksheet, this column divides the water content (wc) by the liquid limit (LL). This ratio can be used to estimate how susceptible fine-grained soils are to liquefaction. This column automatically returns a generic "cohesive" or "cohesionless" label if the required laboratory tests are not done.

Thickness (Column N): The layer thickness is determined by this column. The layer thicknesses are essential for identifying the stresses in the soil profile and the seismic site categorization.

di /Ni and Cumulative di /Ni for site classification (Column O and Column P): These two columns are utilized to compute the individual and total layer thickness values divided by blow count for seismic site classification using SPT blow count. The AASHTO Guide specifications for LRFD seismic bridge design (2nd ed.) Method B of section 3.4.2 Using a LOOKUP command in the Calculation Tables worksheet's Site Classification Based on SPT N Values in the Top 100 ft table, the actual site classification is determined

from these calculations. As mentioned, the big yellow boxes at the top of the worksheet show the final site categorization.

Drill Rod Length with 5' stickup and Rod Length Correction Factor (C_R) (Column Q and Column R): The Drill Rod Length column determines the drill rod's overall length by assuming that it protrudes 5 ft above the ground. The Drill Rod Length, Correction Factor column uses the drill rod length to look up C_R from the Drill Rod Length Correction Factor table in the Calculation Tables worksheet. Table 2 presents the corrections to SPT adopted by Youd et al. (2001).

Table 2. The SPT Blow Count Correction Factors adopted from Youd et al. (2001).

Factor	Equipment variable	Term	Correction
Overburden pressure	—	C_N	$(P_a/\sigma'_{vo})^{0.5}$
Overburden pressure	—	C_N	$C_N \leq 1.7$
Energy ratio	Donut hammer	C_E	0.5–1.0
Energy ratio	Safety hammer	C_E	0.7–1.2
Energy ratio	Automatic-trip Donut-type hammer	C_E	0.8–1.3
Borehole diameter	65–115 mm	C_B	1.0
Borehole diameter	150 mm	C_B	1.05
Borehole diameter	200 mm	C_B	1.15
Rod length	<3 m	C_R	0.75
Rod length	3–4 m	C_R	0.8
Rod length	4–6 m	C_R	0.85
Rod length	6–10 m	C_R	0.95
Rod length	10–30 m	C_R	1.0
Sampling method	Standard sampler	C_S	1.0
Sampling method	Sampler without liners	C_S	1.1–1.3

The calculations performed in column S to column AA are discussed below. For reference purposes, these column headings are presented in Figure 13.

Boring Elevation Calculation Table.								
		In-Situ Stresses						
N_{60} Only Corrected for Energy	Total Unit Weight of the Soil (pcf)	Total Stress in Each Layer (psf)	Actual Total Stress, σ_{vo} (psf)	Pore Water Pressure (psf)	Effective Stress, σ'_{vo} (psf)	Stress Correction Factor, C_N Youd et al. (2001) Eq. 10	Sampler Liner Correction Factor (Cs) Youd et al. (2001) Tbl. 2	$(N_1)_{60}$ Youd et al. (2001) Eq. 8

Figure 13. Column Headers from Column S to Column AA in the "Calculations (Youd)" tab of the SPT-based Worksheet

N_{60} Only Corrected for Energy (Column S): This column calculates the blow count with the hammer efficiency set at 60%. This column is solely used to correlate the unit weight of the soil.

Total Unit Weight of the Soil (Column T): This column uses the LOOKUP function to apply the correlation described in Teng (1962) to the N Value-Unit Weight Correlation table, in the Calculation Tables workbook, to estimate the soil unit weight. The correlation is based on the common soil type and the energy-adjusted blow count (N_{60}). N rather than N_{60} was used in the initial publication of this correlation. However, it was presumed in this article that most hammers at the time were about 60% efficient. Therefore, N_{60} is utilized in the worksheet to correlate unit weight instead of N to estimate unit weight. This correlation will be overridden if the unit weight has been measured and included in the Input Data worksheet.

In-Situ Stresses (Column U to Column X): The elevation values, unit weight, and thickness are used in a four-column series of computations to determine the total, pore water, and effective stresses at each depth. The soil layer's total unit weight is assumed to stay constant throughout the computation of total stress. This assumption is plausible as long as the sample intervals are kept to a minimum.

Stress Correction Factor (C_N) (Column Y): The effective stresses are used to produce the standardized overburden blow count correction factor. The adjusted blow count, as a function of depth, is strongly controlled by C_N. Considering this, the remaining portions of this section concentrate on the numerous C_N correlations. Both the C_N correlations provided by Liao and Whitman (1986) and Kayen et al. (1992) are suggested by Youd et al. (2001). The correlation suggested by Kayen et al. (1992) over Liao and Whitman (1986) is used in the Youd et al. (2001) worksheet that goes with this report because, as stated by Youd et al. (2001), "in these writers' opinion, [Kayen et al. (1992)] provides a better fit to the original

curve specified by Seed and Idriss (1982)". This correlation is presented below in Equation 1, where effective stress is defined previously, and a 1.0 atmospheric pressure (P_a) of 2116 psf is used. This equation limits the maximum C_N value to 1.7.

$$C_N = 2.2/\ (1.2+\sigma'_v/P_a) \qquad \text{(Equation 1)}$$

Sampler Liner Correction Factor, C_S (Column Z): This column calculates the sampler liner correction factor using the table presented in Table 2. If the SPT sampler is used without the liners, the spreadsheet will use an average value of 1.1-1.3, which is 1.2.

$(N_1)_{60}$ (Column AA): All the blow count correction factors (C_N, C_R, C_B, C_E, C_S) are multiplied by the raw blow count (N) to determine the corrected blow count $[N_1)_{60}]$ and rounded to the nearest whole number.

The calculations performed in columns AB–AG are discussed below. For reference purposes, these column headings are presented in Figure 14.

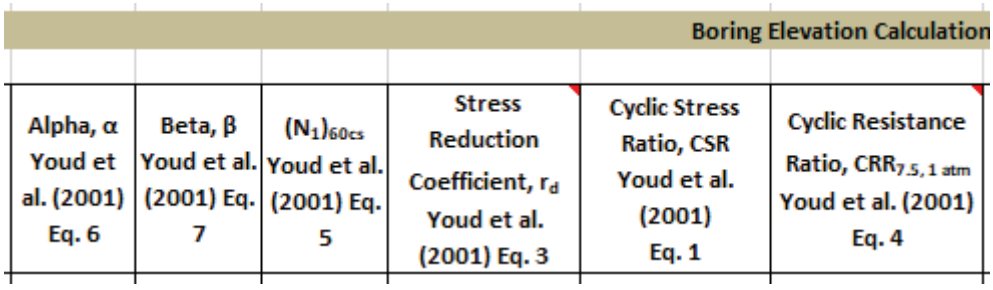

Figure 14. Column Headers from Column AB to Column AG in the "Calculations (Youd)" Tab of the SPT-based Worksheet

Alpha (α) (Column AB): Alpha is calculated based on the fines content information provided in the Input Data worksheet and the formulas detailed in Youd et al. (2001). If fines content has not been input, alpha is conservatively assumed equal to zero. The formulae used to calculate α are shown in Equations 2a to 2c.

$$\alpha = 0; \text{ for FC} \leq 5\% \qquad \text{(Equation 2a)}$$

$$\alpha = \exp\,[1.76 - (190/FC2)];\ \text{for } 5\% < FC < 35\% \qquad \text{(Equation 2b)}$$

$$\alpha = 5;\ \text{for } FC \geq 35\% \qquad \text{(Equation 2c)}$$

Beta (β) (Column AC): Beta is calculated based on the fines content information provided in the Input Data worksheet and the formulas detailed in Youd et al. (2001). If fines content has not been input, beta is conservatively assumed equal to one. The formulae used to calculate α are shown in Equation 3a to Equation 3c.

$$\beta = 1;\ \text{for } FC \leq 5\% \qquad \text{(Equation 3a)}$$

$$\beta = [0.99 + (FC^{1.5}/1000)];\ \text{for } 5\% < FC < 35\% \qquad \text{(Equation 3b)}$$

$$\beta = 5;\ \text{for } FC \geq 35\% \qquad \text{(Equation 3c)}$$

$(N_1)_{60,cs}$ (Column AD): This column utilizes alpha and beta to calculate an equivalent clean sand blow count [$(N_1)_{60,cs}$]. This clean sand equivalent blow count is used to calculate the CRR of the soil. Equation 4 from Youd et al. (2001) used to calculate $(N_1)_{60,\,cs}$ is presented below.

$$(N_1)_{60,cs} = \alpha + \beta^{*}\,(N_1)_{60} \qquad \text{(Equation 4)}$$

Stress Reduction Coefficient (r_d) (Column AE): This column uses a LOOKUP function to determine r_d. The stress reduction coefficient is calculated in the Calculation Tables worksheet within the Stress Reduction Coefficient table. The comment in this column heading is from the r_d figure in Youd et al. (2001), reminding the user that the simplified procedure is not verified with case history data for depths greater than 50 ft. The user will note that a significant scatter exists in various r_d relationships and increases with depth. Youd et al. (2001) adopted the recommendation by Seed and Idriss (1971) for use in determining rd. The use of Equation 5 below a depth of approximately 15 m (50 ft) is not recommended by Youd et al. (2001) because, as stated therein, "evaluation of liquefaction at these greater depths is beyond the depths where the simplified procedure is verified and where routine applications should be applied".

$$r_d = \frac{(1 - 0.4113z^{0.5} + 0.04052z + 0.001753z^{1.5})}{(1 - 0.4177z^{0.5} + 0.05729z - 0.006205z^{1.5} - 0.001210z^{2})} \qquad \text{(Equation 5)}$$

Cyclic Stress Ratio (CSR) (Column AF): This column calculates the cyclic stress ratio imparted by the earthquake, and the same formula is used for all the simplified procedures (Equation 6).

$$CSR = 0.65(a_{max}/g)(\sigma_{vo}/\sigma'_{vo})r_d \qquad \text{(Equation 6)}$$

Cyclic Resistance Ratio ($CRR_{7.5,\ 1\ atm}$) (Column AG): Each technique requires a different computation. According to Youd et al. (2001), CRR7.5 is computed in this workbook using $(N_1)_{60cs}$. If the $(N_1)_{60cs}$ value is greater than 30 blows/ft, the soil is defined as non-liquefiable according to the Youd et al. (2001) approach. Therefore, a high CRR of 2.0 is assigned. The CRR 2.0 assignment renders the FS computation meaningless. This is considered by giving a value of 2.0 to both the preliminary and final factor of safety (Equation 7).

$$CRR_{M=7.5,\ \sigma'_v\ =1\ atm} = \frac{1}{34-(N1)60} + \left(\frac{(N1)60}{135}\right) - \frac{50}{(10*(N1)60+45)^2} + \frac{1}{200} \qquad \text{(Equation 7)}$$

The calculations performed in columns AH-AN are discussed below. For reference purposes, these column headings are presented in Figure 15.

Calculation Table.						Borin
		Fine-grained Soil Screening				
Overburden Correction Factor, Kσ Youd et al. (2001) Eq. 31	Preliminary Factor of Safety, F.S. Youd et al. (2001) Eq. 30	Bray & Sancio (2006) PI Criteria	Bray & Sancio (2006) w_c/LL Criteria	Final F.S.	Soil Susceptibility	Liquefaction Occurrance Check

Figure 15. Column Headers from Column AH to Column AN in the "Calculations (Youd)" Tab of the SPT-based Worksheet

Overburden Correction Factor (K_σ) (Column AH): The exponential factor "f", a component of the K_σ equation whose value depends on the soil's density, provides the basis for the computation of K_σ. According to Youd et al. (2001), this f exponent depends on relative density and varies from 0.6 to 0.8. Thus, using Equation 8 shown below, the relative density has been calculated using the adjusted blow count, $(N_1)_{60}$. According to Youd et al. (2001), the maximum and minimum relative densities suitable to the K_σ assessment are 80% and 40%, respectively. About $(N_1)_{60}$ values, these maximum and minimum relative densities correspond to approximately 30 and 7 blows per foot, respectively. The exponential factor "f" can be calculated once relative densities have been linked. Relative densities below or equal to 40% (i.e., blow counts below or equal to 7) are given an "f" value of 0.8. In contrast, relative densities

above or equal to 80% are given an "f" value of 0.6. (i.e., blow counts greater than or equal to 30). Based on the relative density of the soil, intermediate values of f are linearly interpolated.

$$K_\sigma = (\sigma'_{vo} / P_a)^{(f-1)} \qquad \text{(Equation 8)}$$

Preliminary Factor of Safety (F.S.) (Column AI): The factor of safety against soil liquefaction triggering at each depth is provisionally assessed in this column. In this column, the MSF and K_σ factors are applied to the FS. This FS is preliminary since it only considers the SPT blow count when determining if the soil is loose enough to liquefy and ignores the type of soil. To calculate the final FS, cohesive soils must be further assessed using the Bray and Sancio (2006) fine-grained screening criteria. A preliminary FS of 2.0 is automatically assigned to soil strata having a CRR of 2.0. It is considered that soil layers above the water table are non-liquefiable since they are categorized as "Unsat".

Bray and Sancio (2006) PI and wc/LL Criteria (Column AJ and Column AK): These criteria can be evaluated only when the required laboratory tests have been conducted. These columns will only show the designations "cohesive" or "cohesionless" soil if no laboratory testing has been done. The user will next have to assess whether the cohesive soils are possibly liquefiable. According to the Bray and Sancio (2006) criteria, the calculations made in each column will be used to categorize the soil as susceptible (Susceptible), moderately susceptible (Moderately Susceptible), or not susceptible (Not Susceptible) to liquefaction if the appropriate laboratory tests have been completed. The PI and wc/LL requirements must be satisfied for the soil to be classified as susceptible.

Final F.S. (Column AL): The final factor of safety calculates a final "factor of safety" against soil liquefaction triggering using the preliminary factor of safety and the fine-grained screening criteria. The final FS column may be labeled with any of the following designations: (1) a numerical FS between 0.00 and 2.00; (2) "2.00" (assigned to any soil with a preliminary FS 2.00 based on high penetration resistance); (3) "Unsat" (designated for soils above the water table); (4) "Not Susceptible" (designates that the fine-grained soils were screened and found to be not susceptible in previous columns; (5) "Cohesive" (designates that the fine-grained soils have not had the proper screening tests performed and the preliminary factor of safety is less than 1.0). For "cohesive" soils, the user must utilize engineering judgment to assess their vulnerability to liquefaction.

Soil Susceptibility (Column AM): In this column, the following terms are used: (1) "Unsat" indicates that the soil is above the water table. (2) "Cohesionless" means the soil is coarse-grained according to the USCS classification provided (G, S, ML, CL). (3) "Cohesive" means that the soil is fine-grained/plastic

according to the USCS classification provided (CH or MH). (4) "Susceptible" means the fine-grained soil is determined to be susceptible according to the Bray and Sancio (2006) criteria. And (5) "Not Susceptible" means the fine-grained soil is not susceptible according to the Bray and Sancio (2006) criteria.

Liquefaction Occurrence Check (Column AN): The final safety factor is determined in this column. Here, liquefaction is considered unlikely if the factor of safety is more significant than 1.0; otherwise, it is considered likely if the factor of safety is less than 1.0 (meaning liquefaction is expected). It is important to remember that labels like "Unlikely" or "Likely" do not absolve the user of the need to employ technical judgment when variables of safety are close to convergence. Suppose the preliminary FS is less than 1.0, and no laboratory tests have been conducted to rule out liquefaction susceptibility via the fine-grained screening criteria. In that case, the classification of "Cohesive" is carried forward for silts and clays. The term "Unsat" for soil strata above the water table is carried over from the last FS. When specifying the groundwater level in the Input Data worksheet, the user must make sure that worst-case scenarios, such as changing water levels, are considered.

The probabilistic calculations and liquefaction manifestation analysis performed in columns AO–AS are discussed below. For reference purposes, these column headings are presented in Figure 16.

Boring Elevation Calculation Table.				
Probability of Liquefaction, PL	Liquefaction Potential Index, LPI Iwasaki et al. (1978)	Integrated Liquefaction Potential Index, LPI Iwasaki et al. (1978)	Liquefaction Potential Index, LPI_{ISH} Maurer et al. (2015)	Integrated Liquefaction Potential Index, LPI_{ISH} Maurer et al. (2015)

Figure 16. Column Headers from Column AO to Column AS in the "Calculations (Youd)" Tab of the SPT-based Worksheet

Probability of Liquefaction, PL (Column AO): Although no probabilistic equation is stated in Youd et al. (2001), this worksheet uses data to assist in viewing the comparison between the three methods. The following logic is entered based on the liquefaction occurrence check at a certain depth (if "Unsat", then 0; if "Cohesive", then #NA, if "Likely", then 100%, if "Unlikely", then 0%).

Liquefaction Potential Index, LPI (Column AP and Column AQ): The workbook includes the LPI created by Iwasaki et al. in 1978. The LPI offers a depth-weighted estimate of the likelihood of liquefaction

triggering connected with liquefaction surface manifestation. A linear weighting factor compounds the liquefaction safety factors from 0 to 65.6 ft depth (20 m) below the surface in the LPI method (Equation 9). This indicates that layers close to the surface are more likely than deeper layers to manifest at the surface. The computed LPI spans from 0 to 100, with LPIs under 5 showing minimal liquefaction manifestation, those between 5 and 15 showing moderate liquefaction manifestation, and those over 15 showing severe liquefaction manifestation.

$$\text{LPI} = \int_0^{20\ m} F * w(\ )dz \qquad \text{(Equation 9)}$$

Liquefaction Potential Index, LPI_{ISH} (Column AR and Column AS): Additionally included in the workbook is LPI_{ISH}. LPI_{ISH} is a modification of LPI that incorporates the Ishihara (1985) concept of a non-liquefiable crust that is typical of some Arkansas sites that have a thick layer of clay covering a liquefiable sand layer and uses a power-law depth weighting factor as opposed to a linear depth weighting factor used for LPI. The computed LPI ranges from 0 to 100 from the surface to 65.6 ft depth (20 m). LPI_{ISH} under 5 indicates little liquefaction manifestation, those between 5 and 15 indicate moderate liquefaction manifestation, while LPI_{ISH} over 15 indicates severe liquefaction manifestation.

$$\text{LPI}_{\text{ISH}} = \int_{H_1}^{20\ m} F(FS) * \frac{25.56}{} * d\ , \qquad \text{(Equation 10a)}$$

$$\text{where } F(FS) = I - FS, \text{ if } FS \leq 1 \cap H_1 * m(FS) \leq 3; \text{ otherwise, } 0 \qquad \text{(Equation 10b)}$$

$$\text{and } m(FS) = \exp\left(\frac{5}{25.56*(1-FS)}\right) - 1 \qquad \text{(Equation 10c)}$$

Calculation Tables by Youd et al. (2001)

Seven tables are contained in the Calculation Tables worksheet. The Calculations worksheet uses LOOKUP functions to determine values from the tables. Included in these seven tables are the following: (1) N Value-Unit Weight Correlation (Teng 1962), (2) Drill Rod Length Correction Factor, (3) Borehole Diameter Correction Factor, (4) Stress Reduction Coefficient, (5) General Soil Classification based on USCS, (6) Site Classification based on SPT N Value in the top 100 ft, and (7) Exponential "f" Factor for the K_σ Equation. These tables make it simpler to program and check the formulae in the Calculations worksheet. Additionally, they give the user a visual reference for how the correction factors change depending on the depth, number of blows, etc.

Output and Output Graphs by Youd et al. (2001)

The two output worksheets are described in this section. The user may access graphs in the Output Graphs worksheet to help visualize the examined data. The References worksheet is included so that, if needed, the user may find further information on the processes used to create the workbooks. Data from the Input Data and Calculations worksheet are integrated into the Output Boring El. Worksheet. The main findings from the liquefaction triggering study in reference to the boring surface elevation are presented in a more condensed, printable table in this worksheet (Figure 17). This worksheet reorganizes the input and computations; no new data is entered or calculations are carried out.

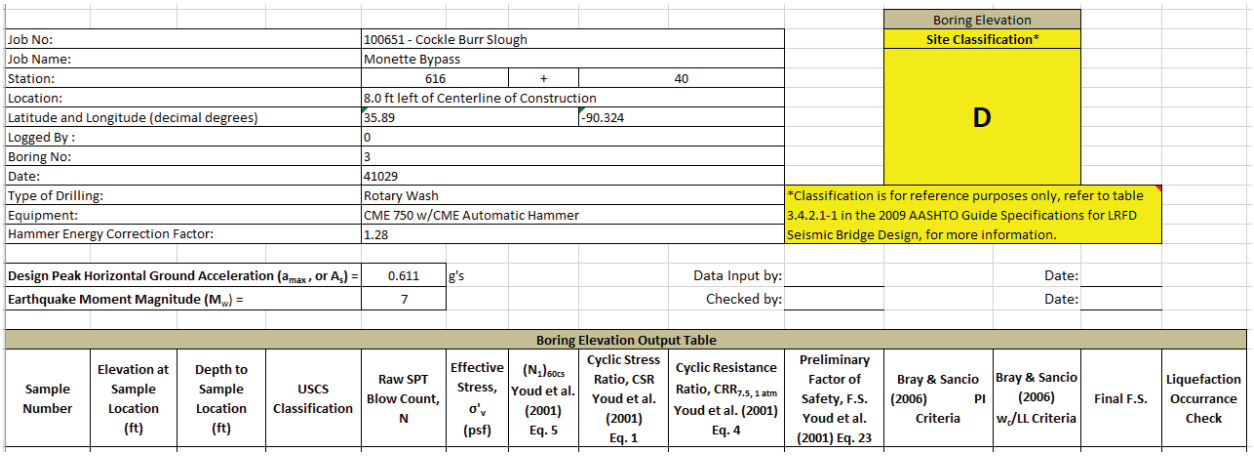

										Boring Elevation			
Job No:	100651 - Cockle Burr Slough									Site Classification*			
Job Name:	Monette Bypass												
Station:	616	+	40							D			
Location:	8.0 ft left of Centerline of Construction												
Latitude and Longitude (decimal degrees)	35.89	-90.324											
Logged By :	0												
Boring No:	3												
Date:	41029												
Type of Drilling:	Rotary Wash									*Classification is for reference purposes only, refer to table			
Equipment:	CME 750 w/CME Automatic Hammer									3.4.2.1-1 in the 2009 AASHTO Guide Specifications for LRFD			
Hammer Energy Correction Factor:	1.28									Seismic Bridge Design, for more information.			
Design Peak Horizontal Ground Acceleration (a_{max}, or A_s) =	0.611	g's							Data Input by:			Date:	
Earthquake Moment Magnitude (M_w) =	7								Checked by:			Date:	

Boring Elevation Output Table													
Sample Number	Elevation at Sample Location (ft)	Depth to Sample Location (ft)	USCS Classification	Raw SPT Blow Count, N	Effective Stress, σ'_v (psf)	$(N_1)_{60cs}$ Youd et al. (2001) Eq. 5	Cyclic Stress Ratio, CSR Youd et al. (2001) Eq. 1	Cyclic Resistance Ratio, $CRR_{7.5,\ 1\ atm}$ Youd et al. (2001) Eq. 4	Preliminary Factor of Safety, F.S. Youd et al. (2001) Eq. 23	Bray & Sancio (2006) PI Criteria	Bray & Sancio (2006) w_c/LL Criteria	Final F.S.	Liquefaction Occurrance Check

Figure 17. Output Summary of the Youd (2001) SPT-based Liquefaction Analysis

The Output Graphs worksheet is made to make it simple and quick for the user to understand the liquefaction results visually. Three graphs for the boring elevation are shown in this worksheet. The final factor of the safety chart, the updated, clean sand base curve, and the Bray and Sancio plots for fine-grained screening criteria are located near the top of the worksheet in columns N–V. The final FS values are depicted on the worksheet as red x marks, with a black line designating an FS of 1.0. This plot will plot "Not Sus" assignments as 2.0 and will not display any data for soils categorized as "Cohesive" or "Unsat". The site-specific data for Youd et al. (2001) adjusted clean sand base curve is shown in the output graphs. As per Youd et al. (2001), the curve has only been extended here up to a maximum $(N_1)_{60cs}$ value of 30, after which, soils are deemed too dense to liquefy. This border is shown as a vertical dashed line. The red x marks on this chart represent the CSR points computed in the Calculations worksheet. The Bray and Sancio (2006) fine-grained screening criteria are shown. Once more, the site-specific information is shown as red x marks.

Calculation and Calculation Tables of Cetin et al. (2018)

Seismic Moment Magnitude Scaling Factor (KM_w) (Cell E29): This worksheet calculates the seismic moment MSF using Equation 11 proposed by Cetin et al. (2018). The mentioned equation is stated below:

$$K_{Mw} = (M_w / 7.5)^{-2.324} \quad \textbf{(Equation 11)}$$

Average Shear wave velocity over top 40 ft (12 meters) ($V^*_{S,12\,m}$) (Cell E30): Cetin et al. (2018) uses the average shear wave velocity over the top 12 m (40 ft) ($V_{s,12m}$) to calculate r_d. If no shear wave velocity data is provided, this workbook can calculate this column using a correlation from Andrus and Stokoe (2000), which converts the corrected blow count ($N_1(_{60})$) to shear wave velocity (measured in meters per second). The average shear wave velocity value is displayed in cell E30 in the Calculations workbook. They are included in these cells because they are non–depth-dependent parameters.

Depth-dependent Calculations

The calculations that differ from those presented in Section 3.2.2.1 for the Youd et al. (2001) workbook will be discussed below.

Drill Rod Length Correction Factor (C_R) (Column S): Using Table 2 from Cetin et al. (2018), the drill rod length correction factor is determined. The Calculation Tables Worksheet's Drill Rod Length Correction Factor for different drill lengths using Table 3 presented below by Cetin et al. (2018). It is prudent to say that for drill lengths 10 m to 30 m, the C_R value is stated as 0.48 in Table 3. This is a typo, so in this worksheet, C_R is used as 1 for these depths. Based on the length of the drill rod, a LOOKUP function is utilized to retrieve the relevant C_R from this database.

Table 3. Recommended Correction Factors for SPT Equipment, Energy, and Procedures from Cetin et al. (2018)

C_N	$C_N = \left(\frac{P_a}{\sigma'_v}\right)^{0.5} \leq 2.0$ where the effective stress, σ'_v, and reference stress,Pa, are in the same units.
C_R	$C_R = 0.48 + 0.225 \cdot \ln(d)$; d ≤ 10 m (T-1) $C_R = 0.48$; 10 m < d < 30m where d = rod length (or "stick-up") from the top of the SPT sampler to the striking point at the top of the rod.
C_S	For samplers with an indented space for interior liners, but with liners omitted during sampling, $C_S = 1 + \frac{N_{1,60}}{100}$ (T-2) with limits of 1.10 ≤ C_S ≤1.30
C_B	Borehole diameter correction (C_B) 65 to 115 mm: 1.00 150 mm: 1.05 200 mm: 1.15
C_E	$C_R = \frac{ER}{60}$ (T-3) where ER (energy efficiency ratio) is the fraction or percentage of the theoretical SPT impact hammer energy actually transmitted to the sampler, expressed as % • The best approach is to directly measure the impact energy transmitted with each blow with instrumented rod. When available, direct energy measurements were employed. • The next best approach is to use a hammer and automatic (mechanical) trip hammer release system that has been demonstrated to deliver repeatable energy, and which has been calibrated based on direct (-instrumented) energy measurements. • Otherwise, ER must be estimated. For good field procedures, equipment and monitoring, the following approximate guidelines for SPT performed with rope and cathead are suggested:

Standard SPT Sampler liner correction (C_S) (Column T): This value will be 1.0 at all depths if the sampler has been used with liners or does not have space for liners, as shown on the Input Data worksheet. On the other hand, if the sampler has space for liners but is operated without them, this adjustment is depth-dependent and becomes a function of $(N_1)_{60}$ part of the circular reference. This correlation is presented in Table 3, where effective stress is defined previously and a 1.0 atmospheric pressure (P_a) of 2116 psf is used. This equation limits the maximum C_N value to 2.0.

Stress Correction Factor (C_N) (Column AA): The effective stresses in the soil column are used to produce the standardized overburden blow count adjustment factor.

Column headings AC–AG are all new within this worksheet and are presented in Figure 18.

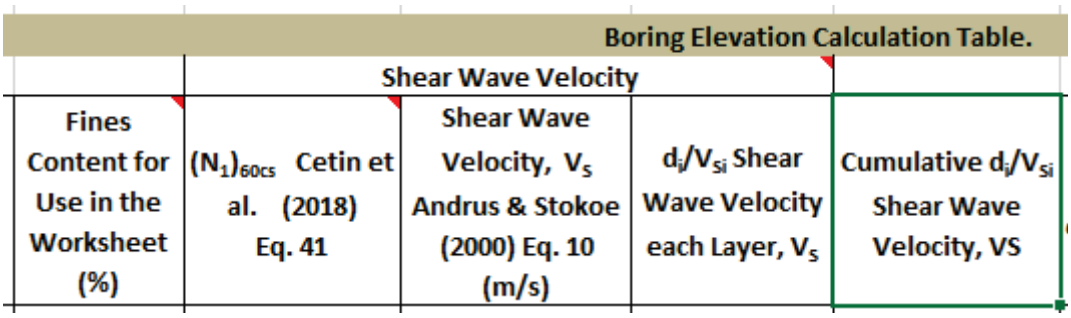

Figure 18**. Column Headers from Column AC to Column AG in the "Calculations (Cetin)" Tab of the SPT-based Worksheet**

Fines Content for use in the Worksheet (%) (Column AC): This column recalls the fines content in column G, and if no data is available in column G, this workbook sets the fines content data at 5%. The fines content for this column ranges from 5% to 35%. It is set to 5% or 35%, this workbook sets a lower limit of 5% (if input fines content is less than 5%) and an upper limit of 35% (if input fines content is greater than 35%) depending on whether the actual fine content is lower or more significant than these numbers.

$(N_1)_{60cs}$ (Column AD): The corrected blow count $(N_1)_{60}$ is combined with the fines content to produce the clean sand corrected blow count, abbreviated as $(N_1)_{60cs}$. The clean sand corrected blow count is used to calculate the CRR using the clean sand corrected blow count directly in the workbook. Equation 12, shown below, is used to calculate the clean sand corrected blow count. Table 4 presents a summary of the model coefficients of the seismic soil-triggering relationship proposed by Cetin et al. (2018).

$$(N_1)_{60cs} = (N_1)_{60} + FC^* (\Theta_1 * (N_1)_{60} + \Theta_4) \quad \text{(Equation 12)}$$

Table 4. A Summary of Model Coefficients of Seismic Soil Liquefaction Triggering Relationship Proposed by Cetin et al. (2018)

θ_1	θ_2	θ_3	θ_4	θ_5	θ_6	θ_7	σ_ε
0.00167	27.352	3.958	0.089	16.084	11.771	0.392	2.95

Shear Wave Velocity (Column AE to Column AG): The average shear wave velocity over the top 12 m is calculated using these three columns (40 ft). Using a correlation created by Andrus and Stokoe (2000), the first column, shear wave velocity, converts the corrected blow count ($N_{1(60)}$) to shear wave velocity

(measured in meters per second). The sample thickness (converted to meters for this computation) is divided by the shear wave velocity in the next column, d_i/V_{si} Shear Wave Velocity per Layer. The cumulative d_i/V_{si} is calculated as a function of depth in the third column, Cumulative d_i/V_{si} Shear Wave Velocity. Cell AG66 uses a LOOKUP function to ascertain which cumulative d_i/V_{si} value corresponds to a depth of 12 m (40 ft) under these columns, and this value is then transferred into cell E30 for use in the r_d equation.

Headings for columns AH–AL are all new within this worksheet and are presented in Figure 19.

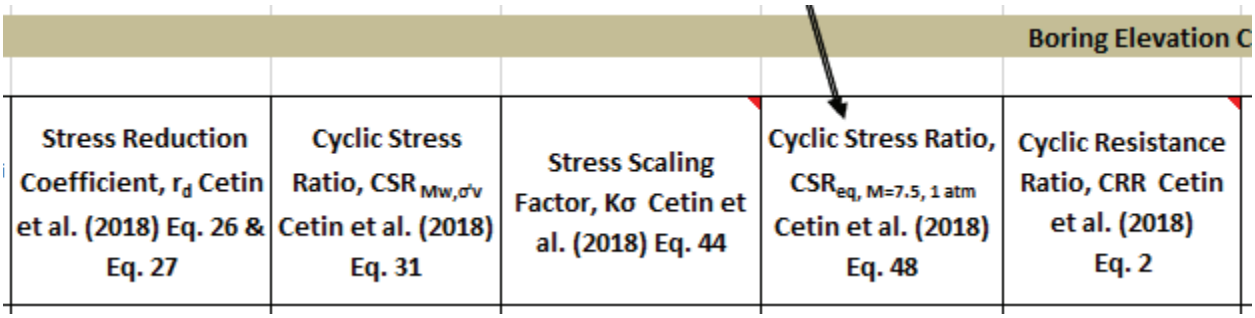

Figure 19. Column Headers from Column AH to Column AL in the "Calculations (Cetin)" Tab of the SPT-based Worksheet

Stress Reduction Coefficient (r_d) (Column AH): The r_d calculation is complex and subject to several factors. In the Calculation Tables worksheet above the Stress Reduction Coefficient tables, the algebraic formulas are broken up and color-coded with assignments of A, B, C, and D to make them easier to grasp. These tables copy data from the Calculations worksheet, compute the r_d, and then display the results. A LOOKUP function in the Calculations worksheet utilizes the tables and provides the correct r_d based on the depth of the sample. Equation 13 and Equation 14, presented below, are adopted from Cetin et al. (2018). All the parameters used in these equations are described in previous sections.

For depth (d) < 20m (~65 ft),

$$r_d = \frac{1+\frac{-23.013-2.949*\ \max+0.999*Mw+0.0525*Vs,12}{16.258+0.201*e\ ^{\wedge}(0.341*(-d+0.0785*Vs,12+7.586))}}{1+\frac{-23.013-2.949*\ ma\ +0.999*Mw+0.0525*Vs,12}{16.258+0.201*e\ ^{\wedge}(0.341*(0.0785*Vs,12+7.586))}} \qquad \textbf{(Equation 13)}$$

For depth(d) ≥ 20m (~65 ft),

$$r_d = \frac{1+\frac{-23.013-2.949*\ max+0.999*Mw+0.0525*Vs,12}{16.258+0.201*e\ ^{\wedge}(0.341*(-20+0.0785*Vs,12+7.586))}}{1+\frac{-23.013-2.949*ama\ +0.999*Mw+0.0525*Vs,12}{16.258+0.201*e\ ^{\wedge}(0.341*(0.0785*Vs,12+7.586))}} - 0.046 * (d-20) \qquad \textbf{(Equation 14)}$$

Stress Scaling Factor (K_σ) (Column AJ): Cetin et al. (2018) recommend effective stress values between 0.25 atm (529 psf) and 1.8 atm (3809 psf). This worksheet uses Equation 15 from Cetin et al. (2018) to calculate this parameter.

$$K_\sigma = \left(\frac{\sigma'v}{Pa}\right)^{-0.336} \qquad \textbf{(Equation 15)}$$

Cyclic Stress Ratio ($CSR_{M=7.5,\ \sigma'v=\ 1atm}$) (Column AK): Before determining the initial factor of safety, Cetin et al. (2018) modify the CSR for the earthquake magnitude (K_{Mw} is the name selected to describe the MSF in Cetin et al. [2018]) and overburden stress (K_σ). Because the K_{Mw} and K_σ factors are applied directly to the factor of safety in the Youd et al. (2001) technique, it should be noted that there is not an equivalent $CSR_{eq\ M,\ K\sigma}$ calculation in Youd et al. (2001).

Cyclic Resistance Ratio (CRR) (Column AL): The CRR in this column is determined by applying Equation 16 from Cetin et al. (2018). The variables Mw = 7.5, σ'v = 1 atm, FC = 5%, and PL = 15% have all been set to a fixed value. Fixing these variables effectively results in the FC 5% clean sand curve of Cetin et al. (2018). In the equations given above, $(N_1)_{60cs}$ is substituted for $(N_1)_{60}$ to account for the FC. Therefore, a CRR of 2.0 is used if the $(N_1)_{60cs}$ value is more than 35, as the soil is primarily thought to be non-liquefiable. Equation 16, presented below, is adopted from Cetin et al. (2018). All the parameters used in these equations are described in previous sections. The model coefficients are presented in Table 4.

$$CRR = \exp\left[\frac{(N1,60*(1+\theta1*FC)-\theta2*\ln(Mw)-\theta3*\ln\left(\frac{\sigma'v}{Pa}\right)+\theta4*FC+\theta5+\sigma\varepsilon*\phi*(-1)*PL)}{\theta6}\right] \qquad \textbf{(Equation 16)}$$

Probabilistic Evaluation (Column AR): The column headings for the probabilistic evaluation performed in columns AR are included in the worksheet using Equation 17 from Cetin et al. (2018). Equation 3–17, presented below, is adopted from Cetin et al. (2018). All the parameters used in these equations are described in previous sections.

$$P_L = \phi\left[\frac{(N1,60*(1+\theta1*FC)-\theta6*\ln(CSR)-\theta2*\ln(Mw)-\theta3*\ln\left(\frac{\sigma'v}{Pa}\right)+\theta4*FC+\theta5}{\sigma\varepsilon}\right] \qquad \textbf{(Equation 17)}$$

The changes to the Calculation Tables worksheet include an updated CR table and chart, a DWFM/MSF table and chart, stress reduction coefficient tables and equations, plus the table titled Exponential "f" factor for K_σ equation. All of which have been discussed previously.

Output and Output Graphs of Cetin et al. (2018)

The Output worksheet is the same for Cetin et al. (2018) as for Youd et al. (2001). The Output graph worksheet includes graphs for each sample elevation, like Youd et al. (2001).

Calculations and Calculation Table Worksheets of Boulanger and Idriss (2014)

The undrained shear strength (S_u) in column J applies only to cohesive soils and should only be entered if the proper laboratory tests have been performed to determine S_u accurately. If the proper laboratory tests have not been performed, this column should be left blank, and a S_u will be estimated based on a correlation with SPT blow count.

Depth-dependent Calculations

The remaining computations are connected to a specific SPT sample site and are all depth-dependent. Again, there are more columns in the Calculations worksheet than in the Input Data workbook. The columns different from the Youd et al. (2001) worksheet will only be discussed here.

Stress Correction Factor (C_N) (Column AB): The equation used to calculate C_N is a function of $(N_1)_{60}$. It is the second circular reference in the Calculations worksheet of Idriss and Boulanger (2014) using Equations 18a and 18b.

$$C_N = \left(\frac{P_a}{\sigma'_v}\right)^m \qquad \textbf{(Equation 18a)}$$

$$m = 0.784 - 0.0768 * \sqrt{(N1)CS} \qquad \textbf{(Equation 18b)}$$

$\Delta(N_1)_{60}$ (Column AD): This column calculates $\Delta(N_1)_{60}$ using Equation 19 from Boulanger and Idriss (2014), which is the change in blow count according to the percentage of fines. This is added to $(N_1)_{60}$ to determine $(N_1)_{60cs}$.

$$\Delta(N_1)_{60} = \exp\left(1.63 + \frac{9.7}{FC+0.01} - \left(\frac{15.7}{FC+0.01}\right)^2\right) \qquad \textbf{(Equation 19)}$$

Columns headings AF–AM are all new within this worksheet and are presented in Figure 20.

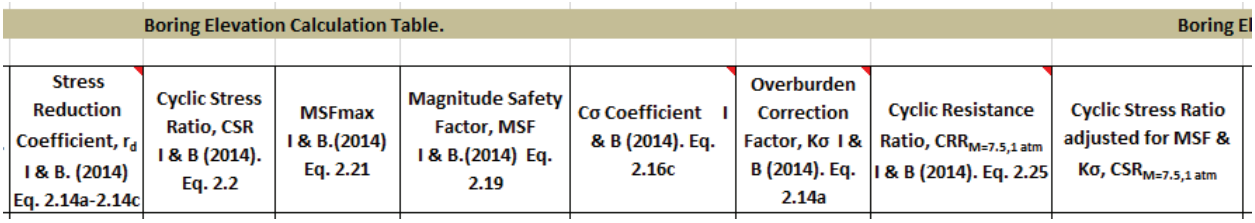

Figure 20**. Column Headers from Column AF to Column AM in the "Calculations (B&I)" Tab of the SPT-based Worksheet**

Stress Reduction Coefficient (r_d) (Column AF) This column looks up the value of r_d from a table in the Calculation Tables worksheet using a LOOKUP function like Youd et al. (2001). In this case, however, details from Equations 20a through 20c are shown below. Due to the increased uncertainty with depth, 20 m (65 ft) is the maximum suggested depth for this r_d correlation to be employed. This workbook uses the r_d relationship to a depth of 36 m (120 ft) against the suggestion. To draw the user's attention to the depth-related increase in uncertainty below a depth of 20 m, the Stress Reduction Coefficient table in the Calculation Tables worksheet has been highlighted in red.

$$r_d = \exp[\alpha(z) + \beta(z)*M] \quad \textbf{(Equation 20a)}$$

$$\alpha(z) = -1.012 - 1.126 \sin(z/11.73 + 5.133) \quad \textbf{(Equation 20b)}$$

$$\beta(z) = 0.106 + 0.188 \sin(z/11.28 + 5.142) \quad \textbf{(Equation 20c)}$$

Magnitude Safety Factor (Columns AH–AI): The proposed relationship to relate MSF_{max} to $(N_1)_{60cs}$ is presented below and adopted from Equation 21a (Idriss and Boulanger 2014). Using the MSF_{max} value found in column AG, the magnitude safety factor is calculated in column AH, and the equation is presented below (Equation 22b) (Idriss and Boulanger 2014).

$$MSF_{max} = 1.09 + ((N_1)_{60cs} / 31.5)^2 \leq 2.2 \quad \textbf{(Equation 21a)}$$

$$MSF = 1 + (MSF_{max} - 1) *(8.64*\exp(-M/4) - 1.325 \quad \textbf{(Equation 21b)}$$

C_σ Coefficient (Column AJ): This column calculates the intermediate variable C_σ, which is used to determine K_σ. C_σ is a function of $(N_1)_{60}$ and relates the relative density of the soil to K_σ (Equation 3–22) (Idriss and Boulanger 2014).

$$C_\sigma = \frac{1}{18.9 - 2.55 * \sqrt{(N1)60cs}} \leq 0.3 \qquad \textbf{(Equation 22)}$$

Overburden Correction Factor (K_σ) (Column AK): K_σ is related to the relative density of the soil via C_σ. Idriss and Boulanger (2006) state, "The interpretation and proper execution of in-situ and laboratory tests [for clays] require a careful accounting of the effective consolidation stress and stress history conditions in the field. Accordingly, as was done for the sand, there is no need to introduce an overburden correction factor for the cyclic strength of clay". Because of this, clay-like and cohesive soils are assigned a $K_\sigma = 1.0$ so that CRR values remain unaffected. Equation 23 presents the formula adopted by Idriss and Boulanger (2014). The limit of 1.1 on the maximum value of K_σ is reached at σ'_v, which varies with the soil's denseness.

$$K_\sigma = 1 - C_\sigma * \ln\left(\frac{\sigma'_v}{Pa}\right) \leq 1.1 \qquad \textbf{(Equation 23)}$$

Cyclic Resistance Ratio ($CRR_{M=7.5, \sigma'_v = 1\ atm}$) (Column AN): The unadjusted CRR is calculated differently depending on the clay-like or sand-like designation. The sand-like soil CRR will be calculated according to $(N_1)_{60cs}$. For sand-like soils, an (N1)60cs ≥ 37.5 is interpreted as too dense to liquefy: These soils are assigned a $CRR_{M=7.5,1\ atm}$ of 2.0, which is carried through the Preliminary FS and Final FS columns.

$$CRR_{M=7.5, \sigma'_v = 1\ atm} = \exp\left(\frac{(N1)60cs}{14.1} + \left(\frac{(N1)60cs}{126}\right)^2 - \left(\frac{(N1)60cs}{23.6}\right)^3 + \left(\frac{(N1)60cs}{137}\right)^4 - 2.8\right) \qquad \textbf{(Equation 24)}$$

Output and Output Graphs of Boulanger and Idriss (2014)

The Output and Output Graphs Worksheets for the Boulanger and Idriss (2014) are the same as in the Youd et al. (2001) workbook. The Output Graphs worksheet includes an FS plot but does not include the plot for fine-grained screening criteria proposed by Bray and Sancio (2006). The Output Graphs worksheet includes a plot representing the clean sand CRR curve recommended by Idriss and Boulanger (2008). The red x marks denote the calculated CSR values, and the vertical dashed line represents the interpreted cutoff between liquefiable and non-liquefiable material.

Comparison

The liquefaction triggering workbooks that have been developed in this work enable easy data transfer between workbooks and facilitate quick and simple comparisons between all three procedures. The "Comparison" tab is created to view the comparative results of the liquefaction analysis (Figure 21). The results of clean sand blow count [$(N_{1,60})_{cs}$], Stress reduction coefficient (r_d), Overburden blow count correction factor (C_N), Overburden correction factor (K_σ), Unadjusted Cyclic Resistance Ratio (CRR), Unadjusted Cyclic Stress Ratio (CSR), Factor of Safety (FS), Sampler liner correction factor (C_S), and Probability of liquefaction (PL) can be viewed in this tab. These outputs have an input number from 3 to 11 in the same order. The user needs to select the input number from the dropdown list at cell D2 to view the desired output. A VLOOKUP function is used, and the corresponding liquefaction analysis results can be viewed from columns D to F. The figure will automatically change according to the input number. The user can view the comparative results of the procedures. It should be noted that except for cell D2, no other cell should be altered.

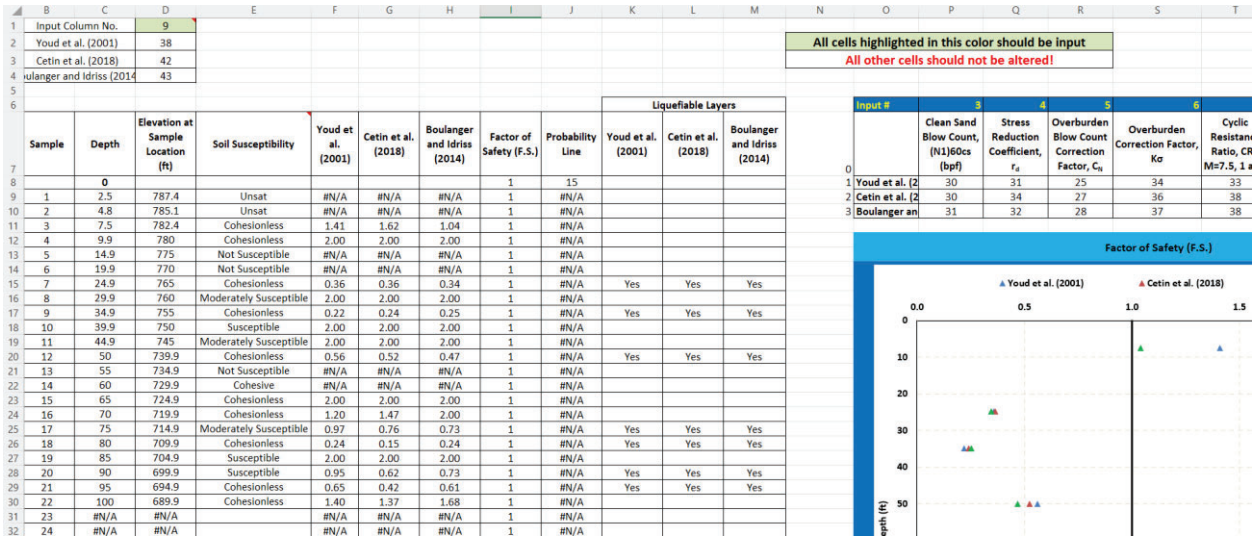

Input Column No.	9	
Youd et al. (2001)	38	
Cetin et al. (2018)	42	
ulanger and Idriss (2014	43	

All cells highlighted in this color should be input
All other cells should not be altered!

Sample	Depth	Elevation at Sample Location (ft)	Soil Susceptibility	Youd et al. (2001)	Cetin et al. (2018)	Boulanger and Idriss (2014)	Factor of Safety (F.S.)	Probability Line	Liquefiable Layers: Youd et al. (2001)	Liquefiable Layers: Cetin et al. (2018)	Liquefiable Layers: Boulanger and Idriss (2014)
	0						1	15			
1	2.5	787.4	Unsat	#N/A	#N/A	#N/A	1	#N/A			
2	4.8	785.1	Unsat	#N/A	#N/A	#N/A	1	#N/A			
3	7.5	782.4	Cohesionless	1.41	1.62	1.04	1	#N/A			
4	9.9	780	Cohesionless	2.00	2.00	2.00	1	#N/A			
5	14.9	775	Not Susceptible	#N/A	#N/A	#N/A	1	#N/A			
6	19.9	770	Not Susceptible	#N/A	#N/A	#N/A	1	#N/A			
7	24.9	765	Cohesionless	0.36	0.36	0.34	1	#N/A	Yes	Yes	Yes
8	29.9	760	Moderately Susceptible	2.00	2.00	2.00	1	#N/A			
9	34.9	755	Cohesionless	0.22	0.24	0.25	1	#N/A	Yes	Yes	Yes
10	39.9	750	Susceptible	2.00	2.00	2.00	1	#N/A			
11	44.9	745	Moderately Susceptible	2.00	2.00	2.00	1	#N/A			
12	50	739.9	Cohesionless	0.56	0.52	0.47	1	#N/A	Yes	Yes	Yes
13	55	734.9	Not Susceptible	#N/A	#N/A	#N/A	1	#N/A			
14	60	729.9	Cohesive	#N/A	#N/A	#N/A	1	#N/A			
15	65	724.9	Cohesionless	2.00	2.00	2.00	1	#N/A			
16	70	719.9	Cohesionless	1.20	1.47	2.00	1	#N/A			
17	75	714.9	Moderately Susceptible	0.97	0.76	0.73	1	#N/A	Yes	Yes	Yes
18	80	709.9	Cohesionless	0.24	0.15	0.24	1	#N/A	Yes	Yes	Yes
19	85	704.9	Susceptible	2.00	2.00	2.00	1	#N/A			
20	90	699.9	Susceptible	0.95	0.62	0.73	1	#N/A	Yes	Yes	Yes
21	95	694.9	Cohesionless	0.65	0.42	0.61	1	#N/A	Yes	Yes	Yes
22	100	689.9	Cohesionless	1.40	1.37	1.68	1	#N/A			
23	#N/A	#N/A		#N/A	#N/A	#N/A	1	#N/A			
24	#N/A	#N/A		#N/A	#N/A	#N/A	1	#N/A			

Input #	3	4	5	6	
	Clean Sand Blow Count, (N1)60cs (bpf)	Stress Reduction Coefficient, r_d	Overburden Blow Count Correction Factor, C_N	Overburden Correction Factor, Kσ	Cyclic Resistan Ratio, CR M=7.5, 1 a
1 Youd et al. (2	30	31	25	34	33
2 Cetin et al. (2	30	34	27	36	38
3 Boulanger an	31	32	28	37	38

Figure 21. "Comparison" Tab of the SPT Liquefaction Triggering Workbook

Liquefaction Manifestation

This tab uses the VLOOKUP function to summarize the results of the liquefaction potential estimation analysis (Figure 22). The user needs to select an option from the dropdown list in cell B2. The results of LPI (Input # 3) and LPI_{ISH} (Input #4) can be viewed, and a corresponding graph will be created. The

calculated total value of LPI and LPI_{ISH} at the top 20 m (65 ft) from all three procedures can also be viewed at cells I7 to I9.

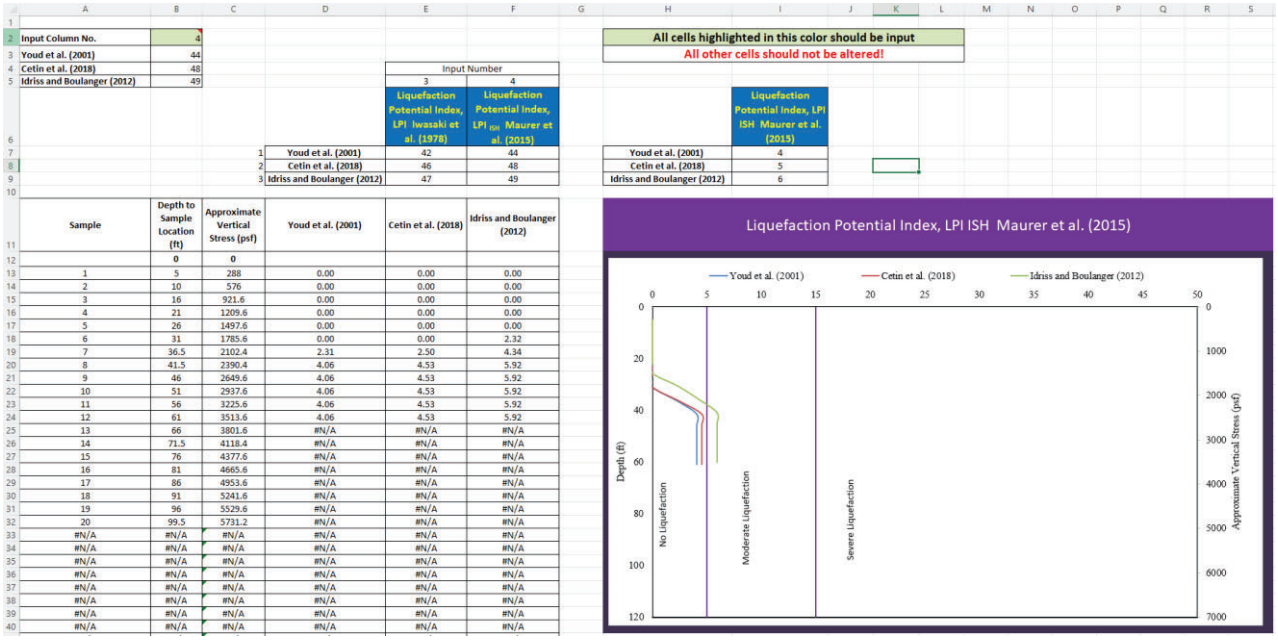

Figure 22. "Liquefaction Manifestation" Tab of the SPT Liquefaction Triggering Workbook

CPT-based Workbook Review

The three most popular CPT-based liquefaction triggering procedures (Youd et al. 2001; Boulanger and Idriss 2014; Moss et al. 2006) and Normalized CPT analysis have been programmed in Microsoft Excel workbooks. The different tabs of this Excel workbook are divided and marked with color codes for better understanding. The "Data Conversion", a red-colored tab, will convert the raw CPT data units to the desired unit (psf, ft), which will be used in the workbook for further calculations. The "Data Processing" tab can process the converted data with a point rolling average. The user can choose the desired option from the dropdown list at cell M2. The "Input data tab", which the user will use to input data for analysis, is red. The red-colored "Water Table" tab can be used to determine the water table if the water table information is not given in the CPT data. The user needs to manually input the value in cell D2 to get the water table value. The "Layer Comparison", "Comparisons", and "Liquefaction manifestation" tabs are purple-colored and show the results of the three liquefaction-triggering procedures used in this Excel workbook. The "CPT Analysis" tab shows the normalized soil behavior calculations and other CPT

calculations. The calculation tab and the supplementary tabs for Youd et al. (2001), Boulanger and Idriss (2014), and Moss et al. (2006) are blue, yellow, and pink, respectively. These tabs are shown in Figure 23. The three calculation tabs for Youd, B & I 2014, and Moss 2006 are as identical as feasible to simplify data entry and information sharing amongst workbooks.

Figure 23. Individual Worksheet Tabs Within the Liquefaction Triggering Workbooks

A thorough discussion about the Youd et al. (2001) workbook will be examined following a brief section highlighting the commonalities between the workbooks. The workbooks from Boulanger and Idriss (2014) and Moss et al. (2006) will be thoroughly examined after the discussion of Youd et al. (2001). The discussion of the Boulanger and Idriss (2014) and Moss et al. (2006) sheets will concentrate on the areas that differ from the workbook by Youd et al. (2001) as many of the computations are identical to Youd et al. (2001). Discussing the overall style and format of the workbook before starting each section is prudent. The Calculation and Tables tabs are for the worksheets that perform the necessary calculations. The Output and Output graphs tabs display information from the Calculations worksheet more graphically.

Data Conversion

The data conversion tab in the workbook can convert the units (Ksf, tsf, and MPa to Psf) of CPT raw data (Tip resistance, Sleeve friction, Pore pressure). It can convert depth units (meters to feet) and shear wave velocity (ft/sec to m/sec). Cell B14, C14, D14, E14, and G14 have a drop-down list where the user can choose the raw units, and it can convert the data to the desired units. The user needs to paste the data in colored cells in column B to column G, and after choosing the raw units, the workbook can convert the units in column I to column N. Cells other than light blue should not be altered. Figure 24 presents an image of the data conversion tab in the Cone penetration test workbook.

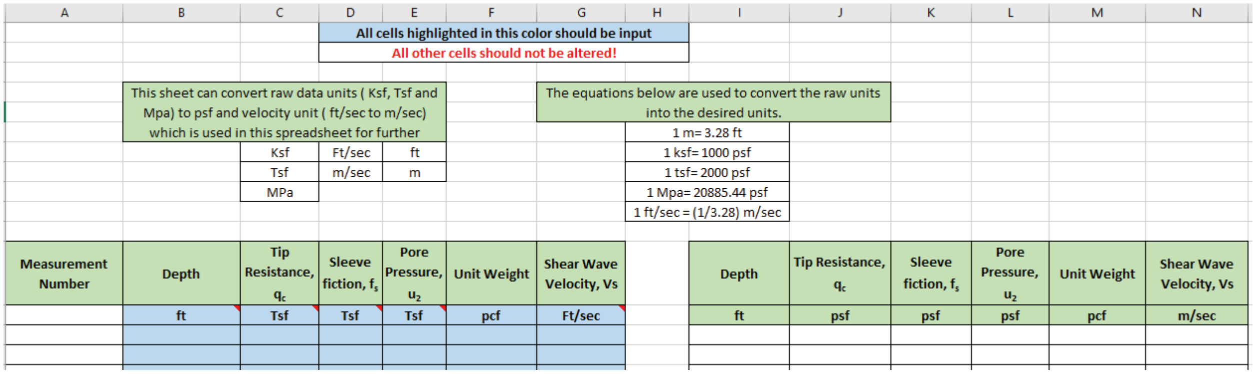

Figure 24**. Data Conversion Tab of the Cone Penetration Test Workbook**

Data Processing

This tab uses a rolling average to smooth the data. In CPT analysis, this may be necessary to better understand the plots. The higher point rolling average can smooth the plots and can help the user to better understand the results and remove large spikes. The M2 cell in this tab has a dropdown list to choose the desired options. The converted data is automatically transferred from the Data conversion tab. The user does not need to input any value except the rolling point average option. Figure 25 presents an image of the data processing tab in the Cone Penetration Test workbook.

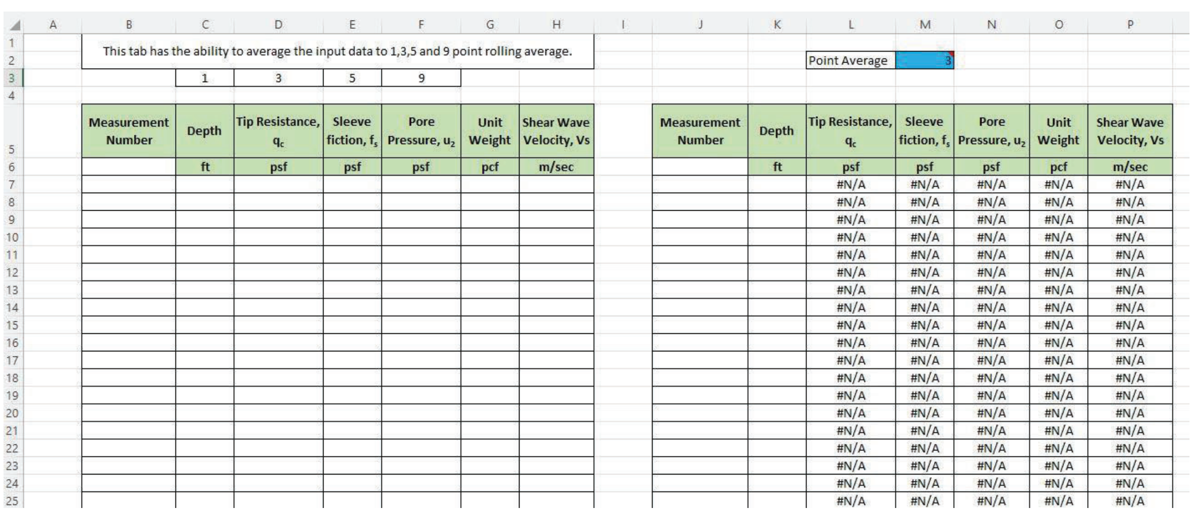

Figure 25**. Data Processing Tab of the Cone Penetration Test Workbook**

Water Table Calculation Tab

The red-colored “Water Table” tab can be used to determine the water table if the water table information is not given in the CPT data. The converted data is automatically transferred from the Data conversion tab. The user estimates a water table depth in cell D2 based on the U2 pore pressure plot. A hydrostatic line equal to the unit weight of water times the depth is projected on the U2 plot to allow the user to adjust the estimated water table depth in cell D2 to the correct depth. Figure 26 presents an image of the water table tab in the Cone penetration test workbook.

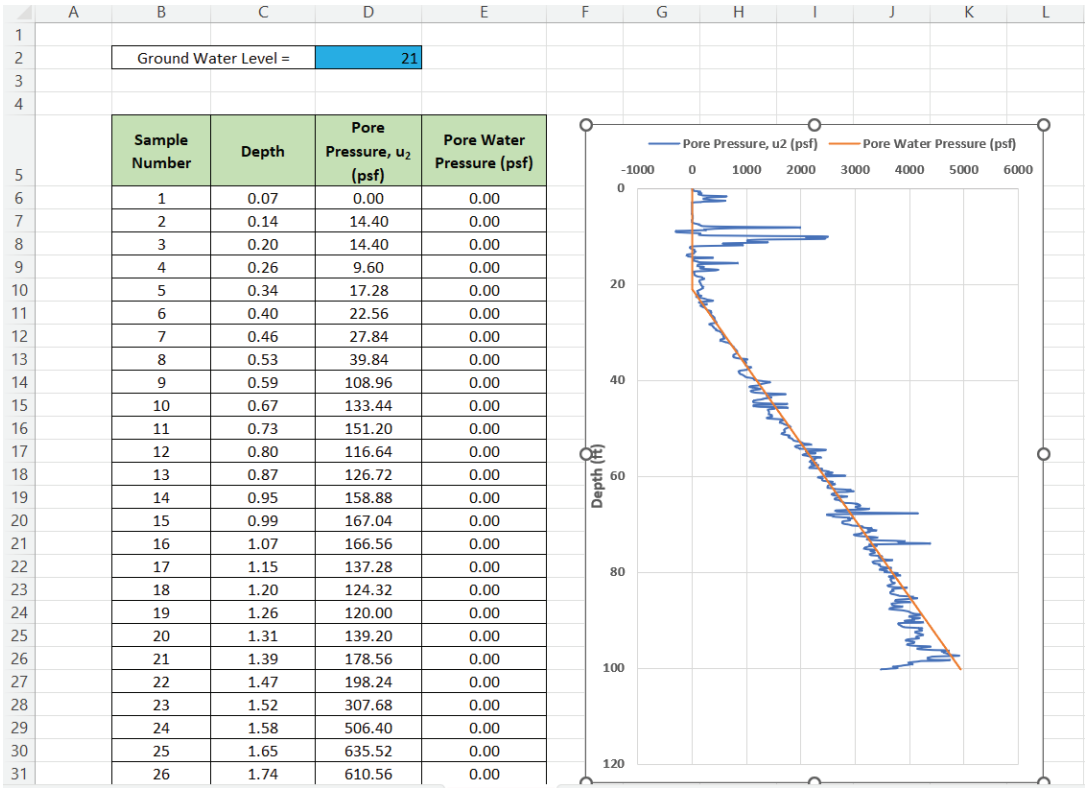

Ground Water Level =	21

Sample Number	Depth	Pore Pressure, u_2 (psf)	Pore Water Pressure (psf)
1	0.07	0.00	0.00
2	0.14	14.40	0.00
3	0.20	14.40	0.00
4	0.26	9.60	0.00
5	0.34	17.28	0.00
6	0.40	22.56	0.00
7	0.46	27.84	0.00
8	0.53	39.84	0.00
9	0.59	108.96	0.00
10	0.67	133.44	0.00
11	0.73	151.20	0.00
12	0.80	116.64	0.00
13	0.87	126.72	0.00
14	0.95	158.88	0.00
15	0.99	167.04	0.00
16	1.07	166.56	0.00
17	1.15	137.28	0.00
18	1.20	124.32	0.00
19	1.26	120.00	0.00
20	1.31	139.20	0.00
21	1.39	178.56	0.00
22	1.47	198.24	0.00
23	1.52	307.68	0.00
24	1.58	506.40	0.00
25	1.65	635.52	0.00
26	1.74	610.56	0.00

Figure 26. Water Table Calculation Tab of the Cone Penetration Test Workbook

Input Data

The Input tab in the workbook is where all site-specific data will be manually added to the workbook. An image of the general input information for the Input tab is provided in Figure 27. Most of the input data required for evaluating soil liquefaction triggering using the CPT will come from the CPT logs collected during the site investigation. The project data should only be updated in the cells marked in light blue.

No cells other than light blue colored cells should be changed in this workbook. Rows E5 to E12, the first set of input fields, are located at the top of the Input Data worksheet and are used to identify jobs by their job number, name, station, location (latitude and longitude), logged by (operator's name), CPT number, date of boring, Type of Rig, and Cone ID. Most of these cells are used for documentation.

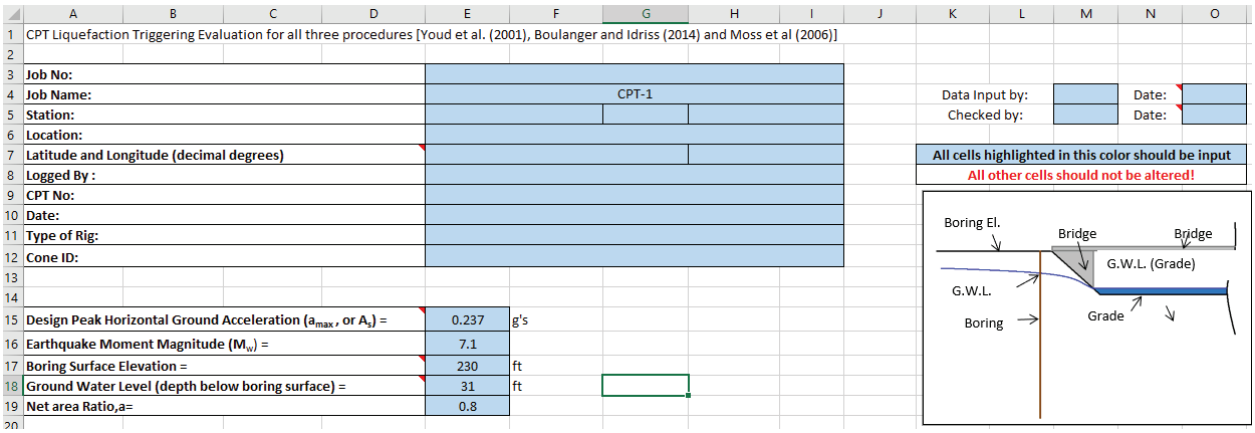

Figure 27. Input Data Worksheet with Job Identification Information and Site-specific Input Options

The input cells E15–E19 contain the design peak horizontal ground acceleration (a_{max} or A_s), earthquake moment magnitude (M_w), boring surface elevation, ground water level (depth below boring surface), and net area ratio. Below, each of these topics is covered in further detail.

Net Area Ratio

The net area ratio is a parameter of the cone used for CPT. It is defined as the ratio of the area of the tip of the CPT cone compared to the area of the back of the cone. It is used to correct the tip resistance for pore pressure acting unequally on the tip and back of the cone. This value is typically provided with the specifications of the cone. Typically, a net area ratio of 0.8 can be used if no value for the net area ratio is provided in the CPT data.

Depth-dependent Input Data

All the remaining input data is depth-dependent. Figure 28 displays the column headers from column A through column I. The numbers in the first two columns, "Measurement Number" and "Elevation at Sample Location", were computed within the workbook. These columns should only contain information to help the user track specific sample locations (depths) across the workbook; the user should enter no

values into them directly. The remaining data input column headers are covered in more detail below to clarify them. The depth at which each CPT sample was taken below the surface is shown in feet. The distance between CPT sample sites is often fixed, such as 50 mm or 0.16 ft. The user must paste the converted data of depth, tip resistance, sleeve friction, pore pressure, measured unit weight, and shear wave velocity from the Data conversion tab. These cells should be left blank if V_s and fines content data are not provided. This workbook can calculate these parameters using correlations, which will be discussed in later sections.

	A	B	C	D	E	F	G	H	I
21			Must Enter: Depth, Tip Resistance,						
22	Measurement Number	Elevation (ft)	Depth (ft)	Tip Resistance, q_c (psf)	Sleeve fiction, f_s (psf)	Pore Pressure, u_2 (psf)	Shear Wave Velocity (m/s)	Measured Unit Weight of Soil (pcf)	Fines Content (%)

Figure 28. Headings for Depth-dependent Parameters in the Input Data Worksheet

Calculations Worksheet of Youd et al. (2001)

The worksheets for calculations and calculation tables provide the framework of the whole workbook. Data is automatically copied into the different worksheets and moved from the Input Data worksheet into these worksheets. These workbooks should be kept the same unless a calculation error is discovered. These workbooks will not have to be examined during typical evaluations if the user is familiar with liquefaction calculations. The users will be given a review of each column so they can comprehend how these worksheets compute and use data. Additionally, many of the column titles in the workbooks have cell comments describing the purpose of the respective column. The users will notice that most inputs into the Input Data worksheet have been copied to the Calculations worksheet when viewing it for the first time (Figure 29). The Calculations worksheet cannot be edited or have data entered again. To avoid this error, the cells are locked. In the cells, E17, E18, E19, and E21, right below the input data, non–depth-dependent parameters—ground water elevation, MSF, the correction factor for sloping ground, and average V_s are provided.

The MSF calculated in cell E18 using Equation 25, obtained from Youd et al. (2001), is provided below.

$$MSF = 10^{2.24}/M_W^{2.56} \qquad \textbf{(Equation 25)}$$

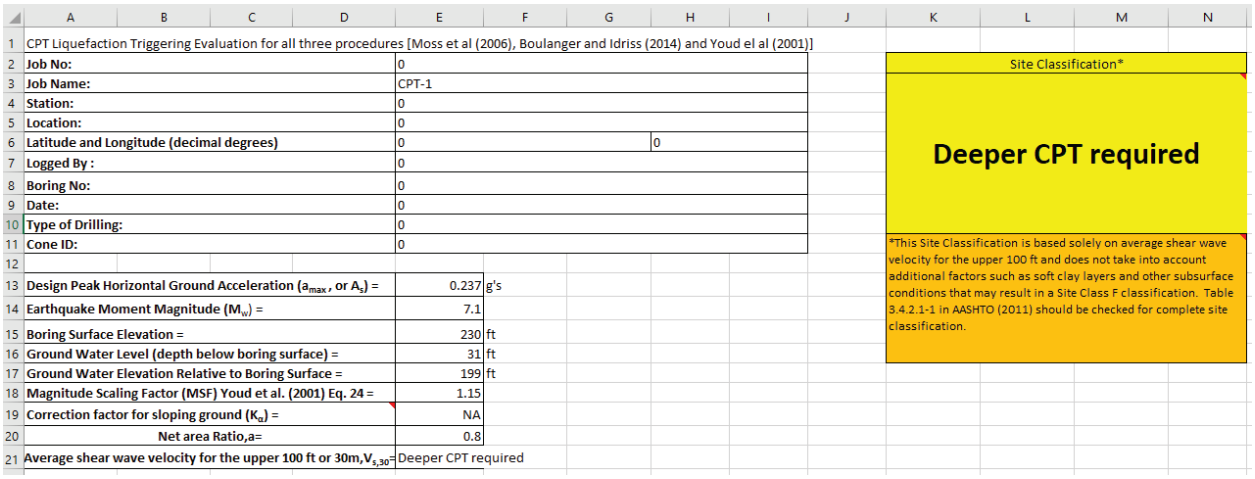

CPT Liquefaction Triggering Evaluation for all three procedures [Moss et al (2006), Boulanger and Idriss (2014) and Youd el al (2001)]		
Job No:	0	
Job Name:	CPT-1	
Station:	0	
Location:	0	
Latitude and Longitude (decimal degrees)	0	0
Logged By :	0	
Boring No:	0	
Date:	0	
Type of Drilling:	0	
Cone ID:	0	
Design Peak Horizontal Ground Acceleration (a_{max} , or A_s) =	0.237	g's
Earthquake Moment Magnitude (M_w) =	7.1	
Boring Surface Elevation =	230	ft
Ground Water Level (depth below boring surface) =	31	ft
Ground Water Elevation Relative to Boring Surface =	199	ft
Magnitude Scaling Factor (MSF) Youd et al. (2001) Eq. 24 =	1.15	
Correction factor for sloping ground (K_α) =	NA	
Net area Ratio,a=	0.8	
Average shear wave velocity for the upper 100 ft or 30m,$V_{s,30}$=	Deeper CPT required	

Site Classification*
Deeper CPT required
*This Site Classification is based solely on average shear wave velocity for the upper 100 ft and does not take into account additional factors such as soft clay layers and other subsurface conditions that may result in a Site Class F classification. Table 3.4.2.1-1 in AASHTO (2011) should be checked for complete site classification.

Figure 29**. "Calculations (Youd)" Tab in the CPT-based Worksheet with Job Identification and Site Classification**

It should be noted that cell E19 was initially designated as the location for the sloping ground correction factor (K_α). However, this function was eliminated from the workbook due to the lack of agreement on handling static driving shear stresses in soil liquefaction triggering. The cell is filled with "NA" to alert the user that this workbook does not consider the correction factor for sloping terrain. Cell E21 calculates $V_{s,30}$; if the boring is terminated before reaching the depth of 100 ft, no site classification can be obtained. If no shear wave velocity is not provided, this worksheet can calculate shear wave velocity based on correlations (Column P).

Depth-dependent Calculations

The remaining calculations are connected to a specific CPT sample site and are all depth-dependent. The user will observe many more filled-in columns in the Calculations worksheet than in the Input Data worksheet (i.e., from column I through column AL). Each column heading in the Calculations worksheet will be examined here in the same order that they are displayed in the worksheet for the sake of clarity. Details on the column's purpose will follow each column title. The user is informed that additional helpful comments may be included in the worksheet's cells. Red triangles in the cell's top right-hand corner denote these comments. The user may readily follow the worksheet development since the equations from the paper by Youd et al. (2001) used for the computations are referenced in the column

titles. Below is a discussion of the calculations made in columns I through R. These column headers are shown in Figure 30 for reference.

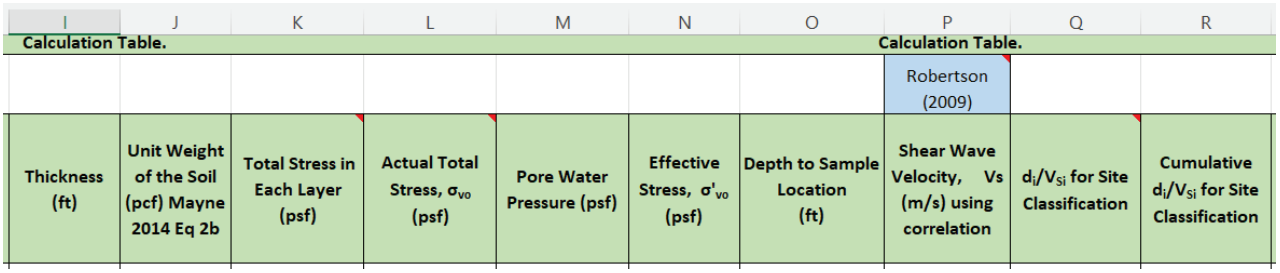

I	J	K	L	M	N	O	P	Q	R
Calculation Table.							Calculation Table.		
							Robertson (2009)		
Thickness (ft)	Unit Weight of the Soil (pcf) Mayne 2014 Eq 2b	Total Stress in Each Layer (psf)	Actual Total Stress, σ_{vo} (psf)	Pore Water Pressure (psf)	Effective Stress, σ'_{vo} (psf)	Depth to Sample Location (ft)	Shear Wave Velocity, Vs (m/s) using correlation	d_i/V_{Si} for Site Classification	Cumulative d_i/V_{Si} for Site Classification

Figure 30. Column Headers from Column I to Column R in the "Calculations (Youd)" Tab in the CPT-based Worksheet

Unit Weight of the Soil (Column J): This column calculates the unit weight of the soil using correlations of Mayne (2014). This column is necessary in CPT analysis if no unit weight data is given in CPT data, which is rarely measured when CPTs are pushed. The adopted correlation from Mayne (2014) is shown in Equation 26.

$$\gamma_t = 12 + 1.5*\ln(f_s + 1), \qquad \text{(Equation 26)}$$

where γ_t is in KN/m^3 and f_s is in Kpa.

In-situ Stresses (Column J–N): These columns have been previously discussed and are not discussed in this section to avoid repetition.

Shear Wave Velocity (Column P): Shear wave velocity measures the speed at which a shear wave propagates through a material, such as soil or rock. Shear waves are seismic waves that travel through a material, causing particles to distort perpendicular to the wave propagation direction. Shear wave velocity is an essential parameter for characterizing the mechanical properties of soil and rock, particularly shear modulus. In this workbook, column P can determine the shear wave velocity using CPT-V_s correlations from Andrus et al. (2007) (Equation 27), Hegazy and Mayne (2006) (Equation 28), and Robertson (2009) (Equation 29). If no shear wave velocity data is provided in the input tab, this workbook uses one of these correlations, based on the user's choice, to determine site classification.

$$V_s = 2.27 * q_t^{0.412} * I_c^{0.989} * z^{0.033} \quad \textbf{(Equation 27)}$$

$$V_s = 10^{0.55*Ic + 1.68} * ((q_t - \sigma_{vo})/Pa)^{0.5} \quad \textbf{(Equation 28)}$$

$$V_s = 0.0831 * q_{c1N} * \exp(1.7861 + Ic)(\sigma'_{vo}/Pa)^{0.25} \quad \textbf{(Equation 29)}$$

Site Classification Calculation (Columns Q and R): The AASHTO seismic site classification in this workbook is based on shear wave velocity as there is no direct method for determining seismic site classification using CPT parameters. Shear wave velocity either has to be measured in the field using the seismic CPT or correlated using a CPT-V_s correlation such as the ones mentioned above. From column Q and column R, cumulative d_i/V_{si} $_{is}$ calculated, and cells R635 and R637 show the cumulative d_i/V_{si} for the top 40 ft and 100 ft, respectively. Cumulative d_i/V_{si} for the top 100 ft is used to calculate $V_{s,100}$ at cell E21.

Below is a discussion of the calculations made in columns S through AD. These column headers are shown in Figure 31 for reference.

S	T	U	V	W	X	Y	Z	AA	AB	AC	AD
Stress Reduction Coefficient, r_d Youd et al. (2001) Eq. 3	Cyclic Stress Ratio, CSR Youd et al. (2001) Eq. 1	Corrected Cone Resistance, qt (psf) Robertson (1990) Eq. 2	q_n	Normalized Friction Ratio, Fr Robertson (2009) Eq. 2	Normalized Pore Pressure Ratio, B_q Robertson (2009) Eq. 3	Soil Behaviour Index, I_c Robertson (2009) Eq. 5	Stress Exponent, n Robertson (2009) Eq. 7	Stress Correction Factor, C_N Youd et al. (2001) Eq. 9	Normalized Cone Resistance, Q_{tn} (atm) Robertson (2009) Eq. 7	Correction Factor, K_c Youd et al. (2001) Eq. 19	Equivalent clean sand value, $(q_{c1N})_{cs}$ Youd et al. (2001) Eq. 18

Figure 31. Column Headers from Column S to Column AD in the "Calculations (Youd)" Tab in the CPT-based Worksheet

Stress Reduction Factor (r_d) and Cyclic Stress Ratio (CSR) (Column S and Column T): These columns have been previously discussed in section 3.2.2.1 and are not discussed in this section to avoid repetition.

Corrected cone resistance, q_t (Column U): The corrected cone tip resistance (q_t) represents the cone tip resistance corrected for pore pressure acting on the cone to obtain a more accurate representation of the cone tip resistance in the soil. This is calculated using Equation 30 (Equation 2) (Robertson 1990).

$$q_t = q_c + u_2 * (1-a) \quad \textbf{(Equation 30)}$$

Normalized friction ratio, F_R (Column W): The normalized friction ratio (F_R) is the ratio of the frictional resistance on the sleeve to the corrected cone resistance (qt) at the same depth. It was first proposed by Robertson et al. (1986) and was further developed and refined by Robertson (1990). F_R is calculated as follows (Equation 31):

$$F_R = f_s*100 / (q_t-\sigma_{vo}) \quad \textbf{(Equation 31)}$$

Normalized pore pressure ratio, B_q (Column X): The normalized pore pressure ratio (B_q) is defined as the ratio of the excess pore pressure generated during the CPT to the total vertical stress at the same depth. Equation 32 presents the formula (Robertson 2009; Equation 3) to calculate the normalized pore pressure ratio.

$$B_q = (u_2 – u_0) / (q_t-\sigma_{vo}) \quad \textbf{(Equation 32)}$$

Soil Behavior Type Index, I_{SBT} (Column Y): The soil behavior type index (I_{SBT}) is a parameter commonly used to estimate the soil type from CPT data. The I_{SBT} is the soil's ability to deform plastically and is related to the grain size and plasticity of the soil. A higher I_{SBT} value indicates that the soil is more clay-like. A lower SBI value indicates that the soil is more sand-like. Equation 33 presents the formula (Robertson 2009; Equation 5) to calculate the soil behavior type index.

$$I_c = [(3.47 – \log Q_{tn})^2 + (1.22 + \log F_r)^2]^{0.5} \quad \textbf{(Equation 33)}$$

Stress exponent, n (Column Z): The stress exponent is a parameter used in soil mechanics to describe the relationship between the shear strength of soil and the applied stress.

The stress exponent "n" is typically assumed to be constant for a given soil type, although it may vary depending on the stress level, strain rate, and other factors. Values of "n" for different soil types have been reported in the literature, ranging from around 0.2 to 1.0. In practice, the stress exponent is often determined through laboratory testing on undisturbed soil samples, although empirical correlations based on CPT data are also commonly used. The choice of "n" can significantly affect the estimated undrained shear strength, and it is vital to use an appropriate value based on the specific soil conditions and application. The relationship to calculate the stress component is presented in Equation 34 (Robertson 2009; Equation 7).

$$n = 0.381 * I_c + 0.05 * (\sigma'_{vo} / P_a) -0.15 \leq 1.0 \quad \textbf{(Equation 34)}$$

Normalized cone resistance, Q_{tn} (Column AB): The normalized cone resistance (Q_{tn}) is used to determine the soil behavior type index (I_c), which is a measure of the soil's shear strength and deformation characteristics. Overall, the normalized cone resistance is an essential parameter in interpreting CPT data. The relationship to calculate the normalized cone resistance is presented in Equation 35 (Robertson 2009; Equation 7).

$$Q_{tn} = [(q_t - \sigma_{vo})/Pa]^* C_N \quad \textbf{(Equation 35)}$$

The grain size characteristics correction factor, K_c (Column AC): The grain size characteristics correction factor (K_c) is calculated for the cells whose I_c is between 2.6 and 1.64. The soil behavior type index, I_c, is greater than 2.6 and is likely to be too clay-rich or plastic to liquefy. The equations of the correction factor for grain characteristics, K_c, are adopted from Robertson and Wride 1998. For $I_c > 2.6$, the K_c curve is shown as a dashed line in Youd et al. (2001) (Figure 6). In this spreadsheet, for $I_c > 2.6$, K_c is taken as 3.5, and for $I_c \leq 1.64$ $K_c = 1$ is used. The relationship to calculate the grain characteristics correction factor is presented in Equations 36a to 36c (Youd et al. 2001; Equation 19).

$$K_c = 1; I_c \leq 1.64 \quad \textbf{(Equation 36a)}$$

$$K_c = -0.403*I_c^4 + 5.571 * I_c^3 - 21.63* I_c^2 + 33.475*I_c ; 1.64 < I_c \text{ ,} 2.6 \quad \textbf{(Equation 36b)}$$

$$K_c = 3.5; I_c \geq 2.6 \quad \textbf{(Equation 36c)}$$

Equivalent clean sand value, $(q_{c1N})_{cs}$ (Column AD): The equivalent clean sand tip resistance parameter is used to calculate CRR. This parameter is calculated by Equation 3–37 obtained from Youd et al. 2001 (Equation 18).

$$(q_{c1N})_{cs} = K_c * Q_{tn} \quad \textbf{(Equation 37)}$$

Below is a discussion of the calculations made in columns AE through AL. These column headers are shown in Figure 32 for reference.

AE	AF	AG	AH	AI	AJ	AK	AL
Cyclic Resistance Ratio, $CRR_{7.5, 1\ atm}$ Youd et al. (2001) Eq. 22	Final F.S.	Liquefaction Occurrance Check	Probability of Liquefaction, P_L	Liquefaction Potential Index, LPI Iwasaki et al. (1978)	Integrated Liquefaction Potential Index, LPI Iwasaki et al. (1978)	Liquefaction Potential Index, LPI_{ISH} Maurer et al. (2015)	Integrated Liquefaction Potential Index, LPI_{ISH} Maurer et al. (2015)

Figure 32. Column Headers from Column AE to Column AL in the "Calculations (Youd)" Tab in the CPT-based Worksheet

Cyclic Resistance Ratio ($CRR_{7.5, 1\ atm}$) (Column AE): Each technique requires a different computation. According to Youd et al. (2001), it is computed in this workbook using $(q_{c1N})_{cs}$. If the $(q_{c1})_{cs}$ value is greater than 160, the Youd et al. (2001) approach considers the soil as non-liquefiable. Therefore, a high CRR of 2.0 is assigned. The CRR 2.0 assignment renders the FS computation meaningless. This is considered by giving a value of 2.0 to both the preliminary and final safety criteria. The adopted relationships to calculate CRR (CRR7.5, 1 atm) are shown in Equation 38a and Equation 38b (Youd et al. 2001; Equation 11a–11b).

$$CRR_{7.5} = 0.833*[(q_{c1N})_{cs}/1000] + 0.05;\ (q_{c1N})_{cs} < 50 \qquad \textbf{(Equation 38a)}$$

$$CRR_{7.5} = 93*[(q_{c1N})_{cs}/1000]^3 + 0.08\ ;\ 50 \leq (q_{c1N})_{cs} < 160 \qquad \textbf{(Equation 38b)}$$

Column AF to column AL have been previously discussed and are not discussed in this section to avoid repetition.

Calculation Tables by Youd et al. (2001)

Three tables are contained in the Calculation Tables worksheet. The Calculations worksheet uses LOOKUP functions to determine values from the tables. Included in these four tables are the following: (1) stress reduction coefficient, (2) site classification based on $V_{s,100}$ in the top 100 ft, (3) adopted CPT and V_s correlations, and (4) Exponential f factor table K_σ calculation.

Output and Output Graphs by Youd et al. (2001)

The two output worksheets are described in this section. The user may access graphs in the Output Graphs worksheet to help visualize the examined data. The Input Data and Calculations worksheet integrates data into the Output Worksheet. The main findings from the liquefaction triggering study are presented in a more condensed, printable table in this worksheet (Figure 33). This worksheet reorganizes the input and computations; no new data is entered or calculations are carried out.

CPT Liquefaction Triggering Evaluation for all three procedures [Moss et al (2006), Boulanger and Idriss (2014) and Youd el al (2001)]

Job No:	0
Job Name:	CPT-1
Station:	0
Location:	0
Latitude and Longitude (decimal degrees)	0 0
Logged By :	0
Boring No:	0
Date:	0
Type of Drilling:	0
Cone ID:	0

Site Classification*

Deeper CPT required

*Classification is for reference purposes only, refer to table 3.4.2.1-1 in th Specifications for LRFD Seismic Bridge Design, for more infor

Design Peak Horizontal Ground Acceleration (a_{max}, or	0.237	g's	Data Input by:	0	Date: 1/0/00
Earthquake Moment Magnitude (M_w) =	7.1		Checked by:	0	Date: 1/0/00

Sample Number	Elevation at Sample Location (ft)	Depth to Sample Location (ft)	Tip Resistance, q_c (psf)	Sleeve fiction, f_s (psf)	Pore Pressure, u2 (psf)	Measured Unit Weight of Soil (pcf)	Actual Total Stress, σ_{vo} (psf)	Shear Wave Velocity, Vs (m/s)	Shear Wave Velocity, Vs (m/s) using correlation	Stress Reduction Coefficient, r_d Youd et al. (2001) Eq. 3	Cyclic Stress Ratio, CSR Youd et al. (2001) Eq. 1	Corrected Cone Resistance, qt (psf) Robertson (1990) Eq. 2	Normalized Friction Ratio, Fr Robertson (2009) Eq. 2	Normalized Pore Pressure Ratio, B_q Robertson (2009) Eq. 3	Soil Beh Inde Robertso Eq.
1	229.84	0.16	4180	691.6	-172	115	18.40		109.26	1.00	0.15	4145.6	16.76	-0.042	3.8
2	229.67	0.33	5880	579.6	-344	115	37.95		110.07	1.00	0.15	5811.2	10.04	-0.060	3.5
3	229.51	0.49	5030	635.6	-258	115	56.35		109.83	1.00	0.15	4978.4	12.91	-0.052	3.7
4	229.34	0.66	8720	531.8	-322.666667	115	75.90		113.50	1.00	0.15	8655.466667	6.20	-0.038	3.3

Figure 33. "Output (Youd)" Tab of the CPT-based Liquefaction Triggering Analysis

Calculation and Calculation Tables of Moss et al. (2006)

Magnitude correlation duration weighting factor (DWF_w) (Cell E21): This worksheet calculates the seismic moment magnitude scaling factor using Equation 39 proposed by Moss et al. (2006) (Equation 7). The mentioned equation is stated below:

$$DWF_w = 17.84 * M_w^{-1.43} \qquad \text{(Equation 39)}$$

Depth-dependent Calculations

The calculations that differ from those presented in the Youd et al. (2001) workbook will be discussed below.

Stress Reduction Coefficient (r_d) (Column O): The r_d calculation is complex and subject to several factors. In the Calculation Tables worksheet above the Stress Reduction Coefficient tables, the algebraic formulas are broken up and color-coded with assignments of A, B, C, and D to make them easier to grasp. These tables copy data from the Calculations worksheet, compute the r_d, and display the results. A LOOKUP function in the Calculations worksheet utilizes the tables and provides the correct r_d based on the depth of the sample. Equation 40a and Equation 40b, presented below, are adopted from Moss et al. (2006) (Equation 8 and Equation 9). All the parameters used in these equations are described in previous sections.

For depth (d) < 20m (~65 ft)

$$r_d = \frac{1+\frac{-9.147-4.173*amax+0.652*Mw}{10.567+0.089*e\ ^{\wedge}(0.089*(-d*3.28-7.760*amax+78.575))}}{1+\frac{-9.147-4.173*amax+0.652*Mw}{10.567+0.089*e\ ^{\wedge}(0.089*(-7.760*amax+78.575))}} \quad \text{(Equation 40a)}$$

for depth(d) ≥ 20m (~65 ft)

$$r_d = \frac{1+\frac{-9.147-4.173*amax+0.652*Mw}{10.567+0.089*e\ ^{\wedge}(0.089*(-d*3.28-7.760*amax+78.575))}}{1+\frac{-9.147-4.173*amax+0.652*Mw}{10.567+0.089*e\ ^{\wedge}(0.089*(-7.760*amax+78.575))}} -0.0014*(d*3.28-65) \quad \text{(Equation 40b)}$$

Below is a discussion of the calculations made in columns X through AE. These column headers are shown in Figure 34 for reference.

X	Y	Z	AA	AB	AC	AD	AE
Normalization Exponent, c Moss et al. (2006) Eq 5	Tip Normalization Factor, C_q Moss et al. (2006) Eq 4	Normalized Tip Resistance, $q_{c,1}$ (psf)	Normalized Tip Resistance, $q_{c,1}$ (atm)	Δq_{c1N} (Mpa) Moss et al. (2006) Eq. 18	Δq_{c1N} (atm)	Modified Normalized Tip Resistance, $q_{c,1,mod}$ (atm)	Cyclic Resistance Ratio, $CRR_{7.5,\ 1\ atm}$ Moss et al. (2006) Eq. 21

Figure 34. Column headers from column X to Column AE in the "Output (Moss 2006)" Tab of the CPT-based Liquefaction Workbook

Normalization Exponent, c (Column X): The proposed procedure to include the inherent variability of several types of soil has been shown in Equation 41, adopted from Moss et al. (2006) (Equation 5). The parameters to calculate the normalization exponent are also provided here for reference.

$$C = f_1 * \left(\frac{R_f}{f_3}\right)^{f_2}$$

$$f_1 = x_1 * q_c^{x2}$$

$$f_2 = -(y_1 * q_c^{y2} + y_3)$$

$$f_3 = abs(\log(10 + q_c))\text{^}z1$$

x_1=0.78, x_2=-0.33, y_1=-0.32, y_2=-0.35, y_3=0.49, z_1=1.21 **(Equation 41)**

Tip Normalization Factor, C_q (Column Y): Equation 42, shown below, is the equation to calculate the tip normalization factor, C_q, which will be used to calculate normalized tip resistance. The reference pressure, P_a = 2116 psf and effective stress from column N is used in this equation (Moss et al. 2006; Equation 4). The maximum value of C_q cannot exceed 1.7.

$$C_q = \left(\frac{P_a}{\sigma'_v}\right)^c \leq 1.7 \quad \textbf{(Equation 42)}$$

Normalized Tip Resistance, $q_{c,1}$ (Columns Z and AA): The normalization of tip resistance, $q_{c,1}$ for a given overburden stress is calculated using Equation 43.

$$q_{c,1} = C_q * q_c \quad \textbf{(Equation 43)}$$

Modified Normalized Tip Resistance, $q_{c,1,\_mod}$ (Columns AB–AD): A modification of normalized CPT tip resistance is introduced by Moss et al. (2006) to account for the friction ratio (Equation 44). Δq_c is accounted as 0 when the friction ratio is between 0.5 to 5.

$$q_{c,1,mod} = q_{c,1} + \Delta q_c \quad \textbf{(Equation 44)}$$

Cyclic Resistance Ratio (CRR) (Column AE): The CRR in this column is determined by applying Equation 45 from Moss et al. (2006) (Equation 21). The variables Mw = 7.5, σ'v = 1 atm, FC = 5%, and PL = 15% have all been set to a fixed value.

$$\text{CRR} = \text{p}\left\{\frac{(qc,1^{1.045} + qc,1(0.110*Rf) + (0.001*Rf) + c(1+0.850*Rf) - 0.848*\ln(Mw) - 0.002*\ln(\sigma'\text{v}) - 20.923 + 1.632*\phi^{(-1)}*\text{PL})}{7.177}\right\}$$

(Equation 45)

Probabilistic Evaluation (Column AG): The column headings for the probabilistic evaluation performed in columns AG are included in the worksheet using Equation 20 from Moss et al. (2006). Equation 46 is presented below. All the parameters used in these equations are described in previous sections.

$$\text{PL} = \phi\left[-\frac{(qc,1^{1.045} + qc,1(0.110*Rf) + (0.001*Rf) + c(1+0.850*Rf) - 7.177*\ln(CSR) - 0.848*\ln(Mw) - 0.002*\ln(\sigma'\text{v}) - 20.923)}{1.632}\right]$$

(Equation 46)

Calculations and Calculation Table Worksheets of Boulanger and Idriss (2014)

Depth-dependent Calculations

The remaining computations are connected to a specific CPT measurement depth and are all depth dependent. Again, there are more columns in the Calculations worksheet than in the Input Data workbook. The columns different from the Youd et al. (2001) worksheet will only be discussed.

Stress Reduction Coefficient (r_d) (Column O): This column looks up the value of r_d from a table in the Calculation Tables worksheet using a LOOKUP function like Youd et al. (2001). The user has an option to select the equations of Boulanger and Idriss (2014), shown in Equations 20a through 20c, or the equations to calculate r_d using the equations of Green et al. (2018), presented in Equation 47a to 47c.

$$r_d = (1 - \alpha)\exp(\frac{-z}{\beta}) + \alpha \quad \textbf{(Equation 47a)}$$

$$\alpha = \exp(-4.373 + 0.4491*M) \quad \textbf{(Equation 47b)}$$

$$\beta = -20.11 + 6.247*M \quad \textbf{(Equation 47c)}$$

Stress Correction Factor (C_N) (Column R): The equation used to calculate C_N is a function of $(q_{c1})_{Ncs}$. It is the second circular reference in the Calculations worksheet of Boulanger and Idriss (2014) using Equations 48a and 48b.

$$C_N = (\frac{P_a}{\sigma'_v})^m \quad \textbf{(Equation 48a)}$$

$$m = 1.338 - 0.249 * (qc1Ncs)\text{^}0.264 \quad \textbf{(Equation 48b)}$$

q_{c1N} (Column S): CPT tip penetration resistance is corrected for overburden stress effects calculated using Boulanger and Idriss (2014) (Equation 2.4). The adopted equation is shown below in Equation 49.

$$Q_{c1N} = C_N * q_c/P_a \quad \textbf{(Equation 49)}$$

Δq_{c1N} (Column T): This column calculates Δq_{c1N} using Equation 50 from Boulanger and Idriss (2014) (Equation 2.22), which is the change in blow count according to the percentage of fines. This is added to q_{c1N} to determine $(q_{c1N})_{cs}$.

$$\Delta q_{c1N} = (11.9+q_{c1N}/14.6)\exp\left(1.63 + \frac{9.7}{FC+2} - \left(\frac{15.7}{FC+2}\right)^2\right) \quad \textbf{(Equation 50)}$$

C_σ Coefficient (Column AB): This column calculates the intermediate variable C_σ, which determines K_σ. C_σ is a function of $(q_{c1})_{Ncs}$ and relates the relative density of the soil to K_σ (Boulanger and Idriss 2014; Equation 51).

$$C_\sigma = \frac{1}{37.3 - 8.27 * qc1Ncs\text{^}0.264} \leq 0.3 \qquad \textbf{(Equation 51)}$$

Cyclic Resistance Ratio ($CRR_{M=7.5, \sigma'_v = 1\ atm}$) (Column AF): The liquefaction triggering correlation derived from the maximum likelihood solution is adopted from Boulanger and Idriss (2014) (Equation 50) and shown in Equation 52.

$$CRR_{M=7.5, \sigma'_v = 1\ atm} = \exp\left(\frac{qc1Ncs}{113} + \left(\frac{qc1Ncs}{1000}\right)\text{^}2 - \left(\frac{qc1N\ s}{140}\right)\text{^}3 + \left(\frac{qc1Ncs}{137}\right)\text{^}4 - 2.6 + 0.2 * \Phi\text{^}(-1) * PL\right) \qquad \textbf{(Equation 52)}$$

Probabilistic Evaluation (Column AJ): The column headings for the probabilistic evaluation performed in column AG are included in the worksheet using Equation 5.26 from Boulanger and Idriss (2014). Equation 53 is presented below. All the parameters used in these equations are described in previous sections.

$$P_L = \phi\left[-\frac{\left(\frac{qc1Ncs}{113}\right) + \left(\frac{qc1Ncs}{1000}\right)^2 - \left(\frac{qc1Ncs}{140}\right)^3 + \left(\frac{qc1Ncs}{137}\right)^4 - 2.6 - in(CSR)}{0.2}\right] \qquad \textbf{(Equation 53)}$$

Worksheets of CPT Analysis

This chapter defines the CPT analysis tab and CPT graphs for better understanding to the user. It is prudent to inform the user that in the CPT analysis workbook, columns A to column X are already explained in Calculation and will not be explained to avoid repetition.

Below is a discussion of the calculations made in columns Y through AH. These column headers are shown in Figure 35 for reference.

Y	Z	AA	AB	AC	AD	AE	AF	AG	AH
Check for Z8 or Z9	Check Z1	Check for Z2 or Z3 or Z4	Zone	Normalized Soil Behavior Type, SBT_n (Robertson 1990; Robertson 2009)	Apparent Fines Content, FC % Robertson and Wride (1998) Eq. 6	Permeability, k (m/s) CPT Guide-2012 pg 52	$N_{(60)}$ CPT Guide-2012 pg 34	Young's Modulus, Es (Mpa) CPT Guide-2012 pg 70	Relative Density, Dr (%) Mayne (2014) Eq 10

Figure 35. Column Headers from Column Y to Column AH in the "CPT Analysis" Tab of the CPT-based Liquefaction Workbook

Soil Behavior Zone (Column Y to Column AB): These columns classify the soil layer based on soil behavior type index (I_{SBT}) and friction ratio (R_f) based on Robertson's (2009) procedure. Zones 2–7 are calculated based on I_{SBT}, whereas Equation 54b is used to classify soil layers as Zone 1. When the friction ratios of soil layers are between 1.5% to 4.5% and follow Equation 54a, it is in Zone 8, and when the friction ratio is greater than 4.5% and follows Equation 54a, the soil layers are defined in Zone 9. Column AB shows the defined zonation of each layer. Table 5 presents the soil behavior type for each zone and the soil behavior type index boundaries for each zone.

$$Q_{tn} \geq \frac{1}{0.006*(R_f-0.9)-0.0004*(R_f-0.9)^2-0.002} \quad \textbf{(Equation 54a)}$$

$$Q_{tn} \geq 12 * e^{(-1.4*R_f)} \quad \textbf{(Equation 54b)}$$

Table 5. Soil Behavior Type and Soil Behavior Index Boundaries for Each Zone

Zone	Soil Behavior Type	I_c
1	Sensitive, fine-grained	Equation 3–54b
2	Organic soils: clay	> 3.6
3	Clays: silty clay to clay	2.95–3.6
4	Silt mixtures: clayey silt to silty clay	2.60–2.95
5	Sand mixtures: silty sand to sandy silt	2.05–2.6
6	Sands: clean sand to silty sand	1.31–2.05
7	Gravelly sand to dense sand	< 1.31
8	Very stiff sand to clayey sand	Equation 3–54a
9	Very stiff, fine-grained	Equation 3–54a

Normalized Soil Behavior Type, SBTn (Robertson 2009) (Column AC): This column provides the normalized soil behavior type based on Robertson's (2009) procedure.

Apparent Fines Content, FC % (Robertson and Wride 1998) (Column AD): This column calculates the apparent fines content of the soil layer based on Robertson and Wride's (1998) procedure and presented below in Equations 55a–55c.

$$\textbf{FC (\%)=0; if } I_c < 1.26 \qquad \textbf{(Equation 55a)}$$

$$\textbf{FC (\%)= } 1.75*(I_c)^{3.75} - 3.7; \textbf{ if } 1.26 \leq I_c \leq 3.5 \qquad \textbf{(Equation 55b)}$$

$$\textbf{FC (\%)=1000, if } I_c > 3.5 \qquad \textbf{(Equation 55c)}$$

Permeability, k (m/s) (Column AE): The correlations mentioned below in Equations 56a and 56b can be utilized to indicate the anticipated variation of soil permeability with depth from a CPT sounding and to offer a rough estimate of soil permeability (k). The suggested relationship between k and I_c is

approximate and should only be used as a general reference because the normalized CPT parameters (Q_{tn} and F_r) respond to the mechanical behavior of the soil and depend on several soil characteristics.

$$k\ (m/s) = 10^{(0.952 - 3.04 * Ic)};\ If\ I_c \leq 3.27 \quad \textbf{(Equation 56a)}$$

$$k\ (m/s) = 10^{(-4.52 - 1.37 * Ic)};\ If\ I_c > 3.27 \quad \textbf{(Equation 56b)}$$

$N_{(60)}$ (Column AF): Jefferies and Davies (1993) suggested the application of the soil behavior type index, I_c, to link with the CPT-SPT correlation. The soil behavior type index, I_c, can be combined with the CPT-SPT ratios for a relationship. Robertson (2012) suggested an update of that relationship that provides improved estimates of N60 for insensitive clays and is presented below in Equation 57.

$$N_{60} = \frac{Q_{tn}}{10^{(1.1268 - 0.2817 * Ic)}} \quad \textbf{(Equation 57)}$$

Young's Modulus, E_s (MPa) (Column AG): CPT data can be employed to calculate a soil's modulus for use in elastic or semi-empirical settlement prediction techniques (Equation 58). Young's moduli (E) and q_c correlations are subject to past stress and strain, age, and soil mineralogy. This relationship can only be applicable when $I_c < I_{c,\ cutoff}$ (Zone 5 to Zone 8).

$$E_s = 0.015 * 10^{(0.55 * Ic + 1.68)} \quad \textbf{(Equation 58)}$$

Relative Density, D_r (%) (Column AH): Kulhawy and Mayne (1990) suggested a more straightforward relationship for estimating relative density, which is presented in Equation 59 and can only be applicable when $I_c < I_{c,\ cutoff}$ (Zone 5 to Zone 8).

$$D_r = \sqrt{\frac{Q_{tn}}{350}} \quad \textbf{(Equation 59)}$$

Below is a discussion of the calculations made in columns AI through AT. These column headers are shown in Figure 36 for reference.

AI	AJ	AK	AL	AM	AN	AO	AP	AQ	AR	AS	AT
State Parameter, Ψ CPT Guide-2012 pg 44	Peak Drained Friction Angle, Θ (◦) Mayne (2014) Eq 17	α_M CPT Guide-2012 pg 58	1-D constrained modulus, M (Mpa) CPT Guide-2012 pg 58	Small Strain Shear Modulus, Go (Mpa) Robertson (2009) Eq 14	Undrained peak shear strength, Su (kPa) Mayne (2014) Eq 29	Remolded undrained shear strength, Su(rem) (kPa) Mayne (2014) Eq 31	k_{OCR}	Over Consolidation Ratio, OCR Robertson (2009) Eq 29	In Situ Stress Ratio, Ko	Soil Sensitivity, St	Effective Stress Friction Angle, ϕ' (Degree)

Figure 36. Column Headers from Column AI to Column AT in the "CPT Analysis" Tab of the CPT-based Liquefaction Workbook

State Parameter, ψ (Column AI): Robertson (2010) suggested a simplified and approximate relationship between ψ and the clean sand equivalent normalized cone resistance, Qtn presented in Equation 60 and can only be applicable when $I_c < I_{c,\ cutoff}$ (Zone 5 to Zone 8).

$$\Psi = 0.56 - 0.33 * \log Q_{tn} \quad \text{(Equation 60)}$$

Peak Drained Friction Angle, Φ' (Column AJ): Kulhawy and Mayne (1990) suggested a relationship for peak drained friction angle for clean, rounded, uncemented quartz sands presented in Equation 61.

$$\phi' = 17.6 + 11 * \log Q_{tn} \quad \text{(Equation 61)}$$

1-D constrained modulus, M (Mpa) (Column AK and Column AL): Estimates of drained 1-D constrained modulus from undrained cone penetration will be approximate. Estimates can be improved with additional information about the soil, such as plasticity index and natural water content, where αM can be lower in organic soils and soils with high water content. 1-D constrained modulus can be estimated from CPT results using the empirical relationship presented in Equation 62a. Robertson (2009) suggested that α_M varies with Q_t, and the adopted relationships to calculate α_M are presented in Equations 62b to 62d.

$$M = \alpha_M (q_t - \sigma_{vo}) \quad \text{(Equation 62a)}$$

$$\alpha_M = q_t \text{ when } q_t < 14; \text{ When } I_c > 2.2 \text{ (fine-grained soils)} \quad \text{(Equation 62b)}$$

$$\alpha_M = 14 \text{ when } q_t > 14; \text{ When } I_c > 2.2 \text{ (fine-grained soils)} \quad \text{(Equation 62c)}$$

$$\alpha_M = 0.0188 * 10^{(0.55Ic + 1.68)};\ I_c < 2.2 \text{ (coarse-grained soils)} \quad \text{(Equation 62d)}$$

Small Strain Shear Modulus, G_o (Mpa) (Column AM): The small strain shear modulus, G_O, can be estimated using Equation 63, which is proposed by Robertson (2009).

$$G_O = 0.0188 * 10^{(0.55 * Ic + 1.68)} * (q_t - \sigma_{vo}) \quad \textbf{(Equation 63)}$$

Undrained peak shear strength, S_u (kPa) (Column AN): It is more common to find geotechnical practitioners directly evaluating S_u from net cone resistance where the factor N_{kt} depends upon the mode of testing (e.g., vane, triaxial compression, simple shear, triaxial extension) and can be calculated using Equations 64a and 64b and can only be applicable when $I_c > I_{c,\ cutoff}$ (Zone 1 to Zone 4 and Zone 9).

$$S_u = \frac{(q_t - \sigma'_{vo})}{N_{kt}} \quad \textbf{(Equation 64a)}$$

$$N_{kt} = 10.5 - 7 * logF_r \quad \textbf{(Equation 64b)}$$

Remolded undrained shear strength, $S_{u(rem)}$ (kPa) (Column AO): The remolded shear strength may be assessed from the sleeve friction (Equation 65) and can only be applicable when $I_c > I_{c,\ cutoff}$ (Zone 1 to Zone 4 and Zone 9).

$$S_{u(rem)} \approx f_s \quad \textbf{(Equation 65)}$$

Over Consolidation Ratio, OCR (Column AP and Column AQ): The overconsolidation ratio can be calculated using Equations 66a and 66b, adopted from Robertson's (2009) procedure, and can only be applicable when $I_c > I_{c,\ cutoff}$ (Zone 1 to Zone 4 and Zone 9).

$$OCR = k_{OCR} * Q_{tn} \quad \textbf{(Equation 66a)}$$

$$k_{OCR} = \left[\frac{Q_{tn}^{0.2}}{0.25 * (10.5 + 7 * \log(F_r))}\right]^{1.25} \quad \textbf{(Equation 66b)}$$

In Situ Stress Ratio, K_o (Column AR): The in-situ stress ratio is calculated using Equations 3–67 and can only be applicable when $I_c > I_{c,\ cutoff}$ (Zone 1 to Zone 4 and Zone 9).

$$K_o = 0.1 * \left(\frac{q_t - \sigma_v}{\sigma_{vo}}\right) \quad \textbf{(Equation 67)}$$

Soil Sensitivity, S_t (Column AS): The sensitivity (S_t) of clay is defined as the ratio of undisturbed peak undrained shear strength to remolded undrained shear strength and can be calculated using Equation 68 and can only be applicable when $I_c > I_{c,\ cutoff}$ (Zone 1 to Zone 4 and Zone 9).

$$S_t = \frac{7.1}{F_r} \quad \textbf{(Equation 68)}$$

Effective Stress Friction Angle, ϕ' (Column AT): In a simplified approach for normally to lightly overconsolidated clays and silts (c' = 0), the effective stress friction angle, ϕ' can be approximated for the following ranges of parameters: 20º ≤ ϕ' ≤ 40º and 0.1 ≤ B_q ≤ 1.0 (Mayne 2006) and presented in Equation 69.

$$\phi' \text{ (deg)} = 29.5^{\circ} * B_q^{0.121} [0.256 + 0.336 \cdot B_q + \log q_t] \quad \text{(Equation 69)}$$

In the CPT graphs tab, columns A to X presented the data found in the CPT analysis. It is prudent to notify the user that, in this workbook total of 24 charts have been displayed: (1) soil behavior type index, I_{SBT} plot (boundary lines for this plot can be viewed in columns AZ to BE); (2) SBTn plot (boundary lines for this plot can be viewed in columns BG to BV); (3) normalized cone resistance, Q_{tn}; (4) normalized friction ratio, F_r; (5) B_q; (6) corrected tip resistance, q_t; (7) tip resistance, q_c; (8) sleeve friction, F_s; (9) pore pressure, U_2; (10) permeability, k; (11) $(N_1)_{60}$; (12) Young's Modulus, E_s; (13) state parameter; (14) drained peak friction angle; (15) shear wave velocity, V_s; (16) 1-D constrained modulus; (17) small strain shear modulus; (18) undrained peak shear strength; (19) remolded undrained peak shear strength; (20) relative density; (21) overconsolidation ratio; (22) in situ stress ratio; (23) soil sensitivity; (24) effective stress friction angle.

Comparison

The liquefaction triggering workbooks that have been developed in this work enable easy data transfer between workbooks and facilitate quick and simple comparisons between all three procedures. The "Comparison" tab was created to view the comparative results of the liquefaction analysis (Figure 37). The results of equivalent clean sand blow count [$(q_{1,CN})_{cs}$], normalized cone resistance, stress reduction coefficient (r_d), overburden blow count correction factor (C_N), overburden correction factor (K_σ), cyclic stress ratio (CSR), cyclic resistance ratio (CRR), factor of safety (FS), and probability of liquefaction (PL) can be viewed in this tab. These outputs have an input number from 3 to 9 in the same order. The user needs to select the input number from the dropdown list at cell D2 to view the desired output. A VLOOKUP function is used, and the corresponding liquefaction analysis results can be viewed from columns E to G. The figure will automatically change according to the input number. The user can view the comparative continuous results of the adopted procedures. It should be noted that except for cell B2, no other cell should be altered.

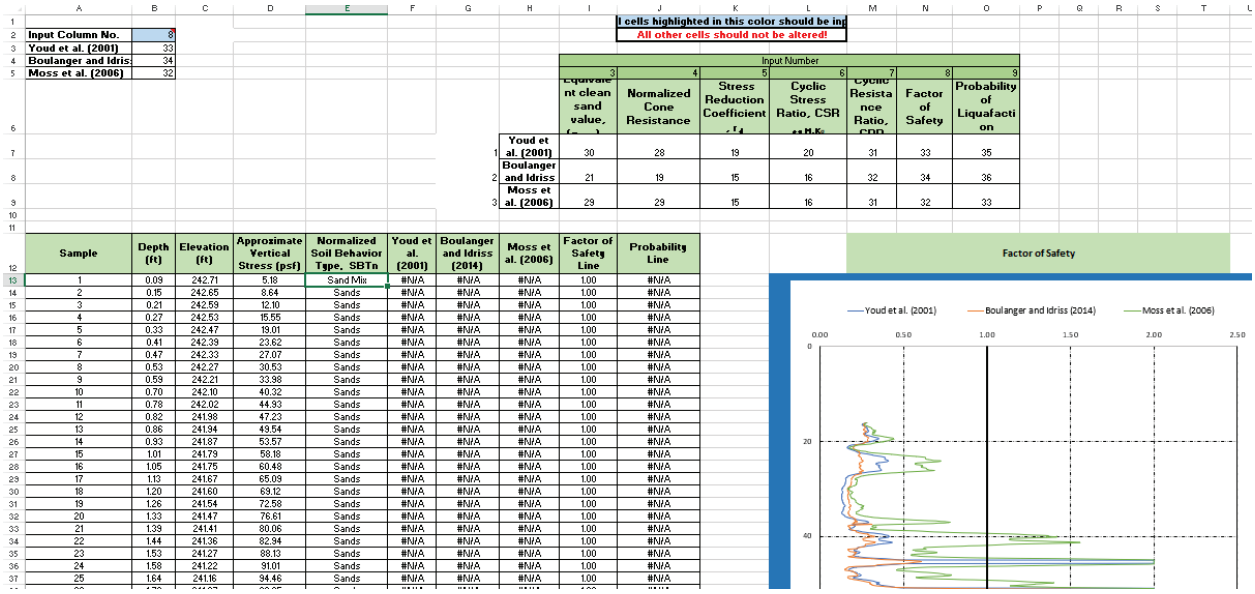

Figure 37. "Comparison" Tab of the CPT-based Liquefaction Triggering Workbook

Layer Comparison

This tab has been developed to provide discontinuous CPT data. One of the purposes of this work is to compare co-located SPT, CPT, and V_s data and complete a sensitivity study using the spreadsheet to understand any differences between the procedures and methods. This tab can convert continuous CPT results into 2.5' or 5' layered discontinuous CPT results. The layout of this tab is the same as the "comparison" tab, described earlier. To view the desired output, the user needs to select the input number from the dropdown list at cell D2. Additionally, the user needs to choose the layer thickness from the dropdown list at cell B7 (Figure 38). It should be noted that, except for cells B2 and B7, no other cell should be altered.

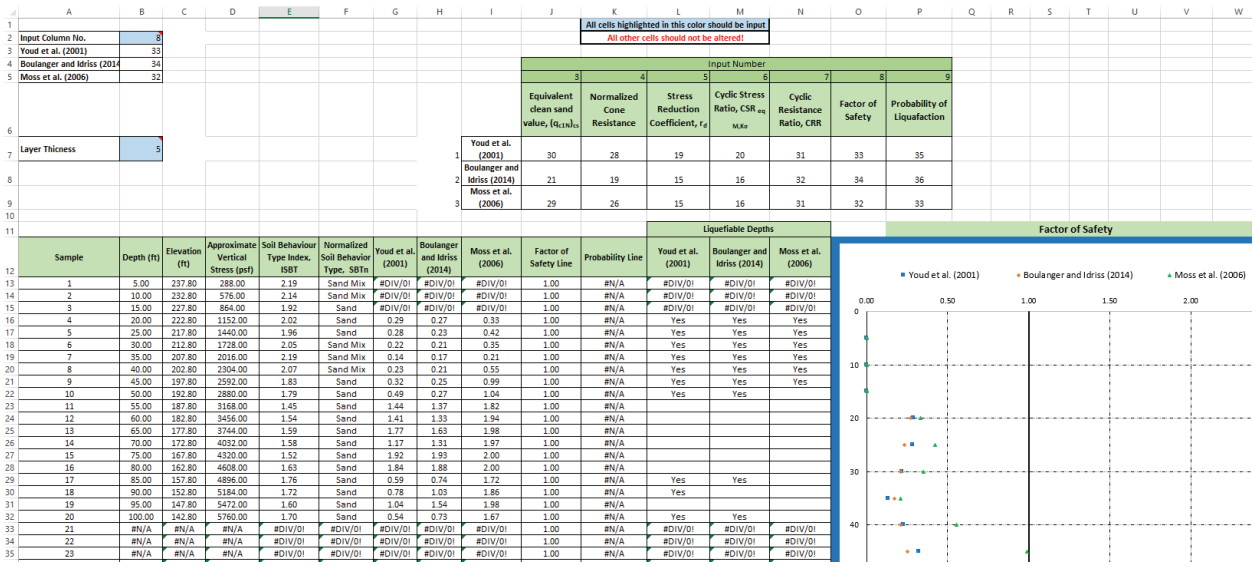

Figure 38**. "Layer comparison" Tab of the CPT-based Liquefaction Triggering Tab**

The user needs to enable the iterative calculation option in Excel before performing CPT analysis. To do this, the user needs to select File > Options > Formulas > Enable Iterative Calculation. Also, in the "CPT Analysis" tab, the user needs to perform iterative calculations manually in column V. The user needs to click the lower left corner of cell V22 to perform the iterative calculation for column V to perform the iterative calculation. Similarly, in the "Calculations (B & I 2014)" tab, the user needs to click the lower left corner of cell U27 to perform iterative calculations for column U.

V_s-based Workbook Review

The two most popular V_s-based liquefaction triggering procedures (Youd et al. 2001; Kayen et al. 2013) have been programmed in Microsoft Excel workbooks. The different tabs of this Excel workbook are divided and marked with color codes for better understanding. The "Data Conversion", a purple-colored tab, will convert the raw V_s data to units of meter per second, which will be used in the workbook for further calculations. The "Input data tab", which the user will use to input data for analysis, is green. The "Layer Comparison", "Comparison", and "Liquefaction manifestation" tabs are red and show the results of the two liquefaction triggering procedures used in this Excel workbook. The calculation tab and the supplementary tabs for Youd et al. (2001) and Kayen et al. (2013) are blue and yellow, respectively. The user can also view the references used in this Excel workbook in the last tab titled References (Figure 39). The two calculation tabs for Youd and Kayen are as identical as feasible to simplify data entry and information sharing amongst workbooks. A thorough discussion about the Youd et al. (2001) workbook will be examined following a brief section highlighting the commonalities between the workbooks. The

workbooks from Kayen et al. (2013) will be thoroughly investigated after the discussion of Youd et al. (2001). The discussion of the Kayen et al. (2013) sheets will concentrate on the areas that differ from the workbook by Youd et al. (2001), as many of the computations are identical to Youd et al. (2001). Discussing the overall style and format of the workbook before starting each section is prudent.

Figure 39**. Individual Worksheet Tabs Within the Liquefaction Triggering Workbooks**

Data Conversion

The data conversion tab in the workbook can convert the units (ft/sec to m/sec and m to ft) (shear wave velocity and depth). Cells D11 and E11 have a drop-down list where the user can choose the raw units, and it can convert the data to the desired units. The user needs to paste the data in colored cells in column D to column E, and after choosing the raw units, the workbook can convert the units in column G to column H. Cells other than light blue should not be altered. If no shear wave velocity is provided for a layer, it would be better to use the shear wave velocity of the adjacent layers. Figure 40 presents an image of the data conversion tab in the shear wave velocity workbook.

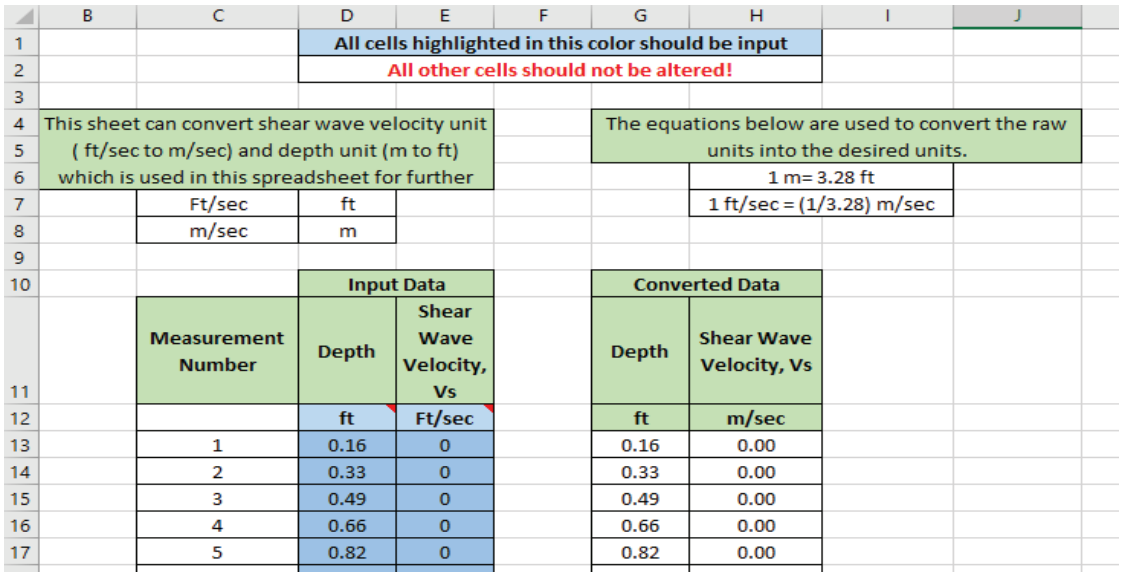

	B	C	D	E	F	G	H	I	J
1			All cells highlighted in this color should be input						
2			All other cells should not be altered!						
3									
4	This sheet can convert shear wave velocity unit					The equations below are used to convert the raw			
5	(ft/sec to m/sec) and depth unit (m to ft)					units into the desired units.			
6	which is used in this spreadsheet for further						1 m= 3.28 ft		
7		Ft/sec	ft				1 ft/sec = (1/3.28) m/sec		
8		m/sec	m						
9									
10			Input Data			Converted Data			
11		Measurement Number	Depth	Shear Wave Velocity, Vs		Depth	Shear Wave Velocity, Vs		
12			ft	Ft/sec		ft	m/sec		
13		1	0.16	0		0.16	0.00		
14		2	0.33	0		0.33	0.00		
15		3	0.49	0		0.49	0.00		
16		4	0.66	0		0.66	0.00		
17		5	0.82	0		0.82	0.00		

Figure 40. Data Conversion Tab for Shear Wave Velocity Workbook

Input Data

The Input tab in the workbook is where all site-specific data will be manually added to the workbook. An image of the general input information for the Input tab is provided in Figure 41. Most of the input data required for evaluating soil liquefaction triggering will come from the V_s measurements collected during the site investigation and other tests. The project data should only be updated in the cells marked in light gray. No other cells should be changed in this workbook. Rows E4 to E9, the first set of input fields, are located at the top of the Input Data worksheet and are used to identify jobs by their job number, name, station, and location (latitude and longitude, etc.). Most of these cells are simply used for documentation. The cells E11–E14 contain the Design Peak Horizontal Ground Acceleration (a_{max} or A_s), Earthquake Moment Magnitude (M_w), Boring Surface Elevation, and Ground Water Level (depth below ground surface). Below, each of these topics is covered in further detail.

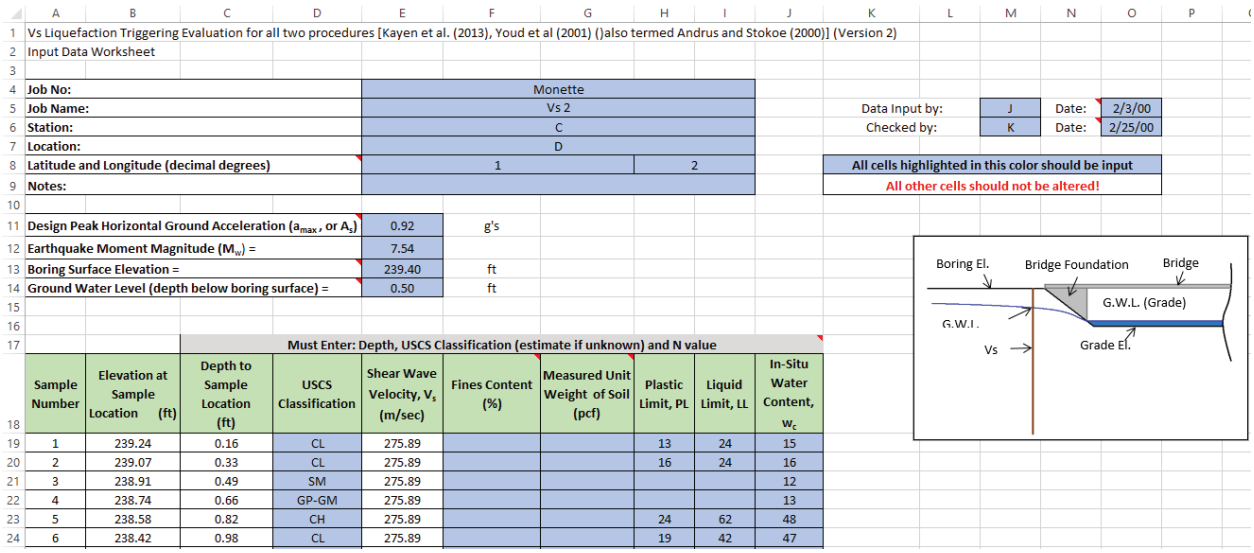

Vs Liquefaction Triggering Evaluation for all two procedures [Kayen et al. (2013), Youd et al (2001) ()also termed Andrus and Stokoe (2000)] (Version 2)

Input Data Worksheet

Job No:	Monette		
Job Name:	Vs 2		
Station:	C		
Location:	D		
Latitude and Longitude (decimal degrees)	1	2	
Notes:			

Data Input by: J Date: 2/3/00
Checked by: K Date: 2/25/00

All cells highlighted in this color should be input
All other cells should not be altered!

Design Peak Horizontal Ground Acceleration (a_{max}, or A_s)	0.92	g's
Earthquake Moment Magnitude (M_w) =	7.54	
Boring Surface Elevation =	239.40	ft
Ground Water Level (depth below boring surface) =	0.50	ft

Must Enter: Depth, USCS Classification (estimate if unknown) and N value

Sample Number	Elevation at Sample Location (ft)	Depth to Sample Location (ft)	USCS Classification	Shear Wave Velocity, V_s (m/sec)	Fines Content (%)	Measured Unit Weight of Soil (pcf)	Plastic Limit, PL	Liquid Limit, LL	In-Situ Water Content, w_c
1	239.24	0.16	CL	275.89			13	24	15
2	239.07	0.33	CL	275.89			16	24	16
3	238.91	0.49	SM	275.89					12
4	238.74	0.66	GP-GM	275.89					13
5	238.58	0.82	CH	275.89			24	62	48
6	238.42	0.98	CL	275.89			19	42	47

Figure 41. "Input Data" Tab of the V_s Worksheet with Job Identification Information and Site-specific Input Options

Depth-dependent Input Data

All the remaining input data is depth-dependent. Figure 42 displays the column headers for columns A through K. The user will notice that columns A, B, C, and E are automatically copied from the data conversion tab. This spreadsheet can calculate the unit weight, so if the unit weight of the soil sample is unknown, it should be kept empty. If other column cells are not available, leave the cell empty, and a conservative value (i.e., an FC of 5%) will be assigned. Plastic Limit, Liquid Limit, and In-situ Water Content assist in establishing the fine-grained liquefaction susceptibility of the soil. Leave these cells empty if this information has not been established or the soil is not plastic.

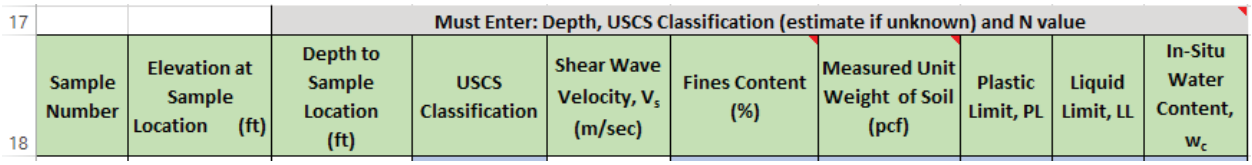

Must Enter: Depth, USCS Classification (estimate if unknown) and N value

Sample Number	Elevation at Sample Location (ft)	Depth to Sample Location (ft)	USCS Classification	Shear Wave Velocity, V_s (m/sec)	Fines Content (%)	Measured Unit Weight of Soil (pcf)	Plastic Limit, PL	Liquid Limit, LL	In-Situ Water Content, w_c

Figure 42. Headings for Depth-dependent Parameters in the "Input Data" Tab of the V_s Worksheet

Calculations Worksheet of Youd et al. (2001)

Depth-dependent Calculations

The remaining calculations are all depth-dependent. The user will observe many more filled-in columns in the Calculations worksheet than in the Input Data worksheet (i.e., from column K through column AL). Each column heading in the Calculations worksheet will be examined here in the same order that they are displayed in the worksheet for the sake of clarity. Below is a discussion of the calculations made in columns K through S. These column headers are shown in Figure 43 for reference.

K	L	M	N	O	P	Q	R	S
Calculation Table.								
General Soil Type	Plasticity Index, PI	w_c/LL	Thickness (ft)	Unit Weight of the Soil (pcf) Mayne 2014 Eq 1	Total Stress in Each Layer (psf)	Actual Total Stress, σ_{vo} (psf)	Pore Water Pressure (psf)	Effective Stress, σ'_{vo} (psf)

Figure 43. Column Headers from Column K to Column S in the "Calculations (Youd) tab of the V_s Worksheet

All the columns, except column O, have been previously discussed and are not discussed in this section to avoid repetition.

Unit Weight of the Soil (Column O): This column calculates the unit weight of the soil using correlations of Mayne (2014). This column is necessary for liquefaction analysis if no unit weight data is provided, which is randomly available. The adopted correlation from Mayne (2014) is shown in Equation 70.

$$\Gamma_t = 8.32*\log(V_s) - 1.61*\log(z), \quad \text{(Equation 70)}$$

where, γ_t is in KN/m^3, V_s is in m/s, and depth, z is in meter.

Below is a discussion of the calculations made in columns U through AC. These column headers are shown in Figure 44 for reference.

U	V	W	X	Y	Z	AA	AB	AC
	Calculation Table.							Calculation Table.
d_i/V_{si} for Site Classification	Cumulative d_i/V_{si} for Site Classification	Stress Reduction Coefficient, r_d Youd et al. (2001)	Cyclic Stress Ratio, CSR Youd et al. (2001) Eq. 1	C_v	Overburden-stress corrected shear-wave velocity, V_{s1}	V_{s1}^* Andrus & Stokoe(1998) Eq 11	Cyclic Resistance Ratio, $CRR_{7.5, 1\ atm}$ Youd et al. (2001) Eq. 22	Preliminary Factor of Safety, F.S. Youd et al. (2001) Eq. 30

Figure 44. Column Headers from Column U to Column AC in the "Calculations (Youd) Tab of the V_s Worksheet

Columns U to X have been previously discussed. These columns are not discussed in this section to avoid repetition.

Stress Correction Factor (C_V) (Column Y): The stress correction factor is calculated using the effective stress calculated at the depth of interest. The adjusted shear wave velocity, as a function of depth, is strongly controlled by C_V. This correlation is presented below as Equation 71 (same as Youd et al. [2001]), where effective stress is defined previously, and a 1.0 atmospheric pressure (P_a) of 2116 psf is used. This equation limits the maximum C_V value of 1.4.

$$C_V = (P_a/\sigma'_v)^{0.25} \leq 1.4 \qquad \textbf{(Equation 71)}$$

Overburden-stress corrected shear wave velocity, V_{s1} (Column Z): The stress correction factor is multiplied by the shear wave velocity to determine the overburden-stress corrected shear wave velocity using Equation 72 described in Youd et al. (2001).

$$V_{s1} = V_s * C_V \qquad \textbf{(Equation 72)}$$

Limiting velocity, V_s^* (Column AA): The limiting velocity for the liquefaction of soils can be measured using Equations 11a to 11c, adopted from Andrus and Stokoe (2000). If the Fines content is less than 5, the limiting velocity is 215, whereas, for layers with Fines content higher than 35, the limiting value is 200. It varies between those values according to Equation 73.

$$V_s^* = 215 - 0.5*(FC - 5) \qquad \textbf{(Equation 73)}$$

Cyclic Resistance Ratio (CRR7.5, 1 atm) (Column AB): Each technique requires a different computation. According to Youd et al. (2001), it is computed in this workbook using V_{s1} and V_s^*. If the V_{s1} is greater

than V_s^*, the soil is considered non-liquefiable, which renders the FS computation meaningless (Equation 74).

$$\mathbf{CRR_{M=7.5,\ \sigma'_v\ =1\ atm}} = \mathbf{0.022} * \left(\frac{V_{s1}}{100}\right)^2 + \mathbf{2.8} * \left(\frac{1}{V_{S1}^* - V_S} - \frac{1}{V_{S1}^*}\right) \qquad \textbf{(Equation 74)}$$

Calculation Tables worksheet of Youd et al. (2001)

Three tables are contained in the Calculation Tables worksheet. The Calculations worksheet uses LOOKUP functions to determine values from the tables. Included in these seven tables are the following: (1) Stress Reduction Coefficient, (2) Soil classification based on USCS, and (3) Site Classification based on $V_{s,100}$ in the top 100 ft. These tables are provided to simplify programming in the Calculations worksheet.

Output and Output Graphs Worksheets of Youd et al. (2001)

The two output worksheets are described in this section. The user may access graphs in the Output Graphs worksheet to help visualize the examined data. The Input Data and Calculations worksheet integrates data into the Output Worksheet. The main findings from the liquefaction triggering study are presented in a more condensed, printable table in this worksheet (Figure 45). This worksheet reorganizes the input and computations; no new data is entered, or calculations are carried out.

The Output Graphs worksheet is made to make it simple and quick for the user to understand the liquefaction results visually. Four graphs are shown in this output graphs worksheet. The necessary data to plot the graphs are summarized in columns A to E. The plots of the factor of safety chart, Bray and Sancio's (2006) criteria, V_{s1} as a function of CSR. A suggested curve is also plotted to visualize the liquefiable soil), and a comparison of Cyclic Stress Ratio (CSR) and Cyclic Resistance Ratio (CRR) as a function of depth is located near the top of the worksheet in columns K to Z.

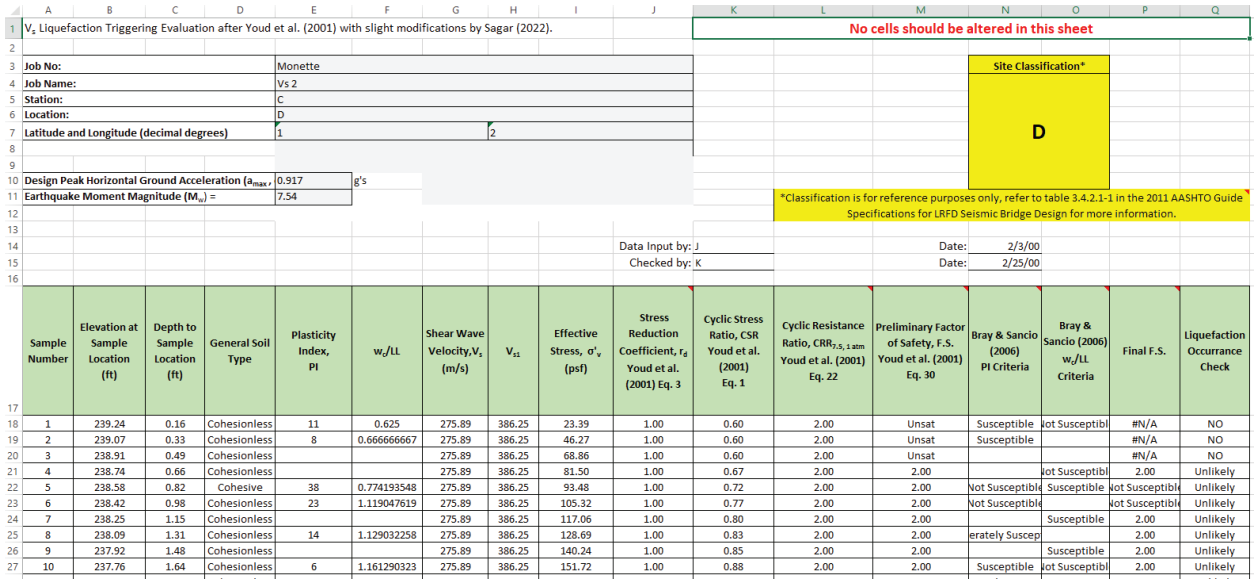

V_s Liquefaction Triggering Evaluation after Youd et al. (2001) with slight modifications by Sagar (2022).

No cells should be altered in this sheet

Job No:	Monette
Job Name:	Vs 2
Station:	C
Location:	D
Latitude and Longitude (decimal degrees)	1 / 2
Design Peak Horizontal Ground Acceleration (a_{max})	0.917 g's
Earthquake Moment Magnitude (M_w) =	7.54

Site Classification*: **D**

*Classification is for reference purposes only, refer to table 3.4.2.1-1 in the 2011 AASHTO Guide Specifications for LRFD Seismic Bridge Design for more information.

Data Input by: J — Date: 2/3/00

Checked by: K — Date: 2/25/00

Sample Number	Elevation at Sample Location (ft)	Depth to Sample Location (ft)	General Soil Type	Plasticity Index, PI	w_c/LL	Shear Wave Velocity, V_s (m/s)	V_{s1}	Effective Stress, σ'_v (psf)	Stress Reduction Coefficient, r_d Youd et al. (2001) Eq. 3	Cyclic Stress Ratio, CSR Youd et al. (2001) Eq. 1	Cyclic Resistance Ratio, $CRR_{7.5,1\,atm}$ Youd et al. (2001) Eq. 22	Preliminary Factor of Safety, F.S. Youd et al. (2001) Eq. 30	Bray & Sancio (2006) PI Criteria	Bray & Sancio (2006) w_c/LL Criteria	Final F.S.	Liquefaction Occurrance Check
1	239.24	0.16	Cohesionless	11	0.625	275.89	386.25	23.39	1.00	0.60	2.00	Unsat	Susceptible	ot Susceptibl	#N/A	NO
2	239.07	0.33	Cohesionless	8	0.666666667	275.89	386.25	46.27	1.00	0.60	2.00	Unsat	Susceptible		#N/A	NO
3	238.91	0.49	Cohesionless			275.89	386.25	68.86	1.00	0.60	2.00	Unsat			#N/A	NO
4	238.74	0.66	Cohesionless			275.89	386.25	81.50	1.00	0.67	2.00	2.00		ot Susceptibl	2.00	Unlikely
5	238.58	0.82	Cohesive	38	0.774193548	275.89	386.25	93.48	1.00	0.72	2.00	2.00	Not Susceptible	Susceptible	ot Susceptibl	Unlikely
6	238.42	0.98	Cohesionless	23	1.119047619	275.89	386.25	105.32	1.00	0.77	2.00	2.00	Not Susceptible		ot Susceptibl	Unlikely
7	238.25	1.15	Cohesionless			275.89	386.25	117.06	1.00	0.80	2.00	2.00		Susceptible	2.00	Unlikely
8	238.09	1.31	Cohesionless	14	1.129032258	275.89	386.25	128.69	1.00	0.83	2.00	2.00	erately Suscep		2.00	Unlikely
9	237.92	1.48	Cohesionless			275.89	386.25	140.24	1.00	0.85	2.00	2.00		Susceptible	2.00	Unlikely
10	237.76	1.64	Cohesionless	6	1.161290323	275.89	386.25	151.72	1.00	0.88	2.00	2.00	Susceptible	ot Susceptibl	2.00	Unlikely

Figure 45. The "Output (Youd)" Tab of the V_s Worksheet with Summary of the Liquefaction Triggering Analysis Results

Calculations Worksheet of Kayen et al. (2013)

Duration weighting factor (DWF) (Cell E16): This worksheet calculates the seismic moment magnitude scaling factor using Equation 75, proposed by Cetin et al. (2018). The mentioned equation is stated below:

$$DWF = 15*(M_w)^{-1.342} \qquad \text{(Equation 75)}$$

Average Shear wave velocity over top 40 ft (12 meters) ($V_{s,12\ m}$) (Cell E18): Kayen et al. (2013) uses the average shear wave velocity over the top 12 m (40 ft) [$V_{s,12\ m}$] to calculate r_d. Cells E30 in the Calculations workbook displays the average shear wave velocity value. They are included in these cells because they are non–non-depth-dependent parameters.

Depth-dependent Calculations

The calculations that differ from those presented in the Youd et al. (2001) workbook will be discussed below.

Stress Correction Factor (C_{vs}) (Column O): This column's overburden stress correction factor is used to produce the standardized shear wave velocity. The stress correction (C_{vs}) is affected by the vertical

effective overburden stress (σ'_v), normalized reference stress (Pa), and the stress exponent 0.25. At shallow depths, where the effective overburden stress is small, the writers recommend that C_{vs} be capped at 1.5 (Equation 76).

$$C_{Vs} = (P_a/\sigma'_v)^{0.25} \leq 1.5 \quad \textbf{(Equation 76)}$$

Stress Reduction Coefficient (r_d) (Column Y): The r_d calculation is complex and subject to several factors. In the Calculation Tables worksheet above the Stress Reduction Coefficient tables, the algebraic formulas are broken up and color-coded with assignments of A, B, C, D, and E to make them easier to grasp. These tables copy data from the Calculations worksheet, compute the r_d, and display the results. A LOOKUP function in the Calculations worksheet utilizes the tables and provides the correct r_d based on the depth of the sample. Equation 77 and Equation 78, presented below, are adopted from Kayen et al. (2013). All the parameters used in these equations are described in previous sections.

For depth (d) < 20 m (~65 ft)

$$r_d = \frac{1+\frac{-23.013-2.949*\ \max+0.999*Mw+0.0525*Vs,12}{16.258+0.201*e\ \hat{}\ (0.341*(-d+0.0785*Vs,12+7.586))}}{1+\frac{-23.013-2.949*\ ma\ +0.999*Mw+0.0525*Vs,12}{16.258+0.201*e\ \hat{}\ (0.341*(0.0785*Vs,12+7.586))}} \quad \textbf{(Equation 77)}$$

for depth(d) ≥ 20 m (~65 ft)

$$r_d = \frac{1+\frac{-23.013-2.949*\ \max+0.999*Mw+0.0525*Vs,12}{16.258+0.201*e\ \hat{}\ (0.341*(-20+0.0785*Vs,12+7.586))}}{1+\frac{-23.013-2.949*ama\ +0.999*Mw+0.0525*Vs,12}{16.258+0.201*e\ \hat{}\ (0.341*(0.0785*Vs,12+7.586))}} \ -0.046*(d-20) \quad \textbf{(Equation 78)}$$

Cyclic Resistance Ratio (CRR7.5, 1 atm) (Column AB): The CRR in this column is determined by applying Equation 3–79 from Kayen et al. (2013). The variables M_w = 7.5, σ'v = 1 atm, FC = 5%, and PL = 15% have all been set to a fixed value. Equation 79, presented below, is adopted from Kayen et al. (2013). All the parameters used in these equations are described in previous sections.

$$CRR = \exp\left\{\frac{(0.0073*V_{s1})\hat{}2.8011+0.0028*FC-0.0099*\ln(\sigma'_v)-2.6168*\ln(Mw)-0.4809*\phi\hat{}(-1)*PL)}{1.946}\right\} \quad \textbf{(Equation 79)}$$

Probability of Liquefaction, P_L (Column AH): The column headings for the probability of liquefaction performed in columns W are included in the worksheet using Equation 80, adopted from Kayen et al. (2013). All the parameters used in these equations are described in previous sections.

$$P_L = \phi\left[\frac{(0.0073*V_{s1})\hat{}2.8011-1.946*\ln(CSR)-0.0099*\ln(\sigma'_v)-2.6168*\ln(Mw)+0.0028*FC)}{0.4809}\right] \quad \textbf{(Equation 80)}$$

The changes to the Calculation Tables worksheet include an updated CR table and chart, a DWFM/MSF table and chart, Stress reduction coefficient tables and equations, plus the table titled Exponential "f" factor for K_σ Equation. All of which have been discussed previously.

Comparison

The liquefaction triggering workbooks that have been developed in this work enable easy data transfer between workbooks and facilitate quick and simple comparisons between all three procedures. The "Comparison" tab is created to view the comparative results of the V_s-based liquefaction analysis (Figure 46). The results of overburden corrected shear wave velocity (V_{s1}), Stress reduction coefficient (r_d), Cyclic Stress Ratio (CSR), Cyclic Resistance Ratio (CRR), Factor of Safety (FS), and Probability of liquefaction (P_L) can be viewed in this tab. These outputs have an input number from 3 to 8 in the same order. The user needs to select the input number from the dropdown list at cell C2 to view the desired output. A VLOOKUP function is used, and the corresponding liquefaction analysis results can be viewed from columns G to H. The figure will automatically change according to the input number. The user can view the comparative continuous results of the adopted procedures. It should be noted that except for cell C2, no other cell should be altered.

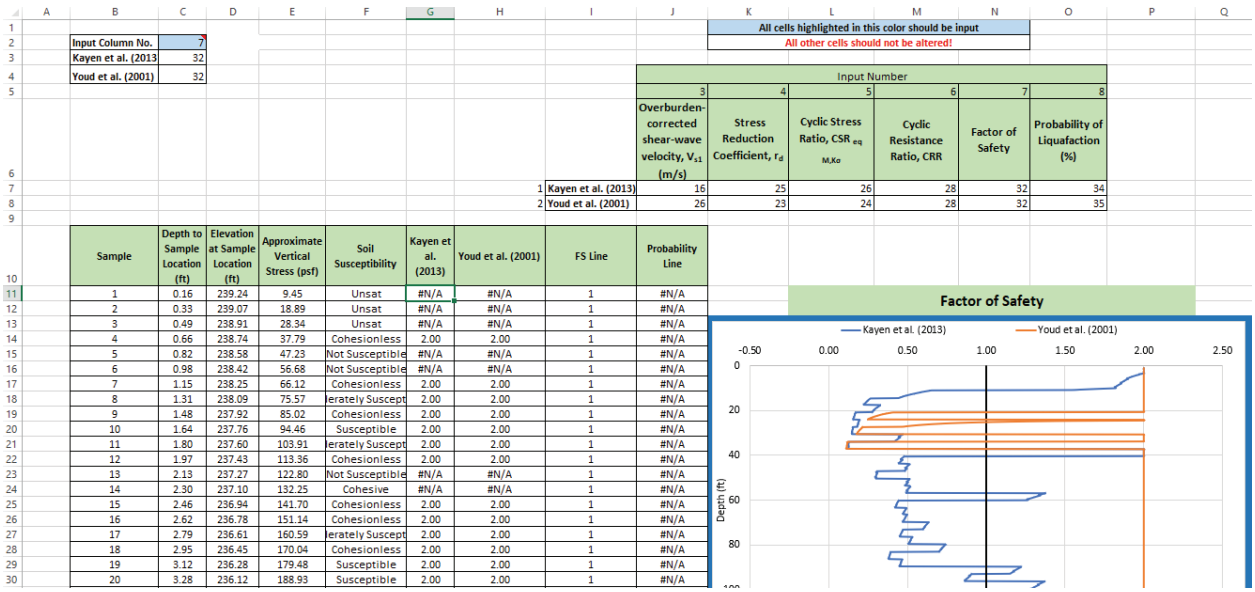

Figure 46. "Comparison" Tab of the V_s-based Liquefaction Triggering Workbook

Layer Comparison

This tab has been developed to provide discontinuous V_s-based liquefaction analysis results. One of the purposes of this work is to compare co-located SPT, CPT, and V_s data and conduct a sensitivity study using the spreadsheet to understand any differences between the procedures and methods. To serve this purpose, this tab can convert continuous V_s results into 2.5' of 5' layered discontinuous V_s results. The layout of this tab is kept the same as the "comparison" tab, as described before. To view the desired output, the user needs to select the input number from the dropdown list at cell B2; also, the user needs to select the layer thickness from the dropdown list at cell B7 (Figure 47). It should be noted that except for cell B2 and cell B7, no other cell should be altered.

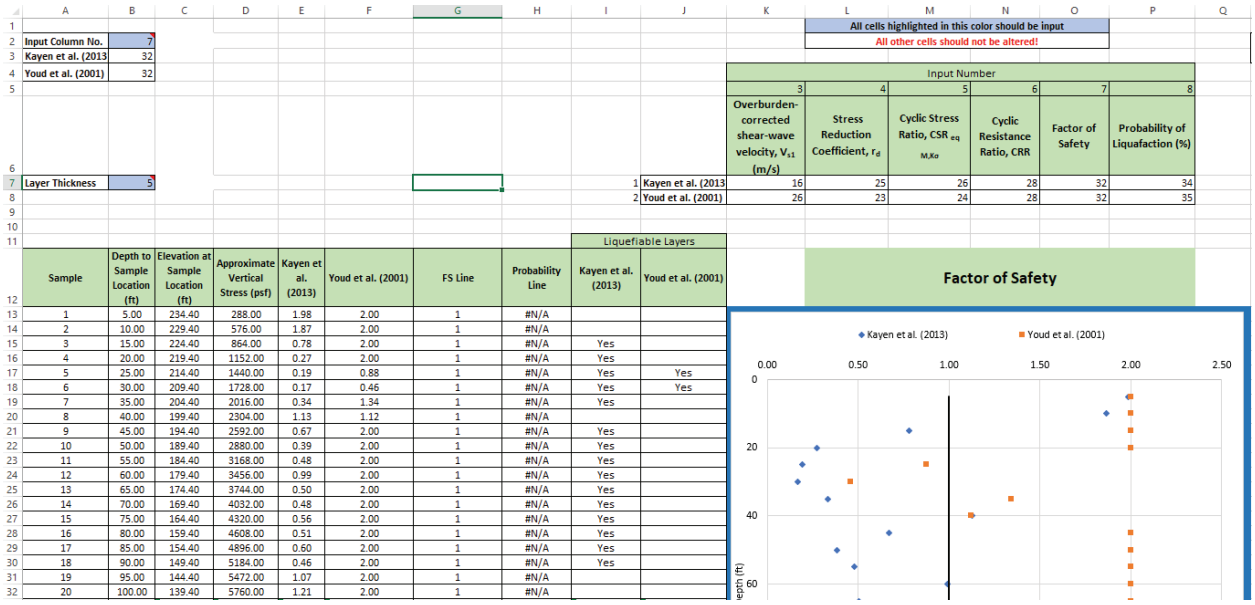

Input Column No.	7
Kayen et al. (2013	32
Youd et al. (2001)	32
Layer Thickness	5

All cells highlighted in this color should be input
All other cells should not be altered!

	Input Number					
	3	4	5	6	7	8
	Overburden-corrected shear-wave velocity, V_{s1} (m/s)	Stress Reduction Coefficient, r_d	Cyclic Stress Ratio, $CSR_{eq\ M,K\sigma}$	Cyclic Resistance Ratio, CRR	Factor of Safety	Probability of Liquefaction (%)
1 Kayen et al. (2013	16	25	26	28	32	34
2 Youd et al. (2001)	26	23	24	28	32	35

	Sample	Depth to Sample Location (ft)	Elevation at Sample Location (ft)	Approximate Vertical Stress (psf)	Kayen et al. (2013)	Youd et al. (2001)	FS Line	Probability Line	Liquefiable Layers: Kayen et al. (2013)	Liquefiable Layers: Youd et al. (2001)
13	1	5.00	234.40	288.00	1.98	2.00	1	#N/A		
14	2	10.00	229.40	576.00	1.87	2.00	1	#N/A		
15	3	15.00	224.40	864.00	0.78	2.00	1	#N/A	Yes	
16	4	20.00	219.40	1152.00	0.27	2.00	1	#N/A	Yes	
17	5	25.00	214.40	1440.00	0.19	0.88	1	#N/A	Yes	Yes
18	6	30.00	209.40	1728.00	0.17	0.46	1	#N/A	Yes	Yes
19	7	35.00	204.40	2016.00	0.34	1.34	1	#N/A	Yes	
20	8	40.00	199.40	2304.00	1.13	1.12	1	#N/A		
21	9	45.00	194.40	2592.00	0.67	2.00	1	#N/A	Yes	
22	10	50.00	189.40	2880.00	0.39	2.00	1	#N/A	Yes	
23	11	55.00	184.40	3168.00	0.48	2.00	1	#N/A	Yes	
24	12	60.00	179.40	3456.00	0.99	2.00	1	#N/A	Yes	
25	13	65.00	174.40	3744.00	0.50	2.00	1	#N/A	Yes	
26	14	70.00	169.40	4032.00	0.48	2.00	1	#N/A	Yes	
27	15	75.00	164.40	4320.00	0.56	2.00	1	#N/A	Yes	
28	16	80.00	159.40	4608.00	0.51	2.00	1	#N/A	Yes	
29	17	85.00	154.40	4896.00	0.60	2.00	1	#N/A	Yes	
30	18	90.00	149.40	5184.00	0.46	2.00	1	#N/A	Yes	
31	19	95.00	144.40	5472.00	1.07	2.00	1	#N/A		
32	20	100.00	139.40	5760.00	1.21	2.00	1	#N/A		

Figure 47. "Layer Comparison" Tab of the V_s-based Liquefaction Triggering Workbook

Study Area

To provide a comparison of the liquefaction-triggering relationships discussed in the study, two locations have been chosen in Arkansas that have a high likelihood of liquefaction in future earthquakes and have SPT, CPT, and V_s data available for comparison. These sites are located within proximity to the Reelfoot

Rift, the primary fault system of the NMSZ. The locations of the study sites are shown in Figure 48. The sites are in Monette and Turrell, Arkansas, and a detailed description is provided in the next sections.

Figure 48**. The Arkansas State Map with the Locations of the Monette and Turrell Sites**

Monette, Arkansas

Monette, Arkansas, is located on the western edge of Craighead County in Northeast Arkansas at a latitude and longitude of 35.890756 and -90.324169, respectively (see Figure 49). The project site is approximately 0.5 miles west of the intersection between AR-18 and AR-139, east of Monette, Arkansas (Figure 49).

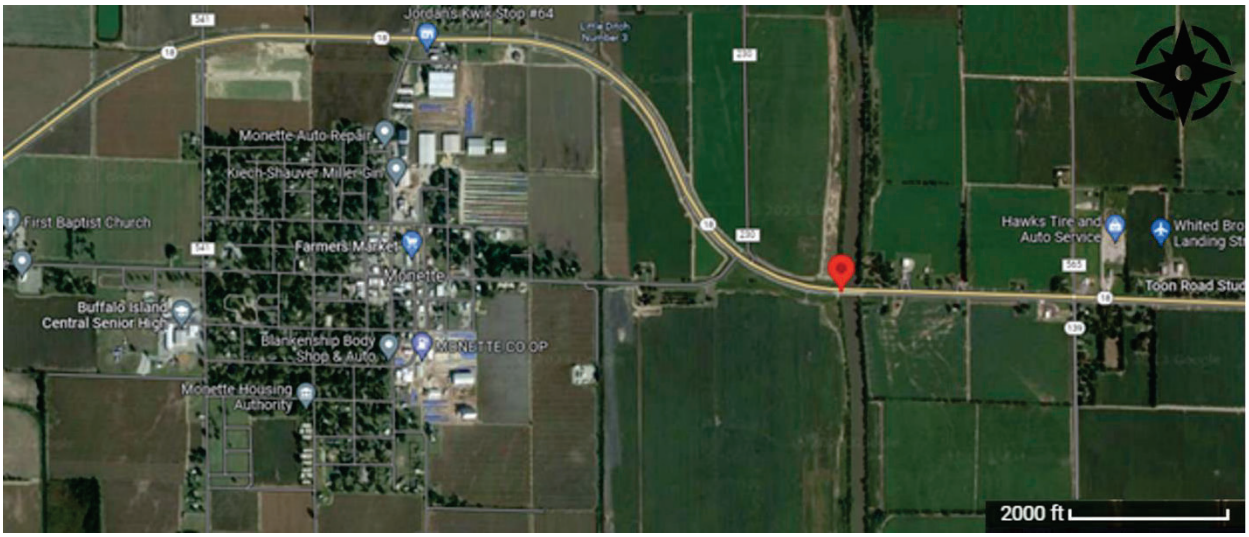

Figure 49. Location of Monette, Arkansas, Bridge Site (Google Map 2023)

Recently, a new 328 ft long by 79 ft wide bridge was built to cross the Cockle Burr Slough as part of a project that increased Highway 18 to four lanes and redirected it to bypass north of Monette. The main components of the bridge include nine 328 ft long continuous steel girders and six pile bents. The lowest bridge chord is 8 ft above the design flood elevation, which is 6.5 ft higher than the height of the preceding canal-crossing structure. Two boreholes (one on each side of the Slough) are drilled by the Arkansas Department of Transportation (ARDOT). The borings with SPT were collected on April 30, 2012. A CME 750 with a CME automatic hammer with rotary wash drilling was used to collect the SPT data. Seismic cone penetration test (SCPT) with shear wave velocity data were collected on April 4, 2023, using a 20-ton, track-mounted Vertek direct-push SCPT rig. Some images of the SCPT equipment and data collection for this site are provided in Figure 50. The locations of the SPT and SCPT at the site are also shown in Figure 51.

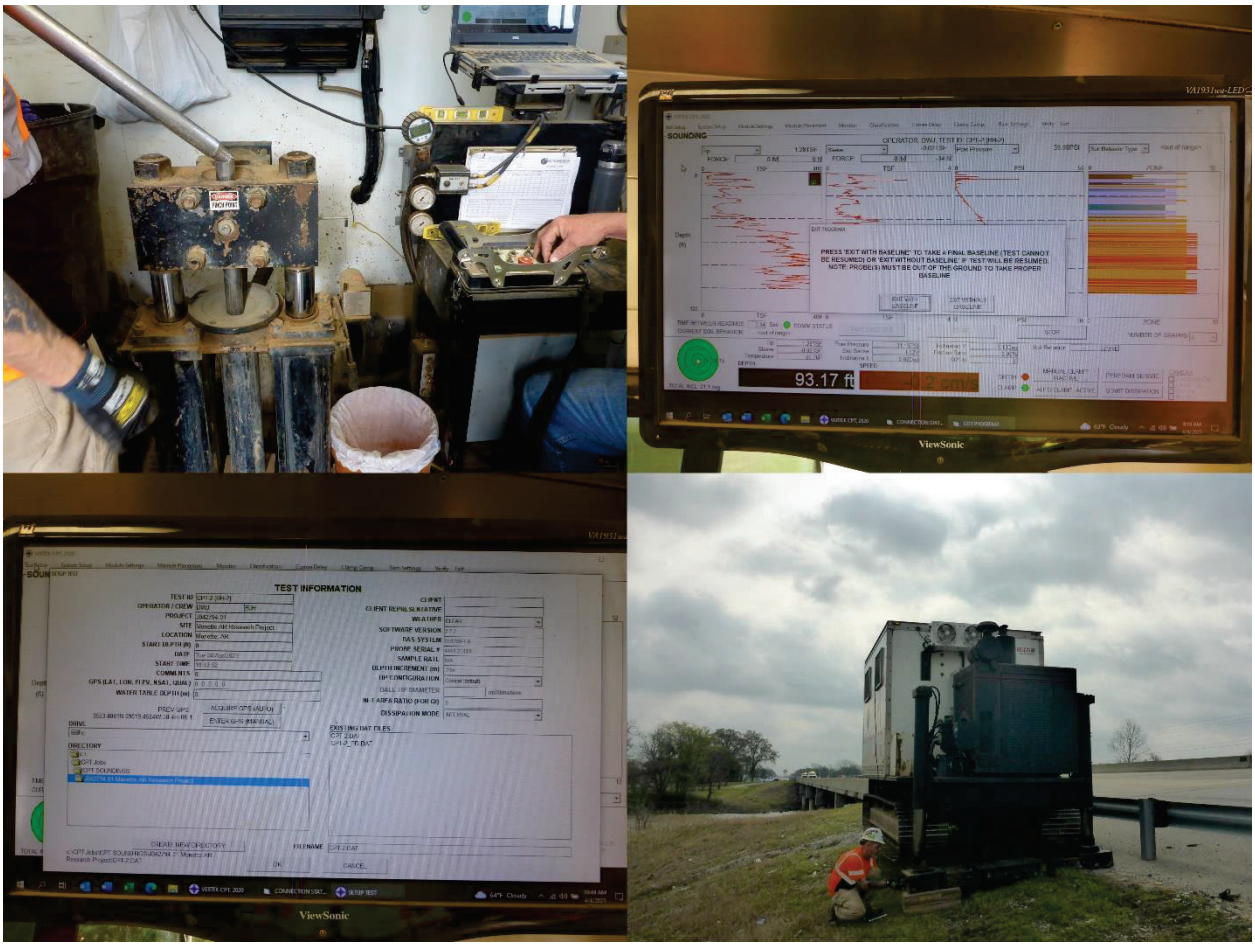

Figure 50. Images of the SCPT Equipment and Data Collection for the Monette Bridge Site

Figure 51. The Locations of SPT Boreholes and SCPT Soundings at the Monette, Arkansas, Bridge Site

According to the ARDOT borings, the subsurface characteristics at the site are primarily sandy soils apart from a clay layer between 10 ft and 20 ft below the existing grade. Some trace gravel exists in layers below 50 ft. A water stratum was encountered in borings from 9 to 9.5 ft with an elevation of 231 ft. Based on blow count and V_s measurements, the site is classified as an AASHTO site class D with a design PGA value of 0.915 g and a moment magnitude (M_w) of 7.54. The design PGA value and moment magnitude (M_w) were determined for the site using procedures discussed in Chapter 3. Deep dynamic site characterization and a site-specific ground motion response analysis (SSGMRA) were conducted for this location by Wood and Baker (2018). A cost-savings analysis was then conducted to determine the potential savings associated with conducting the SSGMRA.

Turrell, Arkansas

The Turrell site is in the Mississippi embayment and the New Madrid Seismic Zone at a latitude and longitude of 35.392250 and -90.274916, respectively (see Figure 52). This site is located within the interchange between the southbound lanes of Highway 63 and the eastbound lanes of Interstate 55 (Figure 52).

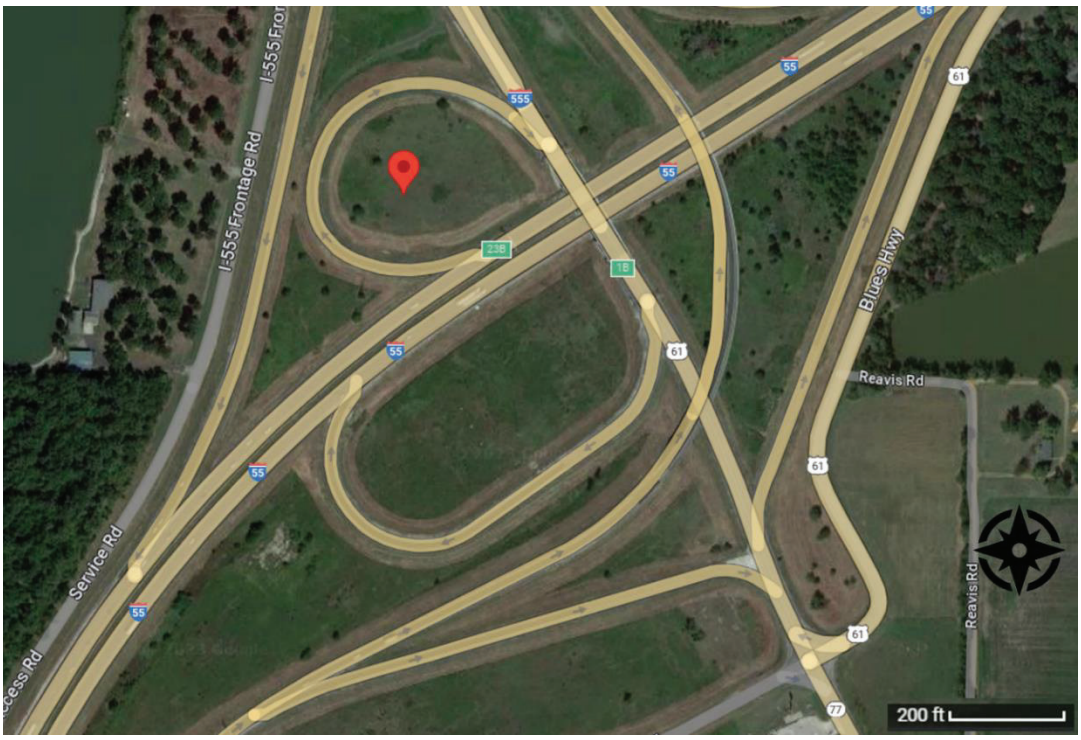

Figure 52. The Location of Turrell, Arkansas, Site (Google Map 2023)

The site is characterized by clean, wet sand overlain by a clay layer that makes up the site's alluvial deposits. The borings with SPT were collected on November 7, 2011. A CME 750 with a CME automatic hammer with rotary wash drilling was used to collect the SPT data. SCPT with V_s data were collected on October 18, 2011, using a Vertek direct-push SCPT rig. Some images of the SCPT equipment and data collection for this site are provided in Figure 53.

Figure 53. Images of the SCPT Equipment and Data Collection for the Turrell Site

The six SPT boreholes drilled by the ARDOT using procedures defined by ARDOT and procedures defined by the University of Arkansas (UofA) as well as the five CPT soundings, completed by the MoDOT, are located as shown in Figure 54.

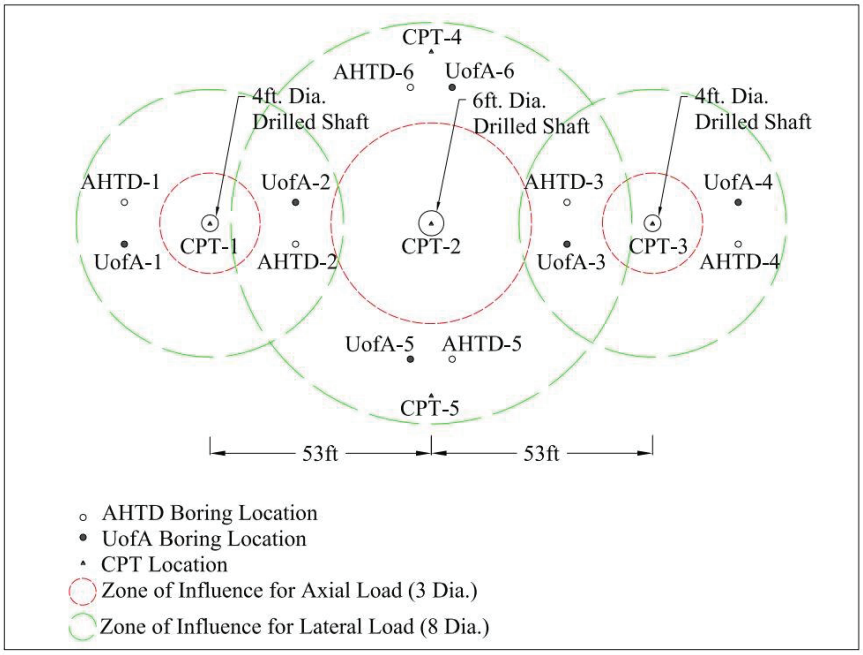

Figure 54. Testing Layouts for Geotechnical Site Investigations (Race and Coffman 2013)

Based on blow count and V_s measurements, the site is classified as an AASHTO site class D with a design PGA value of 0.723 g and a moment magnitude (M_w) of 7.51. The design PGA value and moment magnitude (M_w) were determined for the site using procedures discussed in Chapter 3. Bey performed an analysis in 2014 on this site for drilled shaft foundations to compare the fiscal impacts of the drilling and sampling, in-field and laboratory testing, full-scale load testing, and concrete mixture techniques on the drilled shaft design and performance. In 2013, Race and Coffman performed a full-scale load test on the drilled shaft foundation of this site.

CHAPTER 4: RESULTS AND DISCUSSIONS

The SPT, CPT, and V_s-based liquefaction triggering spreadsheets developed in this study are used in this chapter to understand differences between the methods and analyze real project data from Arkansas. First, the results of constant input analysis are presented and the differences between the procedures are discussed. After that, site-specific comparisons of the SPT, CPT, and V_s liquefaction triggering procedures for two different sites in eastern Arkansas are presented and discussed. The cost savings potential associated with the new liquefaction analysis is also compared to the old analysis to determine if any benefits or cost savings exist. Finally, several q_c-V_s correlations have been used to study the performances of these correlations in the liquefaction study.

CONSTANT INPUT ANALYSIS

After the preparation of the workbooks, several analyses are completed in this chapter using constant raw inputs (SPT-N, q_c, V_s) to compare the liquefaction triggering procedures and understand the contributing factors behind the differences in the procedures. To perform the liquefaction triggering analysis, the design peak horizontal ground acceleration and earthquake moment magnitude are 0.771 g and 7.55, respectively (seismic site class D). These values are often observed in the northeastern corner of Arkansas and are representative of values encountered by ARDOT. The soil was presumed to be sandy, and the groundwater level was set at the surface to create a most susceptible soil profile to liquefaction.

Constant Input Analysis (SPT)

For the SPT analysis, constant SPT-N values of 5, 10, 20, and 40 blows/feet were used from a depth of 5 ft to 100 ft in 5 ft increments. It is prudent to mention that in the old SPT spreadsheet, the K_σ limit for Youd et al. (2001) is set to 1.0, but in the new spreadsheet, the limitation is not used as the limitation is not stated in the Youd et al. (2001) procedure.

For the soft soil profiles (SPT-N = 5 and 10 blows/feet), the entire soil profile was determined to be susceptible to liquefaction (factor of safety less than 1.0) for all procedures. For the dense soil profile (SPT-N = 40 blows/feet), the analysis using Youd et al. (2001) and Boulanger and Idriss (2014) procedures shows that the profile is too dense to liquefy. However, the Cetin et al. (2018) procedure indicates that the deeper layers (more than 75 ft) have the potential to liquefy. These analyses are not shown here but can be viewed in the Appendix.

In Figure 55, the analysis results for a constant SPT-N value of 20 blows/ft are shown. Comparing the procedures in Figure 55a, the overburden stress correction factor (C_N) value for Cetin et al. (2018) is higher in the top 20 ft than the other two procedures. This leads to the equivalent clean sand blow count $(N_1)_{60,cs}$ being higher for the Cetin et al. (2018) procedure at shallow depths compared to the other two procedures. This difference is driven by the upper limit of the C_N to 2.0 for Cetin et al. (2018) ($C_N \leq$ 1.6, Cetin et al. (2004)); whereas the upper value of C_N is 1.7 for Youd et al. (2001) and Boulanger and Idriss (2014) procedures. C_N, along with the other blow count correction factors, directly influences the $(N_1)_{60,\,cs}$ values, which are used in the deterministic SPT procedures to obtain the unadjusted CRR ($CRR_{M=7.5,1atm}$).

The proposed approaches to calculate the K_σ are also found to be varied in the shallower depths as shown in Figure 55c. Boulanger and Idriss (2014) proposed a limiting value of 1.1 for the maximum value of K_σ (Equation 23), though the other two procedures did not state any limitations for the maximum value of K_σ. That leads to differences in K_σ at shallower depths (0–20 ft).

The equation for calculating CRR from the Youd et al. (2001) procedure is only valid for $(N_1)_{60,\,cs} < 30$. For the $(N_{1,60})_{cs}$ values higher than 30, Youd et al. (2001) state that the "clean granular soils are too dense to liquefy and class as non-liquefiable"; that's why a value of 2.0 for CRR is set when $(N_1)_{60,cs} < 30$. However, the other procedures indicate that layers with $(N_1)_{60,cs}$ greater than 30 have the potential to be liquefiable (Figure 55d and 55e). It is also noticeable in Figure 4-1d that the Cetin et al. (2018) procedure has the lower CRR values in deeper layers, though the $(N_{1,60})_{cs}$ is almost the same for all the procedures. Therefore, the factor of safety obtained from this procedure in the deeper layers is the lowest, making this procedure the most conservative of all three procedures.

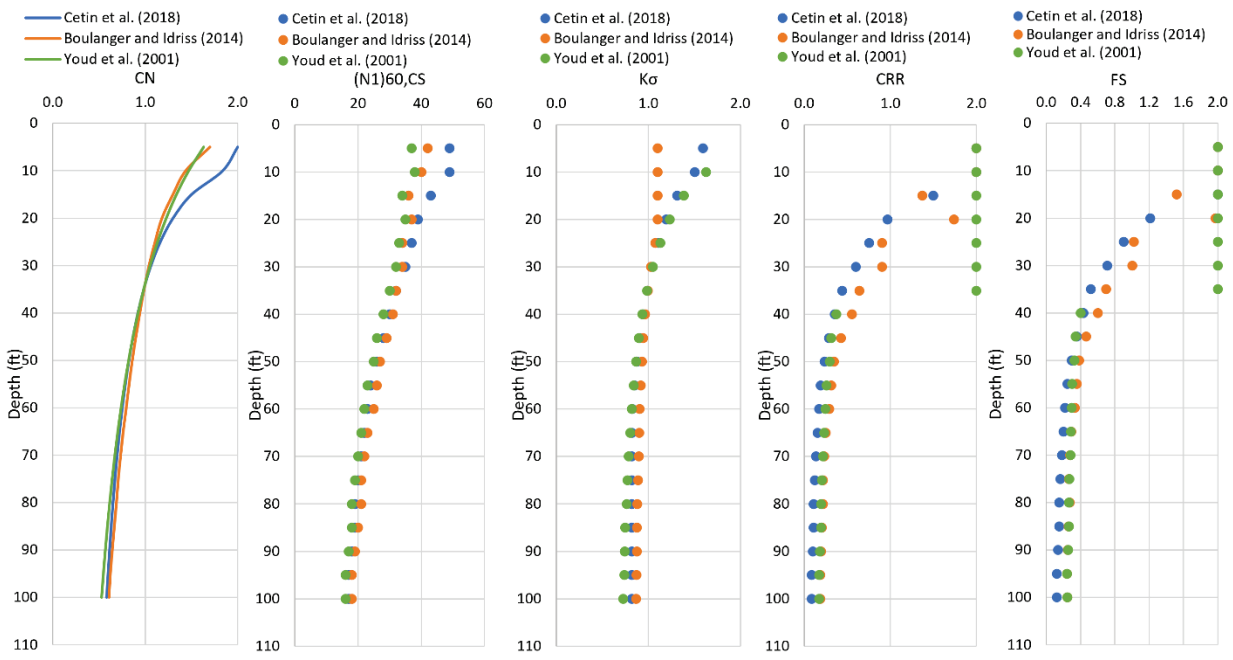

Figure 55. Contant SPT-based Liquefaction Analysis Results for N = 20 blow/ft (a) Overburden Correction Factor (CN), (b) Clean Sand Equivalent Blow Count $(N1)_{60cs}$, (c) K_σ Correction Factor, (d) Unadjusted Cyclic Resistance Ratio (CRR), (e) Factor of Safety

Figure 56a shows the comparison of the factor of safety for constant SPT-N = 20, using the old and new SPT-based liquefaction triggering workbooks. Figure 56b shows the percentage change in the factor of safety between the previous and new procedures as programmed in the workbook. Equation 81 is used to calculate the percentage change in the factor of safety.

$$\text{Percentage change} = \left(\frac{FS_{new\ procedure} - FS_{old\ procedure}}{FS_{old\ procedure}}\right)*100 \qquad \text{(Equation 81)}$$

The FS values from the Cetin et al. (2018) procedure are higher than the Cetin et al. (2004) at shallower depths (< 50 ft). This is caused by the new model coefficients in the probabilistic liquefaction triggering relationship for CRR, which generates higher CRR values at shallow depths. For the other two procedures, the percentage of changes in the factor of safety results is not significant.

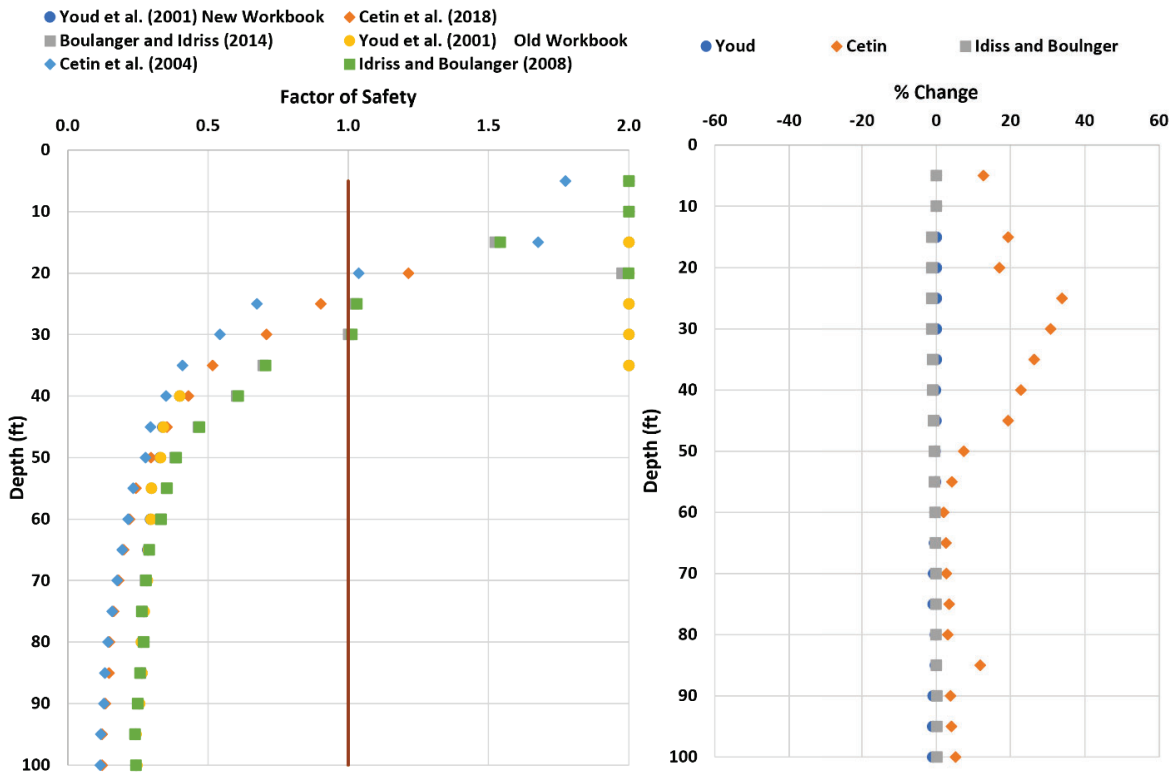

Figure 56. (a) Comparison of Factor of Safety Results Using the Old and New Workbook Methods (Constant SPT-N = 20 blow/ft), (b) Percent Changes of Factor of Safety Results in New Workbook from the Old Workbook (Contant SPT-N = 20 blow/ft)

Constant Input Analysis (CPT)

For the CPT analyses, cone resistance q_c values of 125 ksf, 250 ksf, 375 ksf, and 500 ksf were used. The sleeve friction values are back-calculated using the soil behavior index (I_c) equation by Robertson et al. (2009). The input values are chosen in a way that the I_c is between 1.31 and 2.05 (Figure 57a) so that the soil behavior is in the sand region (see Figure 57a). In this section, the analysis results for a constant q_c of 250 ksf are shown in Figure 57, and the generated results of other analyses are provided in the Appendix, as the results for other q_c follow a similar pattern for each method. From Figure 57b, it is noticeable that in the shallow layers, all three procedures generate almost the same clean sand cone penetration resistance $(q_{c1N})_{cs}$, but the Boulanger and Idriss (2014) procedure generates higher $(q_{c1N})_{cs}$ in deeper layers (greater than 40 ft). It is also noticeable in Figure 57c that Moss et al. (2006) have the lowest CRR for depths shallower than 10 ft, though for greater than 50 ft the CRR values from all three

procedures are almost the same. It is worth noting that the Youd et al. (2001) procedure dictates that for $(q_{c1N})_{cs}$ values higher than 160 are too dense to liquefy, in such cases, the CRR = 2.0 and FS = 2 values are assigned. This is observed in Figure 57d for Youd et al. (2001) procedure for depths less than 25 ft. However, the other two procedures show potential for liquefaction at shallow depths (Figure 57d). It is also noticeable that Moss et al. (2006) yield the lowest FS for depths less than 10 ft, though it is less conservative at depths greater than 25 ft. It is important to note that no probabilistic equation is stated in Youd et al. (2001); this workbook uses data (if FS > 1, PL = 0; if FS ≤ 1, PL = 100) to assist in viewing the comparison between the three methods in Figure 57e.

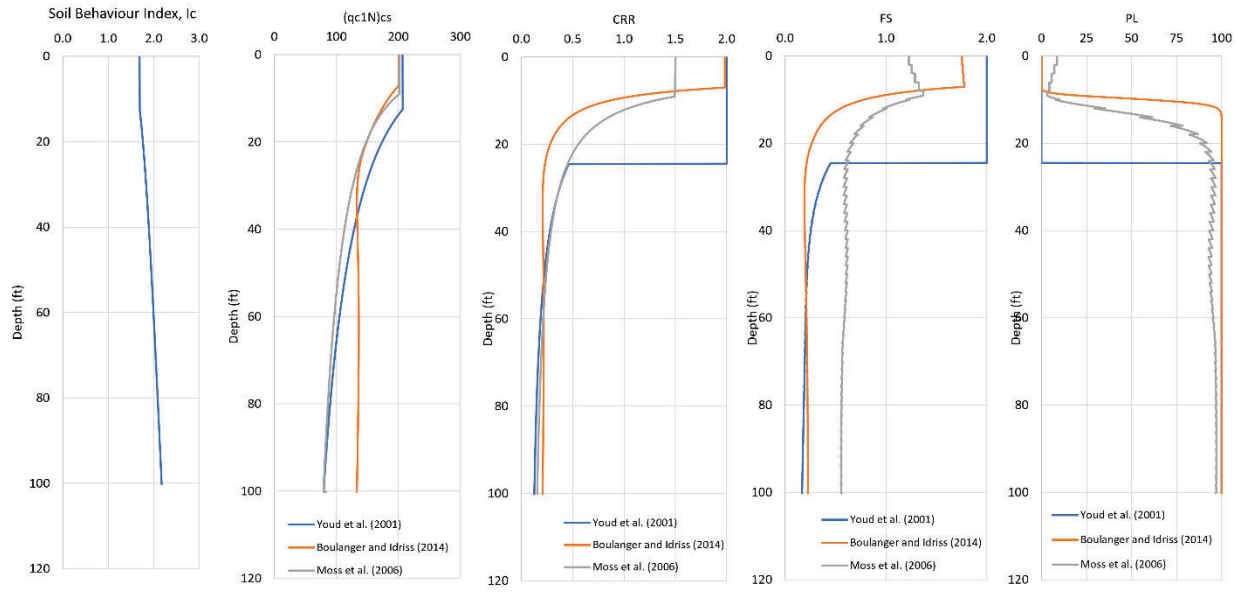

(a) (b) (c) (d) (e) (e)

Figure 57. Contant CPT-based Liquefaction Analysis Results for q_c = 250 ksf (a) Soil Behavior Index (I_C), (b) Clean Sand Equivalent Cone Penetration Resistance $(q_{c1N})_{cs}$, (c) Unadjusted Cyclic Resistance Ratio (CRR), (d) Factor of Safety, (e) Probability of Liquefaction (P_L)

Constant Input Analysis (V_s)

For the V_s-based analyses of constant V_s, shear wave velocity values are 100 m/s, 150 m/s, 200m/s, 250 m/s, and 300 m/s were used. In this section, the analysis results of constant V_s of 200 m/s are shown in Figure 58, and the generated results of other analyses are provided in the Appendix, as the results of the different procedures follow a similar pattern.

The Youd et al. (2001) V_s-based procedure adopts the liquefaction triggering relationship recommended by Andrus and Stokoe (2000), and the maximum factor to correct measured shear wave velocity (C_V) in this procedure is limited to 1.4; whereas Kayen et al. (2013) limited this value to 1.5 in shallow depths (less than 10 ft). That is why the overburden stress-corrected shear wave velocity (V_{s1}) is higher for the Kayen et al. (2013) procedure compared to the one by Youd et al. (2001) (Figure 58a). It is also worth mentioning that Andrus and Stokoe (2000) stated that V_{s1} higher than 200–215 m/s (depending on fines content) is too dense to liquefy; Kayen et al. (2013), on the other hand, indicates that these layers have the potential of being liquefiable (Figure 58b). Although no probabilistic equation is stated in Youd et al. (2001) or Andrus and Stokoe (2000) procedure, this workbook uses data (if FS > 1, PL = 0; if FS ≤ 1, PL = 100) to assist in viewing the comparison between the two methods in Figure 58d.

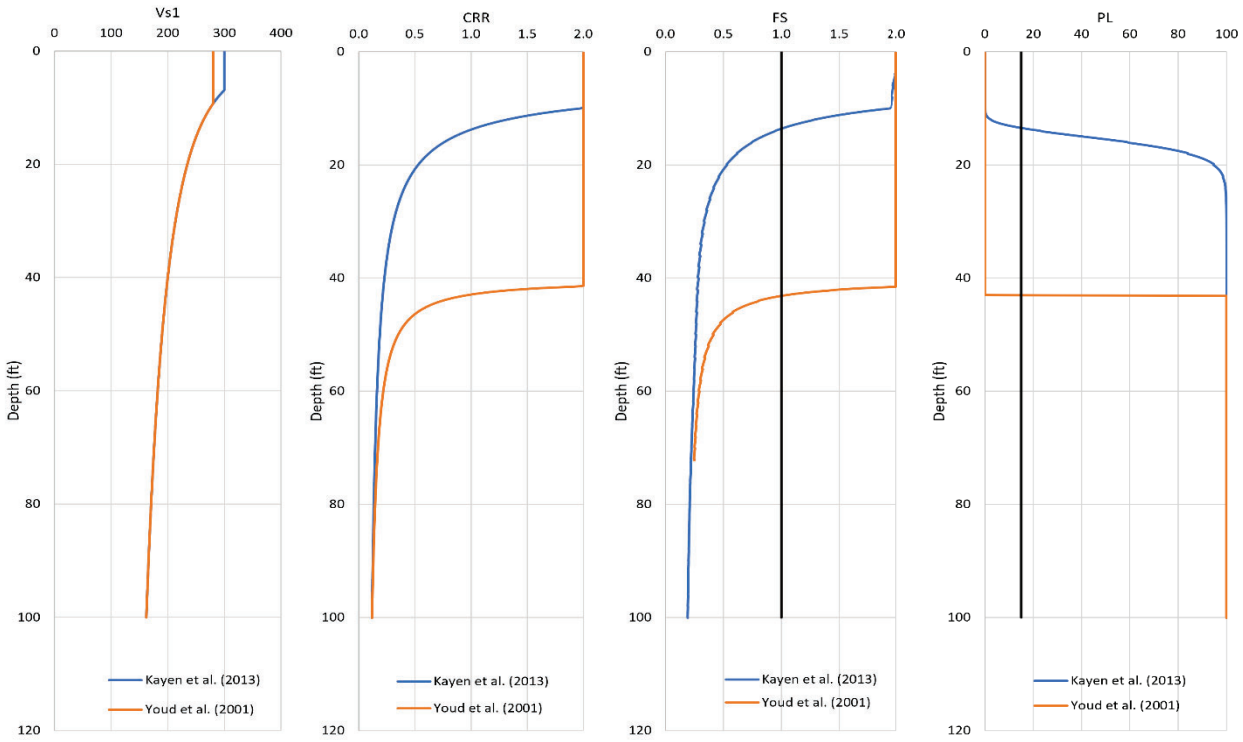

Figure 58. Contant V_s-based Liquefaction Analysis Results for V_s = 200 m/s (a) Overburden Stress Corrected Shear Wave Velocity (V_{s1}), (b) Unadjusted Cyclic Resistance Ratio (CRR), (c) factor of safety, (d) probability of liquefaction (P_L)

SITE-SPECIFIC COMPARISON

This section will present site-specific comparisons of the SPT, CPT, and V_s liquefaction triggering procedures for two different sites in eastern Arkansas.

Analysis **R**esults of **the** Monette Site

The liquefaction analysis results of the Monette bridge site data are discussed in this section. Two sets of SPT data and four sets of SCPT data were collected. The SPT-, CPT-, and V_s -based liquefaction triggering analysis results are discussed below. A detailed description of this site is provided in Chapter 3.

SPT-Based Analysis

In this section, the SPT-based liquefaction analysis results at the Monette site will be discussed. The seismic design information for this site is detailed in Chapter 3. Based on blow count and V_s measurements, the site is classified as an AASHTO site class D with a design PGA value of 0.915 g and a moment magnitude (M_w) of 7.54. The design PGA moment magnitude (M_w) was determined for the site using procedures discussed in Chapter 3. The soil type and raw blow count values of BH-3 and BH-4 are presented in Table 6. From the borehole data, the site consists of clayey material in the top 10–15 ft with medium sand becoming dense to very dense sand as the soil profile gets deeper.

Figure 59a presents a comparison with the raw blow count and the equivalent clean sand blow count values ($(N_1)_{60,cs}$) obtained from all three SPT procedures for Borehole 3 (surface elevation = 237.6 ft, water table = 9 ft). From the raw SPT N values, this profile contains soft sand in the shallow layers, but stiff sand with high SPT N values present in the deeper layers. It is obvious that the multiplication of the correction factors for the Boulanger and Idriss (2014) procedure is more than 1 for the whole profile, and so the $(N_1)_{60,cs}$ is higher than the Raw N; whereas for the other two procedures, the $(N_1)_{60,cs}$ is lower than the Raw N layers deeper than about 75 ft. This caused the unadjusted cyclic resistance ratio ($CRR_{M = 7.5, \sigma'v=1\ atm}$) obtained from the Boulanger and Idriss (2014) to be higher than the other two procedures and resulted in non-liquefiable layers, making this procedure the least conservative approach. Though the $(N_1)_{60,cs}$ obtained from Cetin et al. (2018) is determined to be higher at shallow depths (less than 15 ft), in the deeper layers, it is determined to be less than the $(N_1)_{60,cs}$ obtained from the Boulanger and Idriss (2014) procedure. Also, for layers deeper than 215 ft elevation, the $(N_1)_{60,cs}$ obtained from the Cetin et al. (2018) is observed to be higher than the Youd et al. (2001) procedure but resulted in a lower $CRR_{M = 7.5, \sigma'v=1\ atm.}$ Also, the deeper layers (deeper than 140 ft elevation) are predicted to liquefy for the

Cetin et al. (2018) procedure, while the other two procedures consider the layer non-liquefiable (Figure 59b and Figure 59c).

Table 6. Soil Type and Raw Blow Count Values of BH-3 and BH-4

	BH-3	BH-3	BH-4	BH-4
Depth	Soil Group	SPT- N	Soil Group	SPT- N
(ft)		(blow/ft)		(blow/ft)
5	SC	10	SW	5
10	CL	4	CH	5
15	SM	33	CH	11
20	SW-SM	20	SW	14
25	SW-SM	13	SW	31
30	SW-SM	13	SW	34
35	SW	15	SW	18
40	SW	27	SW	29
45	SW	25	SW	16
50	SW	21	SW	14
55	SW-SM	32	SW	26
60	SW	40	SW	22
65	SW	40	SW	32
70	SW	26	SW	26
75	SW	35	SW	26
80	SW	56	SW	31
85	SW-SM	74	SW-SM	40
90	SW	56	SW-SM	50
95	SW-SM	42	SW-SM	26
100	SW	43	SW-SM	43

In summary, it can be stated that the correction factors obtained from the Boulanger and Idriss (2014) procedure generate higher $(N_1)_{60,cs}$ values than the other two procedures and consequently yield more non-liquefiable layers than the other procedures. Also, the Youd et al. (2001) procedure yields a non-liquefiable layer when the $(N_1)_{60,cs}$ is higher than 30, which agrees with the results found from the Boulanger and Idriss (2014) procedure. The results from the Cetin et al. (2018) procedure do not agree with the other two procedures for these higher blow counts at deeper depths (lower than elevation 145 ft). This difference is driven by the Cetin et al. (2018) procedure having a low $CRR_{M = 7.5,\ \sigma'v = 1\ atm}$ when the $(N_1)_{60,cs}$ values are approximately less than 40, making this procedure the most conservative.

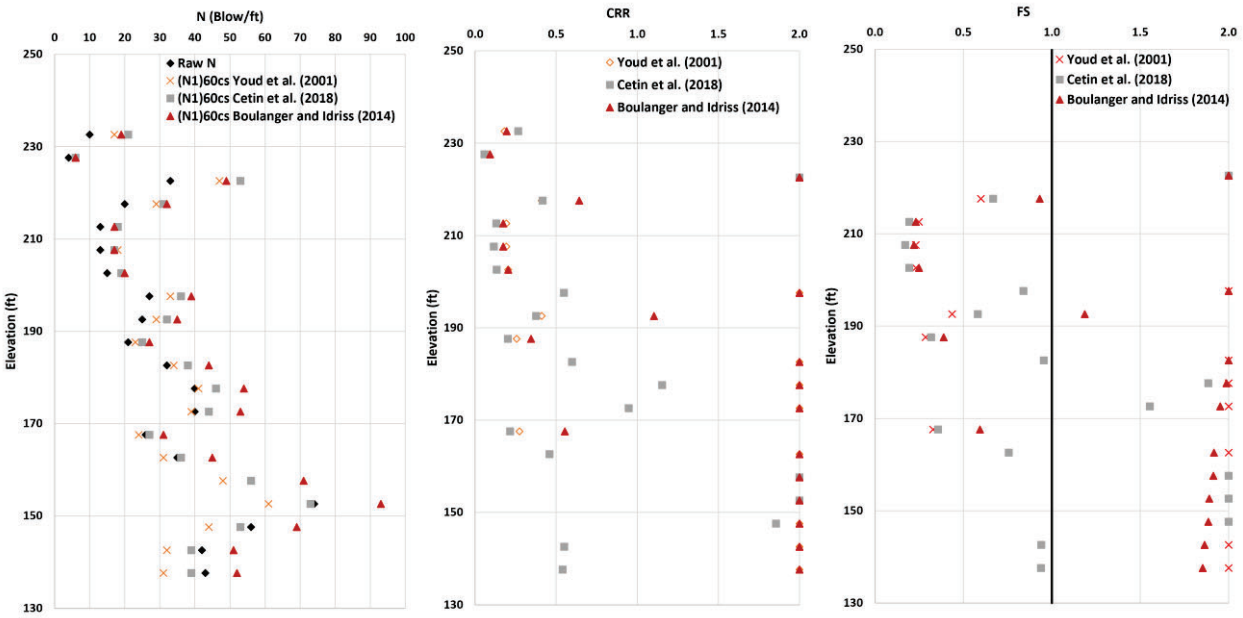

(a) (b) (c)

Figure 59. Comparison of (a) Raw N and Equivalent Clean Sand Blow Count Values, (b) Unadjusted Cyclic Resistance Ratio (CRR), and (c) Factor of Safety Results for BH-3 at the Monette Site

The LPI analysis results for BH-3 at the Monette site are presented in Figure 60. It is important to note that the boundary curves of LPI_{ISH}, developed using a power-law depth weighting function by Maurer et

al. (2015) may be more appropriate than the existing linear form of the LPI, developed by Iwasaki et al. (1978). For BH-3, LPI estimated from all SPT-based procedures suggests that the site is susceptible to severe liquefaction (LPI > 15). LPI_{ISH} estimates less liquefaction manifestation than LPI. LPI_{ISH} calculated using the Boulanger and Idriss (2014) shows moderate liquefaction (5 < LPI < 15), whereas LPI_{ISH} calculated using the other two procedures suggest the possibility of severe liquefaction.

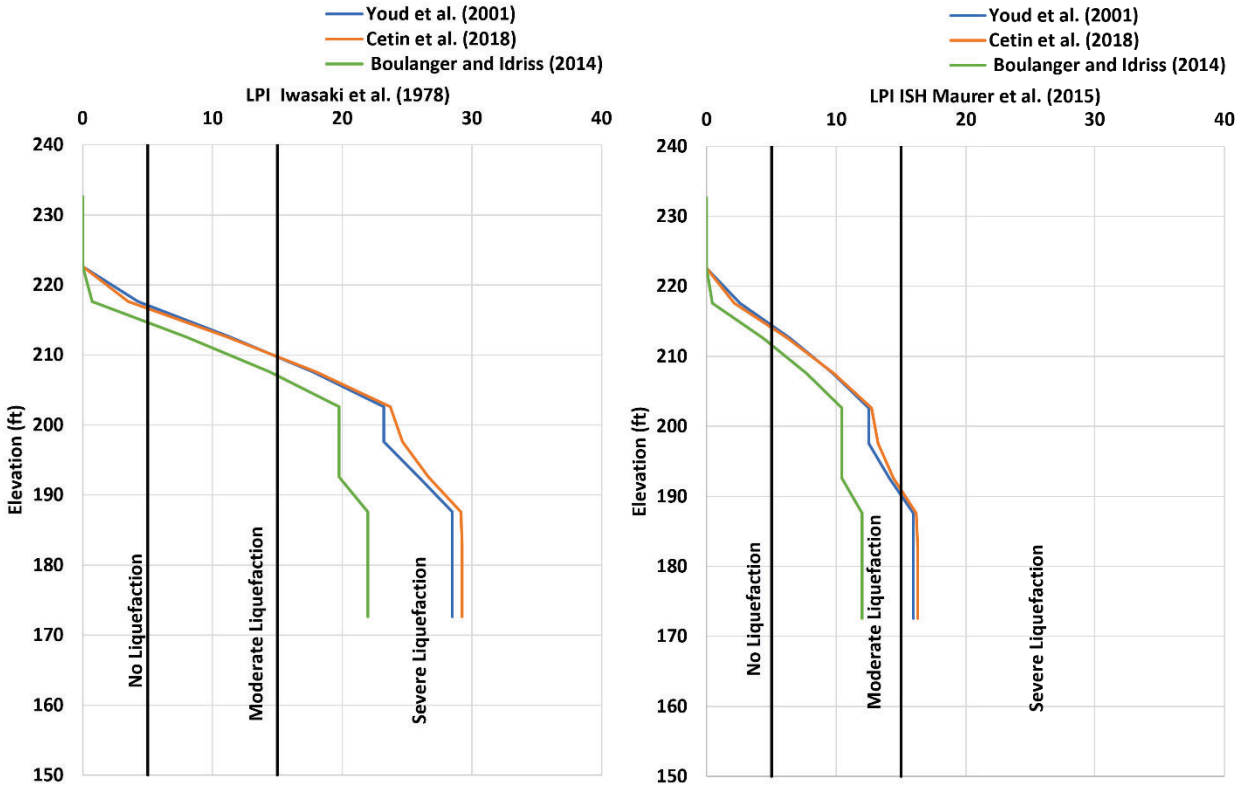

Figure 60. Cumulative (a) LPI by Iwasaki et al. (1978), (b) LPI_{ISH} by Maurer et al. (2015) for BH-3 at the Monette Site

Figure 61 presents the raw SPT-N with the results obtained from the three chosen SPT-based liquefaction procedures for Borehole 4 (surface elevation = 237.7 ft, water table = 9 ft). Borehole 4 has

similar patterns as observed in Borehole 3 and will be compared further in other analyses. The LPI analysis results for BH-4 at the Monette Site are presented in Figure 62. LPI estimated from all SPT-based procedures suggests that the site is susceptible to severe liquefaction (LPI > 15), LPI_{ISH} estimated from all SPT-based procedures shows the moderate severity of liquefaction.

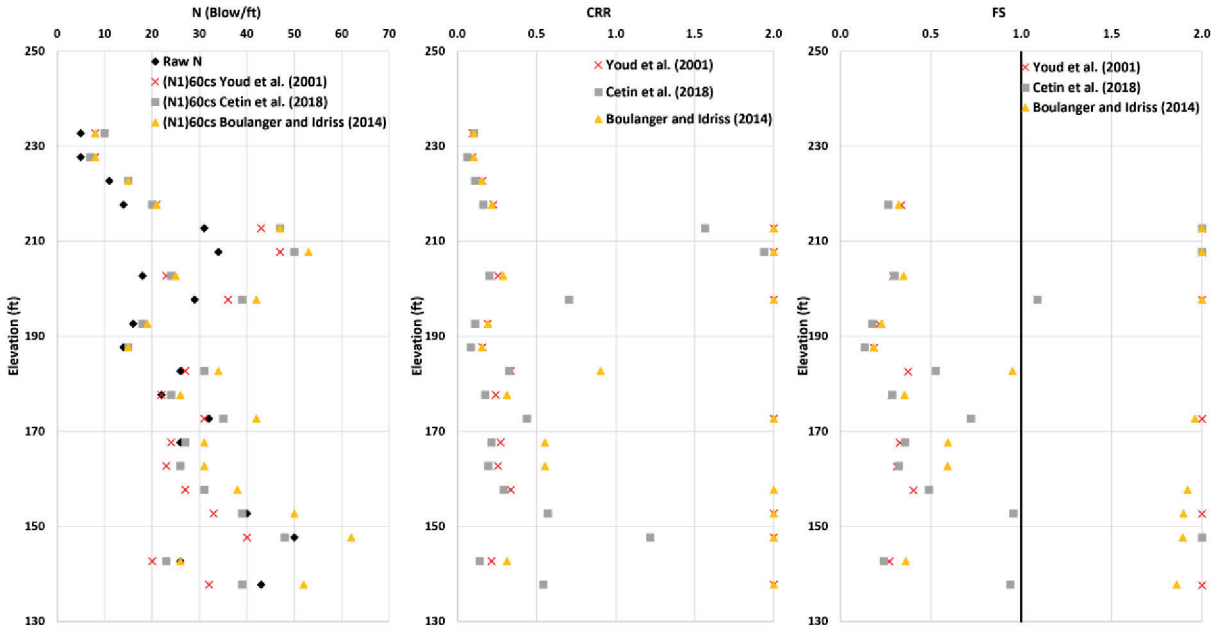

(a) (b) (c)

Figure 61**. Comparison of (a) Raw N and Equivalent Clean Sand Blow Count Values, (b) Unadjusted Cyclic Resistance Ratio (CRR), and (c) Factor of Safety Results for BH-4 at the Monette Site**

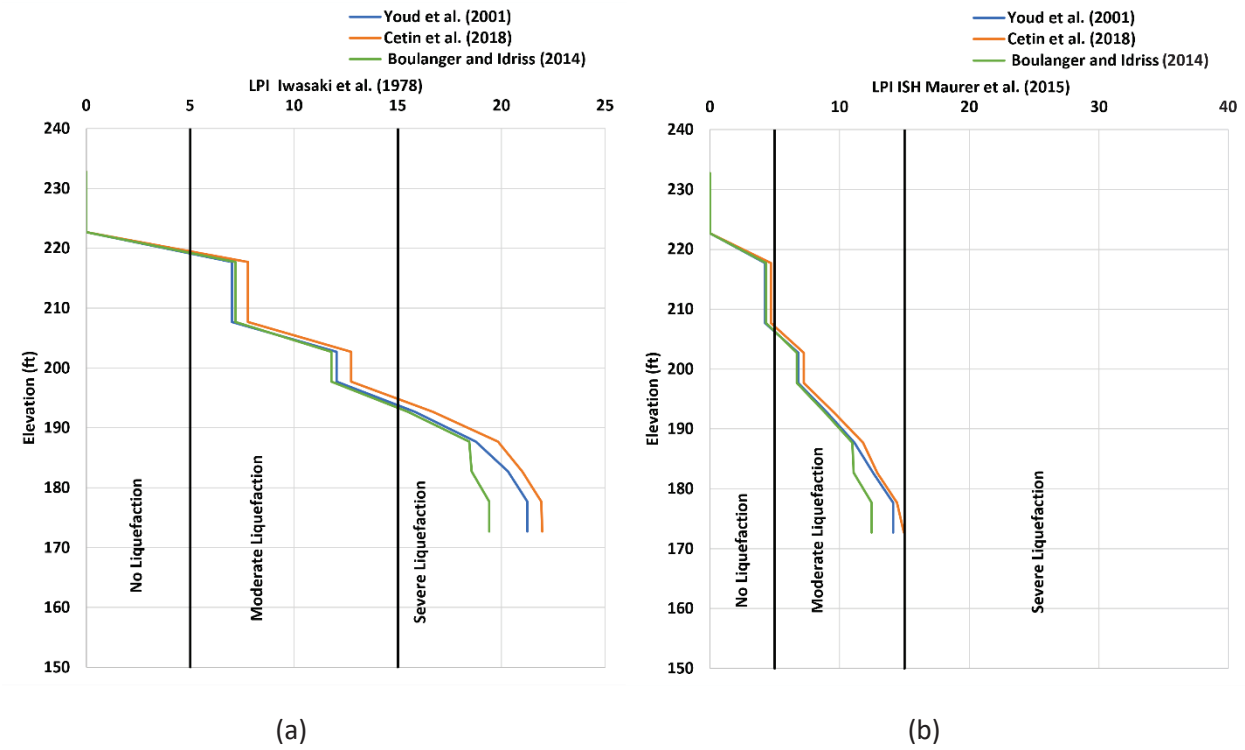

Figure 62. Cumulative (a) LPI by Iwasaki et al. (1978), (b) LPI_{ISH} by Maurer et al. (2015) for BH-4 at the Monette Site

CPT-Based Analysis

In this section, the CPT-based liquefaction analysis results at the Monette site will be discussed. The three CPT-based procedures used in the workbook are evaluated and compared. Four sets of CPT data were collected by ARDOT, and the locations of the CPT soundings are presented in Figure 50. The raw data of CPT 1 (surface elevation = 242.8 ft, water table = 21 ft); CPT 2 (surface elevation = 239.4 ft, water table = 16.5 ft); CPT 3 (surface elevation = 239.4 ft, water table = 15 ft); and CPT 4 (surface elevation = 240.8 ft, water table = 17 ft) are presented, respectively from Figure 63 to 66.

Figures 63, 64, 65, and 66 present the CPT data of CPT 1, CPT 2, CPT3, and CPT 4 respectively. From these CPTs, the surface soils for the site are generally a mix of sand and silts within the top 20 to 25 ft of the surface. Below 20–25 ft, sandy soils then exist. From Figure 63a, the tip resistance is determined to be less than 100 tsf for the top 20 ft, after this depth the tip resistance value increased linearly to almost 400 tsf at the bottom of the profile. The sleeve friction has a gradual increase from the surface to 10 ft, and below this depth, the sleeve friction is found between 0.5 to 2.5 tsf (Figure 63b). From the pore

pressure plot (Figure 63c), the water table depth is observed to be at 21 ft, as below this depth, the pore pressure is linear to the hydrostatic line. No significant difference is observed with the CPTs, except for the changes in groundwater table depth due to the ground surface elevation differences between the CPTs.

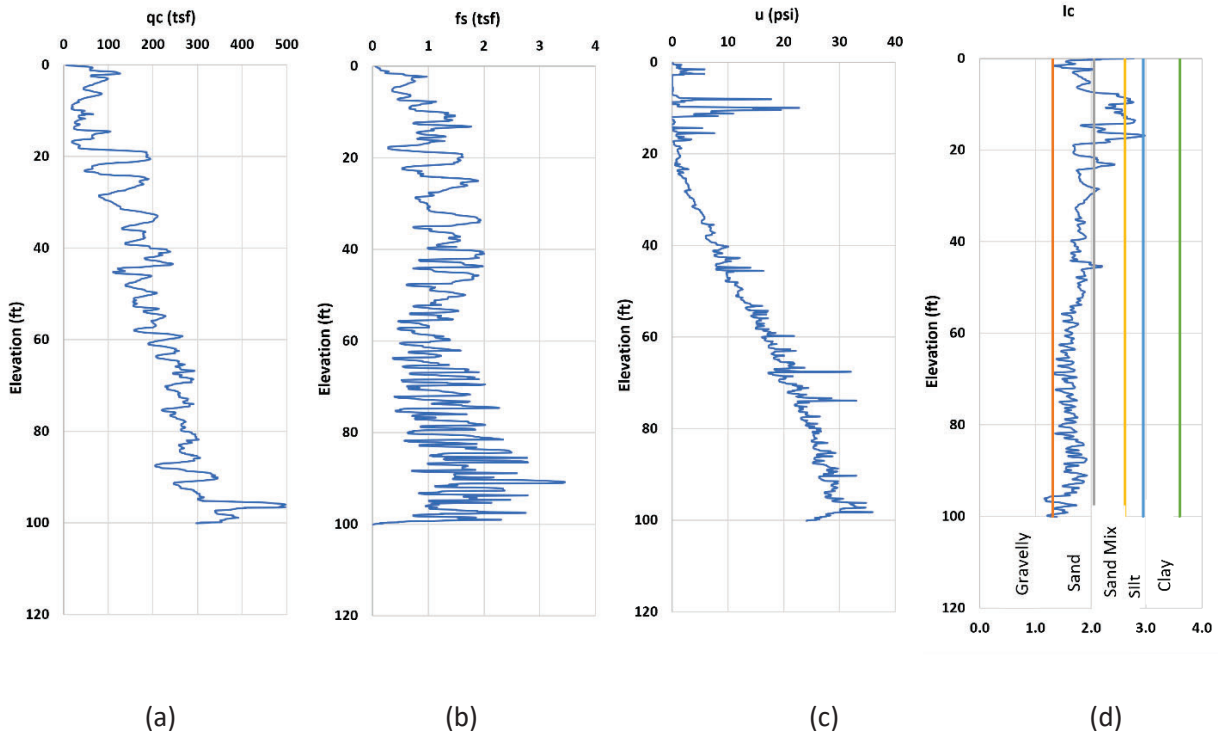

Figure 63. Raw (a) Tip Resistance (q_c), (b) Sleeve Friction (f_s), and (c) Pore Pressure (u), and (d) Normalized Soil Behavior Index (I_C) of CPT 1 at the Monette Site

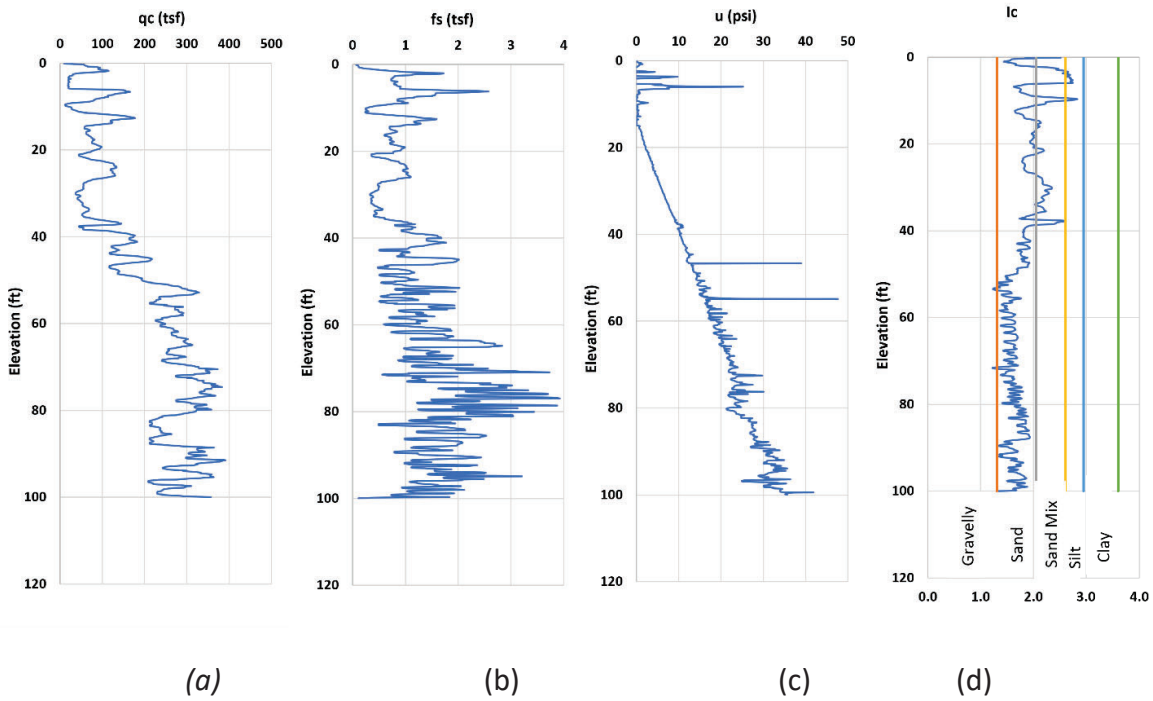

Figure 64**. Raw (a) Tip Resistance (q_c), (b) Sleeve Friction (f_s), and (c) Pore Pressure (u), and (d) Normalized Soil Behavior Index (I_C) of CPT 2 at the Monette Site**

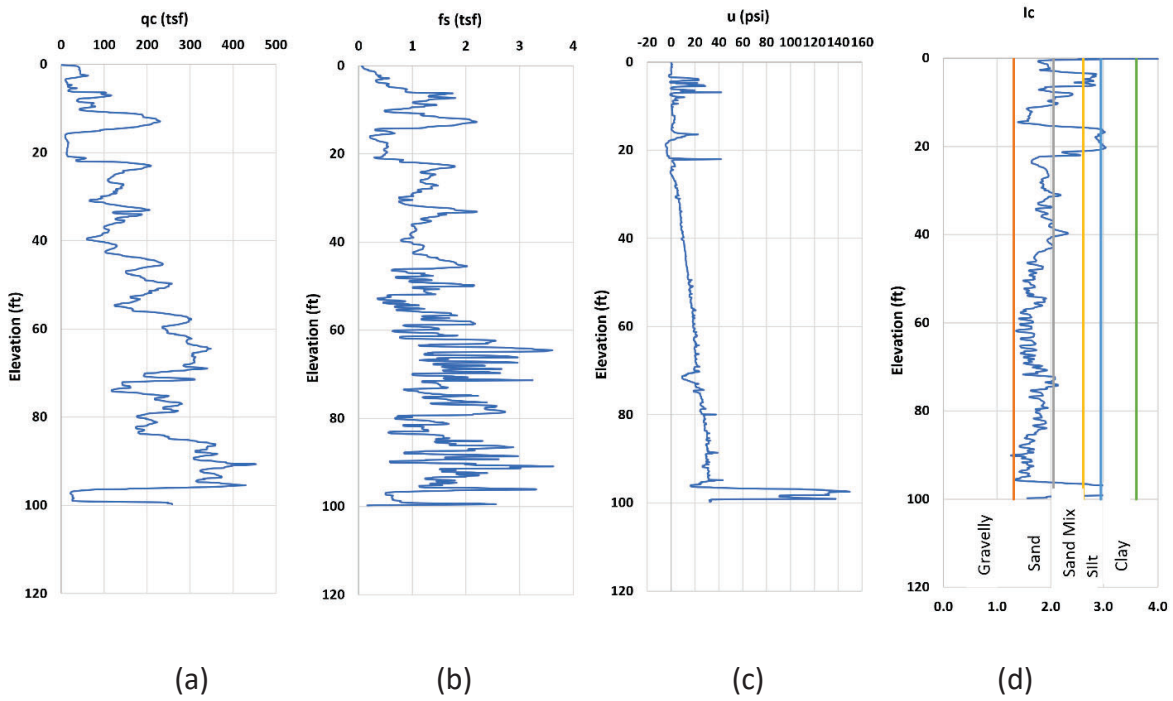

Figure 65**. Raw (a) Tip Resistance (q_c), (b) Sleeve Friction (f_s), and (c) Pore Pressure (u), and (d) Normalized Soil Behavior Index (I_C) of CPT 3 at the Monette Site**

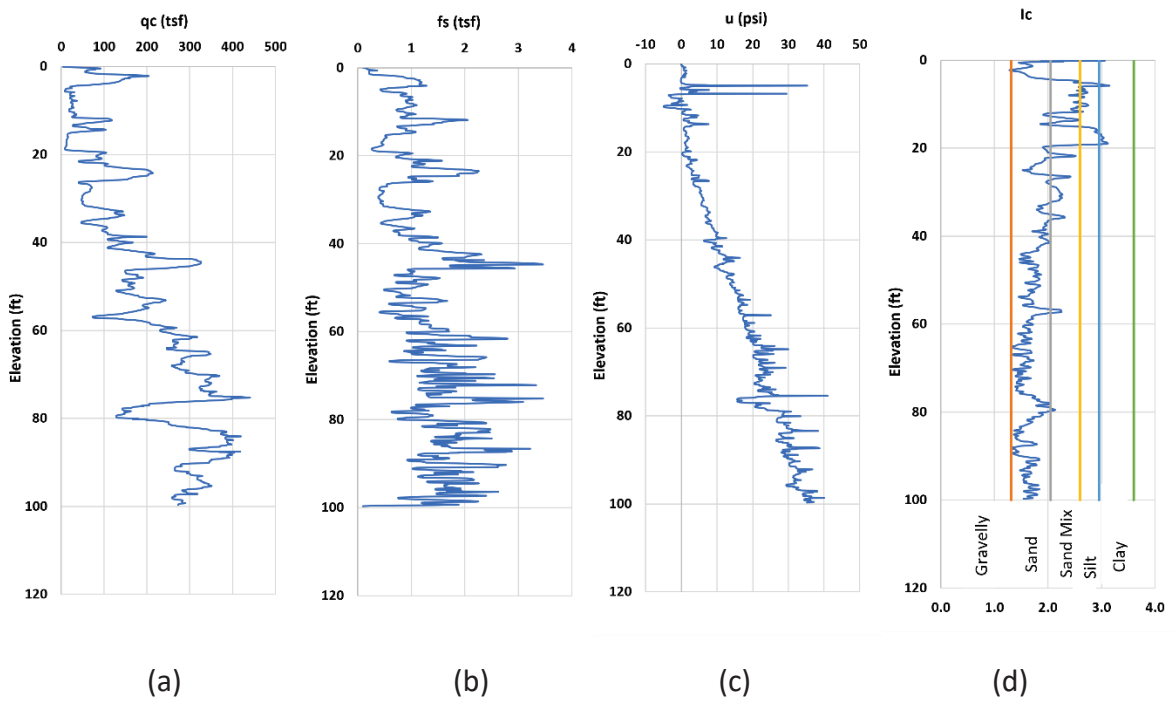

Figure 66. Raw (a) Tip Resistance (q_c), (b) Sleeve Friction (f_s), and (c) Pore Pressure (u), and (d) Normalized Soil Behavior Index (I_C) of CPT 4 at the Monette Site

Figure 67 presents the liquefaction analysis results of the CPT 1 sounding data for the Monette site using the three CPT-based liquefaction triggering procedures. The normalized equivalent clean sand tip resistance ($(q_{c1N})_{cs}$) profiles are presented in Figure 67a. From the ground surface to 225 ft elevation, $(q_{c1N})_{cs}$, obtained from Youd et al. (2001), is the highest of the three procedures, but for elevation lower than 175 ft, Youd et al. (2001) has the lowest $(q_{c1N})_{cs}$. Despite these differences, all the $(q_{c1N})_{cs}$ profiles, obtained from the three procedures, follow the same pattern. Though $(q_{c1N})_{cs}$, obtained from all three procedures are almost the same, Moss et al. (2006) produces higher factors of safety than the other two methods. The factor of safety, obtained from the Youd et al. (2001) and Boulanger and Idriss (2014) procedure are nearly similar from the ground surface to 175 ft elevation. As for elevation lower than 175 ft, Youd et al. (2001) generates the lowest $(q_{c1N})_{cs}$, the factor of safety is also found to be the lowest (Figure 67b). Figure 67c presents the discontinuous factor of safety plot by averaging the factor of safety results in Figure 67d in 5 ft intervals. From the figure, Moss et al. (2006) produces higher factors of safety than the other procedures. The Moss et al. (2006) procedure estimates elevations lower than 210 ft as non-liquefiable, whereas, for the other two procedures, many of the layers are considered

liquefiable. The Youd et al. (2001) procedure shows generally good agreement with the Boulanger and Idriss (2014) procedure, except in the deeper layers (Elevation lower than 160 ft) where the Boulanger and Idriss (2014) estimates most layers are non-liquefiable compared to the Youd et al. (2001) procedure that estimates these layers to be liquefiable. Similar results were observed for CPTs 2–4 at the site, which will be discussed more below.

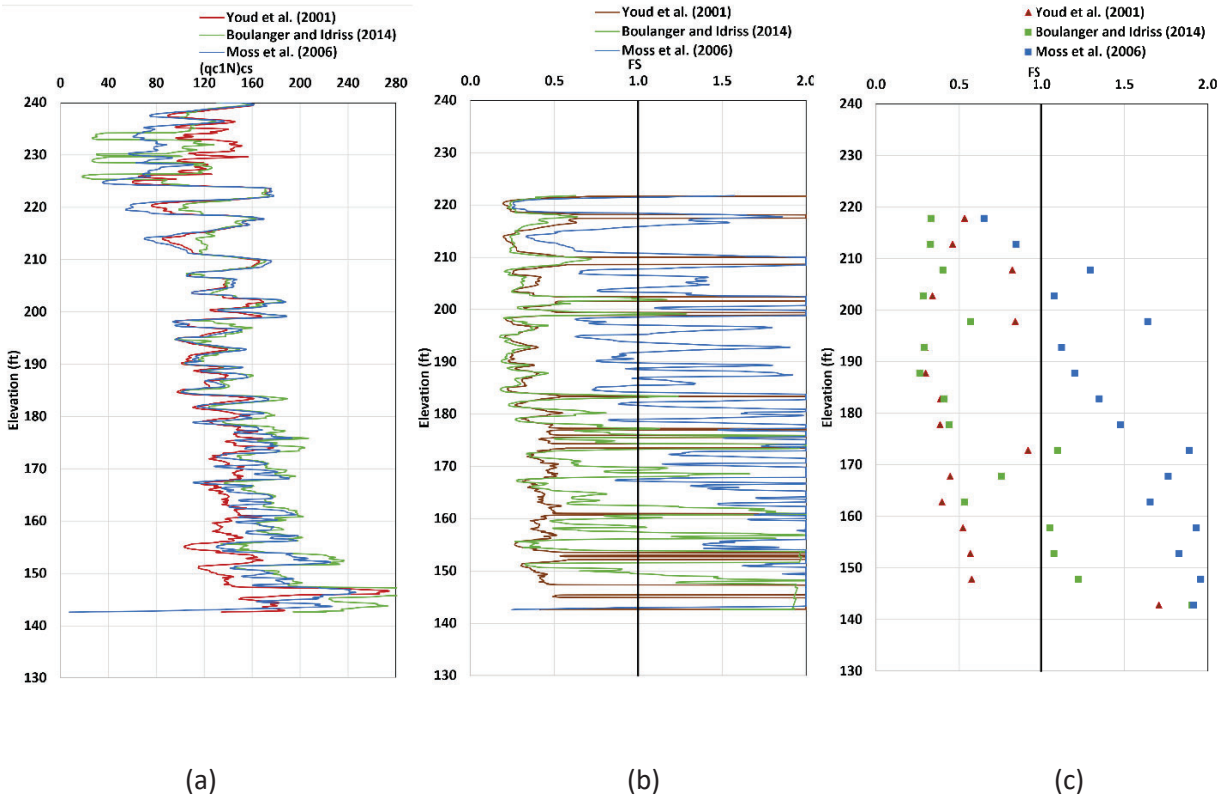

Figure 67. Comparison of (a) Equivalent Clean Sand Cone Penetration Resistance $(q_{c1N})_{cs}$, (b) Continuous Factor of Safety Results, and (c) Discontinuous Factor of Safety Results of CPT 1 Borehole at the Monette Site Using the Three Chosen CPT-based Procedure

The LPI analysis results for CPT 1 at the Monette Site are presented in Figure 68. LPI and LPI_{ISH} estimated from all CPT-based procedures suggest that the site is susceptible to severe liquefaction (LPI > 15), except the Moss et al. (2006) procedure. As the factor of safety calculated from the Moss et al. (2006)

procedure is higher than the other two CPT procedures, the estimated liquefaction severity is found to be less than the others.

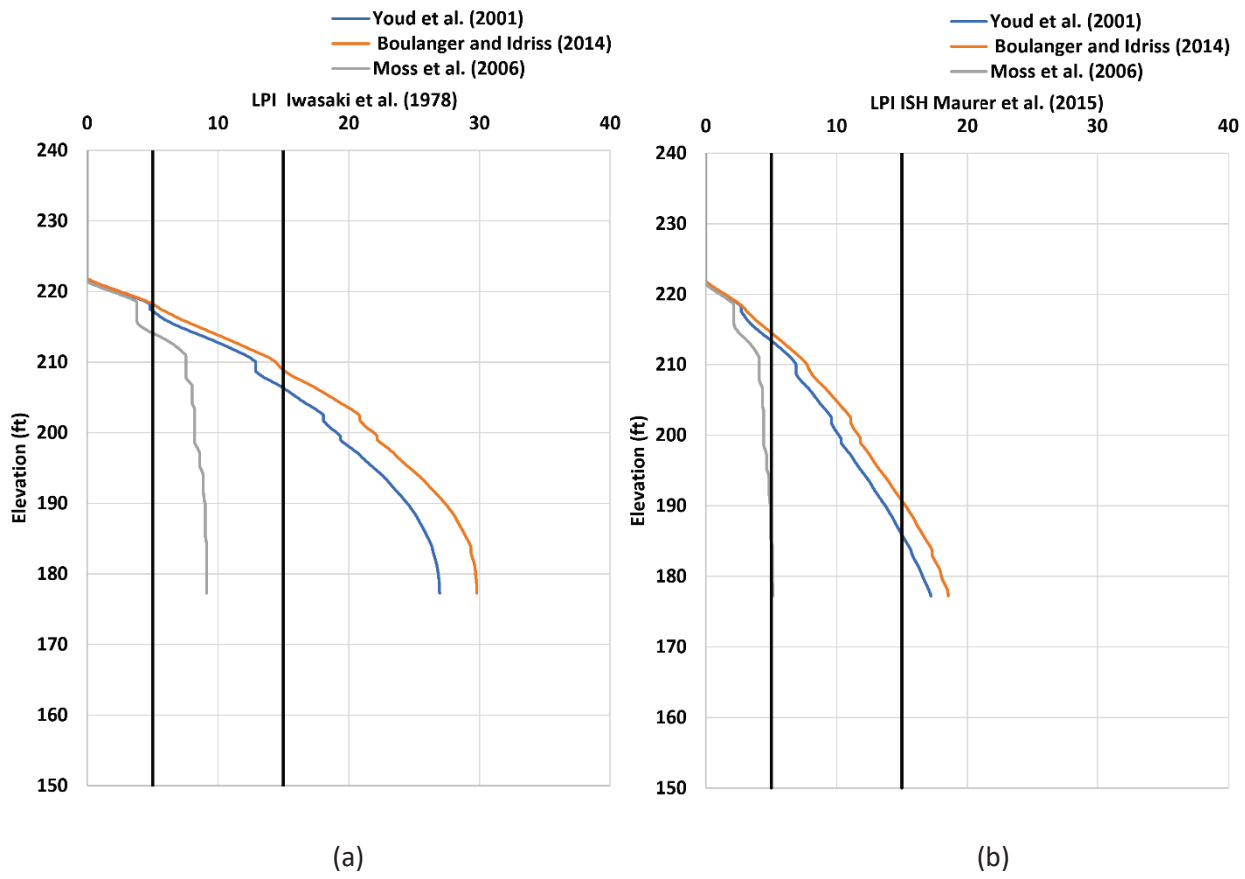

Figure 68. Cumulative (a) LPI by Iwasaki et al. (1978), (b) LPI_{ISH} by Maurer et al. (2015) for CPT 1 at the Monette Site

To understand potential variability in the CPT results at the Monette site, the Boulanger and Idriss (2014) procedure is used to perform further site-specific comparisons between CPTs on each side of the bridge. Figure 69a presents a comparison of the normalized clean sand cone penetration resistance ($(q_{c1N})_{cs}$) for CPT soundings 1 and 2 on the west side of the bridge (see Figure 50), obtained using the Boulanger and Idriss (2014) procedure. CPT 1 (surface elevation = 242.8 ft, water table = 21 ft) has a little higher ground elevation than CPT 2 (surface elevation = 239.4 ft, water table = 16.5 ft). From Figure 69b, the FS results from the two CPTs agree that the west side of the bridge is liquefiable for elevations

above 185–190 ft when below the water table. Below an elevation of 185–190, the CPTs indicate the site is interbedded with layers with an FS greater than and less than 1.0. Generally, CPT 2 is less liquefied than CPT 1, which is supported by the discontinuous plot in Figure 69c.

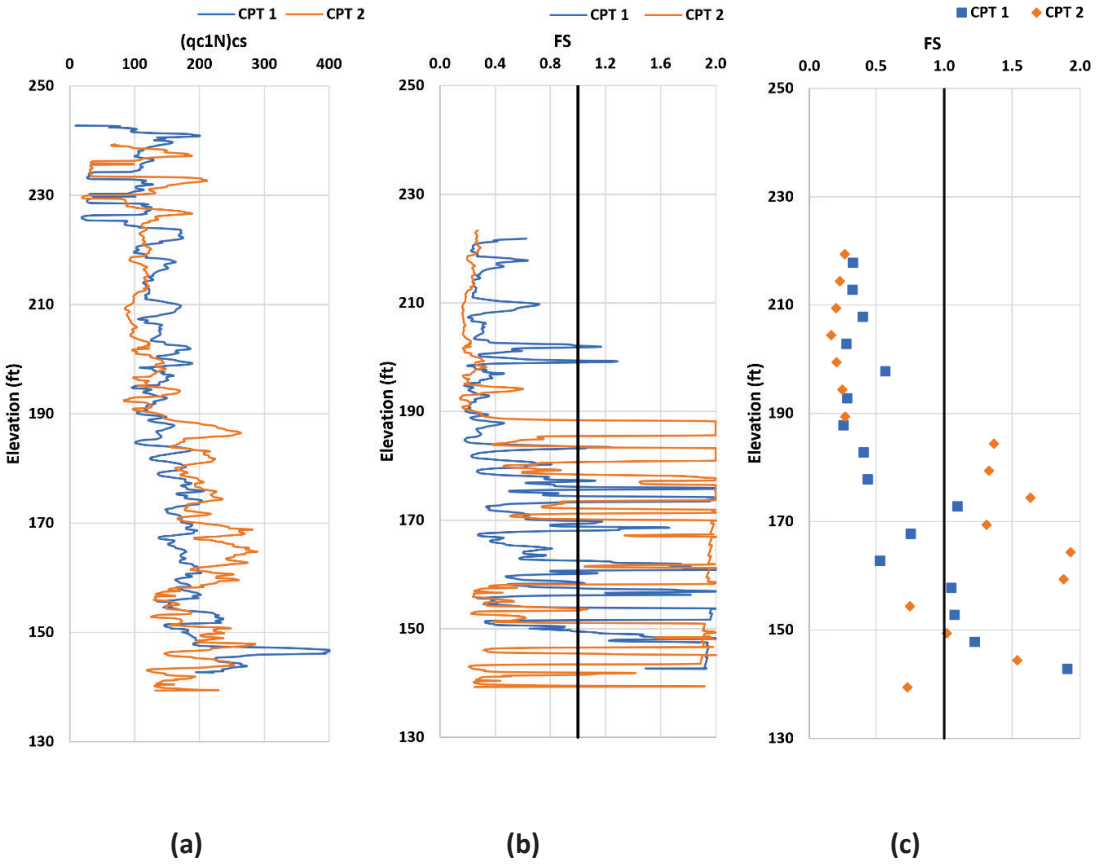

Figure 69**. Comparison of (a) Equivalent Clean Sand Cone Penetration Resistance ($q_{c1N})_{cs}$, (b) Continuous Factor of Safety Results, and (c) Discontinuous Factor of Safety Results of CPT 1 and CPT 2 at the Monette Site Using the Boulanger and Idriss (2014) Procedure**

The LPI analysis results for CPT 1 and CPT 2 at the Monette site using the Boulanger and Idriss (2014) procedure are presented in Figure 70. LPI and LPI_{ISH} estimates suggest that these two sites are susceptible to severe liquefaction (LPI > 15). Additionally, the severity of liquefaction of CPT 2 is higher than CPT 1.

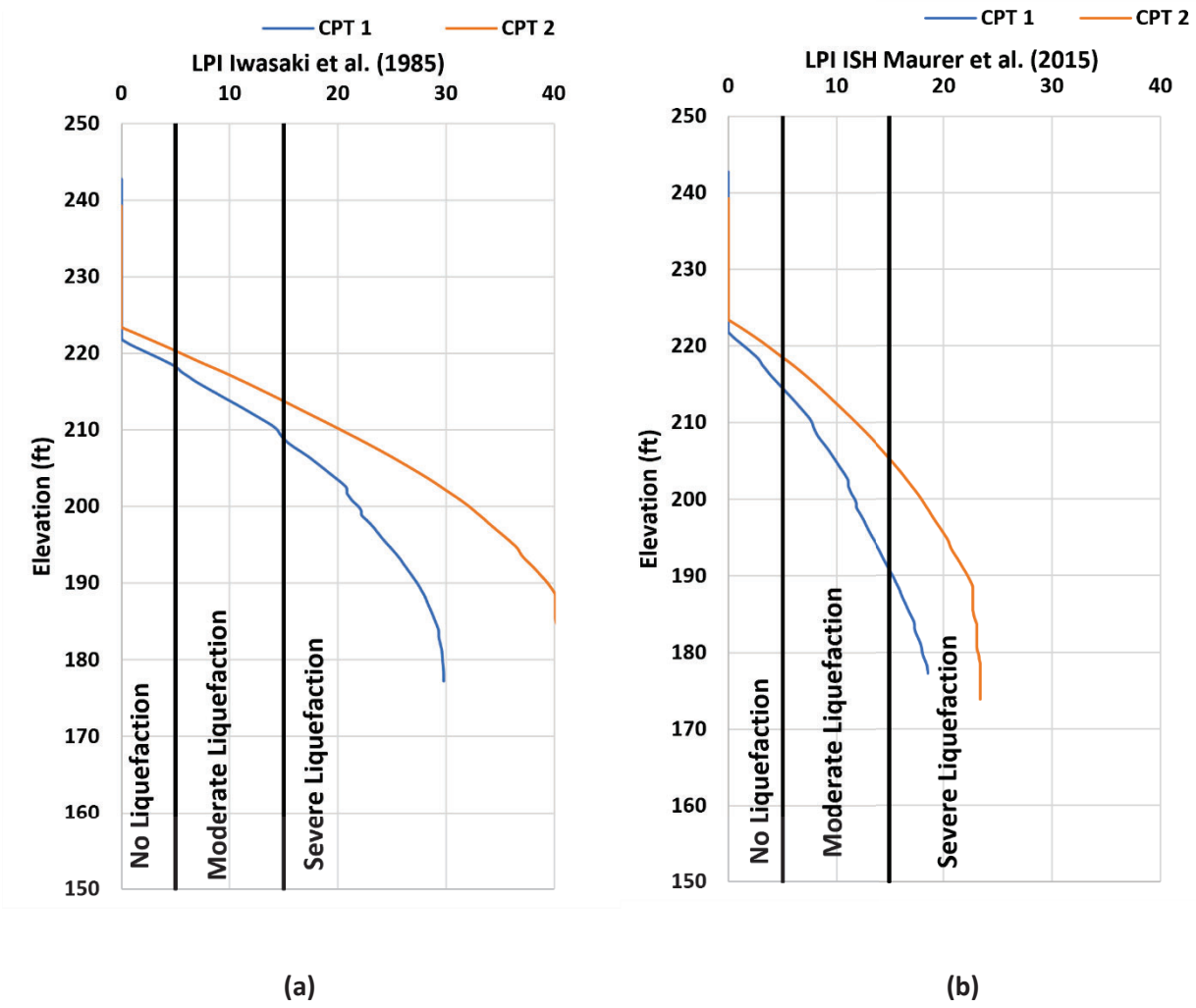

Figure 70. Cumulative (a) LPI by Iwasaki et al. (1978), (b) LPI_{ISH} by Maurer et al. (2015) for CPT 1 and CPT 2 at the Monette Site Using the Boulanger and Idriss (2014) Procedure

Figure 71a presents a comparison of the normalized clean sand cone penetration resistance ($(q_{c1N})_{cs}$) of the CPT soundings 3 and 4 on the east side of the bridge (see Figure 50), obtained from the Boulanger and Idriss (2014) CPT procedures. Though CPT 1 and CPT 2 show differences in liquefiable layers, CPT 3 and CPT 4 are in good agreement with strong similarities throughout the soundings. From Figure 71b and Figure 71c, the profile shows thin, nonliquifiable layers close to the ground surface. However, from

surface elevation 220 ft to 180 ft, and surface elevation 165 ft to 155 ft deep liquefiable layers are encountered. CPT 3 does indicate more liquefiable layers are present in the 165 to 155 ft elevation compared to CPT 4.

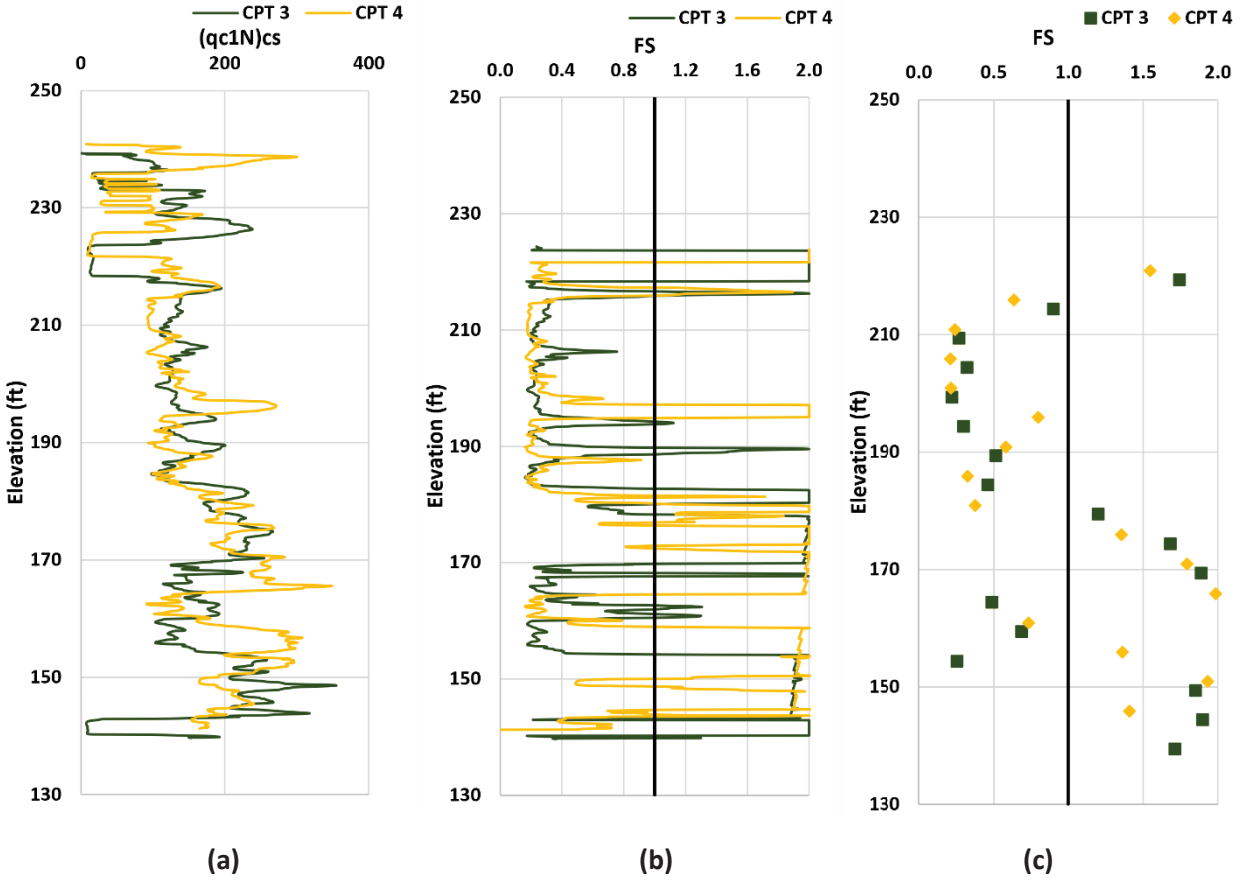

Figure 71. Comparison of (a) Equivalent Clean Sand Cone Penetration Resistance $(q_{c1N})_{cs}$, (b) Continuous Factor of Safety Results, and (c) Discontinuous Factor of Safety Results of CPT 3 and CPT 4 at the Monette Site Using the Boulanger and Idriss (2014) Procedure

The LPI analysis results for CPT 3 and CPT 4 at the Monette site using the Boulanger and Idriss (2014) procedure are presented in Figure 72. LPI and LPI_{ISH} estimates suggest that these two sites are susceptible to severe liquefaction (LPI > 15). Unlike CPT 1 and CPT 2, the liquefaction severity is almost the same for both CPTs on the east side of the bridge.

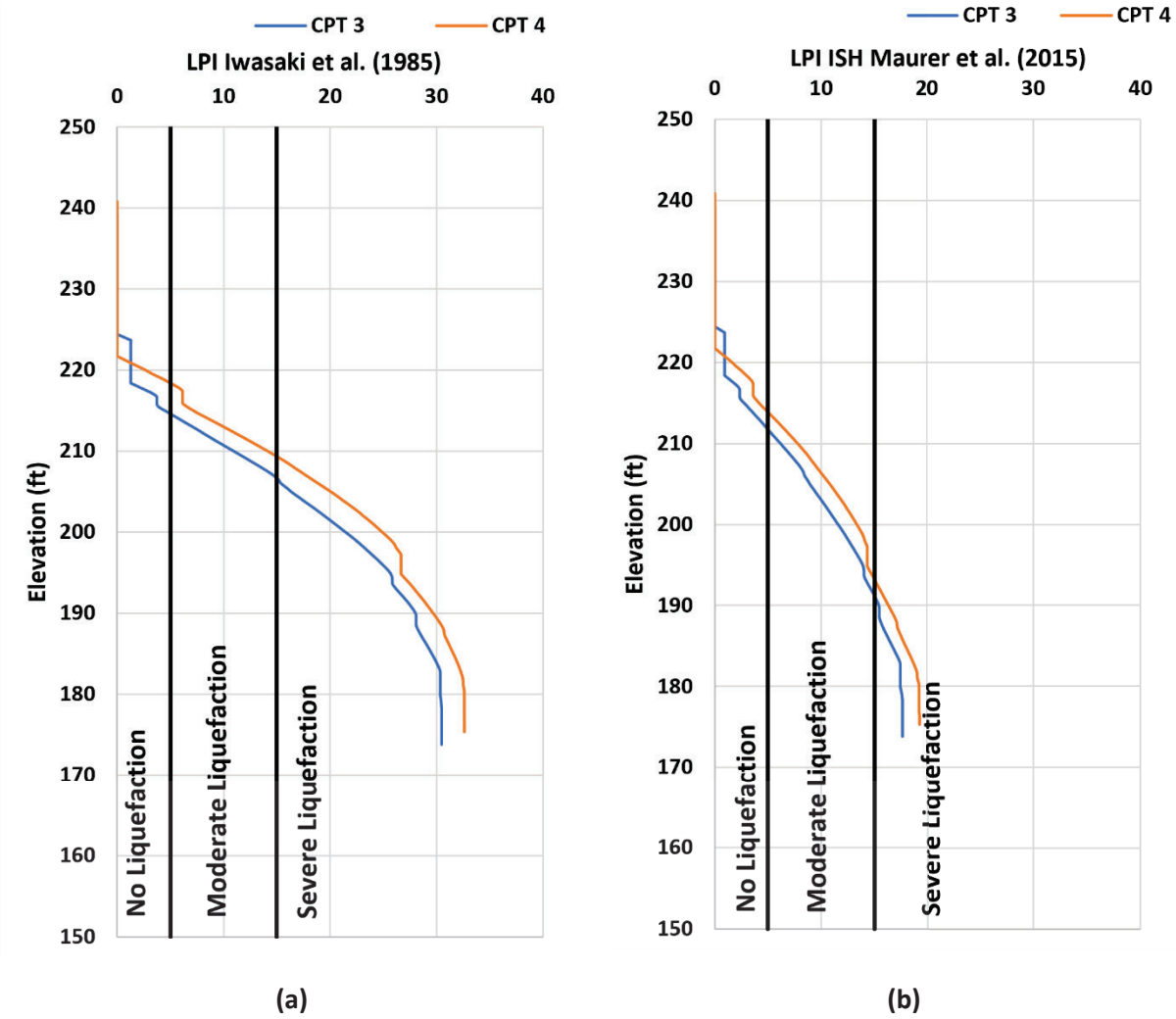

Figure 72. Cumulative (a) LPI by Iwasaki et al. (1978), (b) LPI_{ISH} by Maurer et al. (2015) for CPT 3 and CPT 4 at the Monette Site Using the Boulanger and Idriss (2014) Procedure

V_s-Based Analysis

In this section, the V_s-based liquefaction analysis results of the Monette site will be discussed. The two V_s-based procedures are evaluated and compared. The seismic data from CPT 1–4 at the Monette site are presented in Figure 73. The shear wave velocity is between 150–200 m/s range in the top 12 m (40 ft). Below 12 m (40 ft), the shear wave velocity increases linearly up to almost 300 m/s at the bottom of the profile for all SCPTs.

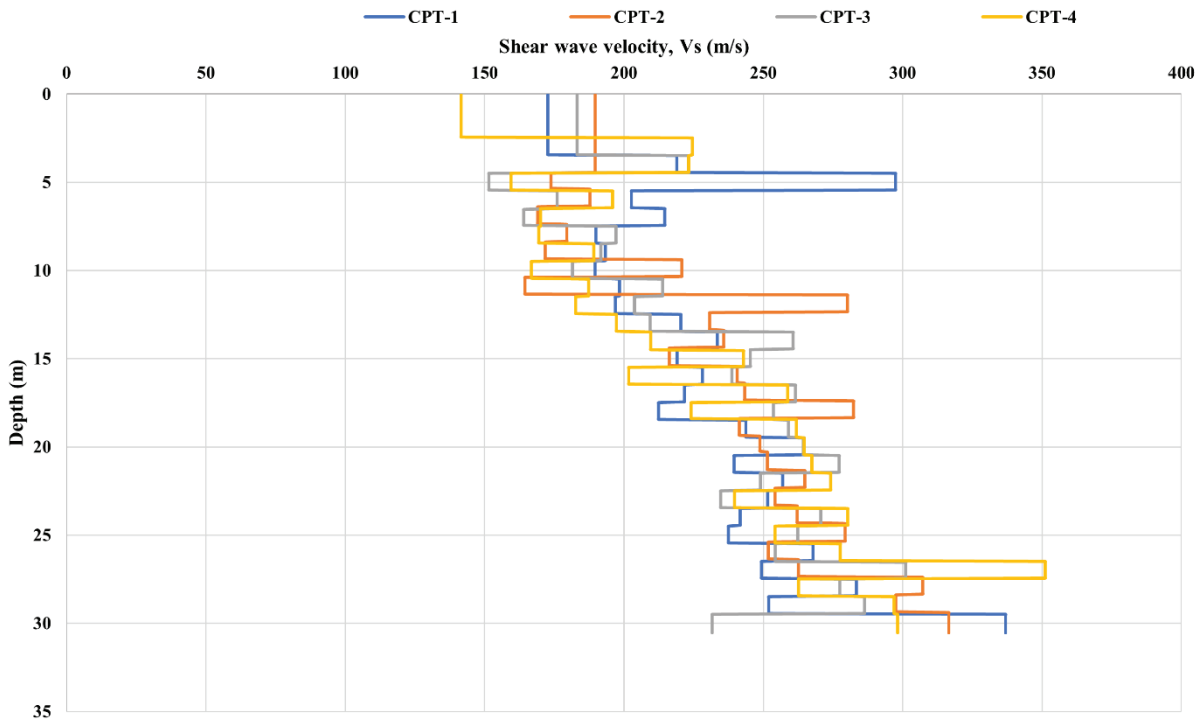

Figure 73**. Comparison of Shear Wave Velocity Data from SCPT 1–4 at the Monette Site**

Figure 74 presents the liquefaction analysis results of the Seismic CPT 1 sounding data of the Monette site using the two chosen V_s-based liquefaction triggering procedures. The obtained overburden stress-corrected shear wave velocity (V_{s1}) profiles are presented in Figure 74a. From the figure, the V_{s1} profiles obtained from the two procedures are nearly the same. Despite the similarity in V_{s1} profiles, Figure 74b presents the differences in the obtained factor of safety between the two procedures. Youd et al. (2001) procedure stated that V_{s1} values higher than 200–215 m/s (depending on fines content) are too dense to liquefy. This is why Youd et al. (2001) indicates many of the soil layers are non-liquefiable when V_{s1} exceeds this limit. However, Kayen et al. (2013) indicates many of these same soil layers are liquefiable. Figure 74c presents the discontinuous factor of safety results of the CPT 1 borehole at the Monette site using the two chosen V_s-based procedures and both procedures show that the soil layers are liquefiable for elevations above 195–215 ft when below the water table.

Wood et al. (2017) examined the performances of the Kayen et al. (2013) and Youd et al. (2001) procedures using 46 V_s-based liquefaction triggering case histories from the 2010–2011 Canterbury

earthquake sequence and concluded that the Kayen et al. (2013) procedure, using the 15% probability of liquefaction curve, provides more accurate predictions than the Youd et al. (2001) deterministic procedure for sites with V_{s1} in the critical layer greater than 180 m/s. In the Monette SCPT 1 data, V_{s1} is greater than 180 m/s for an elevation lower than 200 ft. At elevations lower than 200 ft, Youd et al. (2001) shows that the profile is non-liquefiable, whereas Kayen et al. (2013) shows the possibility of being liquefiable. Based on this data, there is a tendency to believe the Kayen et al. (2013) procedure would provide more accurate liquefaction triggering estimates for this site than the Youd et al. (2001) procedure.

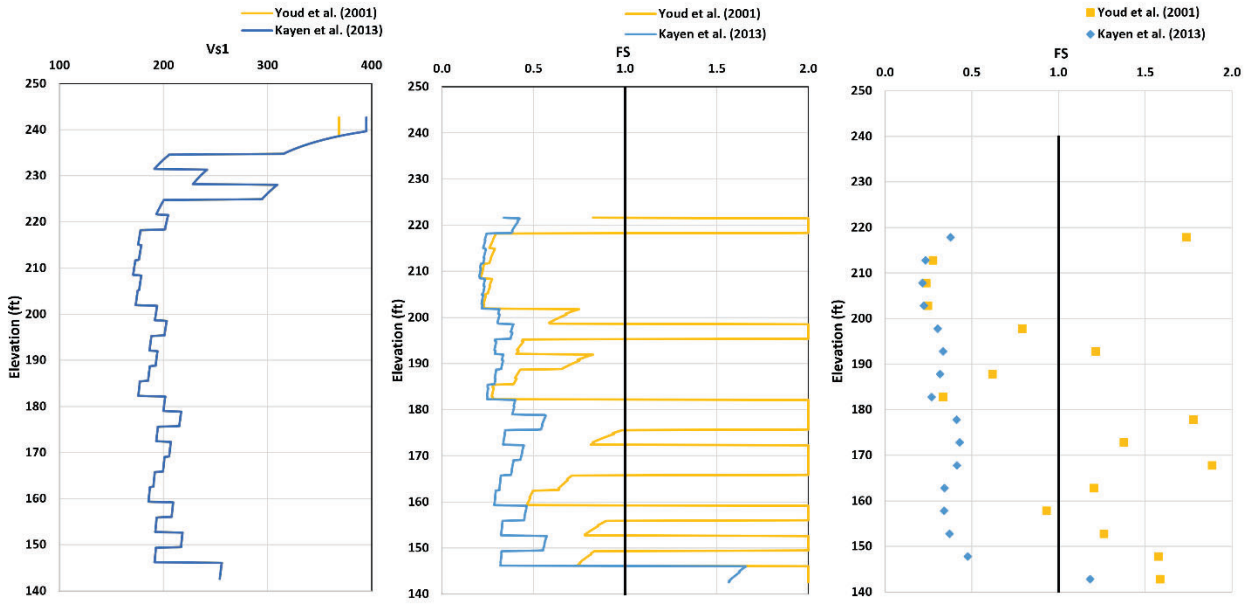

Figure 74. Comparison of (a) Overburden Stress Corrected Shear Wave Velocity (V_{s1}), (b) Continuous Factor of Safety Results, and (c) Discontinuous Factor of Safety Results of SCPT 1 Borehole at the Monette Site Using the Two Chosen V_s-based Procedures

The LPI analysis results for SCPT 1 at the Monette Site are presented in Figure 75. For SCPT 1, LPI estimates from all V_s-based procedures suggest that the site is susceptible to severe liquefaction (LPI > 15). LPI_{ISH} estimates less liquefaction manifestation than LPI. LPI_{ISH} calculated using the Youd et al. (2001)

shows moderate liquefaction (5 < LPI < 15), whereas LPI_{ISH} calculated using the Kayen et al. (2013) procedure suggests the possibility of severe liquefaction.

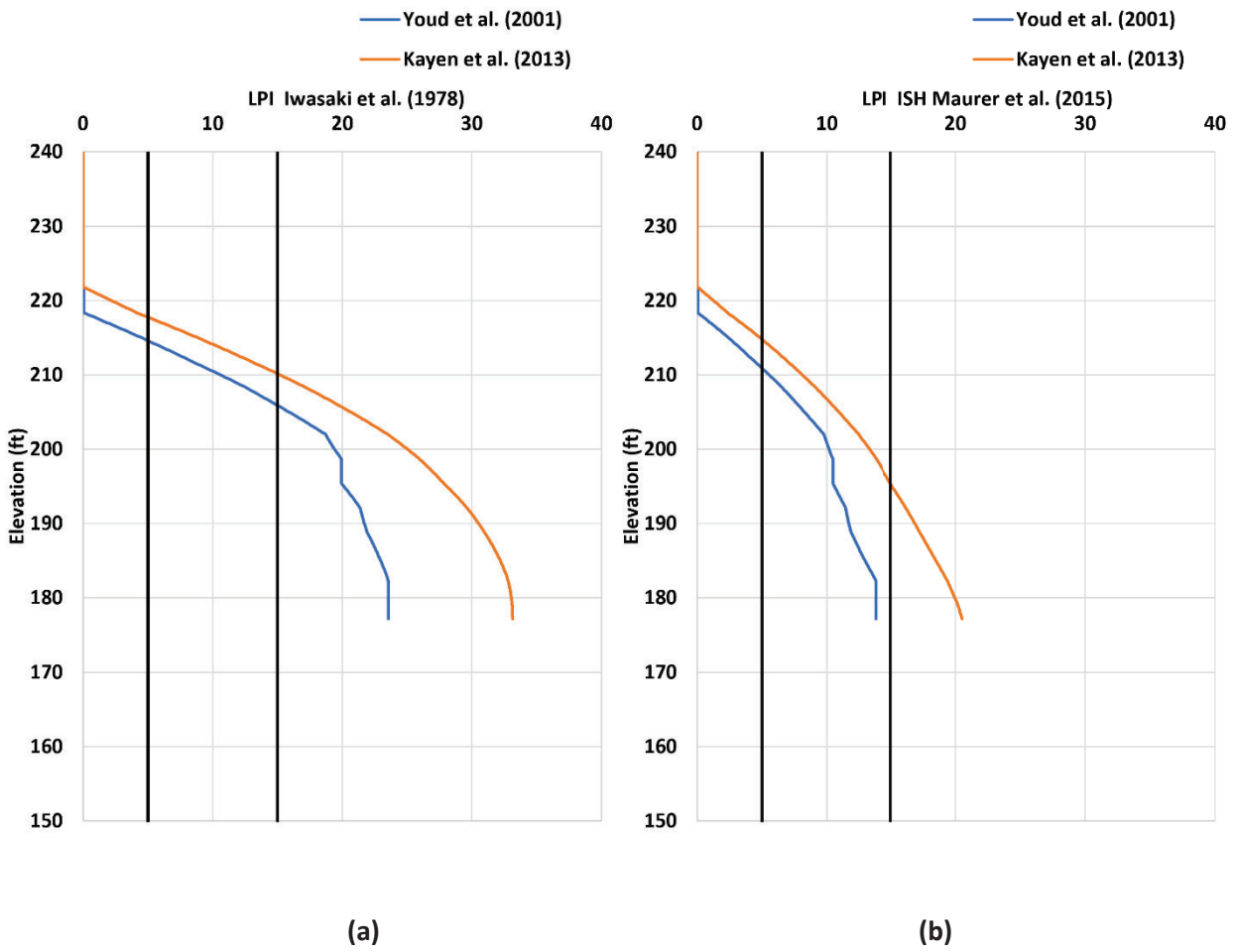

Figure 75. Cumulative (a) LPI by Iwasaki et al. (1978), (b) LPI_{ISH} by Maurer et al. (2015) for SCPT 1 at the Monette Site Using the V_S-based Liquefaction Triggering Procedure

To understand potential variability in the V_s results at the Monette site, the Kayen et al. (2013) procedure is used to perform further site-specific comparisons between SCPT on each side of the bridge. Figure 76a presents a comparison of the overburden stress corrected shear wave velocity for CPT sounding's 1 and 2 on the west side of the bridge (see Figure 50), obtained using the Kayen et al. (2013) procedure. From Figure 76b, the FS results from the two CPTs agree that the west side of the bridge is

liquefiable for elevations above 145–150 ft when below the water table. Both CPTs indicate the site is generally liquefiable at all depths with some thin layers considered non-liquefiable.

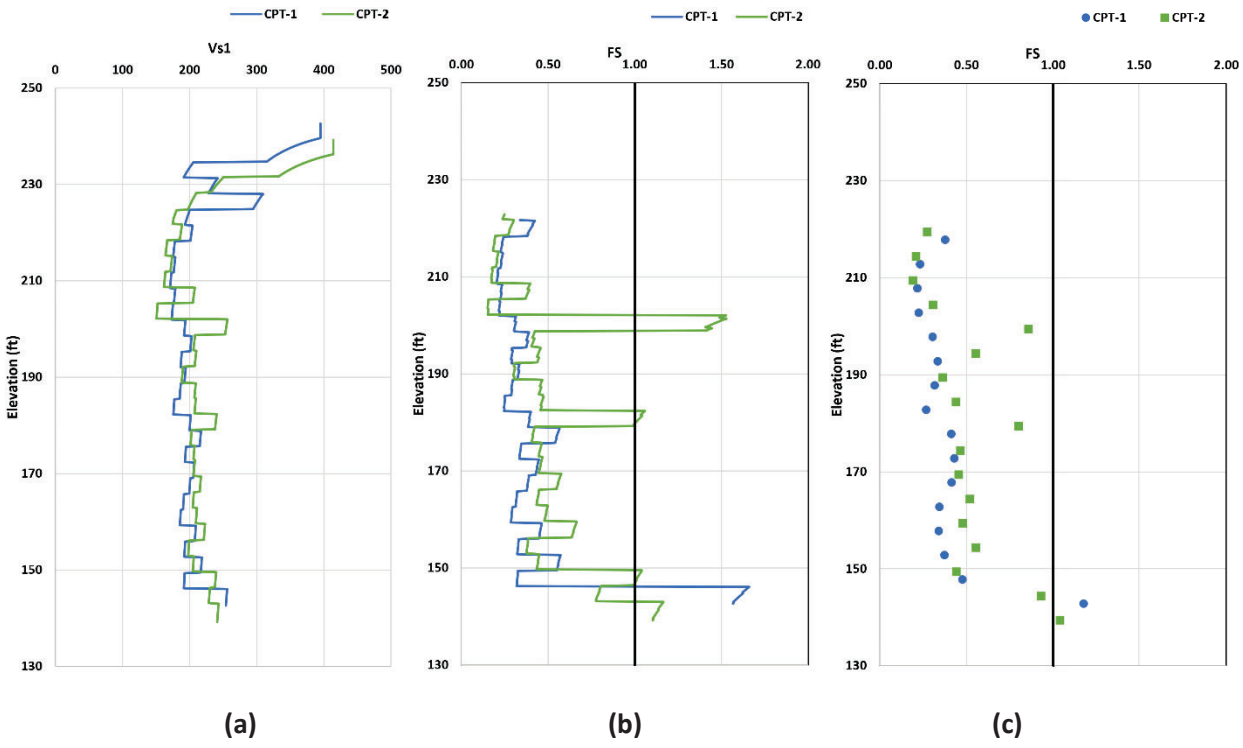

Figure 76. Comparison of (a) Overburden Stress Corrected Shear Wave Velocity (V_{s1}), (b) Continuous Factor of Safety Results, and (c) Discontinuous Factor of Safety Results of SCPT 1 and SCPT 2 at the Monette Site Using the Kayen et al. (2013) Procedure

The LPI analysis results for SCPT 1 and SCPT 2 at the Monette site are presented in Figure 77. LPI and LPI_{ISH} estimated using the Kayen et al. (2013) procedures suggest that the site is susceptible to severe liquefaction (LPI > 15).

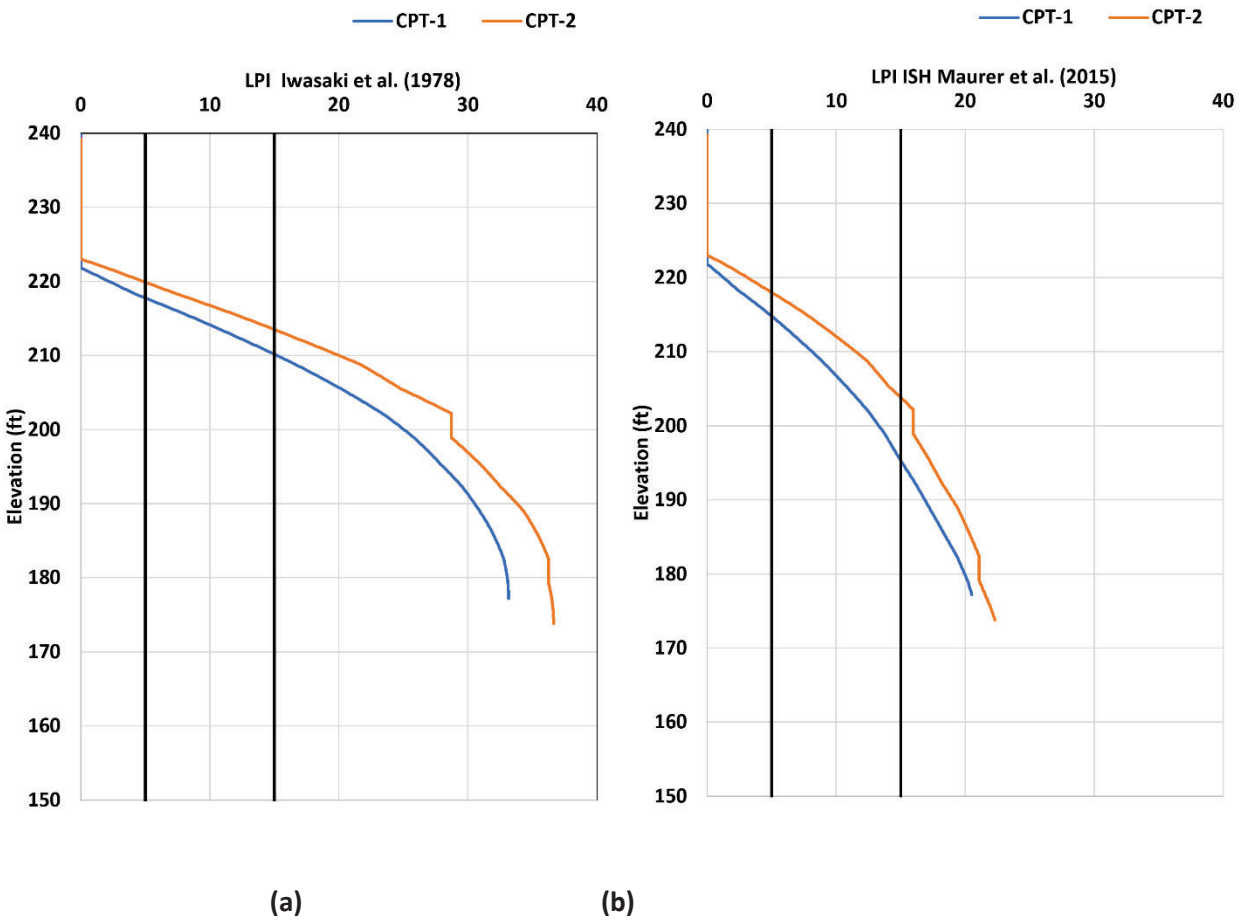

Figure 77. Cumulative (a) LPI by Iwasaki et al. (1978), (b) LPI_{ISH} by Maurer et al. (2015) for SCPT 1 and SCPT 2 at the Monette Site Using the Kayen et al. (2013) Procedure

Figure 78a presents a comparison of the overburden stress corrected shear wave velocity for the CPT soundings 3 and 4 on the east side of the bridge (see Figure 50), obtained using the Kayen et al. (2013) procedure. Similar to CPT 1 and CPT 2, CPT 3 and CPT 4 are in good agreement, indicating very similar patterns in the V_{s1} and factor of safety. From Figure 78b and Figure 78c, both SCPT profiles indicate most layers in the profile are likely to liquefy when below the water table.

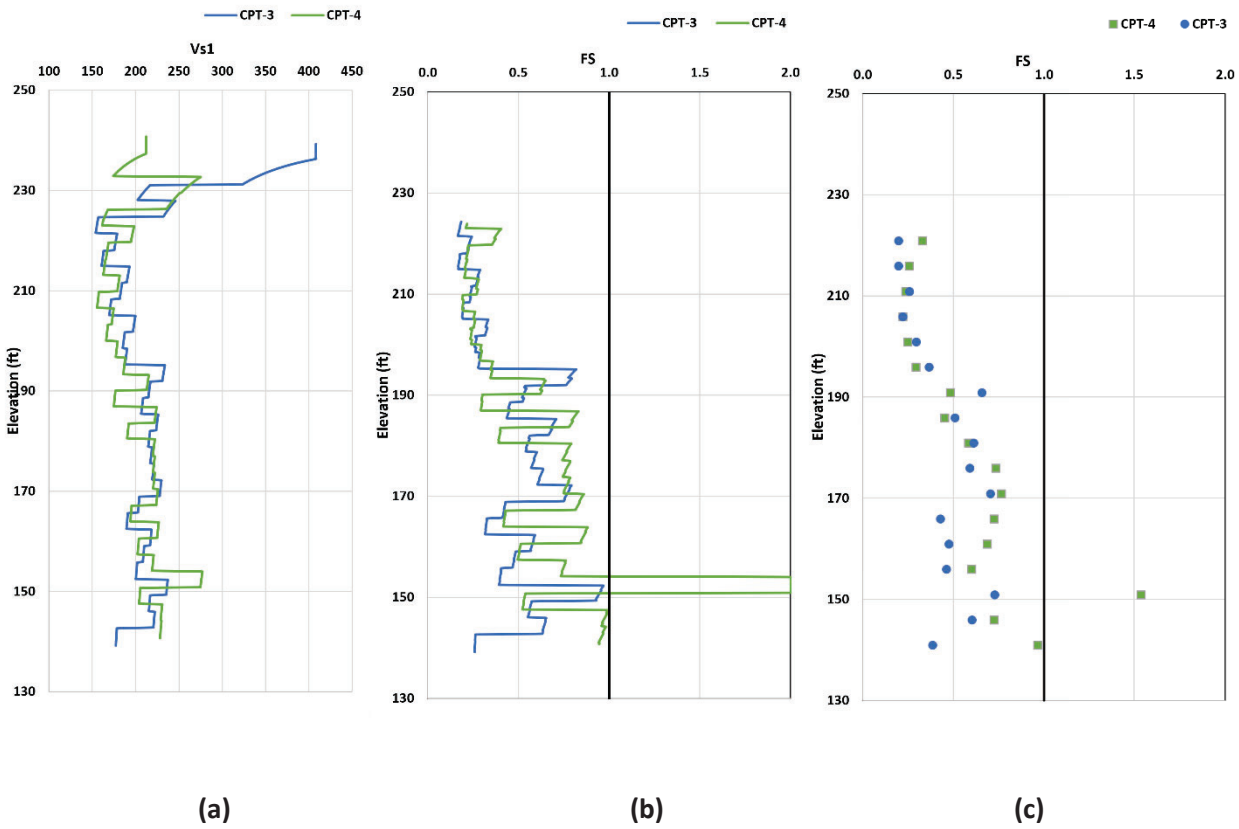

Figure 78. Comparison of (a) Overburden Stress Corrected Shear Wave Velocity (V_{s1}), (b) Continuous Factor of Safety Results, and (c) Discontinuous Factor of Safety Results of SCPT 3 and SCPT 4 at the Monette Site Using the Kayen et al. (2013) Procedure

The LPI analysis results for SCPT 3 and SCPT 4 at the Monette site are presented in Figure 79. LPI and LPI_{ISH} estimated using the Kayen et al. (2013) procedures suggest that the site is susceptible to severe liquefaction (LPI > 15).

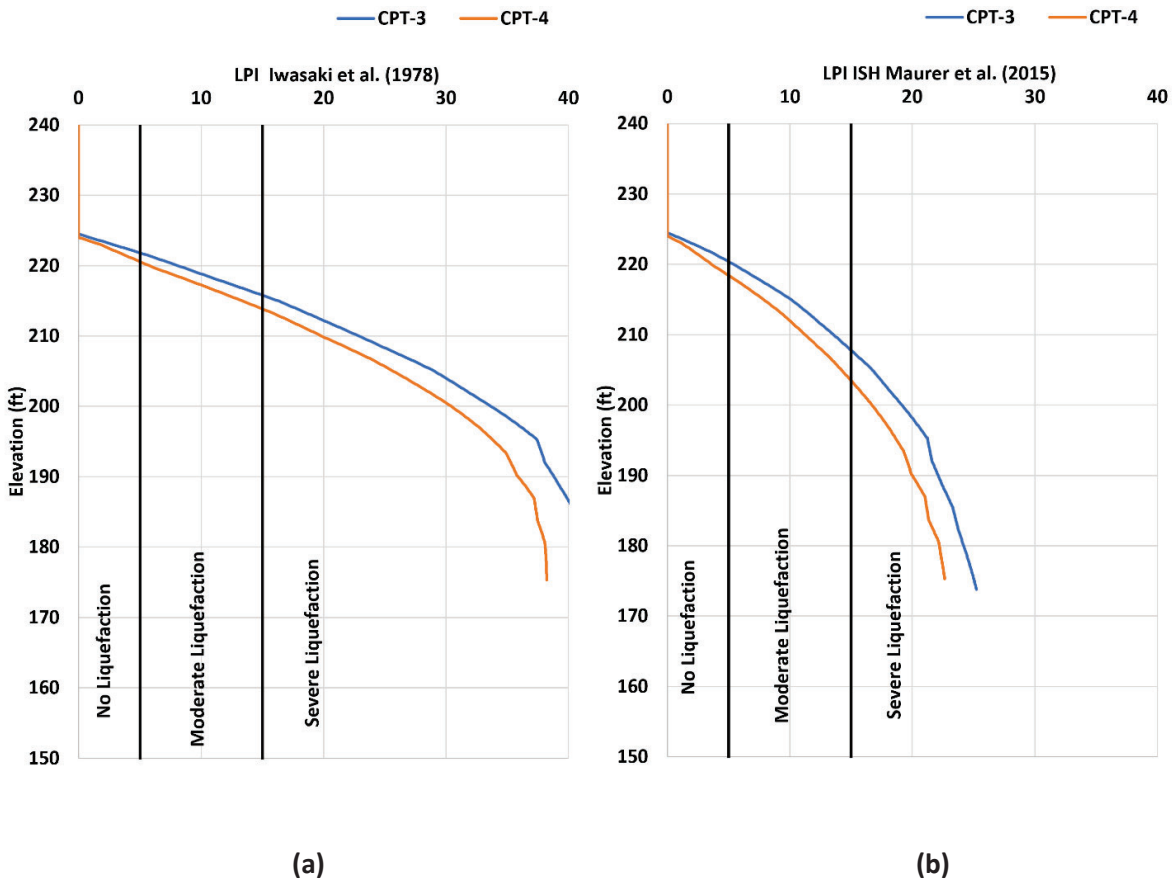

Figure 79**. Cumulative (a) LPI by Iwasaki et al. (1978), (b) LPI_{ISH} by Maurer et al. (2015) for SCPT 3 and SCPT 4 at the Monette Site Using the Kayen et al. (2013) Procedure**

Comparison of In-situ Methods of the Monette Site

In this section, the in-situ results for the Monette site are compared. The CPT and V_s-based results of SCPT 1 and SPT-based results of BH 3 are systematically compared and presented in Figures 80 and 81. In Figure 80, the SPT results are compared with the continuous CPT and V_s results, whereas in Figure 81, the SPT results are compared with the discontinuous CPT and V_s results. From Figures 80a and 81a, the SPT methods are in good agreement with the CPT-based procedure of Boulanger and Idriss (2014) from the surface to 160 ft elevation, at the elevations below that Moss et al. (2006) shows good agreement with the SPT-based results. It is important to note that Youd et al. (2001) and Boulanger and Idriss (2014) CPT-based approaches generally consider the deeper layers more liquefiable than the SPT-based approaches. Due to its discontinuous nature, the SPT methods are unable to resolve the thin layers

observed in the continuous methods. It is also important to note that the SPT-based liquefaction analysis from Boulanger and Idriss (2014) does not agree with the CPT-based liquefaction analysis from Boulanger and Idriss (2014) at an elevation lower than 175 ft. Moreover, Kayen et al. (2013) V_s-based procedure shows similar results to the CPT-based procedure of Boulanger and Idriss (2014) in the shallow depths (from the ground surface to the 180 ft elevation). At elevations lower than 180 ft, the CPT-based procedure of Boulanger and Idriss (2014) shows non-liquefiable layers, whereas the Kayen et al. (2013) method shows a possibility of these layers being liquefiable. This is likely driven by the shear wave velocity measures being averaged more through the soil column making them less sensitive to the rapid changes in stiffness in the soil profile than the CPT results. From the LPI analysis, this site is susceptible to severe liquefaction as all the in-situ methods show LPI and LPI_{ISH} higher than 15.

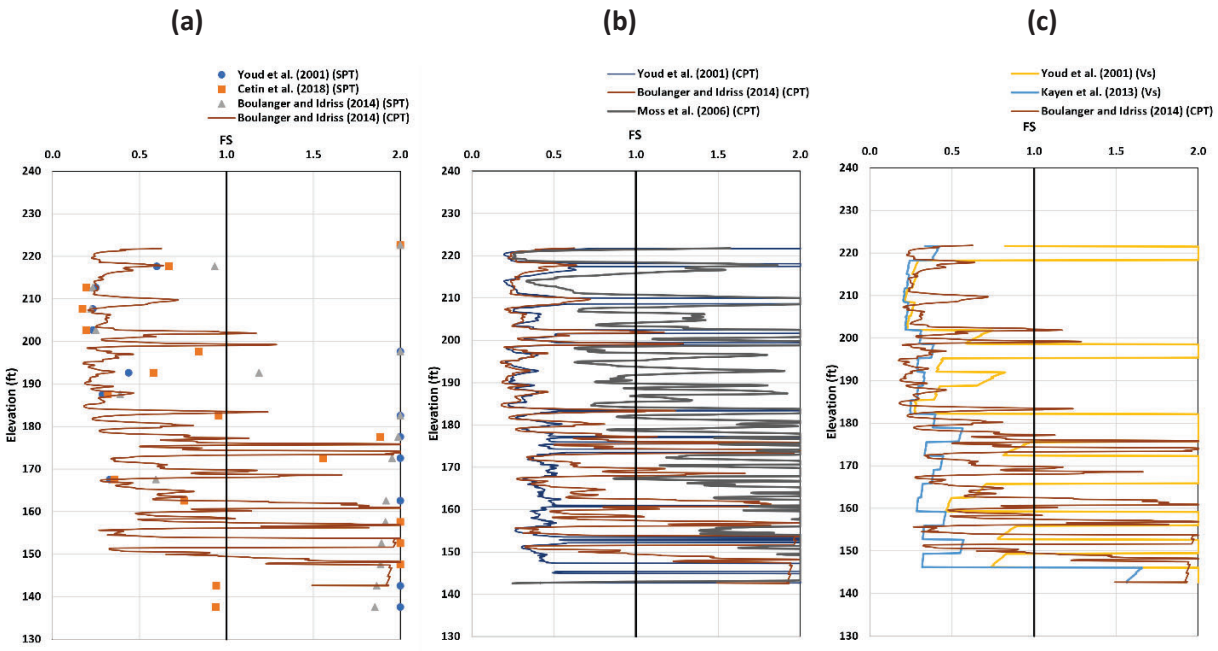

Figure 80. Comparison of SPT Results of BH-3 with Continuous CPT and V_s results of CPT 1 of Monette Site

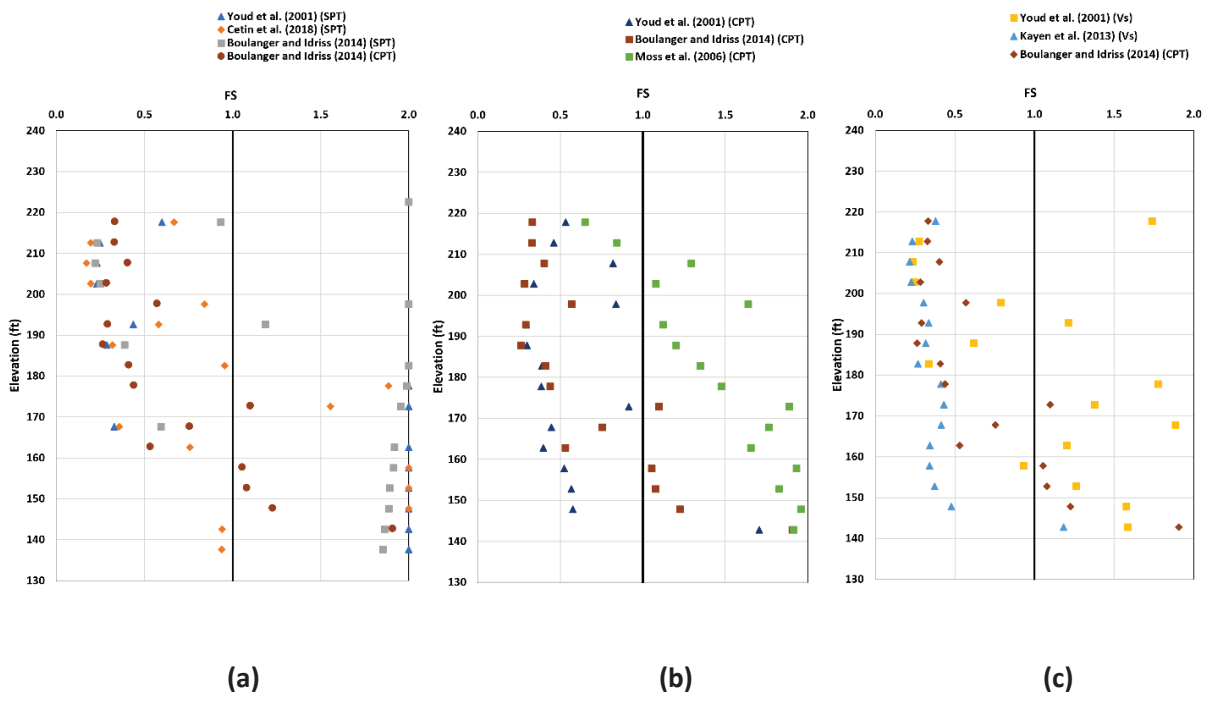

Figure 81. Comparison of SPT Results of BH-3 with Discontinuous CPT and V_s Results of CPT 1 of Monette Site

Analysis Results of Turrell Site

The liquefaction analysis results of the Turrell site data are discussed in this section. Six sets of SPT data were collected by ARDOT, and five sets of CPT data and SCPT data were collected by MoDOT from this site. These data sets are presented in the following sections. Though five CPT and SCPT-sounding data were recorded by MoDOT, only CPT 2 and CPT 4 are used in this analysis as much of the CPT results are considered poor quality. A detailed description of this site is also provided in Chapter 3.

SPT-based Analysis

In this section, the SPT-based liquefaction analysis results of the Turrell site will be discussed. The seismic information of this site is detailed in Chapter 3. Based on blow count, the site is classified as an AASHTO site class D with a design PGA value of 0.723 g and a moment magnitude (M_w) of 7.51. The design PGA and moment magnitude (M_w) were determined using procedures discussed in Chapter 3. The water table depth was determined to be 9.1 ft from the SPT bore logs. An elevation of 230 ft is used

as surface elevation to perform the liquefaction analysis. The soil type and raw blow count values of the boreholes are presented in Tables 7 and 8. From the borehole data, the site consists of clayey material in the top 25–30 ft with medium sand becoming dense to very dense sand as the soil profile gets deeper.

Table 7. Soil Type, Raw Blow Count Values, and Plasticity Index of AHTD-1, AHTD-2, and AHTD-3

	AHTD 1	AHTD 1	AHTD 1	AHTD 2	AHTD 2	AHTD 2	AHTD 3	AHTD 3	AHTD 3
Depth	SPT- N	Soil Group	Plasticity Index	SPT- N	Soil Group	Plasticity Index	SPT- N	Soil Group	Plasticity Index
(ft)	(blow/f			(blow/f			(blow/f		
5	10	CH	55	15	CL		13	CL	25
10	13	CH	61	10	CL		11	CH	62
15	10	CH	47	4	CL		8	CH	56
20	4	CH	41	2	CL-ML		4	CH	45
25	3	CL-ML	6	2	CL-ML		2	ML	NP
30	2	ML	NP	3	CL-ML		1	ML	7
35	7	SM	NP	10	CL-ML		3	SM	NP
40	8	ML	NP	8	SC		4	SM	NP
45	13	SM	NP	3	SW-SC		16	SM	NP
50	27	SM	NP	12	SW-SC		4	ML	NP
55	9	ML	NP	3	SC		19	SW-SM	NP
60	42	SM	NP	32	SW		30	SW	NP
65	29	SW-SM	NP	19	SW		42	SW-SM	NP
70	12	SM	NP	23	SW		28	SW-SM	NP
75	20	SW	NP	31	SW		48	SW	NP
80	22	SW	NP	12	SW		21	SW	NP
85	32	SW	NP	16	SW		25	SW	NP
90	37	SW	NP	11	SW		11	SW-SM	NP
95	94	SW-SM	NP	29	SW		35	SW	NP
100	43	SW	NP	22	SW		36	SW	NP

Table 8. Soil Type, Raw Blow Count Values and Plasticity Index of AHTD-4, AHTD-5, and AHTD-6

	AHTD 4	AHTD 4	AHTD 4	AHTD 5	AHTD 5	AHTD 5	AHTD 6	AHTD 6	AHTD 6
Depth	SPT- N	Soil Group	Plasticity Index	SPT- N	Soil Group	Plasticity Index	SPT- N	Soil Group	Plasticity Index
(ft)	(blow/ft)			(blow/ft)			(blow/ft)		
5	15	CL		14	CL		12	CL	
10	10	CL		10	CL		11	CL	
15	7	CL		4	CL		5	CL	
20	2	CL		2	CL		4	CL	
25	1	CL-ML		2	CL		1	CL	
30	12	CL-ML		3	GC		2	GC	
35	1	SW		3	GC		8	SM	
40	18	SC		14	SM		3	SM	
45	19	SW		14	SW		34	SW	
50	23	SW		25	SW		8	SW	
55	22	SW		5	SW		26	SW	
60	28	SW		26	SW		17	SW	
65	22	SW		18	SW		10	SW	
70	30	SW		12	SW		11	SW	
75	17	SW		40	SW		30	SC	
80	21	SW		14	SW		20	SW	
85	11	SW		21	SW		26	SW	
90	2	SW		39	SW		46	SW	
95	47	SW		39	SW		46	SW	
100	30	SW		94	SW		42	SW	

Figure 82a presents a comparison with the raw blow count and the equivalent clean sand blow count values ($(N_1)_{60,cs}$) obtained from all three SPT procedures for borehole AHTD-6 (surface elevation = 230 ft, water table = 9.1 ft). The analysis results of the other boreholes on this site are presented in the Appendix and are not discussed here to avoid repetition, as they all follow the same pattern.

The multiplication of the blow count correction factors for the Boulanger and Idriss (2014) procedure is more than 1 for the whole profile, and so the $(N_1)_{60,cs}$ is higher than the Raw N, whereas for the other two factors, the $(N_1)_{60,cs}$ is found lower than the Raw N in the deeper layers. This causes the unadjusted cyclic resistance ratio ($CRR_{M=7.5,\ \sigma'v=1\ atm}$) obtained from the Boulanger and Idriss (2014) procedure to be higher than the other two procedures and resulted in non-liquefiable layers (Figure 82b). At the

elevation lower than 185 ft, the $(N_1)_{60,cs}$ obtained from the Cetin et al. (2018) is found to be higher than the Youd et al. (2001) procedure but resulted in a low $CRR_{M=7.5,\ \sigma'v=1\ atm}$ and factor of safety less than 1.0. In summary, the blow count correction factors obtained from the Boulanger and Idriss (2014) procedure generate higher $(N_1)_{60,cs}$ values than the other two procedures and consequently yield more non-liquefiable layers. Also, the Youd et al. (2001) procedure yields a non-liquefiable layer when the $(N_1)_{60,cs}$ is found higher than 30, which agrees with the results using the Boulanger and Idriss (2014) procedure. However, the results from the Cetin et al. (2018) procedure do not agree with the other two procedures. The $CRR_{M=7.5,\ \sigma'v=1\ atm}$ obtained using the probabilistic approach of Cetin et al. (2018) generates FS less than 1, when the $(N_1)_{60,cs}$ values are between 35 and 40, whereas the other two procedures show FS more than 1 for this range. Figure 82c shows that the soil from the elevation of 200 ft to 145 ft, has shown the possibility of being liquefiable as the $(N_1)_{60,cs}$ obtained from all the procedures are less than 30, with a couple of non-liquefiable layers at the elevations of 185 ft and 175 ft with $(N_1)_{60,cs}$ higher than 30.

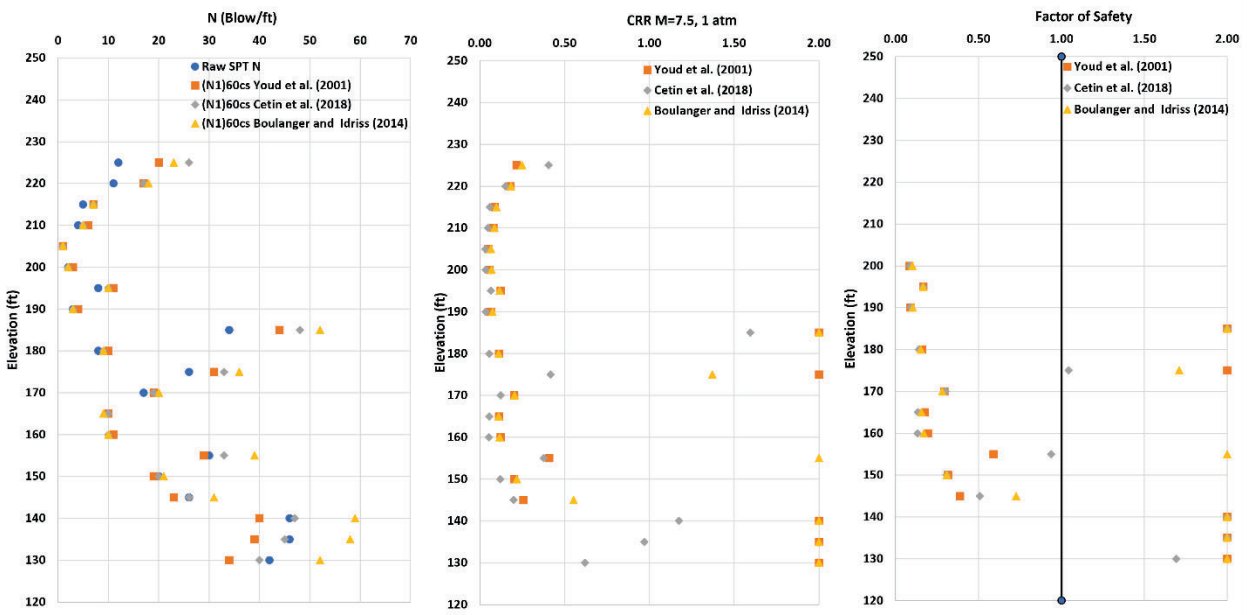

(a) **(b)** **(c)**

Figure 82. Comparison of (a) Raw N and Equivalent Clean Sand Blow Count Value, (b) Unadjusted Cyclic Resistance Ratio (CRR), and (c) Factor of Safety Results of AHTD 6 at the Turrell Site Using the Chosen Three SPT-based Procedures

The LPI analysis results for AHTD-6 at the Turrell Site are presented in Figure 83. It is important to note that the boundary curves of LPI_{ISH}, developed using a power-law depth weighting function by Maurer et al. (2015) may be more appropriate than the existing linear form of the LPI, developed by Iwasaki et al. (1978). For AHTD-6, LPI and LPI_{ISH} estimated from all SPT-based procedures suggest that the site is susceptible to severe liquefaction (LPI > 15).

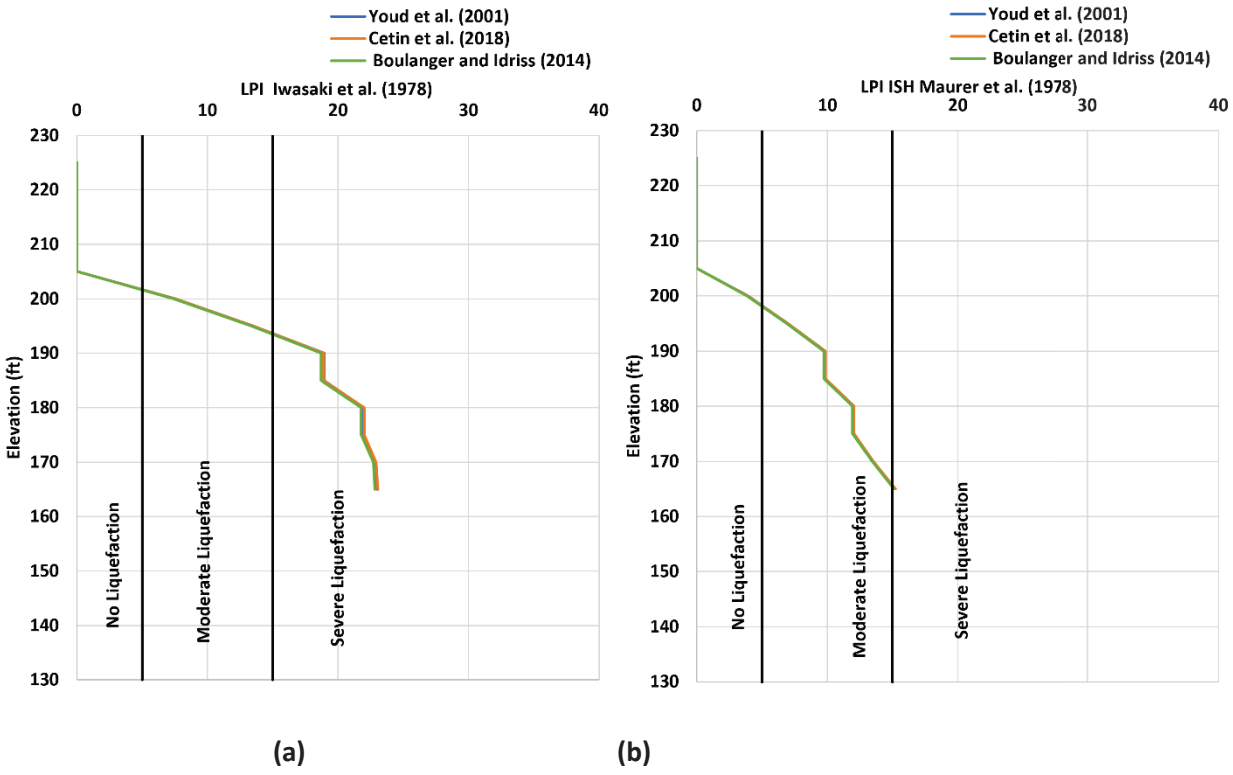

Figure 83. Cumulative (a) LPI by Iwasaki et al. (1978), (b) LPI_{ISH} by Maurer et al. (2015) for AHTD-6 at the Turrell Site Using the SPT-based Triggering Procedures

CPT-Based Analysis

In this section, the CPT-based liquefaction analysis results of the Turrell site will be discussed. Though five CPT-sounding data were recorded by MoDOT, only CPT 2 and CPT 4 are used in this analysis as much of the CPT results are considered poor-quality data. Similar to the SPT-based analysis, the elevations of these soundings are set at 230 ft. From the boring log of this site, the water table depth is known to be 9.1 ft. However, the pore pressure plots (Figure 84c, Figure 85c) of the CPTs disagree with that depth.

From the pore pressure plots, the water table depth is determined to be 35 ft and 45 ft for CPT 2 and CPT 4, respectively. This results in significant differences in the water table depths between the two CPTs. With such a large difference in water table depth estimates from the six CPTs at the site, the reliability of the CPT pore pressure measurements is questionable. Therefore, for the CPT-based analysis of the Turrell site, the water table depth is considered 9.1 ft similar to the SPT-based analysis. The raw data from CPT 2 and CPT 4 are presented in Figure 84 and Figure 85, respectively. From Figure 84 of the CPT 2 dataset, at the top 40 ft, silty clay is observed, and the tip resistance is less than 75 tsf. From 40 to 48 ft depth, sand is found with a high tip resistance ranging from 150 to 350 tsf, followed by a 4 ft thick silty clay layer from 48 to 52 ft with less than 100 tsf tip resistance. Below this depth, sand layers are observed.

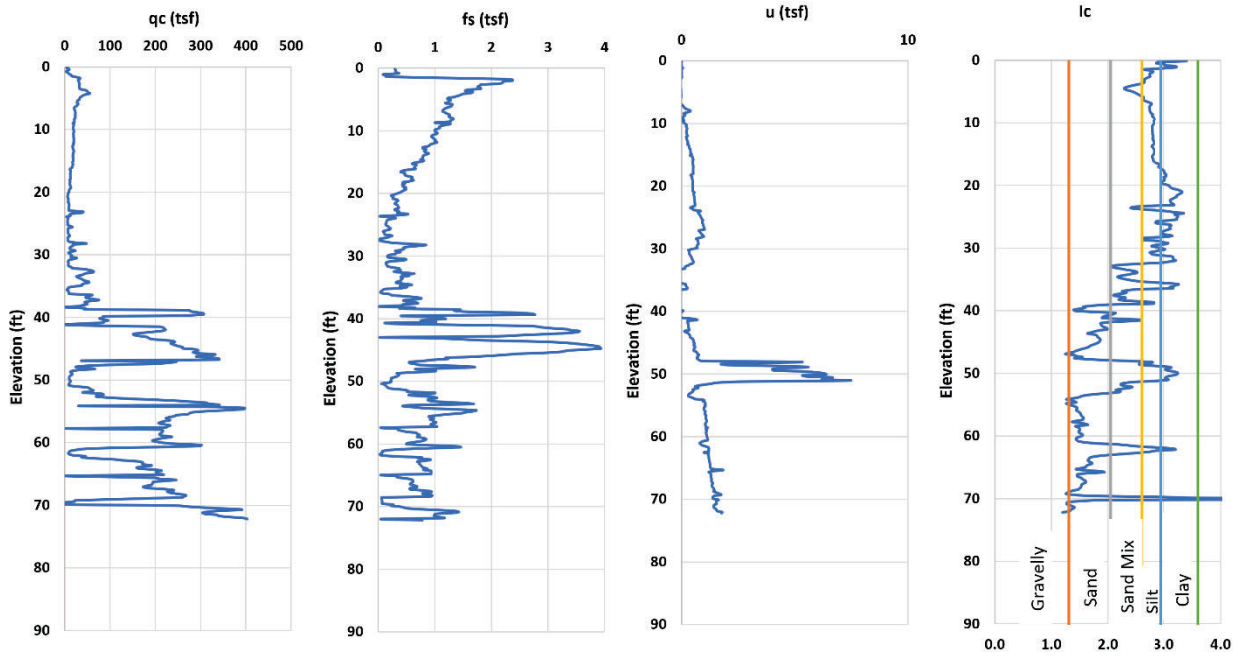

(a) (b) (c) (d)

Figure 84. Raw (a) Tip Resistance (q_c), (b) Sleeve Friction (f_s), and (c) Pore Pressure (u), and (d) Normalized Soil Behavior Index (I_C) of CPT 2 at the Turrell Site

From Figure 85 of the CPT 4 dataset, at the top 31 ft, the silty clay is observed, and the tip resistance is less than 50 tsf. From 31 to 35 ft depth, sand is found with a high tip resistance of 100 tsf, followed by 5 ft of silty clay from 35 to 40 ft with less than 30 tsf tip resistance. Sand layers are observed from 40–55 ft. Another 5 ft silty clay layer is observed from 56 to 61 ft with less than 30 tsf tip resistance. For the rest of the profile, sand layers are found with high tip resistance ranging from 100 to 400 tsf.

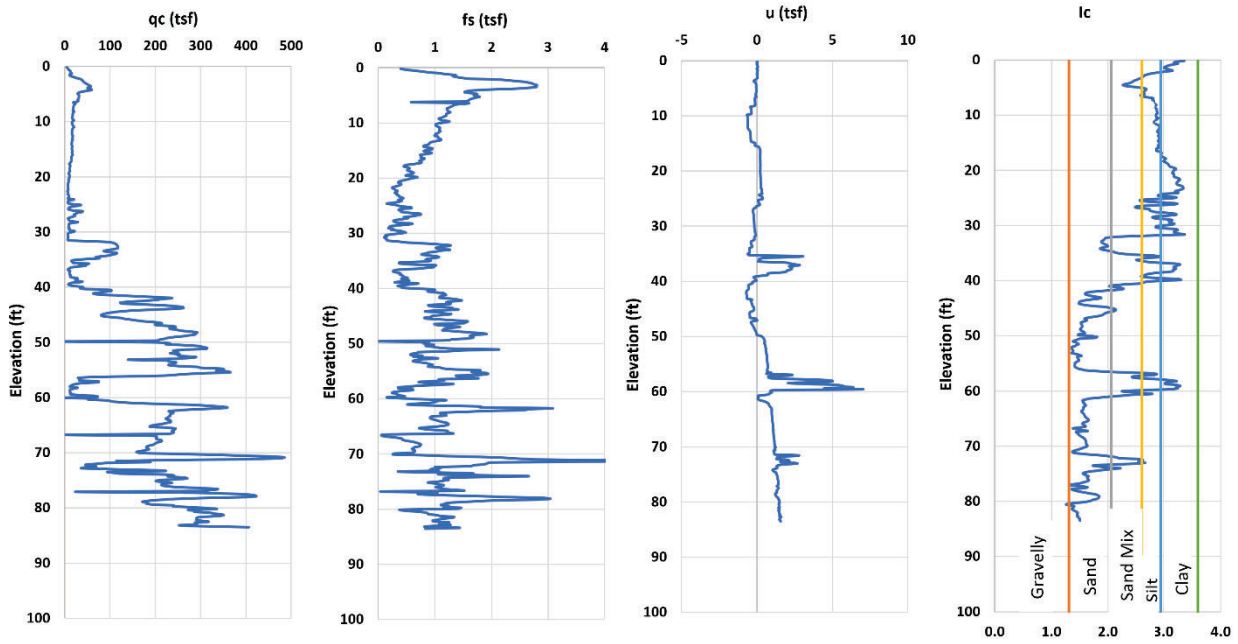

Figure 85**. Raw (a) Tip Resistance (q_c), (b) Sleeve Friction (f_s), and (c) Pore Pressure (u), and (d) Normalized Soil Behavior Index (I_C) of CPT 4 at the Turrell Site**

Figure 86 presents the liquefaction analysis results of CPT 4 from the Turrell site using the three CPT-based liquefaction triggering procedures. The normalized equivalent clean sand tip resistance ($(q_{c1N})_{cs}$) profiles are presented in Figure 86a. The $(q_{c1N})_{cs}$ plot obtained from the CPT-based liquefaction triggering procedures follows the same pattern but has differences in $(q_{c1N})_{cs}$ for elevations above 200 ft. This is caused by the I_C being greater than 2.6 (silts and clays) in this region, and each procedure has a different approach to calculating $(q_{c1N})_{cs}$ for clays and silts that are not liquefiable. Comparing the factors of safety

in Figure 86b and 86c, the Moss et al. (2006) procedure produces a higher factor of safety than the other two methods (ranging from 3 to 169% higher, as the FS is maxed at 2.0, the percent differences get smaller when the FS from the other procedures gets higher). The factor of safety, obtained from Youd et al. (2001) and Boulanger and Idriss (2014) procedure are very similar (Figure 4–32b). Figure 4–32c presents the discontinuous factor of the safety profile at every 5 ft. As Moss et al. (2006) produces a higher factor of safety, the discontinuous factor of safety profile presents the soil at an elevation lower than 165 ft as non-liquefiable, whereas from the other two procedures, the layers have the possibility of being liquefiable. Also, the Youd et al. (2001) procedure shows good agreement with the Boulanger and Idriss (2014) procedure.

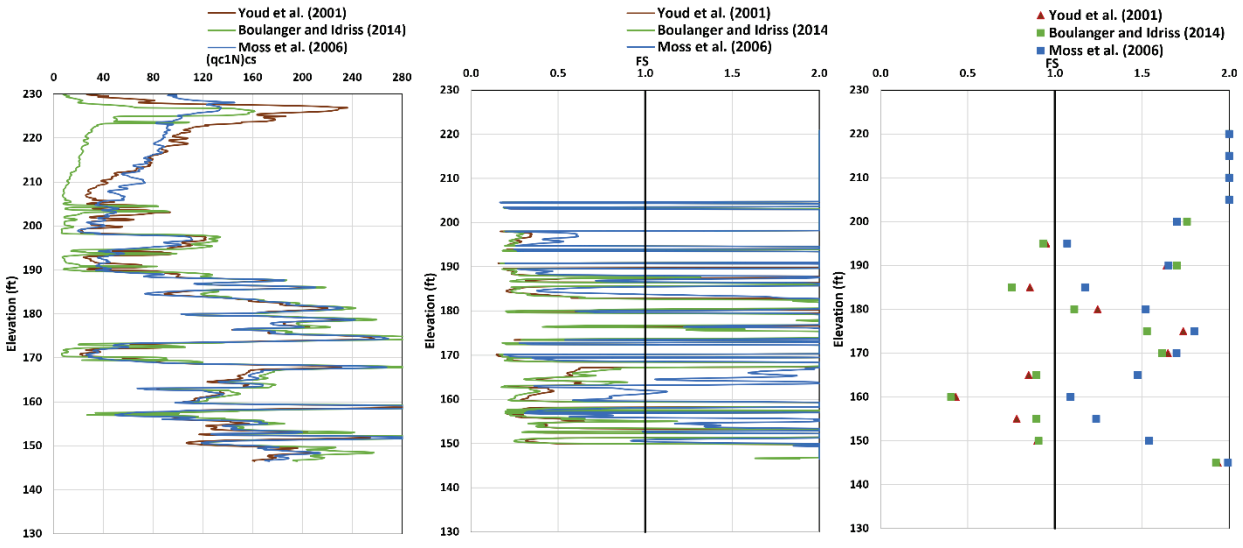

Figure 86**. Comparison of (a) Equivalent Clean Sand Cone Penetration Resistance ($q_{c1N})_{cs}$, (b) Continuous Factor of Safety Results, and (c) Discontinuous Factor of Safety Results of CPT 4 Borehole at the Turrell Site Using the Three Chosen CPT-based Procedure**

The LPI analysis results for CPT 4 at the Turrell Site are presented in Figure 87. The LPI estimated from all CPT-based procedures suggests that the site is susceptible to moderate liquefaction (5 < LPI< 15). LPI_{ISH} estimated from all CPT-based procedures suggests that the site is susceptible to moderate liquefaction,

except Moss et al. (2006) procedure. As the factor of safety calculated from the Moss et al. (2006) procedure is higher than the other two procedures, the estimated liquefaction severity is found to be less than the others. It is also important to note that the LPI and LPI_{ISH} estimated using the CPT-based procedure is less than the SPT-based procedure.

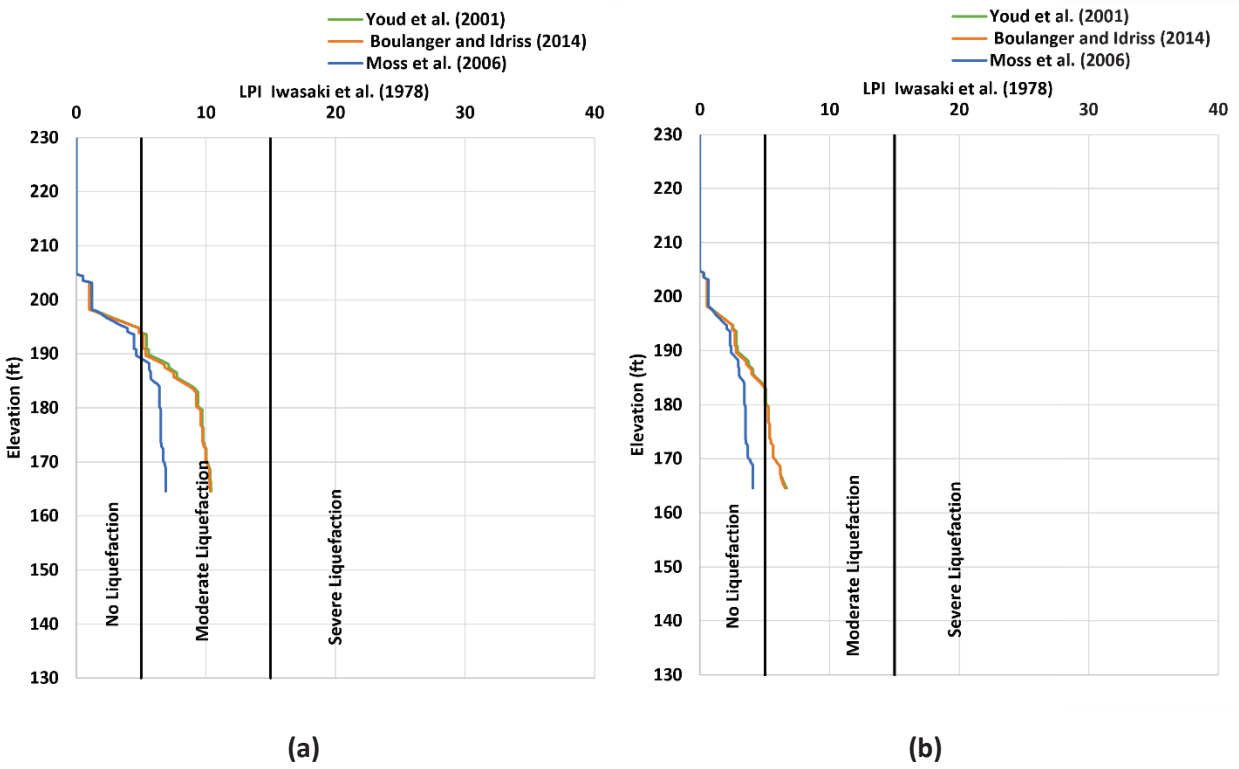

Figure 87. Cumulative (a) LPI by Iwasaki et al. (1978), (b) LPI_{ISH} by Maurer et al. (2015) for CPT 4 at the Turrell Site Using the CPT-based Triggering Procedures

V_s-Based Analysis

In this section, the V_s-based liquefaction analysis results of the Monette site are discussed. The two V_s-based procedures are evaluated and compared. The seismic data of the SCPTs at the Turrell site are presented in Figure 88. For the top 45 ft, the shear wave velocity is less than 200 m/s, with thin layers showing V_s higher than 200 m/s in this depth range. Below this depth, the V_s is higher than 200 m/s.

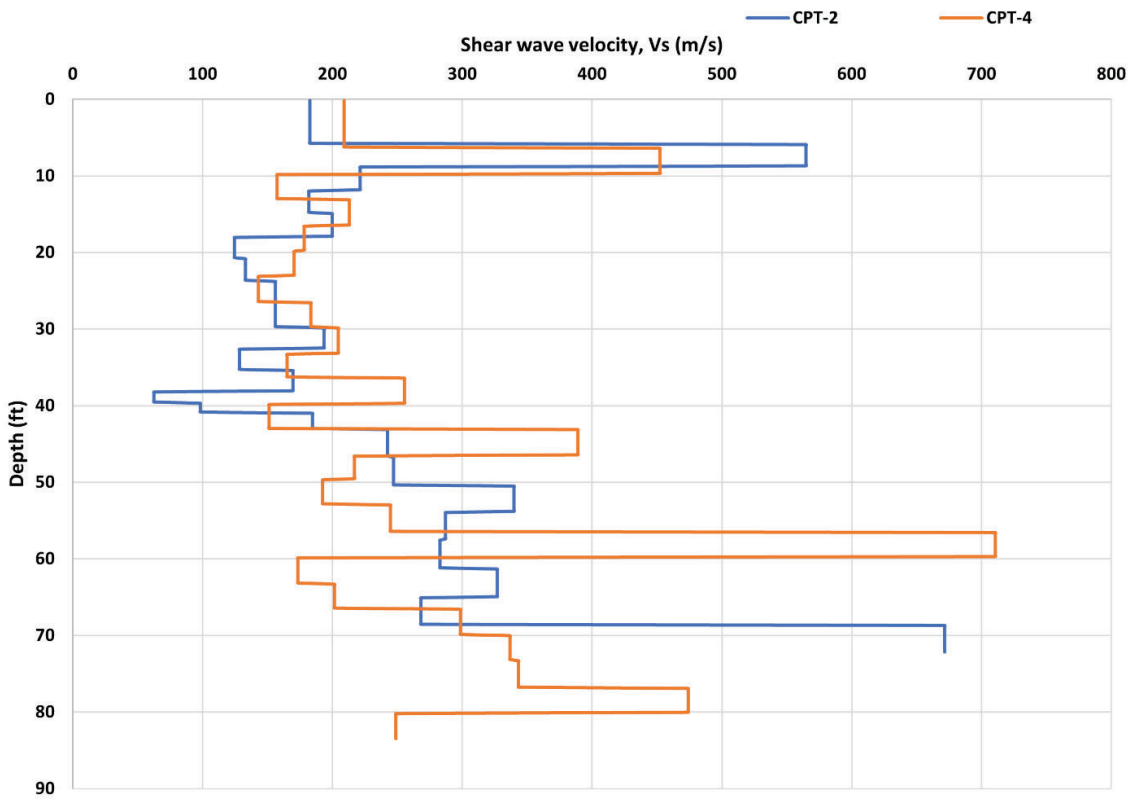

Figure 88**. Comparison of Shear Wave Velocity Data at the Turrell Site**

Figure 89 presents the liquefaction analysis results of the Seismic CPT from the Turrell site using the two V_s-based liquefaction triggering procedures. The obtained overburden stress-corrected shear wave velocity (V_{s1}) profiles are presented in Figure 89a. From that figure, differences in V_{s1} profiles are observed only in the top 10 ft with both methods having the same V_{s1} below that depth. Figure 89b and 89c presents the comparison of the calculated factor of safety for the two procedures with Figure 89c being a discontinuous factor of safety. For both methods, the site has interbedded layers of liquefied and non-liquefiable soils. In general, Youd et al. (2001) indicates more layers are liquefiable than the Kayen et al. (2013) procedure. This is driven by the V_{s1} of the site being near or above 200 m/s. For the Youd et al. (2001) procedure, a V_{s1} value higher than 200–215 m/s (depending on fines content) is too dense for the soil to liquefy whereas the Kayen et al. (2013) procedure estimates layers with V_s above that can liquefy for high CSR values.

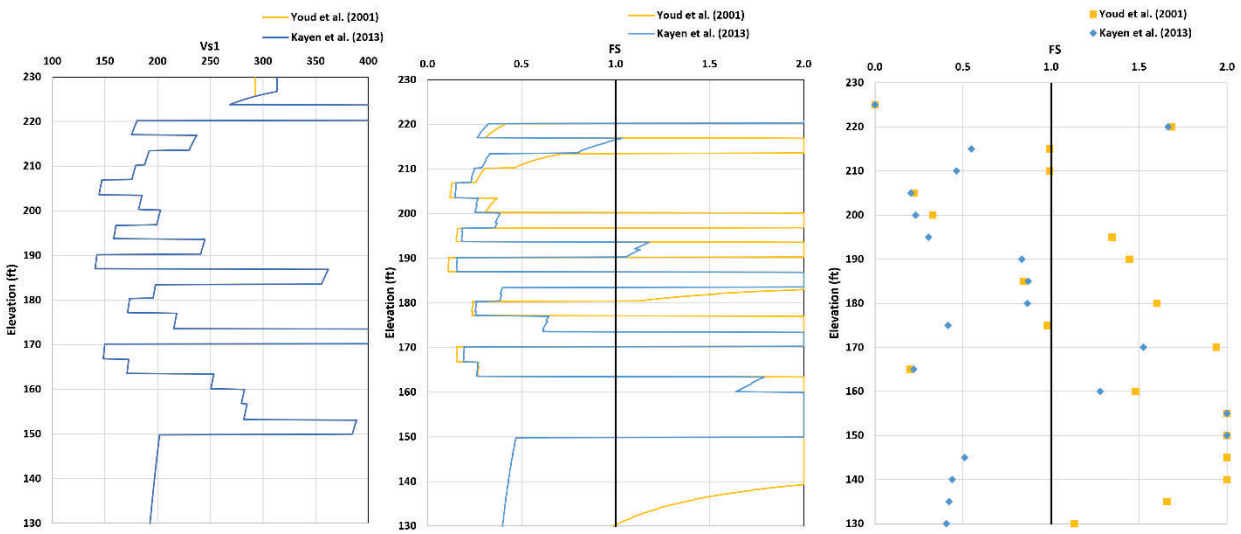

(a) **(b)** **(c)**

Figure 89. Comparison of (a) Overburden Stress Corrected Shear Wave Velocity (V_{s1}), (b) Continuous Factor of Safety Results, and (c) Discontinuous Factor of Safety Results of SCPT 4 Borehole at the Turrell Site Using the Two Chosen V_s-based Procedure

The LPI analysis results for SCPT 4 at the Turrell site are presented in Figure 90. The LPI and LPI_{ISH} estimates suggest that these two sites are susceptible to severe liquefaction (LPI > 15).

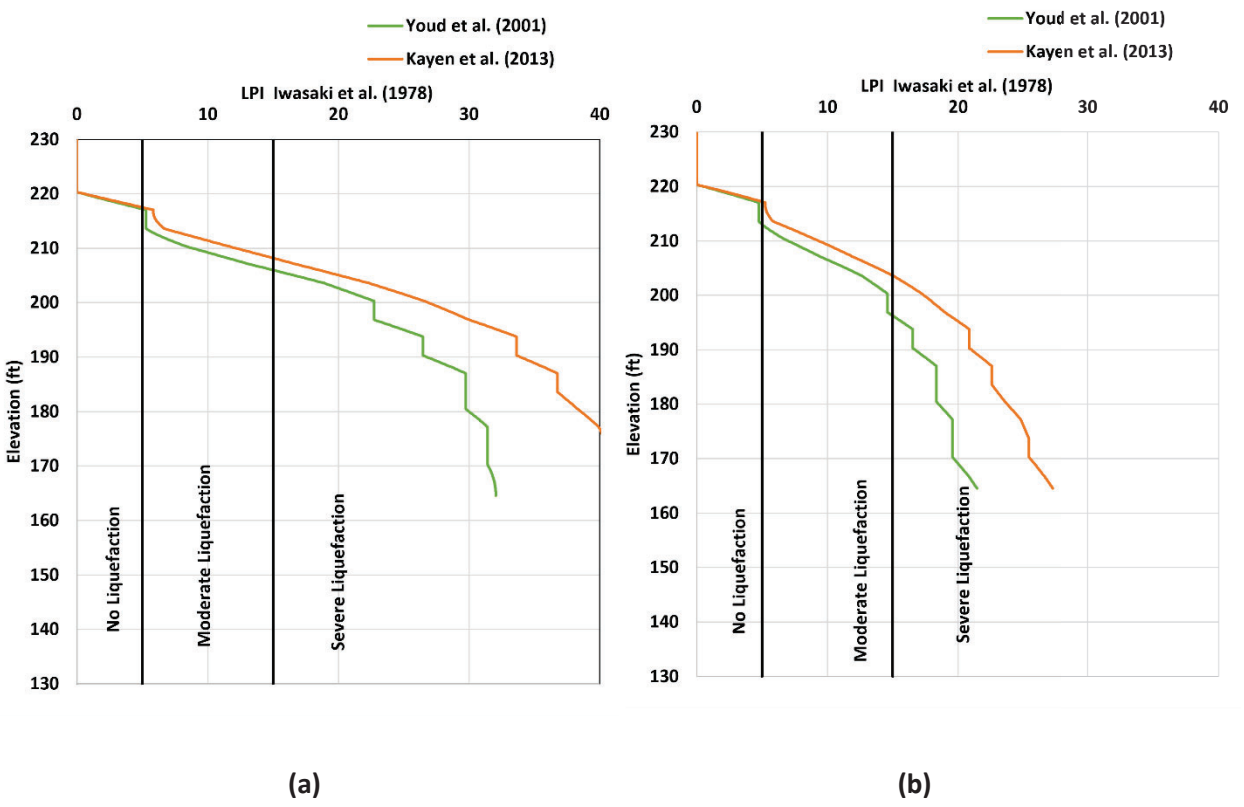

Figure 90. Cumulative (a) LPI by Iwasaki et al. (1978), (b) LPI_{ISH} by Maurer et al. (2015) for SCPT 4 at the Turrell Site Using the V_s-based Triggering Procedures

Comparison of In-situ Methods of the Turrell Site

In this section, the in-situ liquefaction results for the Turrell site are compared. The CPT and V_s liquefaction results from SCPT 4 and the SPT liquefaction results from AHTD 6 are systematically compared and presented in Figures 91 and 92. In Figure 91, the SPT results are compared with the continuous CPT and V_s results, whereas in Figure 92, the SPT results are compared with the discontinuous CPT and V_s results. From Figures 91a and 92a, the CPT-based procedures consistently have a higher factor of safety than the SPT methods, which is quite different from the results observed from the Monette data. This is difficult to see in Figure 91a when continuous CPT data is used as the CPT results swing back and forth over the FS of 1.0 line. However, when looking at the discontinuous CPT results in Figure 92a, it is clear the CPT-based FS is consistently 0.9 or greater compared to the SPT results, which are generally around 0.2. From the discontinuous V_s results, the V_s-based FS is found

higher than the SPT-based FS, but lower than the CPT-based FS at the elevation above 165 ft. At elevations lower than 165 ft, the V_S-based FS from Youd et al. (2001) and Kayen et al. (2013) is higher than both SPT- and CPT-based results. The V_S-based results of Kayen et al. (2013) indicate the layers from elevation 200 ft to 170 ft are liquefiable similar to the SPT-based results but in contrast with the CPT-based results. From the discontinuous FS plot in Figure 92, the Moss et al. (2006) CPT-based procedure and Youd et al. (2001) V_S-based procedure show the least liquefiable layers. All SPT-based procedures and Kayen et al. (2013) V_S-based procedures have the most liquefiable layers. It is important to note that similar to the analysis results of the Monette site, Cetin et al. (2018), Boulanger and Idriss (2014), and Kayen et al. (2013) are found to be the most conservative approach of SPT-based, CPT-based, and V_S-based liquefaction procedures, as these methods generally result in the most liquefiable layers when considering the Monette and Turrell sites. From the LPI analysis results presented in Figures 83, 87, and 90, this site is susceptible to severe liquefaction as the SPT-based and V_S-based analyses show LPI and LPI_{ISH} higher than 15, whereas the CPT-based results show moderate to no liquefaction severity.

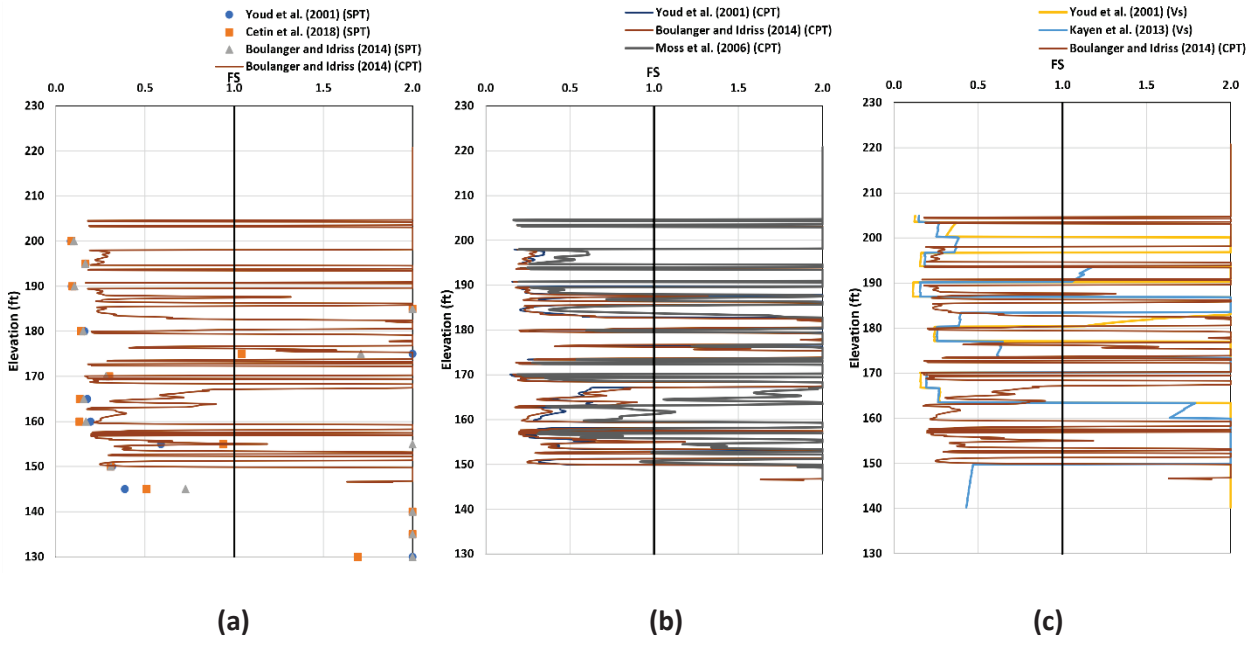

Figure 91. Comparison of SPT Results of AHTD 6 with Continuous CPT and V_s results from CPT 4 of Turrell Site

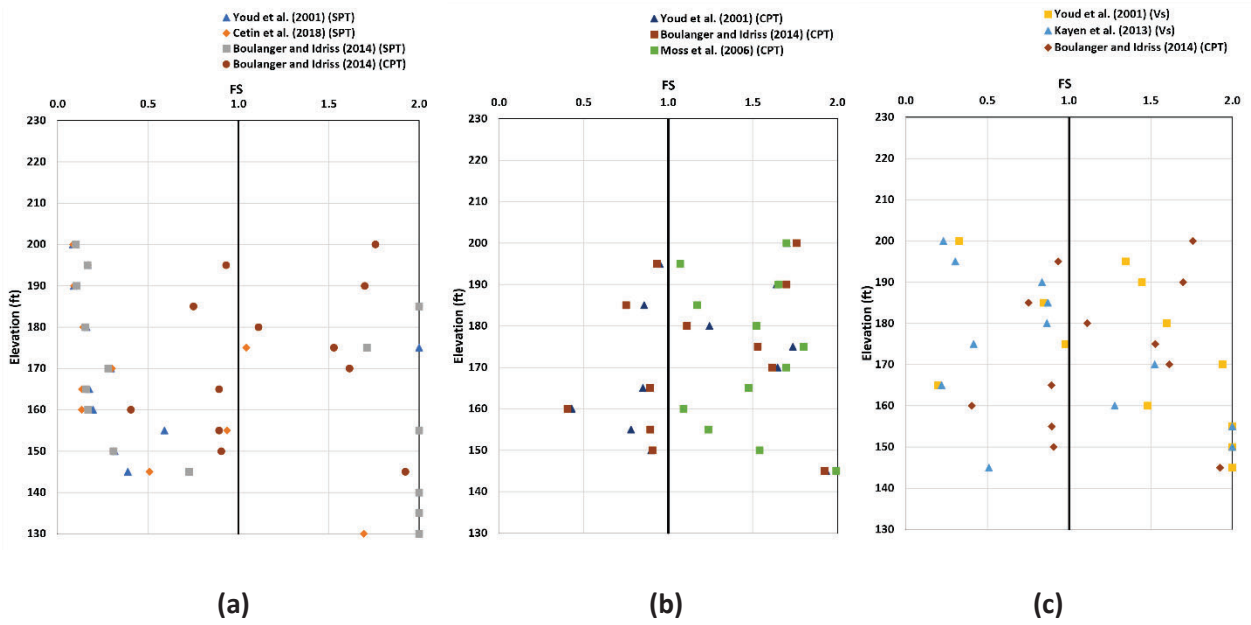

Figure 92. Comparison of SPT Results of AHTD-6 with Discontinuous CPT and V_s Results of CPT 4 of Turrell Site

COST SAVING ANALYSIS

Wood and Baker (2018) conducted deep dynamic site characterization and a site-specific ground motion response analysis (SSGMRA) for the bridge site in Monette, Arkansas, as a part of the TRC 1603 research project. The main components of the bridge include nine 327-foot-long continuous steel girders and six pile bents. The elevation view of the Monette bypass bridge is shown in Figure 93. It is important to note that the Bent 1 pile is located toward the direction of Monette, whereas the Bent 6 pile is located toward Manila City.

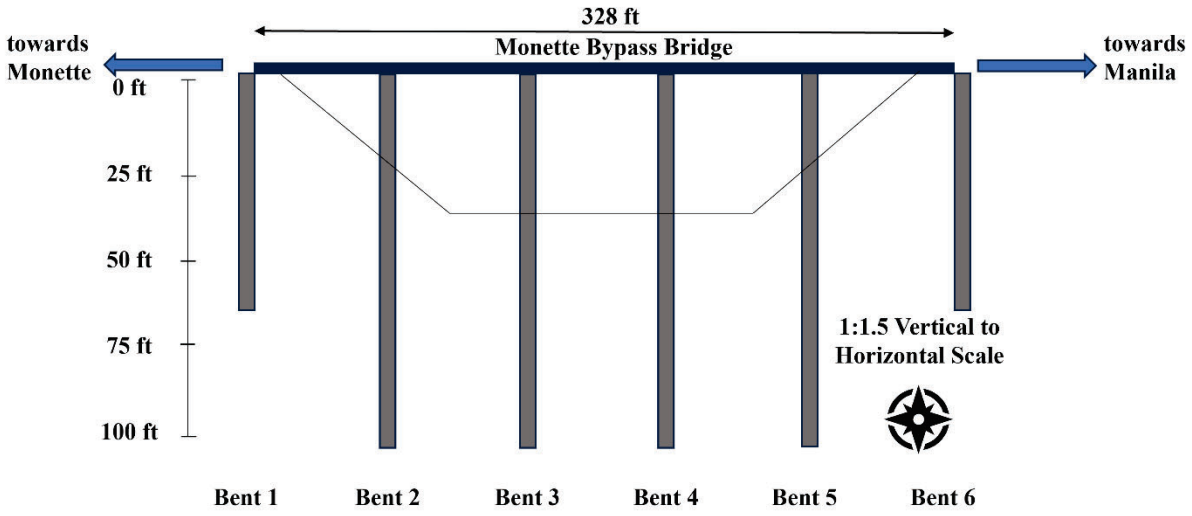

Figure 93**. Elevation View of the Monette Bypass Bridge with Pile Bent Numbering**

The steel girder pile-bent bridge, originally designed using the AASHTO general seismic design procedure (PGA = 0.917 g), was redesigned using the updated seismic demands estimated from a site-specific ground motion response analysis (SSGMRA) (PGA = 0.611 g).

A cost-savings analysis was then conducted to determine the potential savings associated with conducting the SSGMRA. As part of that cost-saving analysis, the required pile length to consider liquefaction potential was calculated. It is important to note that Wood and Baker (2018) used the old SPT-based liquefaction workbook to conduct the study and at the Bent 1 pile, liquefaction analysis results of BH-3 were used, whereas at the rest of the Bent piles liquefaction analysis results of BH-4 were used.

In this section, the cost-saving analysis results of bridge piles, performed by Wood and Baker (2018) are used to compare the in-situ liquefaction analysis results and to find out if any further changes are needed if the updated spreadsheets and new in-situ measurements (i.e., CPT and V_s) are used. It is important to note that in the following figures, each box represents the deterministic analysis result from a 5 ft layer of soil. For the SPT and CPT methods, if at least two or more procedures show the possibility of being liquefiable, the layer is marked with a red box, whereas for the V_s methods, the layers are marked with a red box when at least one procedure shows a factor of safety less than one.

The skin friction resistance of the pile is reduced in layers at which the factors of safety for liquefaction were less than 1.0. According to the study by Wood and Baker (2018), even though there was only a small change in the number of potentially liquefiable layers, the reduction in axial load due to the SSGMRA caused some piles to reach required capacity at shallower depths than in the original design. By using the reduced seismic accelerations in the short period range from SSGMRA, several bridge components were reduced in size and length. It was determined that the bridge pilings could be reduced from 24 inches in diameter to 18 inches in diameter for Bents 2–5. Wood and Baker (2018) calculated the pile length required to meet the axial demand. The required pile length was found to be 45 ft and 35 ft for the end piles, Bent 1 and Bent 6, respectively; for the intermediate piles the required pile length was calculated to be 80 ft when 18-inch diameter piles were used for the intermediate bents bridge. For this analysis, two scenarios referred to as the 24-inch intermediate pile case and the 18-inch intermediate pile case from Wood and Baker (2018) will be considered for further analysis. Moreover, at the Bent 1 pile, liquefaction analysis results from BH-3 and SCPT 2 are used, whereas, at the rest of the Bent piles (2–6), liquefaction analysis results from BH-4 and SCPT 3 are used, which is similar to what was used by Wood and Baker (2018).

Figures 94 and 95 present the comparison of required pile lengths for the 24-inch and 18-inch intermediate pile structure using the AASHTO general seismic design procedure (PGA = 0.917 g). For Bent 1 (the same for each case as Bents 1 and 2 are 18-inch diameter piles for each structure), using the SPT and CPT liquefaction results, the original design piling was tipped at 55 ft. While the pile could reach the required axial capacity at 50 ft, the pile was extended to a non-liquefiable layer at 55 ft to tip the pile end in a non-liquefiable layer. Therefore, there is no change from the original design when using the CPT procedures. The pile is needed to extend to 100 ft to reach the non-liquefiable layer if the V_s results are used. For Bent 6 (the same for both cases), the required pile length to reach axial demand is 50 ft. The SPT results can reach axial demand and be tipped in a non-liquefiable layer at 65 ft, whereas if the CPT and V_s results are used, 60 ft and 100 ft pile lengths are required to be tipped in a non-liquefiable layer. For intermediate piles (Bents 2–5), the original design required the 24-inch piles to extend to 90 ft to reach the required axial capacity if SPT and CPT results are used, whereas 100 ft pile lengths are required to be tipped in a non-liquefiable layer if the V_s results are used (Figure 4–40). If 18-inch diameter piles are used at the intermediate locations (Bents 2–5), the required length is calculated to be 100 ft, which is deeper than the required pile length for 24-inch piles. If SPT and CPT results are used for an 18-inch intermediate pile, the pile can reach a non-liquefiable layer at 100 ft, whereas more than 100 ft pile length are required to be tipped in a non-liquefiable layer if the V_s results are used (Figure 95).

In summary, some cost savings can be achieved in the Bent 6 pile if CPT liquefaction results are used, but no potential cost savings can be achieved if V_s results are used instead of SPT results, using AASHTO general seismic design procedure (PGA = 0.917 g).

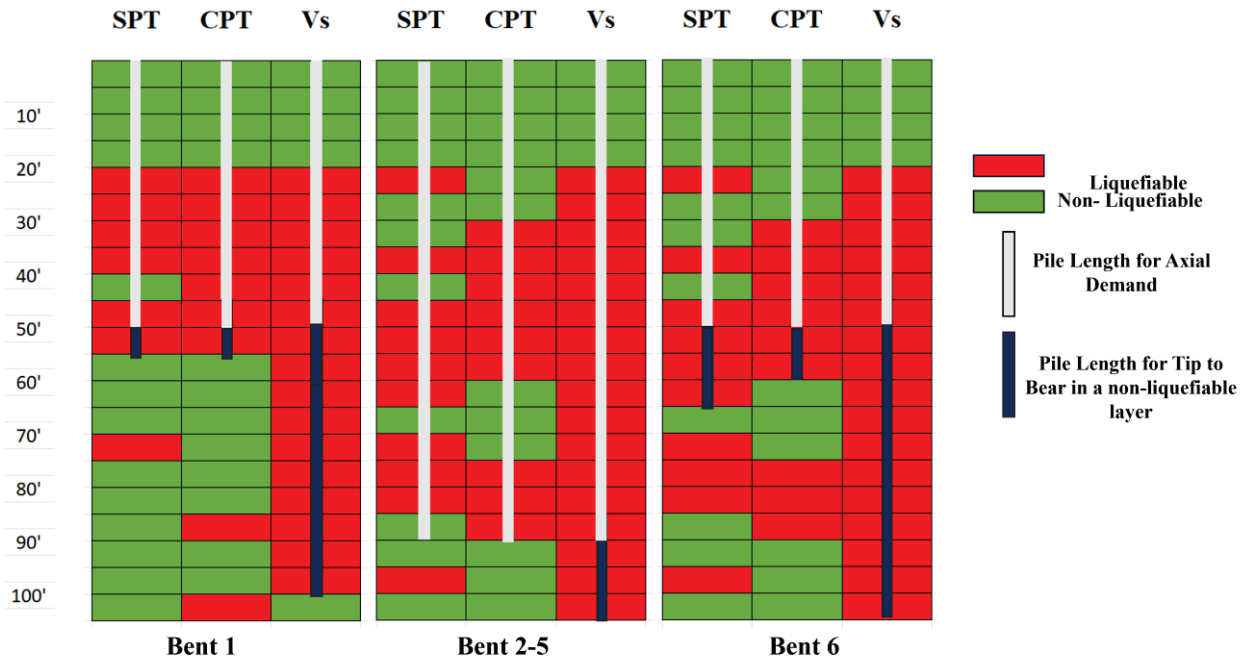

Figure 94. Comparison of Pile Lengths for 24-inch Intermediate Pile Structure Using AASHTO General Seismic Design Procedure (PGA = 0.917 g)

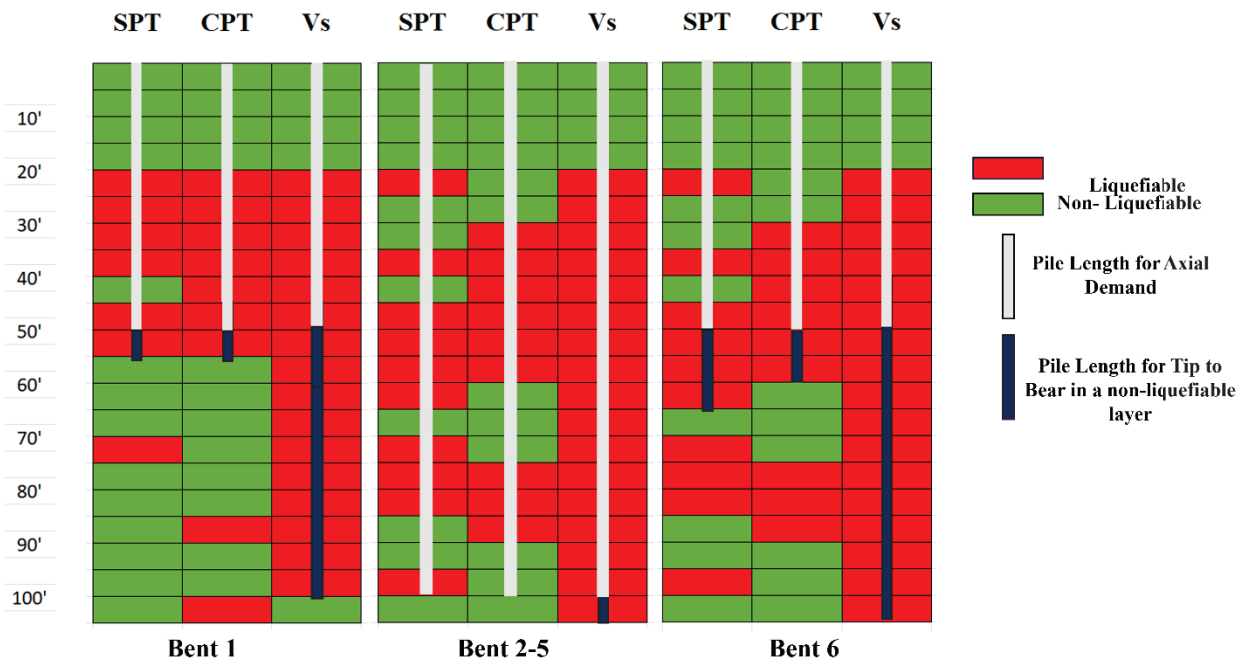

Figure 95**. Comparison of Pile Lengths for 18-inch Intermediate Pile Structure Using AASHTO General Seismic Design Procedure (PGA = 0.917 g)**

No significant differences in pile lengths are observed between 24-inch- and 18-inch-diameter pile structures when the site-specific ground motion response analysis (PGA = 0.611 g) is used. So in this section, only the comparisons of the 18-inch intermediate pile structure are presented. Figure 96 presents the comparison of pile lengths for an 18-inch intermediate pile structure using the site-specific ground motion response analysis (PGA = 0.611 g). For Bent 1, using the SPT and CPT liquefaction results, the original design piling was tipped at 55 ft. While the pile could reach the required axial capacity at 45 ft, the pile was extended to a non-liquefiable layer at 55 ft to tip the pile end in a non-liquefiable layer. The pile is needed to extend to 60 ft to reach the non-liquefiable layer if the V_s results are used. For Bent 6, the required pile length to reach axial demand is 42 ft. The SPT results can reach axial demand and be tipped in a non-liquefiable layer at 42 ft, whereas if the CPT and V_s results are used, 60 ft and more than 100 ft pile lengths are required, respectively, to be tipped in a non-liquefiable layer. For intermediate piles (Bents 2–5), the updated design, using the SSGMRA analysis, required the 18-inch piles to extend to 86 ft to reach the required axial capacity if SPT results are used, whereas if the CPT and V_s results are used, 90 ft and more than 100 ft pile lengths are required to be tipped in a non-liquefiable layer.

When using the AASHTO general seismic design procedure (PGA = 0.917 g), some cost savings can be achieved if the CPT results are used instead of SPT results, no potential cost savings can be made if CPT and V_s results are used instead of SPT results, using site-specific ground motion response analysis (PGA = 0.611 g).

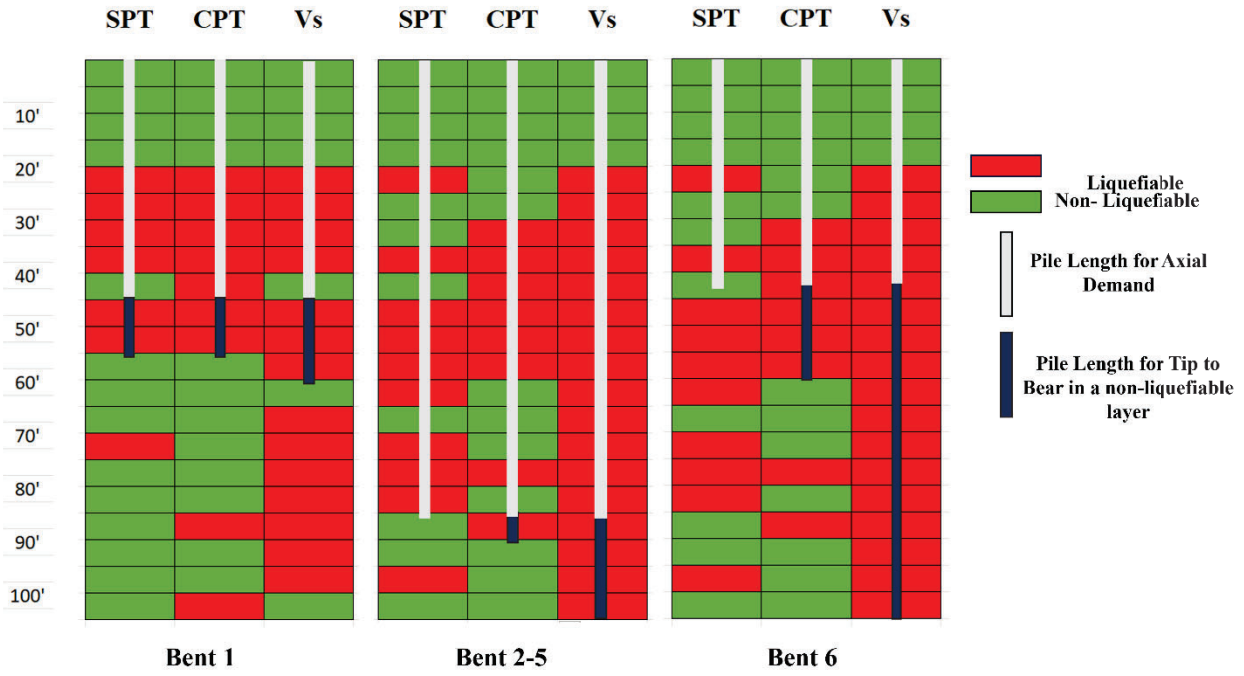

Figure 96. Comparison of Pile Lengths for 18-inch Intermediate Pile Structure Using the Site-specific Ground Motion Response Analysis (PGA = 0.611 g)

It is important to note that even though the CPT and V_s procedures don't offer much in terms of cost savings, these procedures help to provide continuous soil profiles. In this section, the discontinuous CPT and V_s results are used to compare the liquefaction results with the SPT results. The continuous CPT results help to see the transitioning zones in soil layers and perform better in determining the liquefiable layers, especially thin layers, which is not possible in SPT analysis. Due to its continuous nature, the CPT approach provides higher resolution, providing more information on the thickness of potential liquefiable and non-liquefiable layers, which helps add more redundancy to the liquefaction analysis.

q_C-V_S CORRELATION

It is observed from the V_s-based liquefaction analysis of SCPT 1 at the Monette site, the results obtained from the V_s-based results do not always comply with the results obtained from the results of the CPT-based Boulanger and Idriss (2014) procedure. So in this section, several q_c-V_s correlations have been used to study the performances of these correlations in the liquefaction study. Among several correlations, Andrus et al. (2007) (Equation 82), Hegazy and Mayne (2006) (Equation 83), and Robertson (2009) (Equation 84) correlations are chosen to perform this study.

$$V_s = 2.27 * q_t^{0.412} * I_C^{0.989} * z^{0.033} \quad \textbf{(Equation 82)}$$

$$V_s = 0.0831 * q_{c1N} * \exp(1.7861 + I_C)(\sigma'_{v0}/p_a)^{0.25} \quad \textbf{(Equation 83)}$$

$$V_s = [10^{0.55*I_c+1.68}((q_t - \sigma_{v0})/p_a)]^{0.5} \quad \textbf{(Equation 84)}$$

Figure 97a shows the comparison of the V_s data and the V_s obtained from the correlations. It is obvious that, except for Hegazy and Mayne (2006), the other two correlations are similar to the real V_s data. At the top 20 ft, Hegazy and Mayne (2006) underpredicts by 3 to 30%, though it overpredicts below 20 ft by 150 to 200%. The other two correlations also underpredict the shear wave velocity by 10 to 40% above 20 ft, though below 20 ft depth, the prediction is over by 2 to 20%.

The obtained V_s data from the correlations are used to perform the liquefaction analysis and the obtained results using the Kayen et al. (2013) procedure are presented to compare with the CPT-based results from the Boulanger and Idriss (2014) and V_s-based results using the Kayen et al. (2013) procedure of SCPT 1 in Figure 97b to 97d. As expected, the results from Hegazy and Mayne (2006) show a high factor of safety. When the Andrus et al. (2007) correlation is used, the Kayen et al. (2013) procedure fails to show any deep liquefiable layers (Figure 97d).

From this study, the Andrus et al. (2007) (Figure 97c) and Robertson (2009) (Figure 97b) correlations show good compliance with the real data set. If these correlations are used to perform the liquefaction study, it is recommended that the Andrus et al. (2007) should be applicable in depths from the ground surface to 60–65 ft, whereas the Robertson (2009) correlation can be used below these depths, as the results obtained from the above-mentioned correlations showed good agreement in the above mentioned conditions with the CPT-based Boulanger and Idriss (2014) procedure.

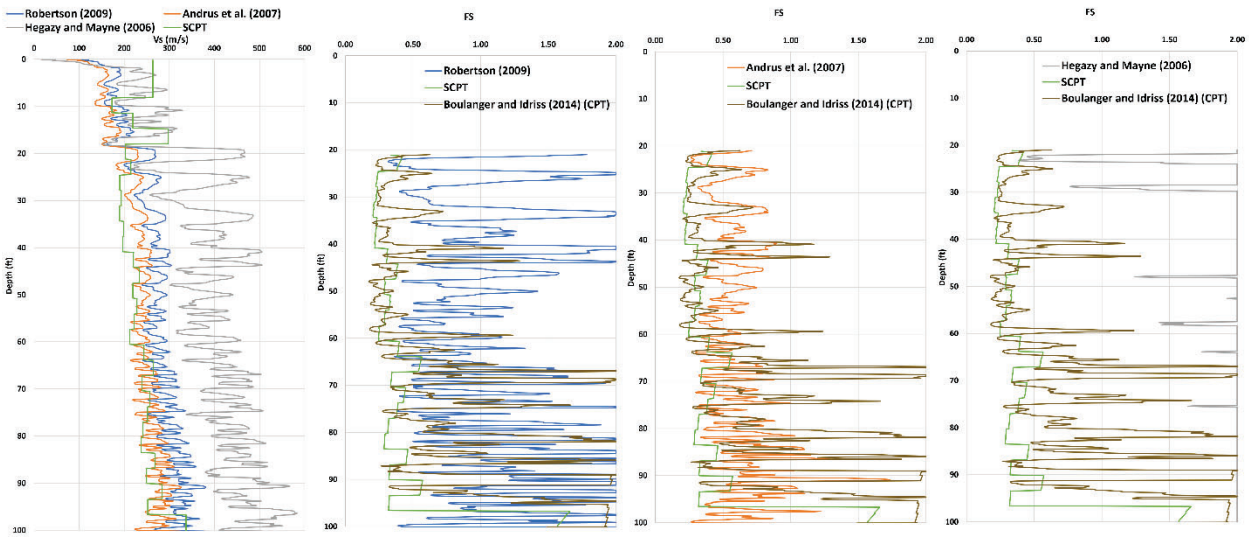

(a) (b) (c) (d)

Figure 97**. Comparison of the V_s-based Analysis Results of the V_s Data and the V_s Obtained from the Correlations for SCPT 1 at the Monette Site**

CHAPTER 5: CONCLUSIONS AND RECOMMENDATIONS

CONCLUSIONS

As a part of this study, the existing ARDOT SPT-based liquefaction triggering spreadsheet is updated with the inclusion of new CPT and V_s-based liquefaction triggering spreadsheets. These SPT, CPT, and V_s-based liquefaction triggering spreadsheets will ultimately aid in evaluating liquefaction triggering using the most up-to-date methods. The format, primary input page, and graphs of these spreadsheets are kept very similar to the existing SPT spreadsheet. This will ensure a minimal learning curve for the user of the basic spreadsheet. Second, extensive manuals for all three spreadsheets are created to aid the users in using these spreadsheets. The manual, provided in Chapter 3, is capable of describing the inputs and outputs of the spreadsheet along with how to utilize the results of the spreadsheet. Also, to understand whether liquefaction manifestation will be an issue, the LPI by Iwasaki et al. (1978) and LPI_{ISH} developed by Maurer et al. (2015) are also included in the spreadsheets. These spreadsheets were verified using previously developed spreadsheets, codes, hand calculations, and commercial software packages.

In the new SPT spreadsheet, the Boulanger and Idriss (2012, 2014) relationship (an update to the Idriss and Boulanger 2008 relationship) and the Cetin et al. (2018) relationship (an update to the Cetin et al. [2004] relationship) for the liquefaction triggering are included. The previous Youd et al. (2001) approach is also still included in the spreadsheet, which has not been revised since 2001 (except for changing the K_σ limit). The Moss et al. (2006), Boulanger and Idriss (2014), and Youd et al. (2001) (also known as Robertson and Wride [1998]) techniques are all included in the CPT spreadsheet. Kayen et al. (2013) and Youd et al. (2001) (also known as the Andrus and Stokoe [2000]) are included in the V_s liquefaction spreadsheet. These spreadsheets can convert the raw data to the desired units required to perform the analysis. In the CPT spreadsheet, a rolling average is programmed into the data analysis to smooth the plots which can help the user to better understand the results and remove large spikes. This spreadsheet can also determine the water table if the water table information is not given in the CPT data. In addition to the continuous comparison tab, a discontinuous 5'/2.5' layered comparison tab is also provided in the CPT and V_s-based spreadsheets to compare co-located SPT, CPT, and V_s data and complete a sensitivity study using the spreadsheet to understand any differences between the procedures and methods.

After developing the SPT, CPT, and V_s-based liquefaction triggering spreadsheets, several analyses are completed using constant raw inputs (SPT-N, q_c, V_s) to compare the liquefaction triggering procedures and understand the contributing factors behind the differences in the procedures. When constant SPT-N values of 20 blows/ft are used in the SPT spreadsheet, the Youd et al. (2001) procedure shows that $(N_{1,60})_{cs}$ values higher than 30, are too dense to liquefy and are classified as non-liquefiable. However, the other two procedures indicate that layers with $(N_{1,60})_{cs}$ greater than 30 have the potential to be liquefiable. Also, the factor of safety obtained from Cetin et al. (2018) in the deeper layers is the lowest, as it generates lower CRR values than others even though $(N_{1,60})_{cs}$ is similar for all three procedures, which makes this method the most conservative of all three SPT procedures. The FS values from the Cetin et al. (2018) procedure are higher than the Cetin et al. (2004) procedure at shallower depths (< 50 ft). This is caused by the new model coefficients in the probabilistic liquefaction triggering relationship for CRR, which generates higher CRR values at shallow depths. For the other two procedures, the percentage of change (old procedure versus new procedure) in the factor of safety results is not significant. In the CPT spreadsheet, constant tip resistance, q_c of 250 ksf are used, and similar to the SPT analysis, the Youd et al. (2001) procedure shows that $(q_{c1N})_{cs}$ values higher than 160, are too dense to liquefy and classifies as non-liquefiable. However, the other two procedures indicate that layers with $(q_{c1N})_{cs}$ greater than 160 have the potential to be liquefiable. In the shallow layers, all CPT procedures generate almost the same clean sand cone penetration resistance $(q_{c1N})_{cs}$, but the Boulanger and Idriss (2014) procedure generates higher $(q_{c1N})_{cs}$ in deeper layers (greater than 40 ft), though this high $(q_{c1N})_{cs}$ yields similar CRR values. The Boulanger and Idriss (2014) analysis results show that the profile is liquefiable in depths deeper than 10 ft, while the Youd et al. (2001) procedure and Moss et al. (2006) procedure show the profile as liquefiable at depths deeper than 10 ft, making the Boulanger and Idriss (2014) procedure the most conservative CPT procedure. From the V_s-based analysis results of constant V_s of 200 m/s, Youd et al. (2001)/Andrus and Stokoe (2000) stated that V_{s1} higher than 200–215 m/s (depending on fines content) is too dense to liquefy, but the Kayen et al. (2013) indicates that these layers have the potential of being liquefiable. The Kayen et al. (2013) procedure analysis results show that the profile is liquefiable at depths higher than 13 ft, while the Youd et al. (2001) procedure shows the profile liquefiable at depths deeper than 10 ft (42 ft), making the Kayen et al. (2013) procedure the most conservative V_s-based procedure.

After the constant input analysis, these spreadsheets are used to understand the differences between the methods and analyze real project data from Arkansas. Site-specific comparisons of the SPT, CPT, and V_s liquefaction triggering procedures for two different sites in eastern Arkansas are presented and

discussed. For the Turrell site, sets of data were produced for the TRC1204 and TRC1502 ARDOT research projects. This dataset includes SPT data gathered by ARDOT, CPT data gathered by MoDOT, and V_s data gathered by MoDOT using seismic CPT. The second dataset was collected in Monette, Arkansas, for an ARDOT project. SPT testing was performed for the initial design efforts while seismic CPT testing was performed as part of this research work. Extensive analyses are conducted using the co-located SPT, CPT, and V_s evaluation data to understand the similarities and differences, and also the driving factors behind these differences.

From the analysis performed at the Monette site using the co-located data, the SPT methods are in good agreement with the CPT-based procedure of Boulanger and Idriss (2014) from the surface to 160 ft elevation (80 ft depth), at the elevations below that, Moss et al. (2006) shows good agreement with the SPT-based results. It is important to note that Youd et al. (2001) and Boulanger and Idriss (2014) CPT-based approaches generally consider the deeper layers more liquefiable than the SPT-based approaches. Moreover, Kayen et al. (2013) V_s-based procedure shows similar results to the CPT-based procedure of Boulanger and Idriss (2014) in the shallow depths (from the ground surface to 180 ft elevation or 60 ft deep). At elevations lower than 180 ft (below 60 ft from the boring surface), the CPT-based procedure of Boulanger and Idriss (2014) shows non-liquefiable layers, whereas the Kayen et al. (2013) method shows the possibility of these layers being liquefiable. This is likely driven by the shear wave velocity measures being averaged more through the soil column, making them less sensitive to the rapid changes in stiffness in the soil profile than the CPT results. From the LPI analysis, this site is susceptible to severe liquefaction as all the in-situ methods show LPI and LPIISH higher than 15.

From the analysis performed at the Turrell site, CPT-based procedures consistently have a higher factor of safety than the SPT methods, which is quite different from the results observed from the Monette data and the CPT-based FS is consistently greater compared to the SPT results. From the discontinuous V_s results, the V_s-based FS is found higher than the SPT-based FS but lower than the CPT-based FS at the elevation above 165 ft. At elevations lower than 165 ft (deeper than 65 ft from the boring surface), the V_s-based FS from Youd et al. (2001) and Kayen et al. (2013) is higher than both SPT- and CPT-based results. The V_s-based results of Kayen et al. (2013) indicate the layers from elevation 200 ft to 170 ft (30 ft to 40 ft deep from the boring surface) are liquefiable, similar to the SPT-based results but in contrast with the CPT-based results. Moss et al. (2006) CPT-based procedure and Youd et al. (2001) V_s-based procedure show the least liquefiable layers for this site, whereas all SPT-based procedures and Kayen et al. (2013) V_s-based procedure have the most liquefiable layers. From the LPI analysis results, this site is

susceptible to severe liquefaction as the SPT-based and V_s-based analyses show LPI and LPI_{ISH} higher than 15, whereas the CPT-based results show moderate to no liquefaction severity.

It is important to note that similar to the analysis results of the Monette site, Cetin et al. (2018), Boulanger and Idriss (2014), and Kayen et al. (2013) are found to be the most conservative approach of SPT-based, CPT-based, and V_s-based liquefaction procedures, as these methods generally result in the most liquefiable layers when considering the Monette and Turrell sites.

Several q_c-V_s correlations have been used to understand the performances of these correlations in the liquefaction study. It is recommended that the Andrus et al. (2007) should be applicable in depths from the ground surface to 60–65 ft, whereas the Robertson (2009) correlation can be used below these depths, as the results obtained from the above-mentioned correlations showed good agreement in the above mentioned conditions with the CPT-based Boulanger and Idriss (2014) procedure.

The cost-saving analysis results from the bridge redesign in Monette, Arkansas, performed by Wood and Baker (2018) as part of the TRC 1603 research project, are used to compare the in-situ liquefaction analysis results and to find out if any further changes are needed if the updated spreadsheets and new in-situ measurements (i.e., CPT and V_s) are used. From the analysis, minor to no potential cost savings can be achieved if CPT and V_s results are used instead of SPT results, using the AASHTO general seismic design procedure (PGA = 0.917 g) and the site-specific ground motion response analysis (PGA = 0.611 g). However, that does not mean using multiple approaches is without benefits. Using more than one approach at a site provides redundancy to the design and the CPT-based approach provides higher resolution, providing more information on the thickness of potential liquefiable and non-liquefiable layers.

The primary task of the research discussed herein is to help ARDOT update the SPT-based procedures used to evaluate earthquake-induced soil liquefaction triggering, particularly for deep soil deposits. The CPT method improves upon this lack of resolution by providing a near-continuous estimate of soil properties with depth. This provides more accurate estimates of liquefaction triggering. In addition, CPT has been shown to provide more accurate estimates of soil strength, especially for softer soils than SPT. The addition of using V_s along with CPT and SPT has the benefits of a better understanding of the aging of the sandy deposits. Aging or cementation in sandy soils increases soil liquefaction resistance. The measurement of aging is improved with V_s as compared to CPT and SPT, which are large strain tests, tending to damage the cementation without fully measuring its contribution to the strength of the soil.

The current liquefaction spreadsheet used by ARDOT is deterministic—meaning, it only provides a yes-or-no answer with a factor of safety. The inclusion of estimates of the severity of surface manifestation has benefits in understanding whether the consequences of liquefaction will be significant for a project. There are times when thin or deep layers are the only ones determined likely to liquefy for a project. In these cases, the impacts of liquefaction are minimized, reducing the need for significant design changes to account for liquefaction.

FUTURE WORK

While the spreadsheet provides a way to evaluate liquefaction triggering using the most up-to-date methods, further investigation is required to comprehend both the possibility for liquefaction to be triggered in deep soil layers (> 50 ft deep) as well as the potential effects from liquefaction at those depths. At the highest levels of geotechnical earthquake engineering, there is currently a discussion about how difficult it is to predict deep soil liquefaction. From the comparisons of the liquefaction triggering results of the in-situ methods at the Monette and Turrell sites, it is noted that the liquefaction potential varies depending on the in-situ method utilized for the evaluation. Therefore, additional sites in and beyond Arkansas are needed where the various in-situ methods can be compared to understand potential bias in the methods.

REFERENCES

American Association of State Highway and Transportation Officials (AASHTO). 2011. *Guide Specifications for LRFD Seismic Bridge Design*, 2nd Ed., Washington, DC.

Andrus, R., Mohanan, N., Piratheepan, P., Ellis, B., and Holzer, T. 2007. "Predicting Shear-wave Velocity from Cone Penetration Resistance", Proc. 4th International Conference on Earthquake Geotechnical Engineering, Thessaloniki, Greece, June 25–28, Paper No. 1454.

Andrus, R. D., and K. H. Stokoe II. 2000. "Liquefaction Resistance of Soils from Shearwave Velocity". *Journal of Geotechnical and Geoenvironmental Engineering* 126, no. 11: 1015–1025.

Boulanger, R. W., and I. M. Idriss. 2014. "CPT and SPT Based Liquefaction Triggering Procedures". Report No. UCD/CGM-14/01. Center for Geotechnical Modeling, Department of Civil and Environmental Engineering, University of California, Davis., 134.

Bray, J. D., and R. B. Sancio. 2006. "Assessment of the Liquefaction Susceptibility of Fine Grained Soils". *Journal of Geotechnical and Geoenvironmental Engineering* 132, no. 9: 1165–1177.

Bey, S. M. (2014). "Cost-Benefit Analyses for Load Resistance Factor Design (LRFD) of Drilled Shafts in Arkansas". Graduate Theses and Dissertations retrieved from https://scholarworks.uark.edu/etd/2274.

Cetin, K. O., H. T. Bilge, J. Wu, A. M. Kammerer, and R. B. Seed. 2009a. "Probabilistic Models for the Assessment of Cyclically Induced Reconsolidation (Volumetric) Settlements". *Journal of Geotechnical and Geoenvironmental Engineering* 135, no. 3: 387–398.

Cetin, K. O., R. B. Seed, R. E. Kayen, R. E. S. Moss, H. T. Bilge, M. Ilgac, K. Chowdhury. 2018. "Examination of Differences Between Three SPT-based Seismic Soil Liquefaction Triggering Relationships". *Soil Dynamics and Earthquake Engineering*, 113: 75–86.

Cetin, K. O., R. B. Seed, A. D. Kiureghain, K. Tokimatsu, L. F. Harder, R. E. Kayen, R. E. S. Moss. 2004. "Standard Penetration Test-Based Probabilistic and Deterministic Assessment of Seismic Soil Liquefaction Potential". *Journal of Geotechnical and Geoenvironmental Engineering*, ASCE 130, no. 12: 1314–1340

Cox, B. and S. Griffiths. 2010. "*Practical Recommendations for Evaluation and Mitigation of Soil Liquefaction in Arkansas*," MBTC dot 3017. https://mack-blackwell.uark.edu/Research/mbtcdot3017.pdf

Green, R. A., J. J. Bommer, A. Rodriguez-Marek, et al. 2019. "Addressing Limitations in Existing 'Simplified' Liquefaction Triggering Evaluation Procedures: Application to Induced Seismicity in the Groningen Gas Field". *Bulletin of Earthquake Engineering* 17: 4539–4557. https://doi.org/10.1007/s10518-018-0489-3

Hegazy, Y. and P. Mayne. 2006. "A Global Statistical Correlation Between Shear Wave Velocity and Cone Penetration Data". Proc. GeoShanghai, Site and Material Characterization (ASCE GSP 149), 243–248.

Idriss, I. M. and R. W. Boulanger. 2008. "Soil Liquefaction during Earthquakes". MNO-12, Earthquake Engineering Research Institute, Oakland, CA.

Ishihara, K., and M. Yoshimine. 1992. "Evaluation of Settlements in Sands Due to Earthquake Shaking". *Soils and Foundations* 32, no. 1: 173–188.

Ishihara, K., 1985. "*Stability of Natural Deposits During Earthquakes"*. In: Proceedings of the 11th International Conference on Soil Mechanics and Foundation Engineering. San Francisco, CA, USA, 1: 321–376.

Iwasaki, T., F. Tatsuoka, K. Tokida, S. Yasuda. 1978. "*A Practical Method for Assessing Soil Liquefaction Potential Based on Case Studies at Various Sites in Japan"*. In: Proceedings of the 2nd International Conference on Microzonation. San Francisco, CA, USA, pp. 885–896.

Juang, C. H., T. Jiang, R. D. Andrus, and D. V. Rosowsky. 2002. "Risk Assessment of Liquefaction Potential Using Bayesian Approach". *Soil Dynamics and Earthquake Engineering* 22, no. 4: 219-230.

Juang, C. H., T. Jiang, R. D. Andrus, and G. Zhang. 2014. "Simplified SPT-based Liquefaction Potential Index Using Logistic Regression Analysis".

Juang, C.H., T. Jiang, R. D. Andrus, and D. V. Rosowsky. 2003. "Risk-based Re-assessment of the Simplified Procedures for Evaluating Liquefaction Potential". *Soil Dynamics and Earthquake Engineering* 23, no. 1: 1–10.

Kayen, R. E., J. K. Mitchell, R. B. Seed, A. Lodge, S. Nishio, and R. Coutinho. 1992. “Evaluation of SPT-, CPT-, and shear wave-based methods for liquefaction potential assessment using Loma Prieta data”. Proc., 4th Japan-U.S. Workshop on Earthquake-Resistant Des. Of Life-line Fac. And Countermeasures of Soil Liquefaction, vol. 1, pp. 177–204.

Kayen, R. R., R. E. S. Moss, E. R. Thompson, R. B. Seed, K. O. Cetin, A. Derkiureghian, Y. Tanaka, and K. Tokimatsu. 2013. “Shear Wave Velocity-based Probabilistic and Deterministic Assessment of Seismic Soil Liquefaction Potential”. *Journal of Geotechnical and Geoenvironmental Engineering* 139, no. 3: 407–419.

Kramer, S. L. and R. T. Mayfield. 2007. “The Return Period of Liquefaction”, *Journal of Geotechnical and Geoenvironmental Engineering*, ASCE, 133, no. 7: 1–12.

Kulhawy, F. H. and P. W. Mayne. 1990. “Manual on Estimating Soil Properties for Foundation Design”. *Electric Power Research Institute*. https://www.osti.gov/biblio/6653074

Liao, S. S. C. and R. V. Whitman. 1986. “Overburden Correction Factors for SPT in Sand”. *Journal of Geotechnical Engineering Division*, ASCE, 112, no. 3: 373–377.

Maurer, B.W., R. A. Green, M. Cubrinovski, and B. A. Bradley. 2015. “Assessment of CPT-Based Methods for Liquefaction Evaluation in a Liquefaction Potential Index (LPI) Framework”. *Geotechnique* 65, no. 5: 328–336.

Mayne, P. W. 2014. *Interpretation of Geotechnical Parameters from Seismic Piezocone Tests*. In Proceedings, 3rd international symposium on cone penetration testing (pp. 47–73).

Moss, R. E. S., R. B. Seed, R. E. Kayen, J. P. Stewart, A. Der Kiureghian, and K. O. Cetin. 2006. “CPT-based Probabilistic and Deterministic Assessment of In Situ Seismic Soil Liquefaction Potential”. *Journal of Geotechnical and Geoenvironmental Engineering* 132, no. 8: 1032–1051.

National Academies of Sciences, Engineering, and Medicine. 2016. *State of the Art and Practice in the Assessment of Earthquake-Induced Soil Liquefaction and Its Consequences*. Washington, DC: The National Academies Press. https://doi.org/10.17226/23474.

P. K. Robertson. 1990. “Soil Classification Using the Cone Penetration Test”. *Canadian Geotechnical Journal* 27, no. 1: 151–158. https://doi.org/10.1139/t90-014

Race, M. L. and R. A. Coffman. 2013. “Effect of Uncertainty in Site Characterization on the Prediction of Liquefaction Potential for Bridge Embankments in the Mississippi Embayment”. https://ascelibrary.org/doi/abs/10.1061/9780784412787.091

Robertson, P. K. and K. L. Cabal. 2012. *Guide to Cone Penetration Testing, Gregg Drilling & Testing*. INC. Corporate Headquarters, Signal Hill, California.

Robertson, P. K. 2009. “Interpretation of Cone Penetration Tests – A Unified Approach”. *Canadian Geotechnical Journal*, 46, no. 11: 1337–1355.

Robertson, P. K. and C. E. Wride. 1998. “Evaluating Cyclic Liquefaction Potential Using the Cone Penetration Test”. *Canadian Geotechnical Journal*, 35, no. 3: 442–459.

Robertson, P. K., R. G. Campanella, D. Gillespie, and J. Grieg. 1986. *Use of Piezometer Cone Data*. In: Proceedings, In-situ ’86, ASCE Specialty Conference, Blacksburg, VA.

Seed, H. B. and I. M. Idriss. 1971. “Simplified Procedure for Evaluating Soil Liquefaction Potential”. Journal of the Soil Mechanics and Foundations Division, 97, no. SM9: 1249–1273.

Seed, H. B. and I. M. Idriss. 1982. “Ground Motions and Soil Liquefaction During Earthquakes”. Earthquake Engineering Research Institute Monograph No. 5, Oakland, California.

Teng, W. C. 1962. “Foundation Design”. Civil Engineering and Engineering Mechanics Series. Prentice-Hall, Inc. Englewood Cliffs, NJ.

van Ballegooy, S., P. J. Malan, M. E. Jacka, V. I. M. F. Lacrosse, J. R. Leeves, and J. E. Lyth. 2012. *Methods for Characterizing Effects of Liquefaction in Terms of Damage Severity*. In Proceedings of the 15th World Conference on Earthquake Engineering, Lisbon, Portugal.

Wood, C. M. and E. R. B. Baker. 2018. “Cost Savings of Implementing Site-Specific Ground Motion Response Analysis in the Design of Short-Period Mississippi Embayment Bridges”. *Earthquake Spectra* 34, no. 3: 1155–1175. doi:10.1193/120517EQS247M

Wood, C., B. Cox, R. Green, L. Wotherspoon, B. Bradley, M. Cubrinovski. 2017. “Vs-based Evaluation of Select Liquefaction Case Histories from the 2010-2011 Canterbury Earthquake Sequence”, *Journal of Geotechnical and Geoenvironmental Engineering* 143, no. 9, 04017066-(1-14).

Youd, T. L., I. M. Idriss, R. D. Andrus, I. Arango, G. Castro, J. T. Christian, R. Dobry, W. D. L. Finn, L. F. Harder, M. E. Hynes, K. Ishihara, J. P. Koester, S. C. C. Liao, W. F. Marcuson III., G. R. Martin, J. K. Mitchell, Y. Moriwaki, M. S. Power, P. K. Robertson, R. B. Seed, and K. H. Stokoe II. 2001. "Liquefaction Resistance of Soils: Summary Report from the 1996 NCEER and 1998 NCEER/NSF Workshops on Evaluation of Liquefaction Resistance of Soils". *Journal of Geotechnical and Geoenvironmental Engineering*, 127:817–833.

Zhang, G., P. K. Robertson, and R. W. I. Brachman. 2002. "Estimating Liquefaction Induced Ground Settlements from CPT for Level Ground". *Canadian Geotechnical Journal*, 39: 1168–1180.

Zhou, S. and G. Chen. 2007. "Modification of Liquefaction Potential Index and Its Application to Liquefaction Zoning Map of Sand Deposits."

APPENDIX

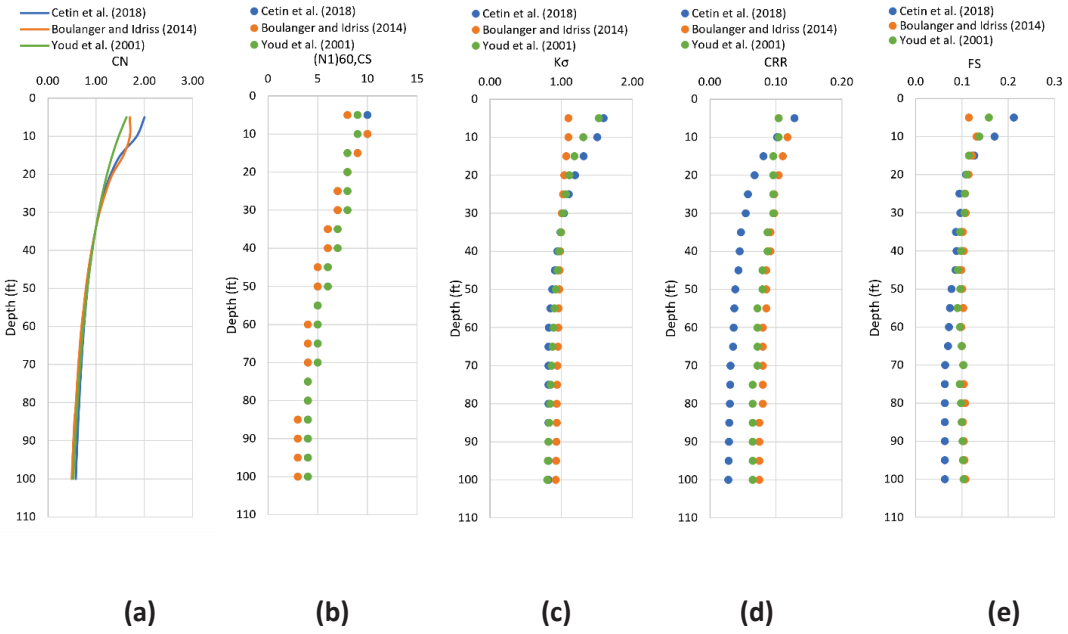

Figure 98. Contant SPT-based Liquefaction Analysis Results for N = 5 blow/ft (a) Overburden Correction Factor (C_N), (b) Clean Sand Equivalent Blow Count, $(N_1)_{60cs}$, (c) K_σ Correction Factor, (d) Unadjusted Cyclic Resistance Ratio (CRR), (e) Factor of Safety

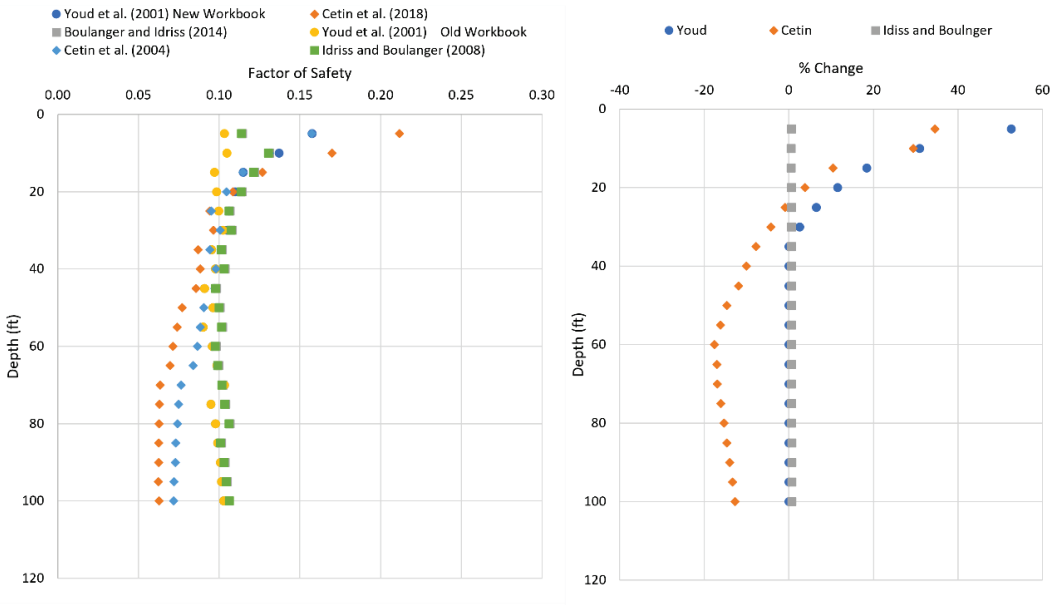

(a) **(b)**

Figure 99. (a) Comparison of Factor of Safety Results Using the Old and New Workbook Methods (Contant SPT-N = 5 blow/ft), (b) Percent Changes of Factor of Safety Results in New Workbook from the Old Workbook (Contant SPT-N = 5 blow/ft)

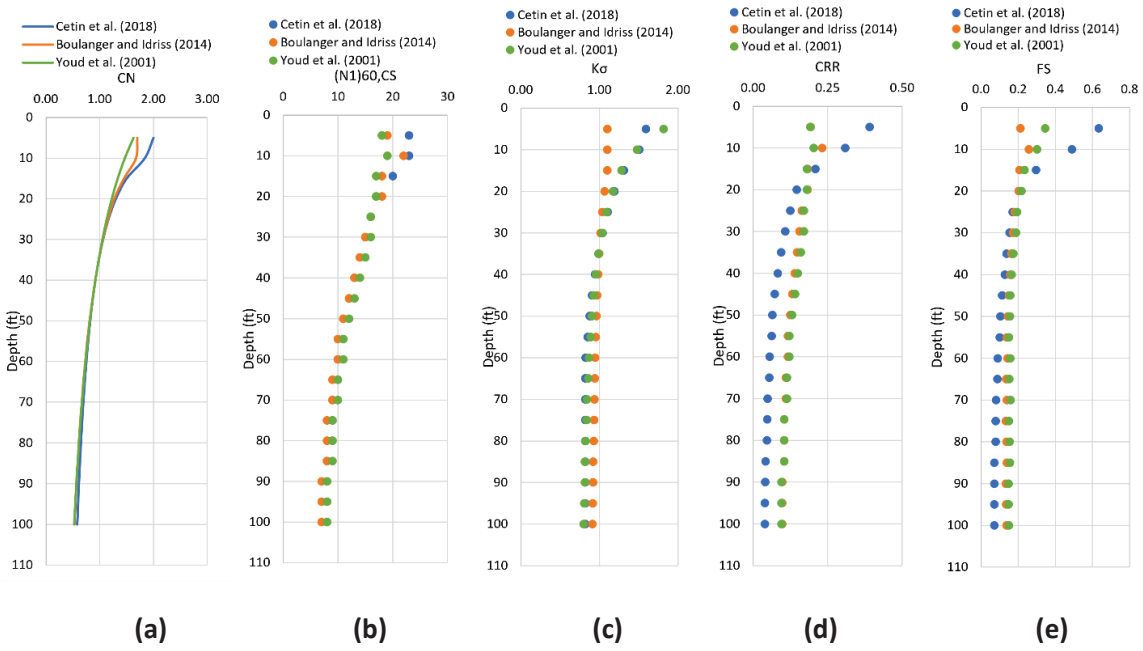

Figure 100. Contant SPT-based Liquefaction Analysis Results for N = 10 blow/ft (a) Overburden Correction Factor (C_N), (b) Clean Sand Equivalent Blow Count, $(N_1)_{60cs}$, (c) K_σ Correction Factor, (d) Unadjusted Cyclic Resistance Ratio (CRR), (e) Factor of Safety

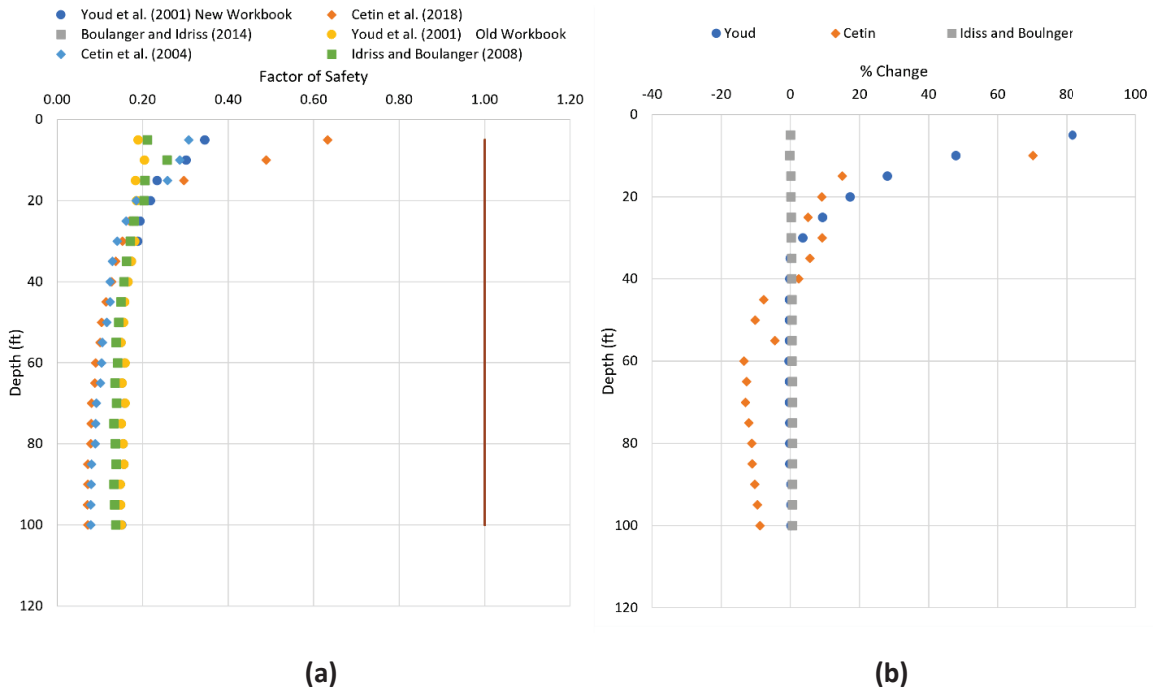

Figure 101**. (a) Comparison of Factor of Safety Results Using the Old and New Workbook Methods (Contant SPT-N = 5 blow/ft), (b) Percent Changes of Factor of Safety Results in New Workbook from the Old Workbook (Contant SPT-N = 5 blow/ft)**

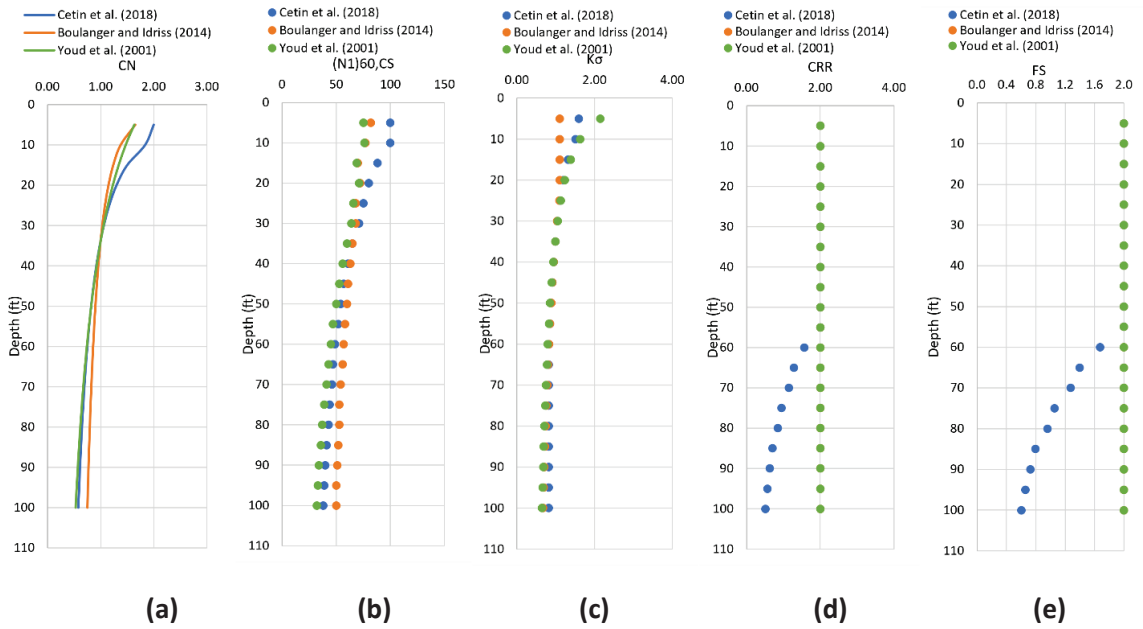

Figure 102. Contant SPT-based Liquefaction Analysis Results for N = 40 blow/ft (a) Overburden Correction Factor (C_N), (b) Clean Sand Equivalent Blow Count $(N_1)_{60cs}$, (c) K_σ Correction Factor, (d) Unadjusted Cyclic Resistance Ratio (CRR), (e) Factor of Safety

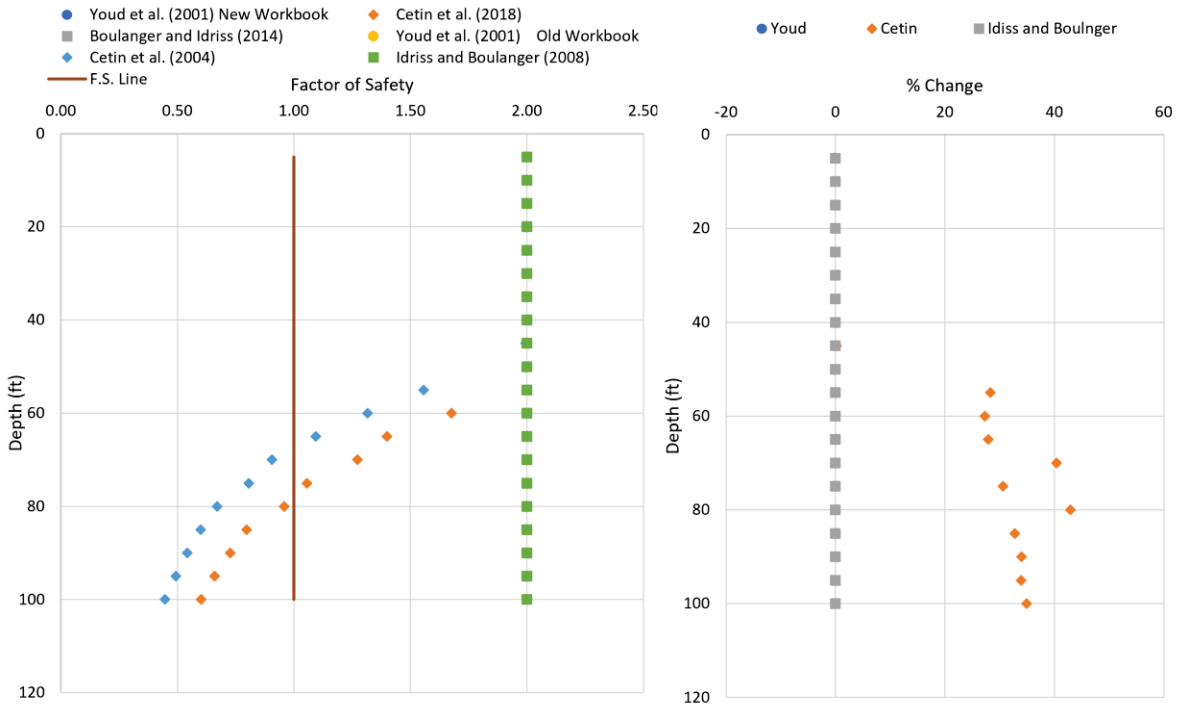

(a) **(b)**

Figure 103. (a) Comparison of Factor of Safety Results Using the Old and New Workbook Methods (Contant SPT-N = 5 blow/ft), (b) Percent Changes of Factor of Safety Results in New Workbook from the Old Workbook (Contant SPT-N = 5 blow/ft)

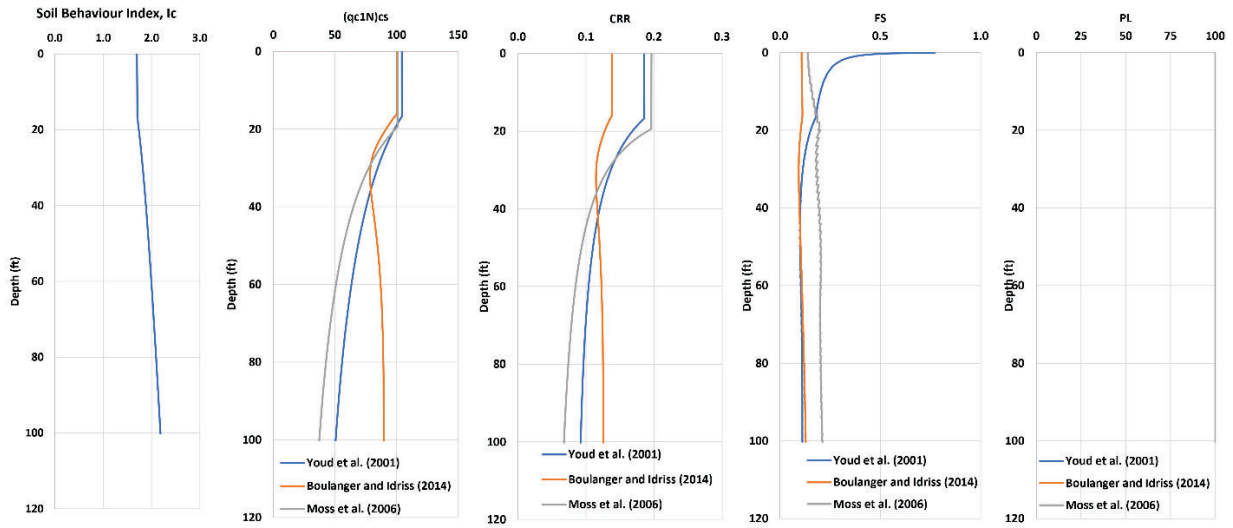

(a) (b) (c) (d) (e)

Figure 104. Contant CPT-based Liquefaction Analysis Results for q_c = 125 ksf (a) Soil Behavior Index (I_C), (b) Clean Sand Equivalent Cone Penetration Resistance, $(q_{c1N})_{cs}$, (c) Unadjusted Cyclic Resistance Ratio (CRR), (d) Factor of Safety, (e) Probability of Liquefaction

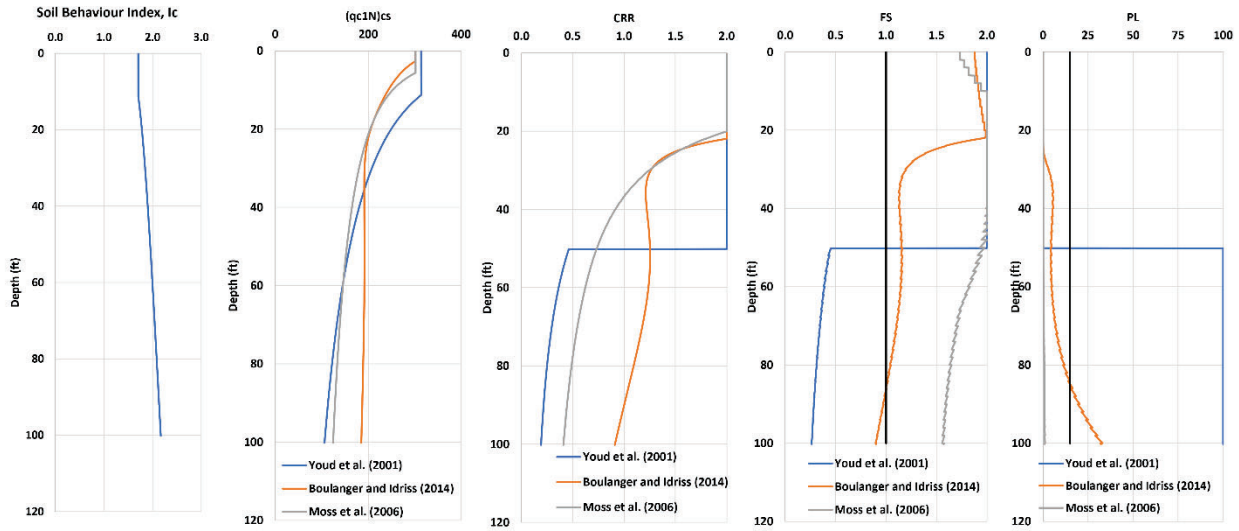

(a) (b) (c) (d) (e)

Figure 105. Contant CPT-based Liquefaction Analysis Results for q_c = 375 ksf (a) Soil Behavior Index (I_C), (b) Clean Sand Equivalent Cone Penetration Resistance, $(q_{c1N})_{cs}$, (c) Unadjusted Cyclic Resistance Ratio (CRR), (d) Factor of Safety, (e) Probability of Liquefaction.

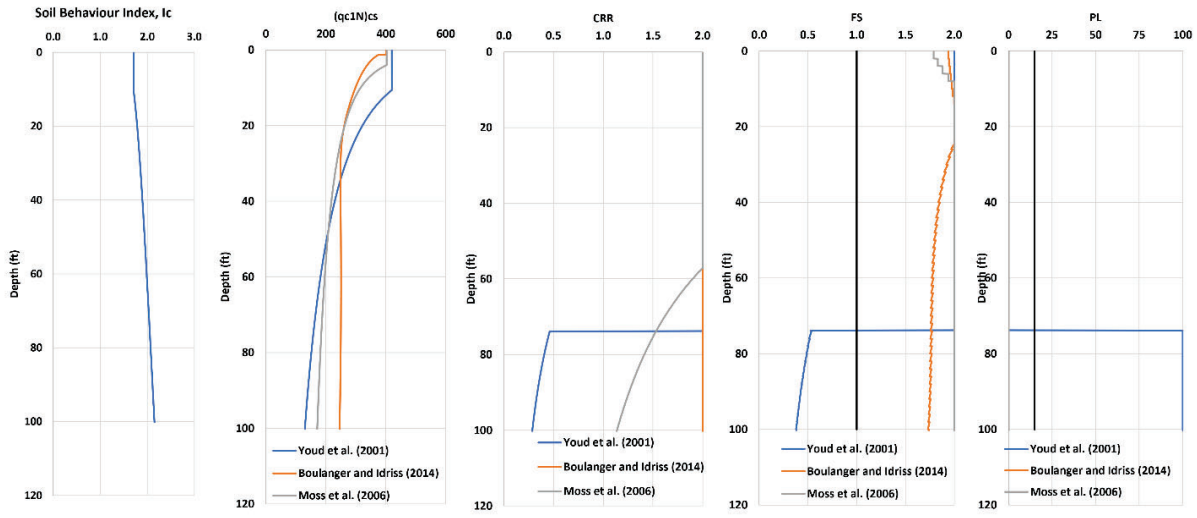

(a) (b) (c) (d) (e)

Figure 106. Contant CPT-based Liquefaction Analysis Results for q_c = 500 ksf (a) Soil Behavior Index (I_C), (b) Clean Sand Equivalent Cone Penetration Resistance, $(q_{c1N})_{cs}$, (c) Unadjusted Cyclic Resistance Ratio (CRR), (d) Factor of Safety, (e) Probability of Liquefaction

Appendix A1.

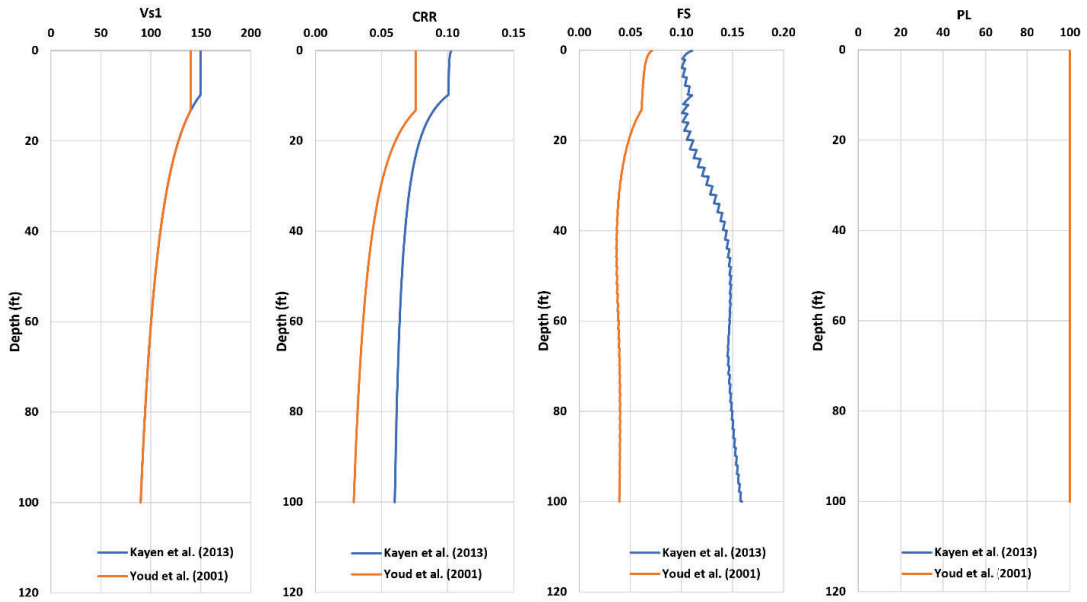

Figure 107**. Contant V_s-based Liquefaction Analysis Results for V_s = 100 m/s (a) Overburden Stress Corrected Shear Wave Velocity (V_{s1}), (b) Unadjusted Cyclic Resistance Ratio (CRR), (c) Factor of Safety, (d) Probability of Liquefaction (PL)**

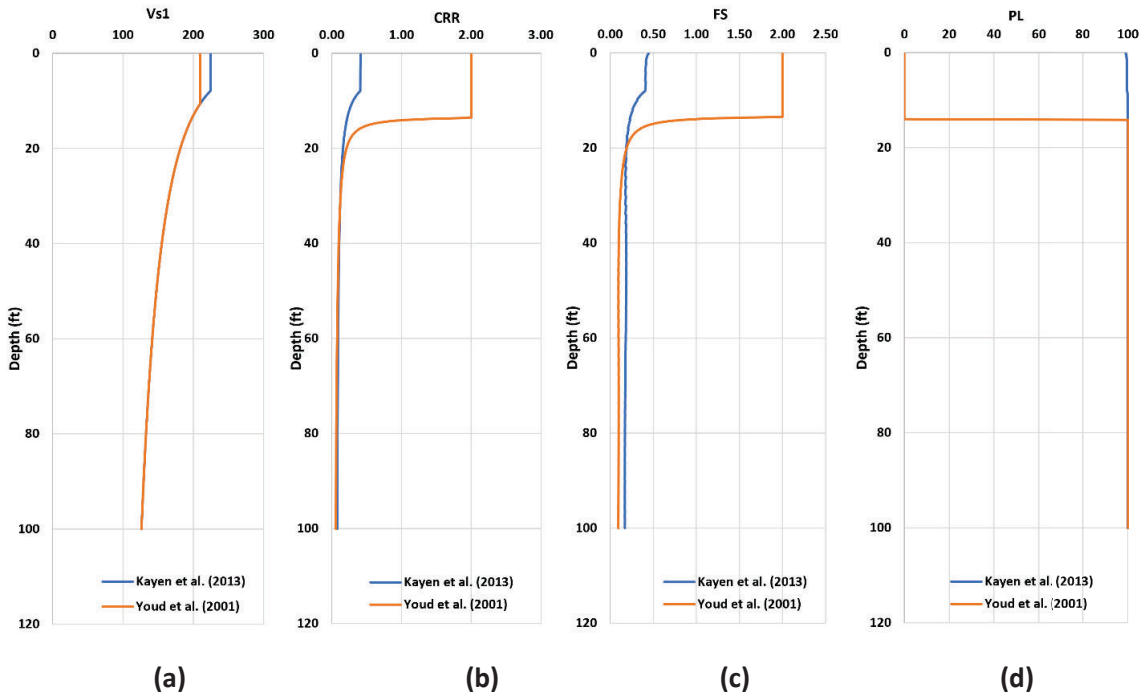

Figure 108. Contant V_s-based Liquefaction Analysis Results for V_s = 150 m/s (a) Overburden Stress Corrected Shear Wave Velocity (V_{s1}), (b) Unadjusted Cyclic Resistance Ratio (CRR), (c) Factor of Safety, (d) Probability of Liquefaction (PL)

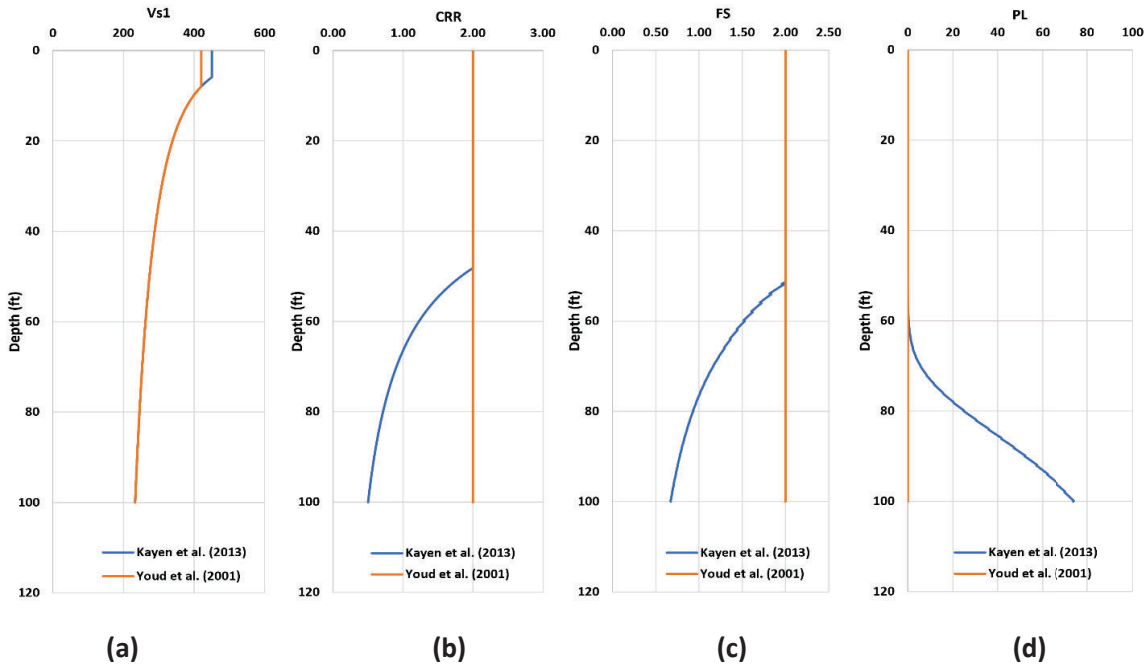

Figure 109**. Contant V_s-based Liquefaction Analysis Results for V_s = 300 m/s (a) Overburden Stress Corrected Shear Wave Velocity (V_{s1}), (b) Unadjusted Cyclic Resistance Ratio (CRR), (c) Factor of Safety, (d) Probability of Liquefaction (PL)**

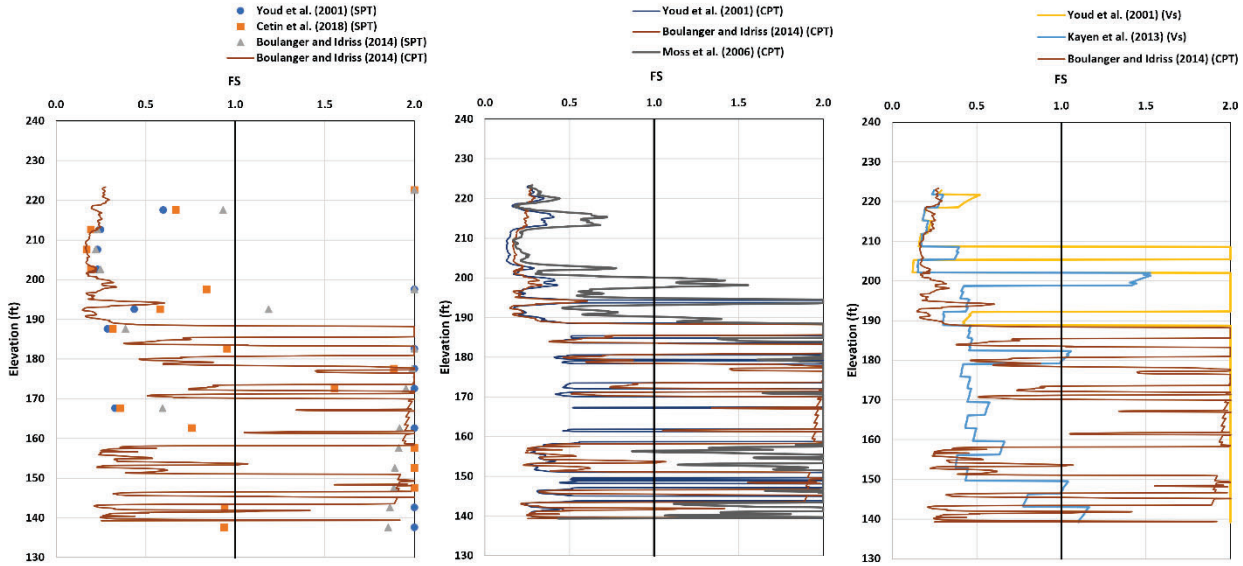

Figure 110**. Comparison of SPT Results of BH-3 with Continuous CPT and V_s results of CPT 2 of Monette Site**

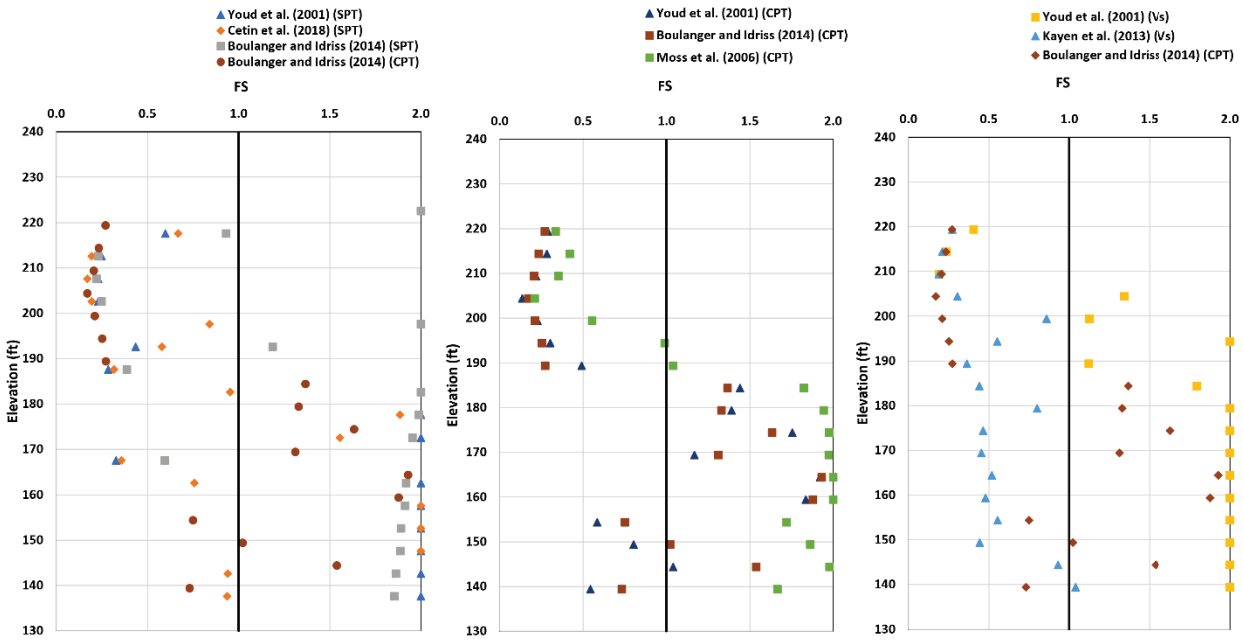

Figure 111. Comparison of SPT Results of BH-3 with Discontinuous CPT and V_s results of CPT 2 of Monette Site

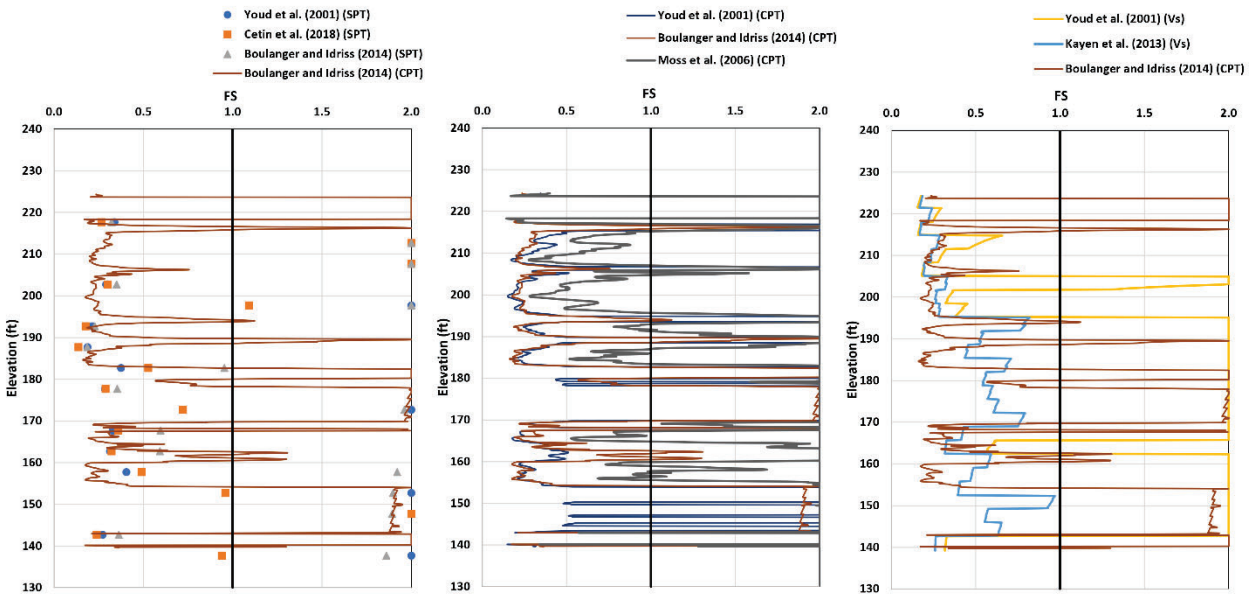

Figure 112. Comparison of SPT Results of BH-4 with Continuous CPT and V_s Results of CPT 3 of Monette Site

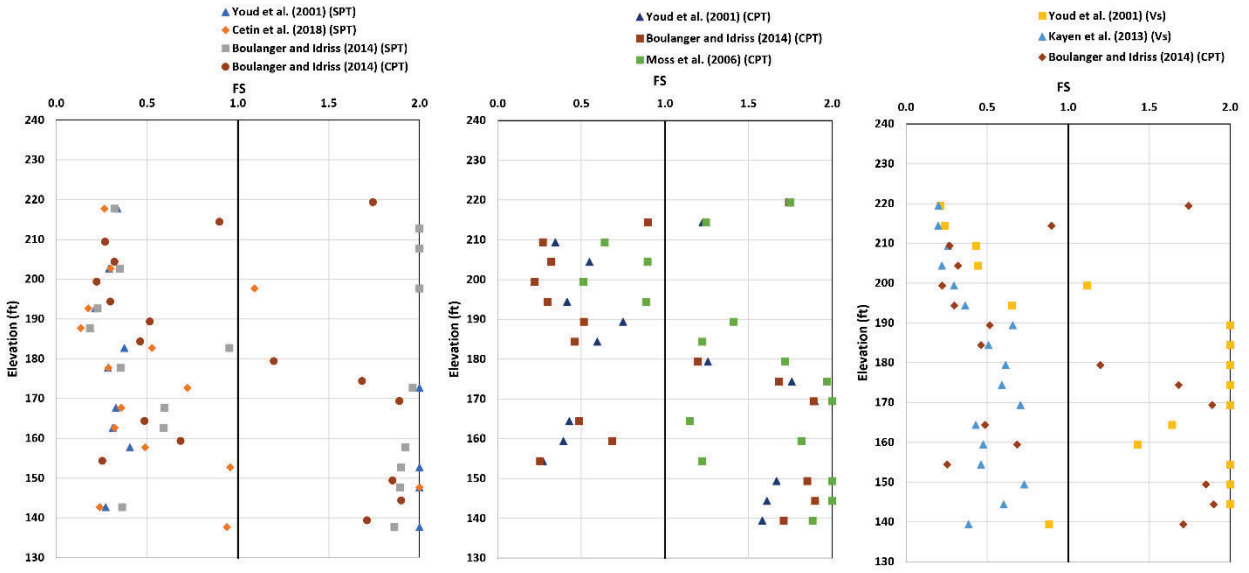

Figure 113. Comparison of SPT Results of BH-4 with Discontinuous CPT and V_s Results of CPT 3 of Monette Site

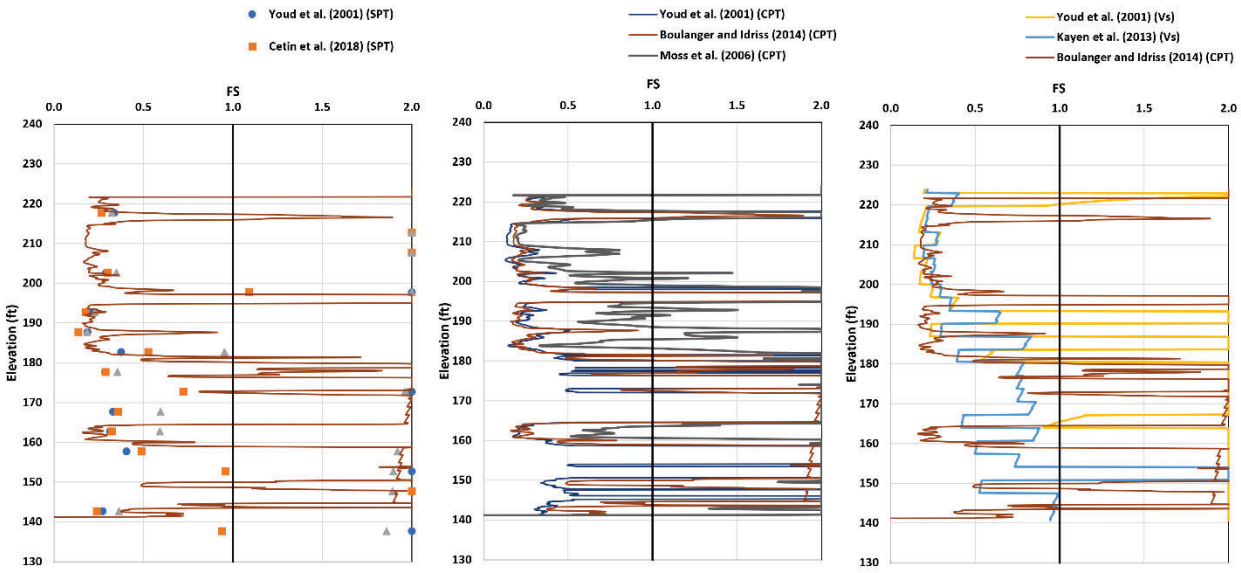

Figure 114. Comparison of SPT Results of BH-4 with Continuous CPT and V_s Results of CPT 4 of Monette Site

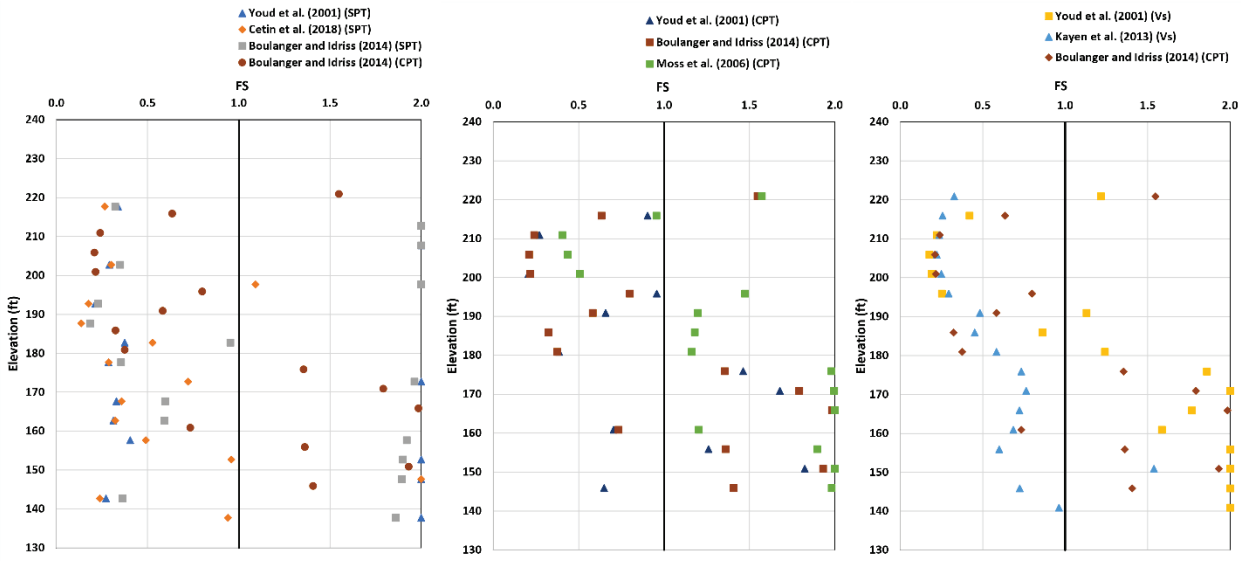

Figure 115. Comparison of SPT Results of BH-4 with Continuous CPT and V_s Results of CPT 4 of Monette Site

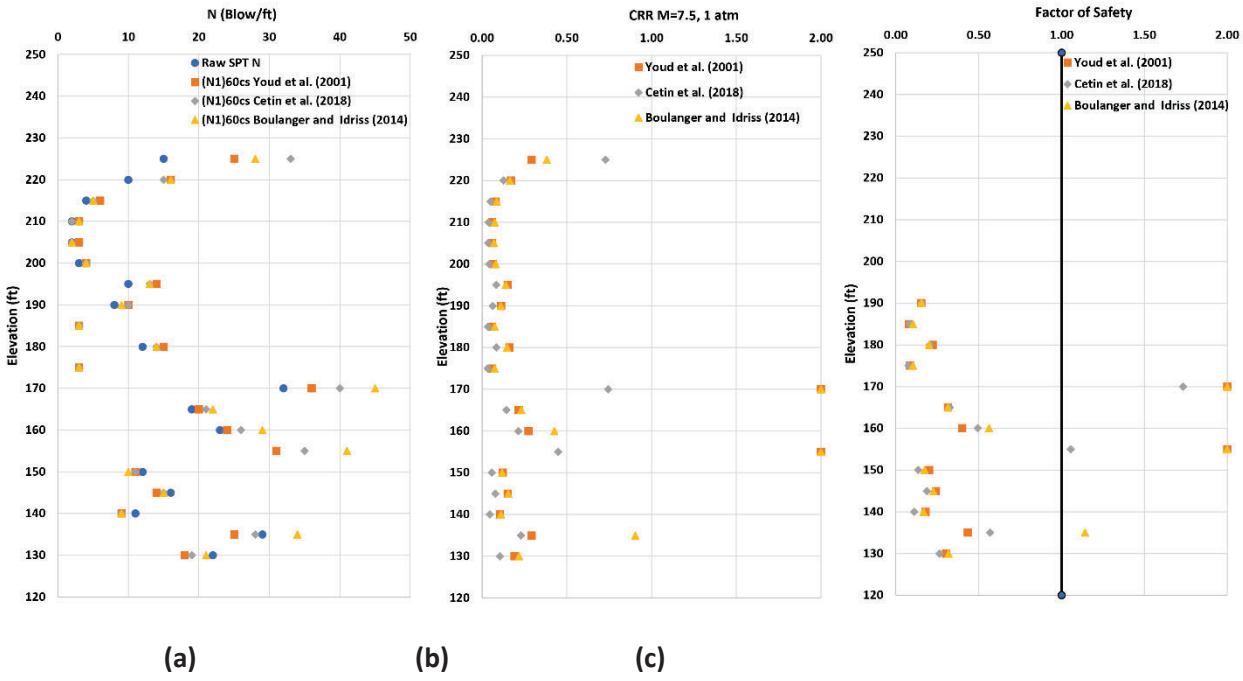

Figure 116**. Comparison of (a) Raw N and Equivalent Clean Sand Blow Count Value, (b) Unadjusted Cyclic Resistance Ratio (CRR), and (c) Factor of Safety Results of AHTD 1 at the Turrell Site Using the Chosen Three SPT-based Procedures**

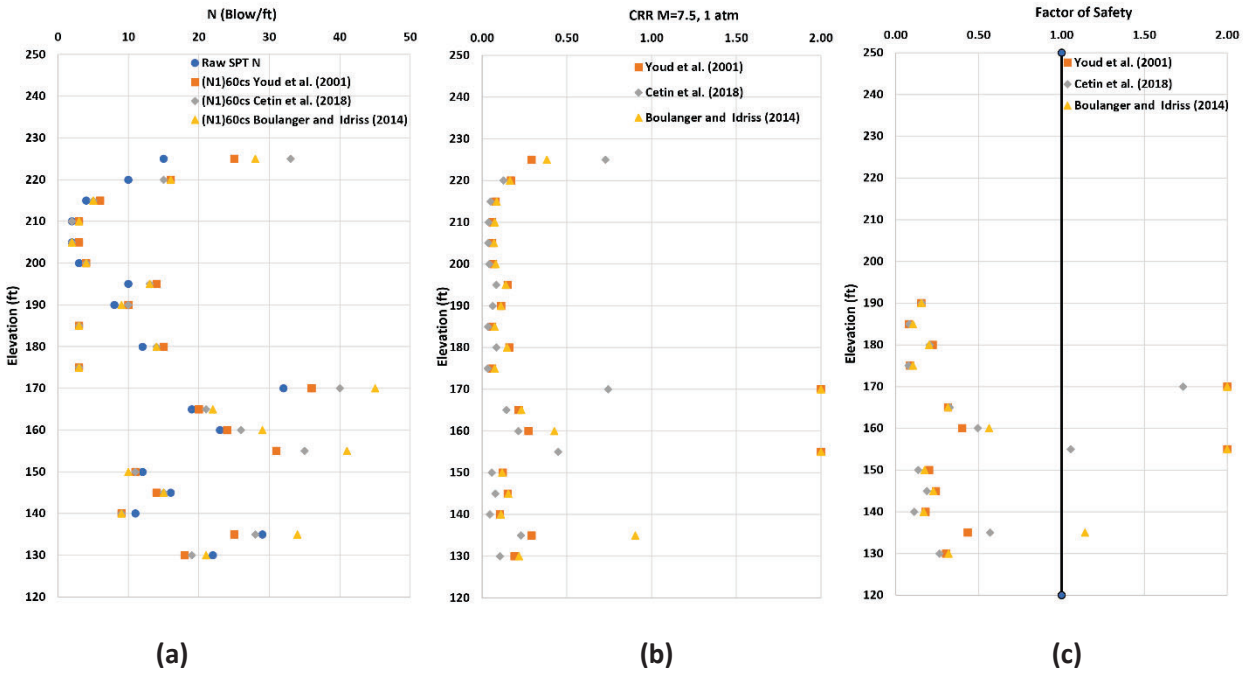

Figure 117. Comparison of (a) Raw N and Equivalent Clean Sand Blow Count Value, (b) Unadjusted Cyclic Resistance Ratio (CRR), and (c) Factor of Safety Results of AHTD 2 at the Turrell Site Using the Chosen Three SPT-based Procedures

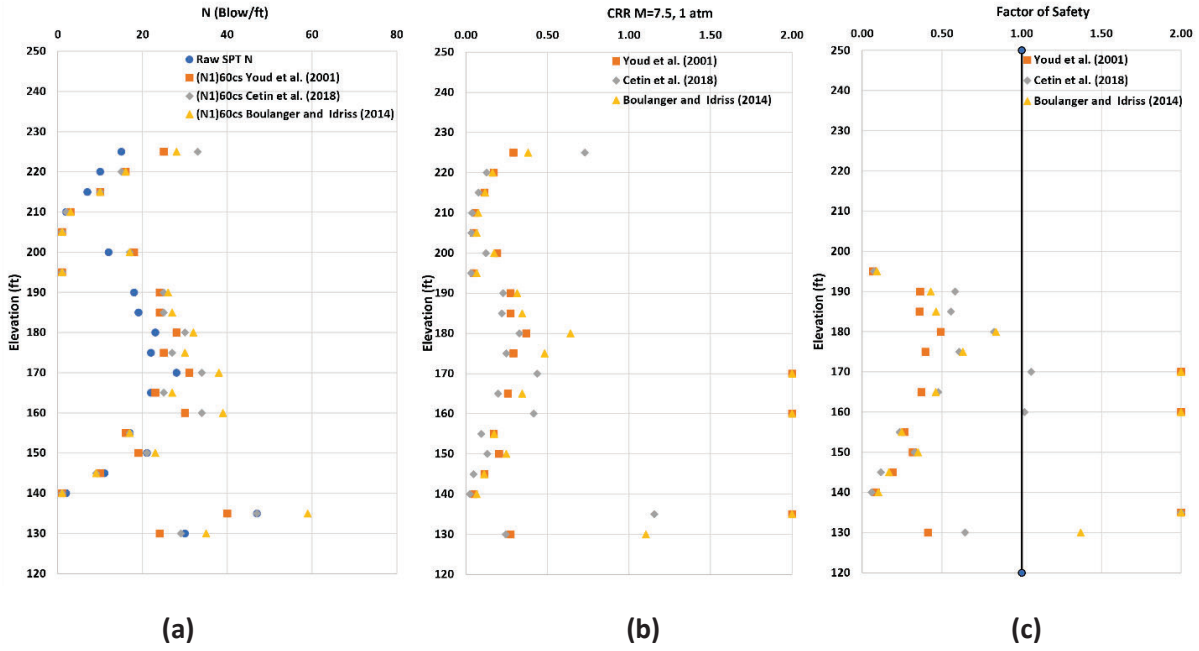

Figure 118**. Comparison of (a) Raw N and Equivalent Clean Sand Blow Count Value, (b) Unadjusted Cyclic Resistance Ratio (CRR), and (c) Factor of Safety Results of AHTD 3 at the Turrell Site Using the Chosen Three SPT-based Procedures**

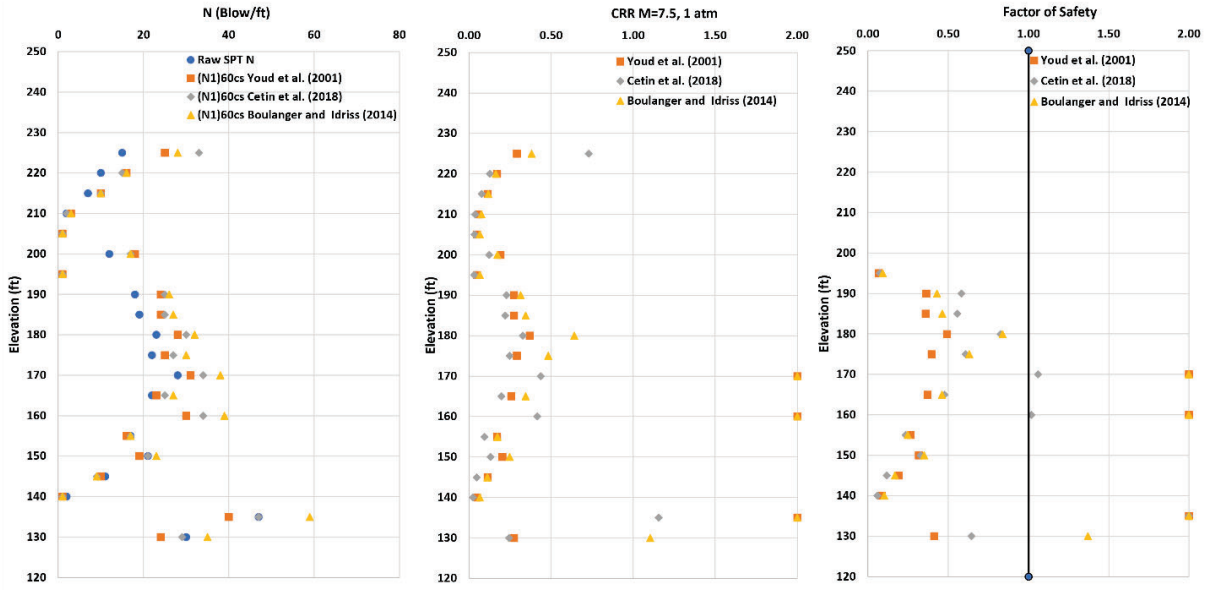

Figure 119**. Comparison of (a) Raw N and Equivalent Clean Sand Blow Count Value, (b) Unadjusted Cyclic Resistance Ratio (CRR), and (c) Factor of Safety Results of AHTD 4 at the Turrell Site Using the Chosen Three SPT-based Procedures**

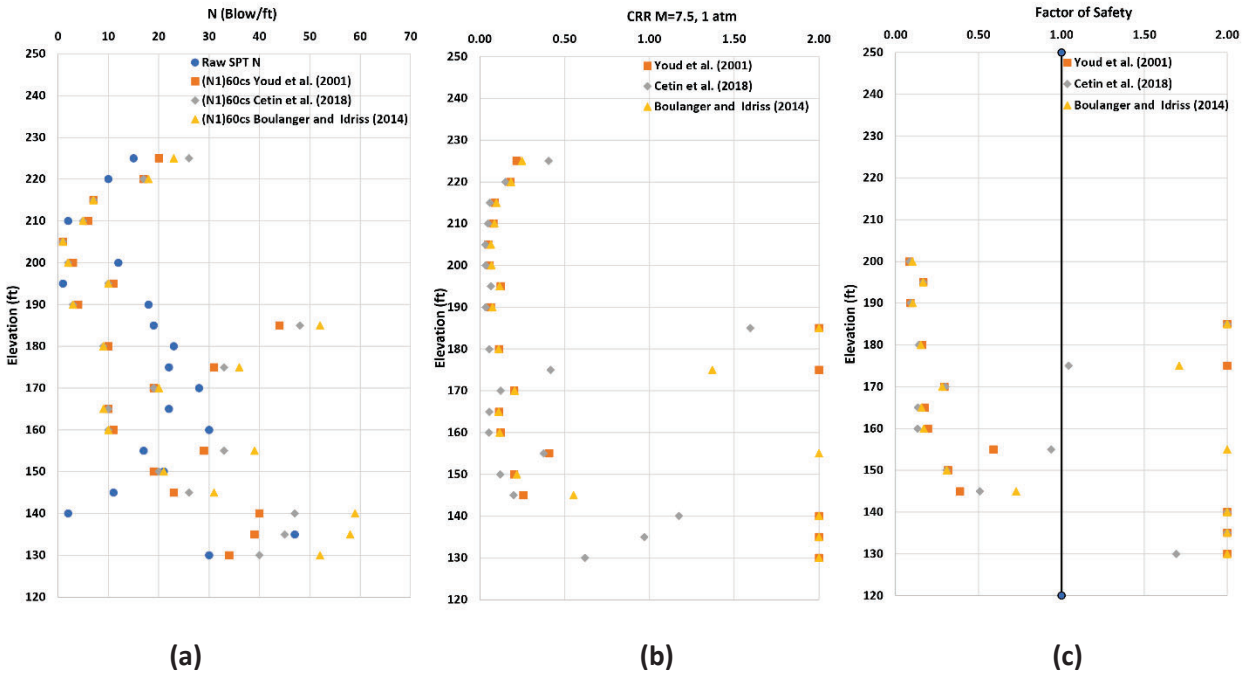

Figure 120. Comparison of (a) Raw N and Equivalent Clean Sand Value, (b) Unadjusted Cyclic Resistance Ratio (CRR), and (c) Factor of Safety Results of AHTD 5 at the Turrell Site Using the Chosen Three SPT-based Procedures

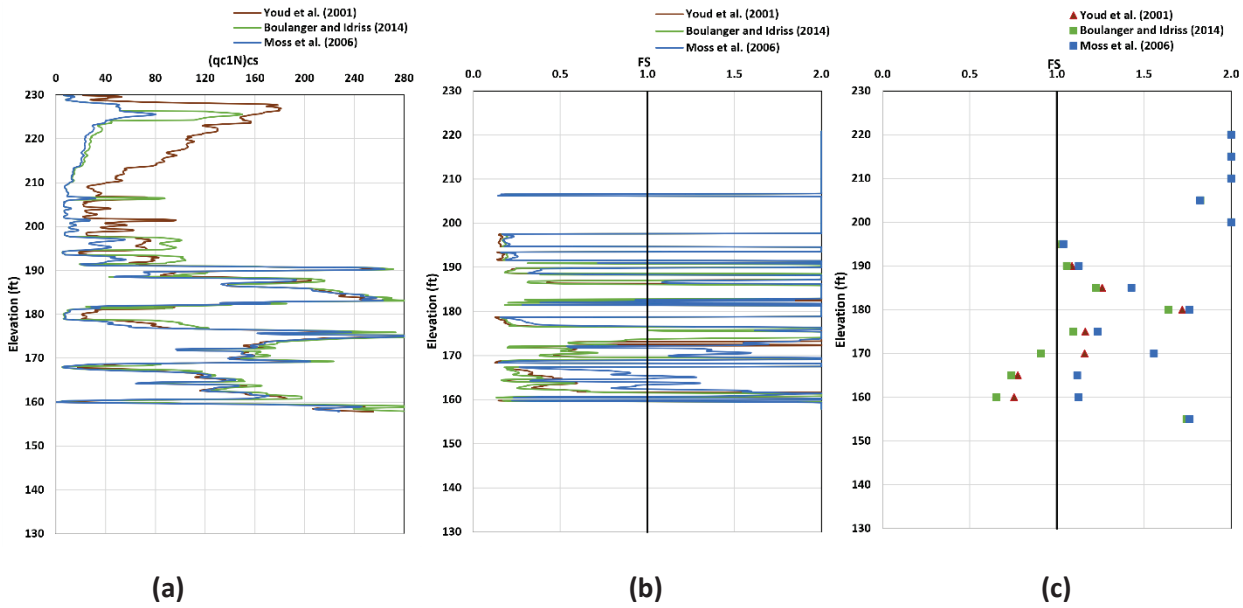

Figure 121. Comparison of (a) Equivalent Clean Sand Cone Penetration Resistance (qc1N)cs, (b) Continuous Factor of Safety Results, and (c) Discontinuous Factor of Safety Results of CPT 2 Borehole at the Turrell Site Using the Three Chosen CPT-based Procedure

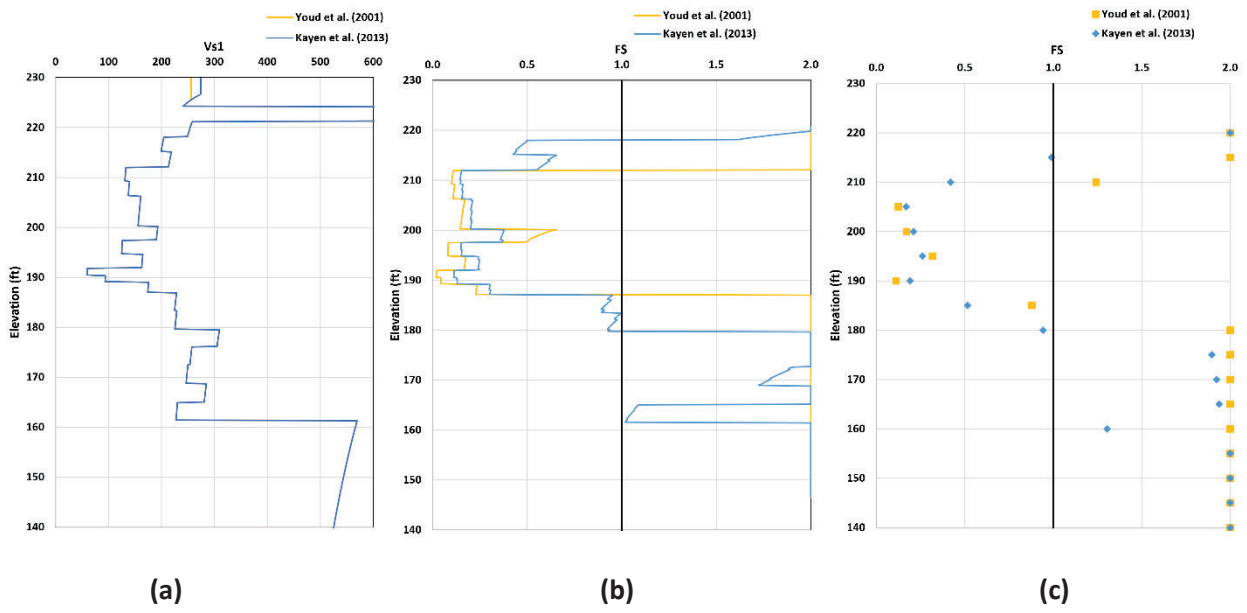

Figure 122. Comparison of (a) Overburden Stress Corrected Shear Wave Velocity (V_{s1}), (b) Continuous Factor of Safety Results, and (c) Discontinuous Factor of Safety Results of CPT 2 Borehole at the Turrell Site Using the Two Chosen V_s-based Procedures

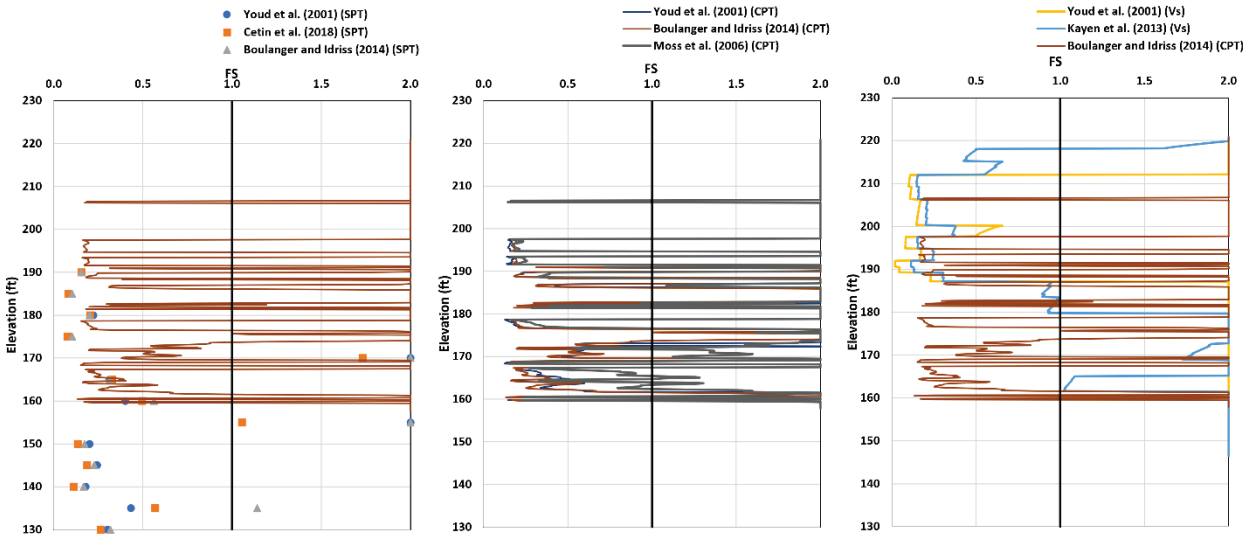

Figure 123. Comparison of SPT Results of AHTD-2 with Continuous CPT and V_s Results of CPT 2 of Turrell Site

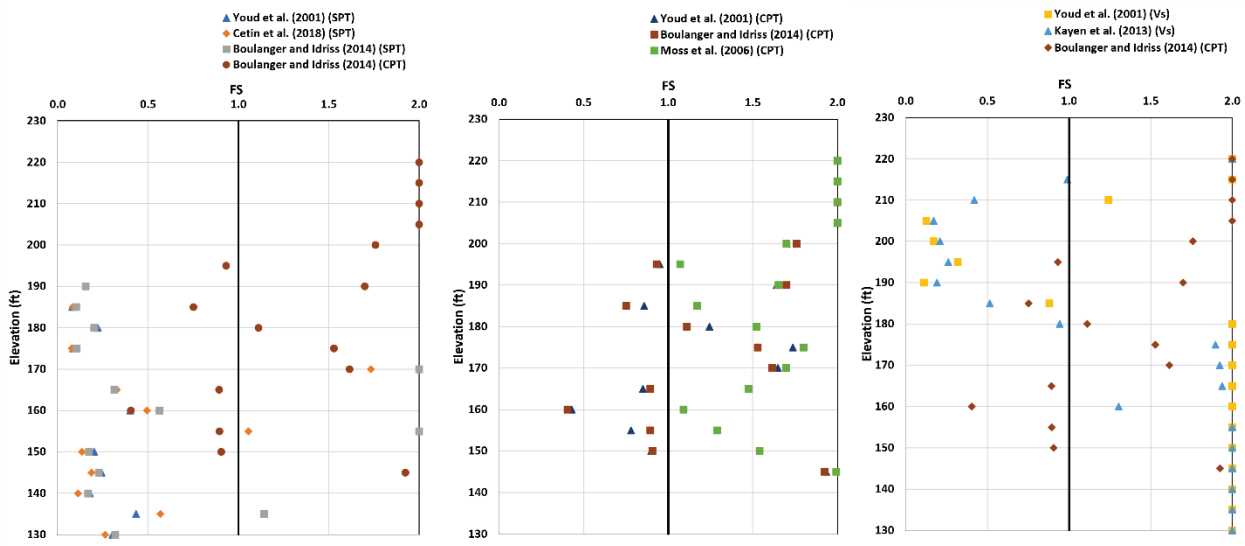

Figure 124. Comparison of SPT Results of AHTD-2 with Discontinuous CPT and V_s Results of CPT 2 of Turrell Site